R-08-105

Porewater in the rock matrix

Site descriptive modelling
SDM-Site Forsmark

H N Waber, T Gimmi
Rock-Water Interaction, Institute of Geological Sciences
University of Bern

J A T Smellie, Conterra AB

June 2009

Svensk Kärnbränslehantering AB
Swedish Nuclear Fuel
and Waste Management Co

Box 250, SE-101 24 Stockholm
Phone +46 8 459 84 00

ISSN 1402-3091
SKB Rapport R-08-105

Porewater in the rock matrix

Site descriptive modelling
SDM-Site Forsmark

H N Waber, T Gimmi
Rock-Water Interaction, Institute of Geological Sciences
University of Bern

J A T Smellie, Conterra AB

June 2009

Preface

This report describes the porewater investigation carried out on drillcore material from deep boreholes within the Forsmark Site Investigation programme. Porewater residing in the low permeability matrix of a rock body cannot be sampled by conventional groundwater sampling techniques, but has to be characterised by indirect methods based on drillcore material. Such determination is subjected to various types of induced perturbations, which need to be understood for the interpretation of the data at *in situ* conditions. Once the produced data can be judged to reliably represent *in situ* conditions they might be used for the characterisation of the exchange between porewater and fracture groundwater and to establish a conceptual model of the palaeohydogeological evolution.

At the Forsmark and Laxemar sites, porewater investigations based on various diffusion experiments utilising fresh drillcore material have been conducted for the first time in crystalline rocks. This required a rigorous control of the acquired data and supporting experiments in order to understand possible perturbation effects such as stress releases, the drilling process, and by sample desaturation. The present report presents applied methods and their uncertainties, the chemical and isotopic porewater data generated from the raw data, model attempts for the *in situ* porewater composition, and transport properties of the rock. A particular section is devoted to the quantitative evaluation of perturbing effects induced on porosity and porewater composition by stress release and drilling process on behalf of drillcore material collected from about repository depth and drilled with spiked drilling fluid. Finally, implications of the porewater geochemistry on the palaeohydrogeological evolution of the Forsmark site are discussed. Special emphasis is given to the integration of other geological, hydrogeochemical, hydrological and palaeo-climate data from the overall Forsmark descriptive model and, when appropriate, *vice-versa.*

The original works by the ChemNet modellers are presented in five level III reports containing complementary information for the bedrock hydrogeochemistry Forsmark Site Descriptive Model (SDM-Site Forsmark, R-08-47) level II report.

There is also one additional level III report: Fracture mineralogy of the Forsmark area by Sandström et al. R-08-102.

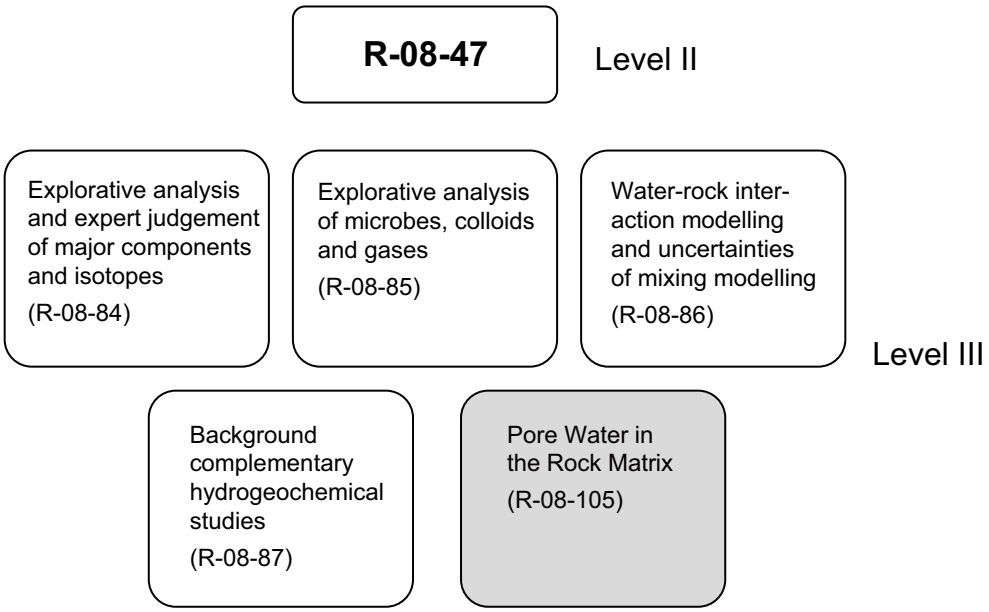

Summary

Porewater investigations at the Forsmark investigation site were aimed at elaborating the hydrogeochemical evolution of the site based on the potential of porewater acting as an archive to events that have happened over recent geological time (i.e. several thousands to a few millions of years), and to define the potential of matrix diffusion to contribute to solute transport in the geosphere.

A chemical and isotopic signature established in the porewater in the past might be preserved over long geological time periods. The degree of preservation depends on: a) the distance of the porewater sample to the nearest water-conducting fracture in three dimensions (i.e. the fracture network), b) the solute transport properties of the rock (i.e. diffusion coefficient, porosity), and c) the period of constant boundary conditions (i.e. constant fracture groundwater composition). Complex situations occur in the case of overlap or superimposition of changes induced by variable boundary conditions in Holocene and Pleistocene times when frequent climatic and hydrogeological changes occurred. As a consequence, no simple correlation between two independent natural tracers (e.g. Cl^- and $\delta^{18}O$) can be expected and the porewater data have to be interpreted by taking all these influencing factors into account. Furthermore, porewater data obtained for a single sample from a borehole can only be interpreted to a limited degree. More information can be extracted if profiles are sampled along a borehole, and/or small-scale profiles sampled from a water-conducting fracture into the host rock, and by comparing such data to present day fracture groundwater compositions in the nearest water-conducting fracture(s).

Porewater residing in the rock matrix cannot be sampled by conventional groundwater sampling techniques and therefore needs to be characterised by indirect methods based on drillcore material. Most importantly, this requires carefull evaluation of the produced porewater data for potential artefacts induced during drilling and sample processing in order for their interpretation in terms of *in situ* conditions. Within the SKB site investigation programmes at Oskarshamn and Forsmark, porewater investigations have been developed and tested for the first time in crystalline rocks /Waber and Smellie 2008/.

The effects of stress release and the drilling processes on the porewater concentration of conservative compounds are evaluated by employing indirect methods to core material drilled at about 550 m depth using traced drilling fluid. It is shown that the effect of the drilling disturbed zone on the water content and the porewater composition is less than 1%. For the rocks of the Forsmark site the cummulated effects of stress release on the porewater composition are shown to be less than 10%.

Porewater composition, the structural evolution in the rocks of the Forsmark investigation site and the transport properties of the rocks, differ greatly between rock sequences with a high frequency of transmissive fractures and rock sequences with a low frequency of transmissive fractures. Whereas these sequences generally correspond with the footwall bedrock segment and hanging wall bedrock segment defined by the geological fracture domains and deformation zones, there is some overlap in properties from one segment to the other, especially in boreholes KFM02B and KFM06A. Therefore, the porewater data have been interpreted in terms of footwall bedrock and hanging wall bedrock *sensu lato (s.l.)*, and are more biased on the frequency of transmissive fractures compared to the purely geological features.

Solute transport in the rock matrix is dominated by diffusion and matrix diffusion is identified to occur at least over several decametres into the rock matrix as shown by the natural tracer profiles developed in the gently dipping deformation zones ZFMA2 and ZFMF1 which demarcate the geologically defined footwall bedrock from the hanging wall bedrock. Pore diffusion coefficients for Cl^-, D_{pCl}, derived on kilogramme size samples show little variation among different rocks types and with sample depth and vary between 1.2×10^{-10}–8.1×10^{-11} m^2/s. Similarly, little variation among different rock types exists for the water-loss porosity, but differences exist between the rocks from the footwall bedrock s.l. (0.23–0.42 Vol.%) and the hanging wall bedrock s.l. (0.35–0.90 Vol.%).

In the footwall bedrock s.l. (i.e. fracture domains FFM01, FFM02 and FFM06, but excluding the highly transmissive part of borehole KFM06A which extends from the bedrock surface to at least 340 m depth), porewater chemical types change rather continuously with depth from dilute Na-Ca-HCO_3 type to brackish Na-Ca-Cl-(HCO_3) type and saline Ca-Na-Cl type. Indications for the most recent hydrologic events during the Holocene (e.g. glacial water, Littorina and/or Baltic Sea water) are

restricted mainly to local occurrences in the shallowest levels within fracture domain FFM02. Below in fracture domain FFM01, Cl^- concentrations are between about 2,000–3,500 mg/kg_{H2O} with associated isotope values enriched in the heavy isotopes ($\delta^{18}O$ = –2‰ to –8‰ VSMOW) down to about 500 m depth.

The dilute Na-Ca-HCO_3 type and brackish Na-Ca-Cl-(HCO_3) porewater types have originated from interaction with fracture groundwater of meteoric origin that infiltrated under warmer climatic conditions than today based on the moderate Cl^- concentration, the absence of Mg^{2+} (as an indicator for Littorina and/or Baltic Sea water), rock-water interaction which controlled Sr^{2+} and $^{87}Sr/^{86}Sr$, and the absence of distinct cold climate type $\delta^{18}O$ and $\delta^{2}H$ signatures. Combined with the large distances (generally > 20 m) from the nearest water-conducting fractures and the established transient state to the higher mineralised fracture groundwater, this suggests a very old origin (most probably pre-Pleistocene) for these porewaters. This is in agreement with the estimated very long average residence times of at least hundreds of thousands of years for fracture groundwaters at these depths based on ^{36}Cl and ^{4}He /Smellie et al. 2008/. Towards greater depth a gradual change to saline Ca-Na-Cl type porewaters with Cl^- concentrations up to 14,600 mg/kg_{H2O} and less enriched isotope compositions ($\delta^{18}O$ = –4 to –10‰ VSMOW) occur, although this transition varies from borehole to borehole. These very old porewaters show the greatest chemical and isotopic affinity to the different rock types and their composition seems to be largely controlled by rock-water interactions.

The porewaters in the footwall bedrock s.l. thus indicate that before the beginning of the Pleistocene-Holocene the entire rock volume was saturated with dilute meteoric water of warm climate origin, possibly as far back as Tertiary times, down to at least 640 m depth. Changes induced by fracture groundwater during Pleistocene and Holocene times are restricted to porewater of the shallowest zone and a few highly altered zones penetrating to greater depths (e.g. more transmissive episyenite). Based on the porewater data, the footwall bedrock appears to have been a weakly active hydraulic system at least during Holocene and Pleistocene times.

A different picture arises for the highly transmissive hanging wall bedrock s.l., i.e. fracture domain FFM03 which extends from the bedrock surface to 431 m depth in borehole KFM02B, and fracture domain FFM01 which extends in the same borehole from 431–512 m depth. Borehole KFM02B also intercepts two major gently dipping deformation zones ZFMA2 and ZFMF1 between about 400–500 m depth. The hanging wall bedrock s.l. also includes the highly transmissive upper part of borehole KFM06A (i.e. fracture domains FFM02, FFM01 and the steeply dipping deformation zones ENE0060B and A down to about 340 m depth or 400 m borehole length). In these localities the porewater is of a dilute Ca-Na-HCO_3 type and Na-Ca-HCO_3 type that alternate irregularly with depth and are more correlated to major deformation zones. Chloride concentrations are mainly below 1,500 mg/kg_{H2O} and associated isotope values indicate a meteoric origin covering the range from present day to cold temperature climatic conditions ($\delta^{18}O$ = –8 to –15‰ VSMOW) down to about 550 m depth in the hanging wall s.l. Most of the porewaters contain elevated Mg^{2+} concentrations indicating an influence by Littorina and/or Baltic Sea water. More saline porewaters with conspicuously high Mg^{2+} concentrations and more enriched in the heavy isotopes typical for Littorina Sea water occur in samples around the gently dipping deformation zones ZFMA2 and ZFMF1. At these depths such types of signatures superimpose on previously established glacial meltwater signatures in the porewater. Down to about 560 m a transient state between porewater and fracture groundwater is established with respect to Cl^- concentrations, with the Cl^- concentrations being higher in the fracture groundwater due to either a Littorina and/or Baltic Sea water component. The high Mg/Cl ratios and isotope signatures developed in the porewater indicate that the interaction of such marine water must have occurred with a dilute porewater of cold climate (glacial) origin that was previously present in the rock matrix. Based on the short distances (< 10 m, generally < 5 m) between porewater samples and nearest water-conducting fractures this cold climate signature has to be attributed to the last glaciation (Weichselian). Since then, this cold climate porewater signature has become overprinted with a brackish marine-type signature as indicated by Cl^-, Mg^{2+} and $\delta^{18}O$ in porewaters sampled closer to the water-conducting fracture. In the shallow zone, this brackish marine signature is now becoming overprinted by the circulation of present day meteoric groundwaters.

In the hanging wall bedrock s.l., the large compositional variability preserved in porewater samples located at similar short distances from different water-conducting fractures indicate that the porewater composition is dominated by fracture groundwater and the hydraulic system is more active compared to the footwall bedrock s.l.

Contents

1 Introduction

Crystalline rocks are generally characterised by two hydraulic regimes, namely the water-conducting zones related to regional and/or local fracture networks and the bedrock mass of low permeability between the water-conducting zones. In the first regime, the hydraulic transmissivity is generally above 10^{-9} m^2s^{-1} and solute transport takes place by advection. In the second regime, the rock matrix, the hydraulic transmissivity is low to very low ($T << 10^{-10}$ m^2s^{-1}) and solute transport is increasingly dominated by diffusion. The mass of porewater present in the rock matrix of a crystalline rock, however, is significant and its influence on fracture groundwater and future deep repositories needs to be understood.

Porewater in the rock matrix and groundwater in the fracture network always tend to reach chemical and isotopic equilibrium. This interaction depends on the existence of an interconnected pore system in the rock matrix that contains a solvent, i.e. porewater, where solute transport can take place, and on the residence time of groundwater in the water-conducting zones. During such interaction, the porewater (and rock matrix) acts either as a sink or a source for solutes depending on the concentration gradient established between porewater and fracture water. Thus, the porewater does not only act as an archive of past fracture groundwater compositions and therefore of the palaeo-hydrogelogical history of a site, but also as a possible sink for radionuclides (e.g. /Neretnieks 1980/).

In contrast to groundwater flowing in a fracture network, porewater that resides in the low permeable rock matrix cannot be sampled by conventional groundwater sampling techniques. The chemical and isotopic composition of porewater has, therefore, to be derived by indirect extraction techniques based on originally saturated drillcore material. This requires thoroughly tested core preservation techniques and a concerted logistical effort extending from the drilling process to sampling to the laboratory investigations. In addition, the obtained data need to be carefully evaluated for potential perturbations induced, for example, by drilling activities, stress release, sample treatment in the laboratory, and to what degree they are representative of *in situ* conditions.

The matrix of crystalline rocks contains different types of pore spaces where different types of pore fluid reside (cf. /Pearson 1999, Waber and Smellie 2008/ for discussion). This total pore space, the *physical porosity*, is described by the ratio of void volume to the total volume of the rock. It includes the volume not occupied by mineral grains such as pore spaces between mineral grains, dead-end pores, micro-fractures, porous minerals (often secondary minerals) and mineral fluid inclusions /Norton and Knapp 1977/. The *connected porosity* of a rock describes the volume of connected pore space between mineral grains and is smaller than the total porosity. Exchange between (quasi) stagnant porewater and flowing groundwater can only occur in the porosity accessible for solute transport. Transport of a substance can take place either by advection or by diffusion and only through pores of which the minimum pore throat size is larger than the maximum size of the substance transported and where no charge exclusion effects occur.

In the case of advective flow and transport, the Darcy flux and the linear velocity of a tracer are related by the *advective transport porosity*. This advective transport porosity does not include isolated pores or dead-end pores and is smaller than the connected porosity. In the low permeable rock matrix, solute transport by diffusion becomes important. The porosity accessible to diffusion, the *diffusion porosity*, is determined by various diffusion experiments (in-, out-, and through-diffusion). As for other porosity measurements, the porosity derived from diffusion experiments might have different numerical values depending: a) on the rock texture (e.g. anisotropy due to foliation and bedding, grain size variations), and b) on the solute used in the experiments (e.g. ions with large hydration spheres versus ions with small hydration spheres). For the diffusion of the water molecules themselves, the diffusion porosity becomes close to the water-loss porosity. For the diffusion of solutes the diffusion porosity is less than the water-loss porosity, but higher than the advective transport porosity (cf. /Pearson 1999/ for discussion).

The bulk of the fluid contained in the physical porosity of the rock matrix, the *'matrix pore fluid'*, cannot be sampled by conventional groundwater sampling techniques. Because of the above mentioned different accessibility of the total pore space, the matrix pore fluid is composed of

different fluid types. These include: a) the water in microfractures where minor advective flow might occur, b) the water in the pore space of a rock that is only accessible by diffusion, c) the water residing in isolated pores, and d) the fluid enclosed in mineral fluid inclusions.

The term *'porewater'* as used here refers to the water in the connected pore space of the rock matrix that is accessible for diffusion-dominated interaction with groundwater circulating in nearby (micro-) fractures.

A chemical and isotopic signature established in the porewater at a certain time in the hydrogeological evolution of a site might be preserved over long, geological time periods. For chemically conservative compounds, the degree of the preservation of such signature depends on: a) the distance of the porewater sample to the nearest water-conducting fracture in three dimensions (i.e. the fracture network), b) the solute transport properties of the rock (i.e. diffusion coefficient, porosity), and c) the boundary conditions (i.e. the fracture-groundwater composition). Constant boundary conditions over the time period considered greatly facilitate the interpretation of an observed porewater signature. In reality, however, overlaps of changes induced by variable boundary conditions seem more common, certainly in the first few metres of the rock matrix from the nearest water-conducting fracture and over the Holocene and Pleistocene time periods of concern here during which frequent climatic and hydrogeologic changes occurred. In addition, the significance of the signature (with respect to the measurement error) depends on the chemical gradient between porewater and fracture groundwater.

Within the SKB Site Investigation programmes at Forsmark and Oskarshamn /Waber et al. 2009/, porewater investigations have been developed and tested for the first time in the crystalline rocks. The investigations aimed a) to elaborate the hydrogeological evolution of a site due to the potential of porewater acting as an archive of what has happened over recent geological time (i.e. several hundreds to a few millions of years), b) to define the potential of matrix diffusion to contribute to the retardation of radionuclide transport in the geosphere, and c) to provide the basis for a better constrained treatment of the interaction between porewater and repository barrier materials (e.g. bentonite, canister), potentially leading to a deterioration in their physical properties. For safety assessment considerations, it is therefore important to know the composition of the porewater and its evolution over recent geological time, certainly during the last thousands to hundreds of thousands of years in accordance with the expected lifespan of a repository.

From the Forsmark area samples for porewater investigations have been collected from five different boreholes (KFM01D, KFM02B, KFM06A, KFM08C and KFM09B). These deep boreholes have been drilled at different inclinations up to about 1,000 m borehole length. The boreholes are situated in different geological, fracture and hydraulic domains and also penetrate different deformation zones /Olofsson et al. 2007, Follin et al. 2007, Stephens et al. 2008a/. In contrast, the mineralogy of all encountered rocks is similar being mainly of granitic to granodioritic compositions with some intercalations of tonalitic, aplitic, pegmatitic and amphibolitic rock types. In all five boreholes hydraulic logging has been performed and several groundwater samples could be collected from water-conducting fractures.

This report summarises the results obtained from the porewater investigations carried out on rock material from boreholes KFM01D, KFM02B, KFM06A, KFM08C and KFM09B from the Forsmark area. The hydrogeological background of the investigated boreholes and the applied sampling strategy and methods are first presented (cf. /Waber and Smellie 2008/). This is followed by a quantitative evaluation of perturbing effects induced on the rock porosity and porewater composition by stress release and drilling processes. The quality controlled porewater data considered to be representative for *in situ* conditions are then compared to the hydraulic and fracture groundwater data obtained from the same boreholes. Finally, the porewater data are integrated with other geological, hydrogeochemical, hydrological and palaeo-climate data and the implications of the porewater geochemistry on the palaeohydrogeological evolution of the Forsmark site are discussed.

2 Hydrogeological background

The candidate area of the Forsmark site investigation programme (Figure 2-1) is divided into the footwall bedrock segment to the northwest and the hanging wall bedrock segment to the southeast according to geological and structural criteria. The two gently dipping deformation zones ZFMA2 and ZFMF1 form the divide between these two bedrock segments (Figure 2-2).

Boreholes used for porewater investigations are KFM01D, KFM02B, KFM06A, KFM08C and KFM09B. As shown in this report, the porewater composition and evolution strongly depends on hydrogeologic features such as the frequency of transmissive fractures in addition to the geologic and structural features. At certain locations, especially in boreholes KFM02B and KFM06A, the frequency of transmissive fractures (and connected to that the porewater compositions) do not completely overlap with the geologically defined footwall and hanging wall bedrock segments. This required an adaptation of these terms to account for the porewater occurrences and to facilitate the description of the porewater evolution, which is more biased towards the hydraulic than the geologic properties of a rock. Based on the findings from the porewater investigations, the geologically defined footwall and hanging wall bedrock segments were thus extended and further referred to as footwall bedrock *sensu lato (s.l.)* and hanging wall bedrock s.l.

The footwall bedrock s.l. comprises fracture domains FFM01, FFM02 and FFM06 as in the geological model, but excludes the highly transmissive parts of these domains in boreholes KFM02B (i.e. FFM01 from 431–573 m depth) and KFM06A (i.e. FFM02/FFM01 from the bedrock surface to about 340 m depth). From the porewater point of view, the footwall bedrock s.l. thus comprises rock from boreholes KFM01D, KFM08C, KFM09B and the low transmissive part of borehole KFM06A below about 340 m depth (400 m borehole length) (Figure 2-3).

The hanging wall bedrock s.l. mainly comprises the highly transmissive fracture domain FFM03 as in the geologic model, but includes also the highly transmissive parts in boreholes KFM02B and KFM06A. This conspicuously higher frequency of interconnecting water-conducting fractures is related to a series of gently dipping deformation zones of which ZFMA2 and ZFMF1 are the most important in borehole KFM02B, and also the steeply dipping deformation zones ENE0060B and ENE0060A which influence borehole KFM06A in the upper part of fracture domain FFM01; the near-surface fracture domain FFM02 is also highly transmissive. From the porewater point of view the hanging wall bedrock s.l. thus comprises the entire borehole KFM02B and the upper 340 m (400 m borehole length) of borehole KFM06A (Figure 2-3).

This chapter provides a short summary of background information about the geology and hydrology of the rock domains encountered in the boreholes that were used for porewater investigations. For complete and detailed descriptions and the conceptual models derived about the geology, fracture domains, hydraulic situation and bedrock hydrochemistry of the Forsmark area, the reader is referred to /Follin et al. 2007, Follin 2008, Laaksoharju et al. 2008, Nordquist et al. 2008, Olofsson et al. 2007, Sandström et al. 2008, Söderbäck (ed) 2008, Stephens et al. 2008a, b/ and references therein.

2.1 Geology

2.1.1 Boreholes in the footwall bedrock *sensu lato*

In the footwall bedrock s.l., borehole KFM01D was drilled in the western part of the candidate area (Figure 2-1) to obtain detailed geological, hydrogeological and hydrochemical information of the rock volume representing the central part of a potential repository target area (Figure 2-2). The dominant rock type encountered is a metagranite which locally becomes slightly granodioritic in composition /Petersson et al. 2006a/. In the drillcore the metagranite is mainly fine grained from 191–499 m borehole length and more medium grained at greater depth. Pegmatitic granite occurs in sections of commonly less than 2 metres thickness and constitutes about 20% of the entire drillcore. Subordinate fine- to medium-grained metagranitoids of granitic to granodioritic composition and amphibolites are present. Rock foliation is frequently developed leading to a distinct anisotropy and to a gneissic

appearance of certain core sections. Tectonisation, rock alteration and frequency of open fractures are high in the first about 200 m borehole length, after which they decrease systematically with increasing depth. In open fractures calcite, epidote and chlorite are the most abundant minerals over the entire core lengths /Petersson et al. 2006a/. Pyrite occurs only rarely, while oxidised iron phases (hematite, iron hydroxides) are present throughout and are abundant in the three tectonised zones at about 490 m, 690 m, and 770 m borehole length.

Borehole KFM06A was drilled in the footwall bedrock s.l. close to the small lake Puttan, north of Bolundsfjärden, with a 60° inclination towards the north-west to investigate the existence of N–S and NE–SW trending, brittle deformation zones in the northeastern part of the candidate area (Figure 2-1). The upper part of the borehole down to about 340 m depth (400 m borehole length) comprises fracture domain FFM02 to 122 m depth (146 m borehole length) and fracture domain FFM01 to 340 m depth, whereas the lower part of borehole KFM06A from about 340–827.5 m depth (400–1,000.6 m borehole length) consists of fracture domains FFM01 and FFM06 (Figure 2-3). As mentioned above, from a hydrogeological point of view fracture domain FFM02 and the upper part of fracture domain FFM01 contain a high frequencey of transmissive fractures, the latter related to the steeply dipping deformation zones ENE0060B and ENE0060A. Therefore, this upper part of borehole KFM06A is treated together with the highly transmissive hanging wall bedrock s.l., whereas the lower part of the borehole below 340 m depth continues to be treated as the footwall bedrock s.l. In the lower part from 400 m to 580 m borehole length the drillcore consists mainly of

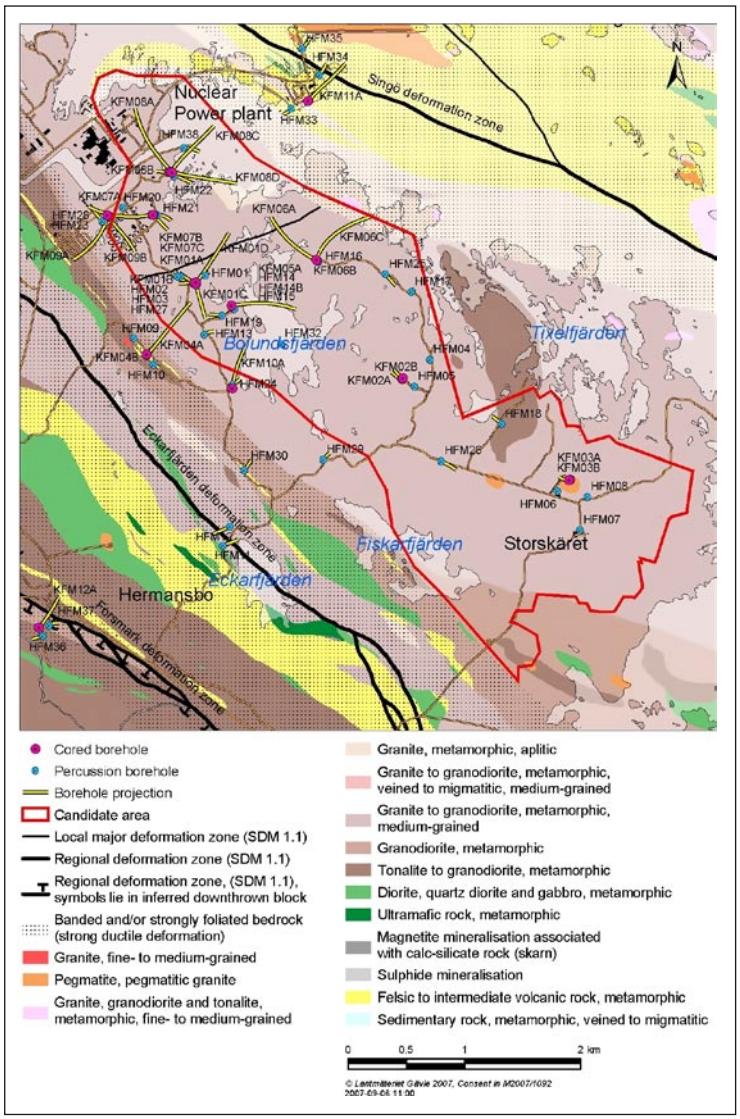

Figure 2-1. *Generalised geological map of the Forsmark site investigation area showing the location of boreholes KFM01D, KFM02B, KFM06A, KFM08C and KFM09B used for porewater characterisation.*

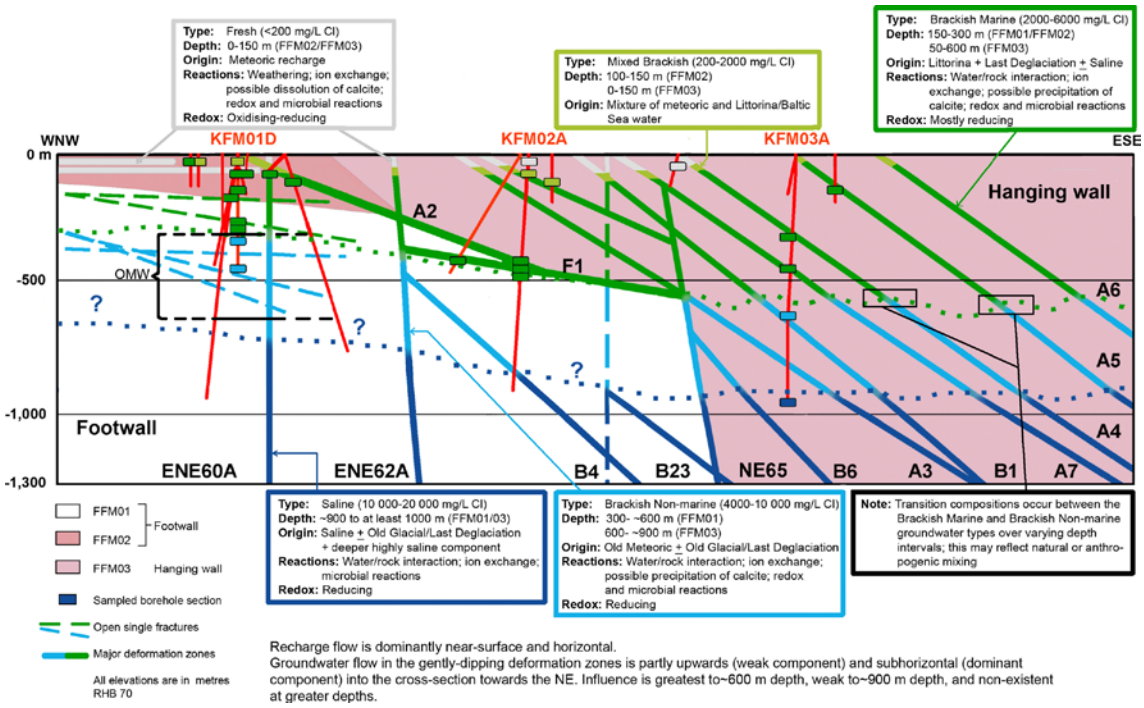

Figure 2-2. *Schematic cross-section through the central part of the candidate area in a WNW-ESE direction showing the geologcially defined footwall (FFM01, FFM06 and FFM02) and hanging wall (FFM03) bedrock segments that are separated by the gently dipping deformation zones ZFMA2 and ZFMF1 (labelled as A2 and F1) and the steeply dipping deformation zone ZFMNE0065 (labelled as NE65). Also given is the distribution of the major fracture groundwater types. The dotted lines in different colours represent the extrapolation of the approximate penetration depths of the major groundwater types along hydraulically active fracture zones (from /Smellie et al. 2008/).*

medium-grained, equigranular metagranite to granodiorite /Petersson et al. 2005/. From 580 m to the end of the borehole at 1,000.6 m the drillcore is comprised of fine- to finely medium-grained metagranitoids of granitic to granodioritic composition with an intercalated fine-grained, whitish, often aplitic leucogranite that extends from 755 m to 966 m borehole length. The bleached appearance of this rock type is due to an albitic alteration and the occurrence of hornblende instead of biotite as the most abundant ferromagnesian phase. Other rock types of limited extent and absent from the porewater rock samples include various amphibolites and dykes or veins of pegmatite, aplitic granite and leucogranite. Although fractures are abundant in the lower part of borehole KFM06A, by far the majority of them are sealed with laumontite, calcite, chlorite, hematite-stained adularia, pyrite and quartz /Petersson et al. 2005/. In the few open fractures calcite, clay minerals and pyrite dominate as infilling minerals and Fe-hydroxides were only observed in one open fracture at 503.4 m borehole length.

Borehole KFM08C was drilled in the northeastern part of the candidate area at the western shore of Asphällsfjärden (Figure 2-1) to investigate the hydrogeology at repository depths close to the boundary of the candidate area. Initially it was intended also to carry out hydrochemical characterisation of the borehole, but this was suspended because of a lack of suitable sampling locations. The dominant rock type encountered is a medium-grained metagranite of greyish-red to grey in colour, similar to that found in other deep boreholes from the site /Petersson et al. 2006b/. Other rock types that commonly occur only over a few metres along the drillcore include pegmatitic granites, fine- to medium-grained metagranitoids, and a few amphibolite dykes. Rock foliation is well developed producing a distinct anisotropy and a gneissic appearance to some of the core sections. Besides, intense ductile and brittle ductile deformation occurs locally in the drillcore.

The most prominent alteration phenomena include oxidation of the bedrock when related to fracture concentrations down to about 700 m borehole length and an albitisation of the rocks between 342.2–546.5 m and again between 603.5–616.8 m borehole length /Petersson et al. 2006b/. This oxidation, apparent as a more or less strong hematite pigmentation of the feldspar grains, defines

fracture domain FFM06 /Olofsson et al. 2007/ (Figure 2-3). The albitisation is characterised by a bleached appearance and the occurrence of hornblende instead of biotite as most abundant ferromagnesian phase, the latter predominating elsewhere in the metagranites. Between 455–532 m borehole length, several approximately three metre long intervals occur that are composed of episyenitic rock exhibiting selective quartz dissolution. These zones, associated with the geologically defined steeply dipping deformation zone NNE2312 /Olofsson et al. 2007/ (Figure 2-3), are highly porous, for example, as shown by porewater sample KFM08C-4 from 455.7 m borehole length. Fractures are abundant and occur over the entire drillcore at a frequency of about 5 fractures per metre and, as in the other boreholes, the majority of the fractures are sealed /Petersson et al. 2006b/. Calcite and chlorite are the most abundant minerals in open fractures often accompanied by clay minerals (illite, corrensite) and pyrite /Petersson et al. 2006b/. Less abundant are apophyllite, analcime, pyrite, laumontite, Fe-hydroxides, and asphalt, the latter being restricted to depths above 150 m borehole length. In closed fractures there occur in addition epidote, quartz, prehnite, adularia, unspecified sulphides, and sometimes biotite.

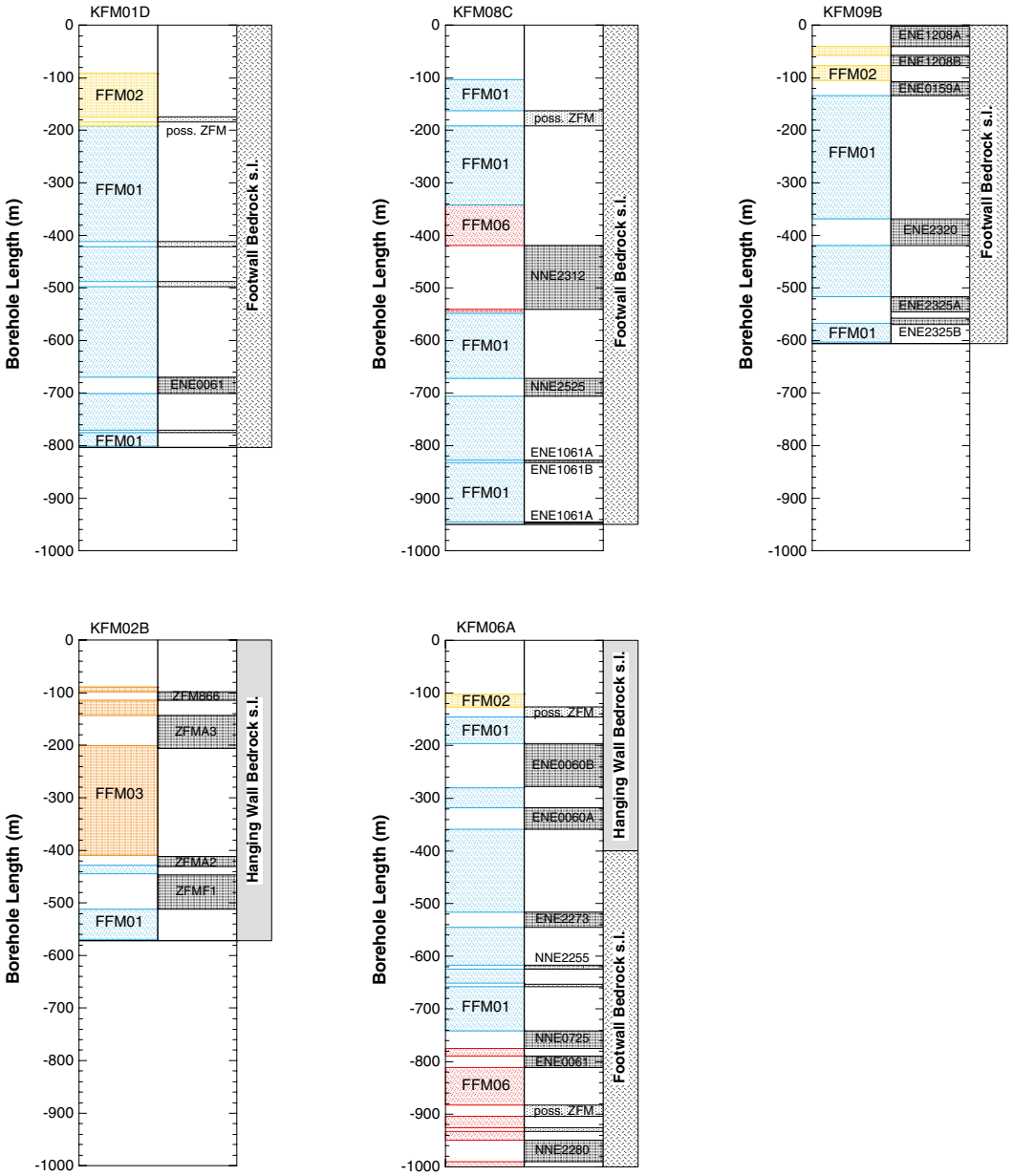

Figure 2-3. *Boreholes used for porewater investigations and their relation to the geologically defined fracture domains (FFM) and deformation zones (ZFM, ENE etc, data from /Olofsson et al. 2007, Stephens et al. 2008a/) and the allocation of footwall bedrock s.l. and hanging wall bedrock s.l. used in this report (cf. Figures 2-1 and 2-2 for borehole location).*

Borehole KFM09B was drilled at the northwestern boundary of the candidate area south of the Forsmark nuclear power plant (Figure 2-1) to investigate the hydrogeology and hydrogeochemistry of the rock mass that may be used for a potential access tunnel to the central part of a potential repository. The dominant rock type encountered is a medium-grained metagranite of greyish-red to grey colour, similar to that found in other deep boreholes from the site /Petersson et al. 2006c/. About 25% of the drillcore consists of granitic pegmatite, which commonly occurs in thicknesses of a few decimetres to metres. In borehole KFM09B samples for porewater investigations were restricted to a 13 m interval starting at 573.47 m borehole length and representing a transition between episyenitic rock and the dominant medium-grained metagranite just below deformation zone ENE2325B (556–568 m borehole length, cf. Figure 2-3). The highly porous and conductive episyenitic rock exhibiting quartz dissolution occurs in the interval from 568.92–573.45 m borehole length and is similar to the episyenite at 455 m borehole length observed in borehole KFM08C.

2.1.2 Boreholes in the hanging wall bedrock *sensu lato*

In the hanging wall bedrock s.l., borehole KFM02B was drilled in the southeast sector of the candidate area (Figure 2-1) in fracture domain FFM03 and eventually into fracture domain FFM01 towards completion of the borehole (Figures 2-2 and 2-3). The objectives of the borehole were: a) to confirm or otherwise the existence of two gently dipping deformation zones ZFMA2 and ZFMF1 (Figures 2-2 and 2-3) and investigate their effect on the local stress field, b) to conduct cross-borehole tracer tests, c) to sample a continuous profile away from a water-conducting zone into the surrounding rock matrix either in deformation Zone ZFMA2 or ZFMF1 for matrix porewater investigations, and d) to investigate the effects of possible drilling fluid contamination on porewater samples. Except for five samples from the last 14 m of the borehole, which comprised intact rock from fracture domain FFM01 and were used for the contamination studies, all porewater samples from borehole KFM02B were selected from fracture domains FFM03 and FFM01 affected by deformation zones ZFM866, ZFMA3, and ZFMA2, ZFMF1, respectively (Figure 2-3). The dominant rock types encountered in borehole KFM02B are a fine- to medium-grained, lineated metagranite-granodiorite that comprises about 59% of the drillcore /Samuelsson et al. 2007, Carlsten et al. 2007/. Pegmatitic granite comprises about 19% and a lineated fine- to medium-grained granite about 14% of the drillcore. Over the entire drillcore amphibolite, fine- to medium-grained metagranitoid and medium-grained metadiorite-gabbro are present in percentages of < 3% and other rock types such as aplitic metagranite, quartz-dominated hydrothermal veins, calc-silicate rock and felsic to intermediate metavolcanic rock contribute less than 1% of the drillcore. Rock foliation is frequently developed leading to a distinct anisotropy and to a gneissic appearance of most of the core sections. Six zones with increased brittle deformation and an accumulation of closed and/or open fractures occur between 98–115 m, 145–204 m, 411–431 m, 447–451 m, 461–473 m, and 485–512 m borehole length /Carlsten et al. 2007/. The crushed sections at 449 m and 471 m borehole length are highly altered, containing clay minerals, hematite and calcite. The remaining crushed sections contain chlorite, clay minerals, calcite, prehnite and also epidote. Pyrite occurs rarely below about 400 m, while oxidised iron phases (hematite, iron hydroxides) are present throughout and are abundant in the tectonised zones.

The upper part of borehole KFM06A includes fracture domain FFM02 (upper 122 m of bedrock; 146 m borehole length) and the upper part of fracture domain FFM01 from about 122–340 m depth (146–400 m borehole length) and affected by the steeply dipping deformation zones ENE0060B and ENE0060A (Figure 2-3). As described in Section 2.1.1, this interval contains a conspicuously higher frequency of interconnecting water-conducting fractures (cf. also Section 2.2.2). Therefore, based on the hydrological criteria, the uppermost 340 metres of borehole KFM06A are treated together with borehole KFM02B under the heading of hanging wall bedrock s.l. The rocks of this uppermost interval of borehole KFM06A consist of medium-grained metagranite to granodiorite /Petersson et al. 2005/. Texturally, the rock is equigranular with elongated quartz domains, alternating with feldspar-dominated domains and thin streaks of biotite. Rock foliation is frequently developed leading to a distinct anisotropy and to a gneissic appearance of most of the core sections used for porewater investigations. Other rock types with an extent of < 1m and not present in the porewater samples include several pegmatites and two amphibolite dykes. Open and closed fractures are frequent in the upper part of borehole KFM06A and open fractures are much more abundant than in the lower part of the borehole (i.e. in the footwall bedrock). Open fractures are often free of visible coatings or contain clay minerals, hematite, Fe-hydroxide, calcite, and sometimes pyrite and asphaltite /Petersson et al. 2005/.

2.2 Hydrology

2.2.1 Boreholes in the footwall bedrock *sensu lato*

In the footwall bedrock s.l. characterised by borehole KFM01D, tectonisation, rock alteration and frequency of open fractures are high in the first approximately 140 m of bedrock comprising mainly fracture domain FFM02 (to approximately 200 m borehole length, Figure 2-3), after which they decrease systematically with increasing depth in fracture domain FFM01. Below about 400 m borehole length open fractures are limited and occur only in a few tectonised zones at about 490 m, 690 m, and 770 m borehole lengths /Petersson et al. 2006a/. An accumulation of highly transmissive fractures (up to 10^{-5} m^2/s) was observed between 100–200 m borehole length based on differential flow logging (PFL, /Väisävaara et al. 2006a/). At greater depth the hydraulic transmissivity of the fractures decreases drastically and the deepest located 5 m interval with a measurable transmissivity (2×10^{-7} m^2/s) is located between 568 m and 573 m borehole length.

In the lower part of borehole KFM06A from about 400–1,000.6 m borehole length (fracture domains FFM01 and FFM06, cf. Figure 2-3) open fracture are rare. Of the 99 open fractures that provided a measurable groundwater flow in the differential flow logging (PFL), only 4 occur in the lower part of borehole KFM06A /Rouhiainen and Sokolnicki 2005/. The hydraulic transmissivity of the 5 m borehole length intervals is about 2×10^{-9} m^2/s at 620 m and 650 m, 3×10^{-6} m^2/s at 740 m and 3×10^{-7} m^2/s at 666 m. Below 770 m borehole length in fracture domain FFM06 no more transmissive fractures could be detected.

In borehole KFM08C open fractures are especially abundant in the tectonised and/or hydrothermally altered (episyenite) intervals at 161–191 m, 230–250 m, 419–542 m, 673–705 m, 829–832 m, and 946–949 m borehole length. In spite of the intense alteration, the differential flow logging (PFL) revealed only 21 flowing fractures in borehole KFM08C /Väisäsvaara et al. 2006b/. About half of these water-conducting fractures occur between 100–300 m borehole length (fracture domain FFM01) with a low hydraulic transmissivity ranging from 10^{-9} to 10^{-8} m^2/s. The remaining transmissive fractures (up to 10^{-7} m^2/s) are concentrated in the strongly altered zone, which includes the episyenite between about 450 m and 530 m along borehole (deformation zone NNE2312, cf. Figure 2-3). The deepest water-conducting fracture was observed at 683 m borehole length in deformation zone NNE2525 with a hydraulic transmissivity of 6.6×10^{-8} m^2/s. The frequency and depth distribution of water-conducting fractures in borehole KFM08C is thus similar to borehole KFM01D.

In borehole KFM09B the interval from 568.92–573.45 borehole length (fracture domain FFM01 adjacent to deformation zone ENE2325B, cf. Figure 2-3) considered for porewater sampling comprises porous episyenitic rock that exhibits selective quartz dissolution and is similar to the episyenite at 455 m borehole length observed in borehole KFM08C (see above). This interval has a high frequency of open fractures (approx. 10 fractures per metre /Petersson et al. 2006c/) with a hydraulic transmissivity of 2.4×10^{-8} m^2/s and 4.3×10^{-8} m^2/s within the 5 m borehole length intervals from 564.5–569.5 and 569.5–574.5 m, respectively, and as obtained from injection tests (PSS, /Gustavsson et al. 2006/). In the adjacent intact metagranite the hydraulic transmissivity immediately drops to values around 2×10^{-10} m^2/s.

2.2.2 Boreholes in the hanging wall bedrock *sensu lato*

In the hanging wall bedrock s.l., borehole KFM02B intersects deformation zone ZFMA2 at about 411–431 m borehole length (408–433 m depth) and deformation zone ZFMF1 at 462–512 m (467–511m depth; Figures 2-2 and 2-3). The interval between these intersections and also the bedrock at greater depth belong to fracture domain FFM01. In the intervals between 462–473 m and 485–512 m in ZFMF1, distinct high frequencies of open fractures and crushed zones are observed (Figure 2-4). Based on these observations, the sample intervals for porewater samples were reduced from 470 m downwards and a continuous profile of porewater samples was collected starting at 512 m borehole length in fracture domain FFM01, which at this depth is still highly affected by deformation zone ZFMF1. Unfortunately, this was already about 10 m distant from the water-conducting zone initially planned, as shown later by the differential flow logging, and underlines the difficulty of accurately predicting the intersection depths of deformation zones prior to drilling.

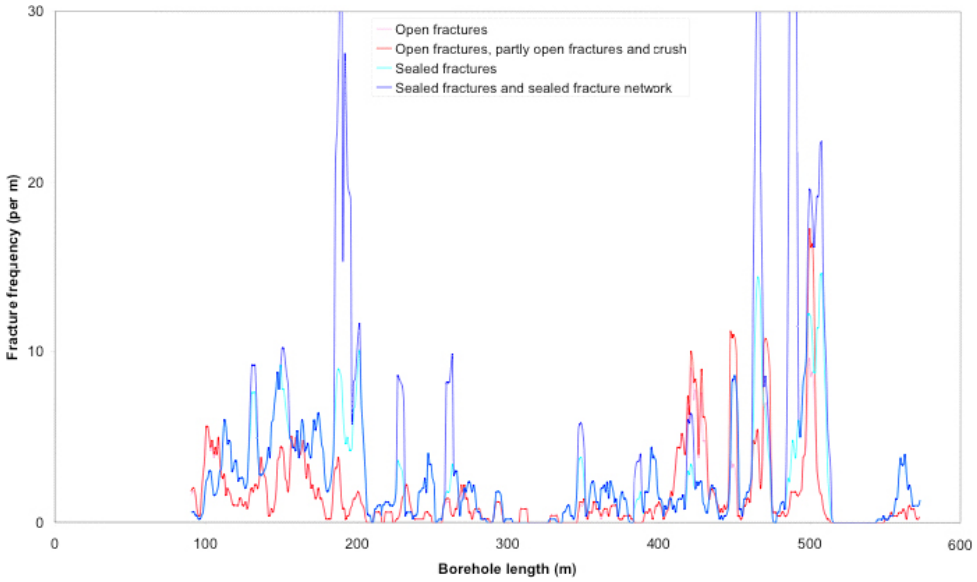

Figure 2-4. *Borehole KFM02B: Fracture frequency as a function of borehole length and expressed as a moving average with a 5 m window and 1 m steps (from /Carlsten et al. 2007/). Note the distinct high frequency of open fractures between about 100–200 m and 400–500 m borehole length, the latter representing deformation zones ZFMF1 and ZFMA2.*

From differential flow logging (PFL) of borehole KFM02B, a high frequency of highly transmissive fractures (up to 10^{-5} m^2/s) are observed between 86–126 m and 411–431 m borehole length /Väisäsvaara and Pöllänen 2007/. High transmissivities of more than 10^{-5} m^2/s were also observed in the highly deformed zones between 461–473 m and 485–512 m, but here mainly restricted to discrete inflow points at 470–471 m and 500–501 m borehole lengths. Differential flow logging was concluded at 568 m borehole length without identifying the inflow points between 558–569 m borehole length, which correspond to the first section drilled with spiked drilling fluid. Neither geological nor hydrological borehole logging is available for the last 6 m of the borehole.

In borehole KFM06A the uppermost 340 m (400 m borehole length) are highly fractured and the frequency of open fractures shows similarities to borehole KFM02B. The frequency of open fractures is about 1.1 fracture per metre and maximum apertures can reach up to 7 mm /Petersson et al. 2005/. Of the 99 open fractures that provided a measurable groundwater flow during the differential flow logging (PFL) of 5 m intervals, 95 fractures occur in the upper part of borehole KFM06A /Rouhiainen and Sokolnicki 2005/ and are related to the geologically defined steeply dipping deformation zones ENE0060B and ENE0060A (/Olofsson et al. 2007/, cf. Figure 2-3). The highest transmissivity (1.9×10^{-5} m^2/s) was detected in a fracture at 130.3 m borehole length. Highly conductive fractures with a transmissivity between about 10^{-5} to 10^{-6} m^2/s, associated with geologically defined steeply dipping deformation zones /Olofsson et al. 2007/, were also found at 181.2 m, 218.2 m, 238.0 m and 269.3 m borehole length. Below about 360 m borehole length the transmissivity of the 5 m intervals drops to values below 10^{-7} m^2/s and to less than 10^{-9} m^2/s below about 400 m borehole length.

3 Sampling strategy and data acquisition

Porewater residing in the rock matrix cannot be sampled by conventional groundwater sampling techniques and needs to be characterised by indirect extraction techniques applied to drillcore material. Such indirect techniques present several challenges concerning drilling and sampling on site and the experimental and analytical procedures conducted in the laboratory on the selected drillcore material. A detailed description of the applied procedures and first evaluation of potential perturbing effects (e.g. different sources for solutes in experiment solutions, desaturation and stress release of rock samples etc) can be found in /Waber and Smellie 2006, 2008/. A quantitative description of possible effects induced by the drilling process and stress release in particular is given in Chapter 4 of this report.

The success of porewater investigations relies on obtaining the original freshly drilled saturated rock core material from boreholes and immediate on-site conditioning of such material within minutes after drillcore recovery. This requires a concerted effort between the teams on the drill site and in the laboratory, including immediate sample preservation on site, rapid transport of the sample to the laboratory and sample preparation for the individual experiments. In addition, rather large sized core samples are required due to the low porewater content and to minimise possible artefacts induced from the time of drilling to the time of analysis. Finally, there is also the great difficulty attached to predicting the location and orientation of a water-conducting fracture in a future borehole. Therefore, the porewater investigations initially aimed to characterise the composition of porewater that resides in as large as possible non-fractured and homogeneous rock portions. In these cases, core samples have been collected at regular intervals of about 50 metres along complete core lengths at least 5 metres from the nearest open fracture visible in the drillcore. Only at a later stage in the programme an attempt has been conducted to also sample a fracture profile, i.e. samples collected continuously along a profile extending from a water-conducting zone into the undisturbed host rock matrix.

For legibility reasons, the samples in this report are labelled with a subsequent numbering with depth using the borehole name as prefix (Table A-1); similar labelling was used for the laboratory studies. The conversion of this sample description to the SKB sample number is given in Table A-1. The complete sets of experimental data produced on porewater samples from the different boreholes can be found in /Waber and Smellie 2005, 2007, 2009/.

In order to differentiate generally between an approximate borehole length or borehole elevation, and more specifically when designating accurately a depth interval or sample location, the following terminology is used:

- A specific depth interval is labelled as –415 to –445 m, i.e. elevation between –415 to –445 m.a.s.l (metres above sea level).
- An approximate depth or depth interval is labelled ‘about or approximately 400 m depth’ or ‘about or approximately 400 to 600 m depth’.
- Any location related to borehole length is signified specifically as ‘685 m borehole length’, or generally as ‘about or approximately 700 m borehole length’ or ‘about or approximately 500 to 700 m borehole length’.
- Repository depth refers to –400 to –700 m elevation.

3.1 Porewater sampling

From boreholes KFM01D, KFM02B, KFM06A and KFM08C drillcore sections of about 25–45 cm in length were taken at regular depth intervals of approximately 50 m from homogeneous, non-fractured bedrock volumes at least 5 metres away from any water-conducting fractures. In addition, sections were taken from fracture zones or along pre-defined depth profiles away from a water-conducting zone in boreholes KFM02B and KFM09B. The depth along the borehole and the elevation, the latter corresponding to the sample reference depth corrected for borehole inclination and altitude, of the porewater samples are given in Table A-1. This table contains in addition information about the lithology of the samples and their relation to water-conducting fractures.

In borehole KFM02B at about 470 m the sampling intervals were reduced based on the observation of the highly tectonised zone between 462–473 m in deformation zone ZFMF1. A continuous profile of porewater samples, the so-called fracture profile, was collected starting at 512 m borehole length just below the tectonised zone from 485–512 m in deformation zone ZFMF1 with its high frequency of open fractures (cf. Figure 2-4). The continuously sampled profile extended to about 517 m borehole length. Further downwards the sampling intervals were again increased to a few metres and this continued to the end of the borehole. As later shown by the differential flow logging, the fracture profile unfortunately started at a depth of about 12 m beyond the correct position which coincided with the water-conducting fracture of interest, i.e. a fracture with a transmissivity of more than 10^{-5} m^2/s /Väisäsvaara and Pöllänen 2007/. However, fortunately some core sections were taken from this 12 m borehole length as part of the overall systematic sampling protocol.

A profile with increased porewater sample frequency was also collected in borehole KFM09B. The purpose of this sampling was to obtain information about the fracture water-porewater interaction between a highly porous episyenite zone that exhibits selective quartz dissolution and the unaltered and non-fractured host bedrock. A total of 8 samples were collected for porewater characterisation at increasing intervals from decimetres to metres from the episyenite zone downwards along the borehole. The first sample, KFM09B-1, taken at the contact of the episyenite to the metagranite, is strongly altered with bleached quartz and plagioclase and reddish-coloured K-feldspar. Two open and two closed fissures with a green infill steeply cut the drillcore along the borehole axis. All other samples consist of medium-grained, equigranular metagranite that are free of any fractures, but display a distinct foliation. The metagranite is mainly grey in colour with reddish-coloured K-feldspar due to hematite pigmentation.

At the Forsmark investigation site, the effects of stress release and drilling fluid contamination on the drillcore have been quantitatively investigated for the first time in a deep borehole drilled into crystalline rock. This was conducted in borehole KFM02B at a borehole length of 560–574 m (–544 m to –558 m elevation) towards the end of the borehole where drilling was performed with a spiked drilling fluid. The five samples collected were treated in exactly the same way as all other porewater samples. In addition, however, the added inorganic tracer was monitored during out-diffusion (see Chapter 4).

To preserve the original water saturated state of the rock material sampled and to minimise potential perturbing effects induced by exposure of the rock sample to air, the drillcore samples were immediately gently cleaned using a dry towel following drilling and selection, then wrapped into two heavy-duty PVC bags and finally sealed in plastic coated aluminium-foil. All three layers were repeatedly flushed with nitrogen, evacuated and heat sealed. The time for the sample selection and packing was minimised to less than 10–15 minutes after core recovery. The packed samples were then air freighted to the laboratory in Bern where they were immediately stored at 4°C in a cool room and prepared for the various measurements and experiments within about 24 hours after arrival.

3.2 Porewater data

Information about the chemical and isotopic composition of porewater in the low-permeability rock matrix was obtained by combining the data of different porewater extraction experiments, different porosity measurements and geochemical modelling.

Following arrival at the laboratory, the core sections were unpacked, wrapped in parafilm™ to minimise evaporation, and cut by dry sawing for subsamples to be used for out-diffusion experiments, diffusive equilibration technique for water isotopes (diffusive isotope exchange), determination of the water content, grain density, and mineralogical investigations where applicable.

3.2.1 Water content and porosity

The water content of the rock samples was determined by two largely independent methods. It should be noted that reliable results for the water content and the water-loss porosity are only obtained if the measurements are conducted on originally saturated core material, i.e. no evaporation of porewater and/or re-saturation of the rock sample has occurred.

The first method is the commonly used gravimetric measurement of the water loss from the saturated to the desaturated state of a rock sample. Here the water content by drying, WC_{Drying}, has been derived by heating the samples at 105°C until the onset of stable weight conditions (± 0.002 g). If possible, three subsamples consisting of an intact piece of core and broken core material with a mass between about 100 g and 500 g were dried to stable weight conditions to account for effects of textural heterogeneity of the rocks and artefacts, which may have been induced by drilling and/or possible stress release. Depending on the sample mass, the drying process lasted up to 20 weeks for the low permeable rock samples from the Forsmark area. For most of the samples, the core section used in the out-diffusion experiment with a mass of about 1,000 g was also dried to stable weight conditions, something which could take up to 9 months.

In the second method, the water content, $WC_{IsoExch}$, was derived by the diffusive equilibration technique for water isotopes (see below). As for the isotopic composition, the relative error of $WC_{IsoExch}$ could be reduced from about 5–10% in the early stages to less than 3% in the final stages of the Forsmark site investigation programme.

The water-loss porosity or connected porosity, Φ_{WL}, was calculated from the water content derived by either of the above methods and known grain density, ρ_{grain}, according to:

$$\Phi_{WL} = \frac{WC_{wet} \cdot \rho_{grain}}{WC_{wet} \cdot \rho_{grain} + (1 - WC_{wet}) \cdot \rho_{water}} \qquad \text{(Equation 3-1)}$$

where WC_{wet} is the water content based on the wet weight of the sample, ρ_{grain} is the grain density and ρ_{water} is the density of the porewater.

Alternatively, the bulk wet density, $\rho_{bulk,\,wet}$, was determined from the volume and mass of large scale samples used for the out-diffusion experiments /Waber and Smellie, 2005, 2007, 2009/. For these samples Φ_{WL} is approximated according to:

$$\Phi_{WL} = WC_{wet} \cdot \frac{\rho_{bulk,\,wet}}{\rho_{water}} \qquad \text{(Equation 3-2)}$$

3.2.2 Out-diffusion experiments

Experimental Set-up

Out-diffusion experiments were performed on complete core samples of about 120 mm to 190 mm in length by immersion into ultra-pure water (about 70–80 ml and 100–110 ml depending on core length). To accelerate the out-diffusion, the vapour tight PVC containers containing the core samples were placed into a constant temperature (45°C) water bath that was gently rotated throughout the experiment to avoid chemical stratification of the experiment solution. Blank experiments were run with each batch of prepared drillcore samples. The weight of the core sample, the experiment container, and the artificial test water used was measured before and after the experiment to ensure that no loss of test water occurred during the entire experiment. Weighing of the core before and after the experiment gives additional valuable information about the saturation state of the core at the beginning of the experiment.

After equilibrium with respect to chloride was achieved (see below), the core was removed from the container and the experiment solution was immediately analysed for pH and alkalinity (by titration). The remaining solution was split into different aliquots for chemical and isotopic analyses. Major cations and anions were analysed by ion-chromatography with a relative error of ±5% (2σ) based on multiple measurements of standard solutions. Dissolved silicon was analysed by photometry with a relative error of ±5% (2σ). In all experiments batches, cation and anion concentrations of the final solution of the blank experiments were below or at detection limit, which is 0.1 mg/L for Cl^-. On aliquots of some selected samples, chlorine ($\delta^{37}Cl$) and strontium isotope ($^{87}Sr/^{86}Sr$) analyses were performed by mass spectrometry at the University of Waterloo and University of Bern, respectively.

The complete data sets for the individual boreholes are given in /Waber and Smellie, 2005, 2007, 2009/.

Equilibrium control of the out-diffusion experiment

The out-diffusion experiments were run under closed system conditions. The control of the mass flux of chloride and, towards the end of the experiment, the equilibrium control of the diffusive exchange occurred by taking small samples (0.5 mL) of the experiment solution at regular intervals and analysing their anion content. The experiments were terminated and the supernatant solution removed for chemical and isotope analyses well after the chloride concentrations had reached a plateau as a function of time, i.e. when equilibrium conditions were reached. Modelling of these time series gave indications about the marginal zone in the drillcore sample disturbed by the drilling process (drilling disturbed zone, DDZ) and stress release and possible contamination by drilling fluid induced by such disturbance of the drillcore material. It further allowed an estimation of the chloride pore diffusion coefficient (Chapter 5). The experiments run at 45°C were terminated after about 90–110 days and those run at 20°C after about 190 days. The extracted 0.5 mL time-series samples were analysed using specially designed ion-chromatographic equipment. The analytical error of these determinations is about ±10% (2σ) based on multiple measurements of the standard solutions of equally small volumes.

Conversion of final solution concentrations to porewater concentrations

Porewater concentrations can be converted from the chloride concentration of the final experiment solution by mass balance calculations given that equilibrium conditions in the out-diffusion experiment are achieved. At equilibrium, the chloride concentration in the connected porosity of the rock sample will be equal to that of the experiment solution. With knowledge of the mass of porewater in the rock sample, the chloride concentration of the porewater can be calculated according to:

$$C_{PW} = \frac{\left(M_{PW} + M_{TEWi} - \sum^{n} M_S\right) \cdot C_{TEW\infty} - (M_{TEWi} \cdot C_{TEWi}) + \sum^{n} M_S \cdot C_S}{M_{PW}} \qquad \text{(Equation 3-3)}$$

For the analysis of the time series with a model neglecting the removal of solution (cf. Chapter 5), the measured concentrations were approximately corrected according to:

$$C_{equil,corrected} = \frac{C_{TW_\infty} \cdot \left(M_{TWi} - \sum^{n} M_S\right) + \sum^{n} M_S C_S}{M_{TW_i}} \qquad \text{(Equation 3-4)}$$

where C = concentration, M = mass, n = number of samples and the subscripts PW = porewater, TEW = experiment solution, S = small-sized sample taken for chloride time-series, i = at beginning of experiment, and ∞ = at end of experiment.

The last term in (Equation 3-3), $\Sigma M_S \cdot C_S$, describes the amount of chloride removed from the initial experiment solution by the chloride time-series samples. The final measured concentration of chloride in the experiment solution, $C_{TEW\infty}$, is corrected for the mass of solution removed by the chloride time-series samples from the initial mass of the experiment solution, M_{TEWi}, in order to obtain the Cl^- concentration in the experiment solution at steady state, $C_{equil.corrected}$ (Equation 3-4). A correction for chloride in the initial experiment solution ($M_{TEWi} \cdot C_{TEWi}$) is necessary if this solution is not entirely free of chloride.

The unit of porewater concentrations is given as mg/kg_{H2O} (and not mg/L) because it is derived on a mass basis rather than a volumetric basis. This is because the density of the porewater is not known beforehand. In reality and within the overall uncertainty band, the difference between mg/kg_{H2O} and mg/L becomes only important at an ionic strength of the calculated porewater above that of sea water (~0.7 M) corresponding to a total mineralisation of ~35 g/L.

3.2.3 Diffusive exchange technique for water isotopes

The stable isotope composition of the porewater was determined by the diffusive isotope exchange technique that was originally developed for argillaceous rocks /Rogge 1997, Rübel 2000/ and later adapted to crystalline rocks /Waber and Smellie 2005, 2006, 2008/. This method is based on the premise that the known water isotope composition of test water will equilibrate with the unknown composition of porewater in a rock sample using the gas phase as a diaphragm in a vapour-tight container. For each rock sample, two equilibration experiments with test water of different isotopic composition are conducted in a vapour-tight glass container. After complete equilibration (commonly about 20–30 days, depending on the size and hydraulic properties of the rock samples), the two test water are analysed by conventional ion-ratio mass spectrometry with the results being reported relative to the VSMOW standard with a precision of ±0.15‰ for $\delta^{18}O$ and ±1.5‰ for $\delta^{2}H$.

The water content of a rock sample and the stable isotope composition of its porewater are calculated from mass balance relationship of the experiments according to:

$$M_{PW} \cdot C_{PW}\big|_{t=0} + M_{TW} \cdot C_{TW}\big|_{t=0} = \left(M_{PW} + M_{TW}\right) \cdot C_{TW}\big|_{t=\infty} \qquad \text{(Equation 3-5)}$$

where M = mass, C = isotope ratio, PW = porewater, TW = test water, and the concentrations on the left side of the equation are prior to equilibration (t = 0), while the concentration on the right side is after equilibration is achieved (t = ∞) in the experiment.

Each equilibration experiment reveals two independent equations of the type (Equation 3-5) for $\delta^{18}O$ and $\delta^{2}H$. Conducting two experiments with different test water and thus obtaining four equations allows the calculation of the three unknowns, which are the porewater mass and the $\delta^{18}O$ and $\delta^{2}H$ of the porewater.

By applying Gauss' law of error propagation, it can be shown that the error of the isotope determination depends mainly on the mass ratio of test water to porewater and on the difference in isotopic composition between the two water types. While the latter is easy to achieve, the optimisation of the mass ratio of test water to porewater is more difficult in crystalline rocks with water contents of generally below 0.2 wt.% VSMOW. During the course of the Forsmark site investigation programme, the propagated error of the isotope diffusive-exchange technique could be reduced from about ± 2.6‰ for $\delta^{18}O$ and ±26‰ VSMOW for $\delta^{2}H$ in the early stages (borehole KFM06A) to about ± 1.3‰ VSMOW for $\delta^{18}O$ and ± 12‰ VSMOW for $\delta^{2}H$ in the final stages (borehole KFM02B) by optimising experimental and analytical procedures.

4 Evaluation of perturbations by drilling and stress release

A rock sample brought to the surface from great depth will tend to release the stress it is exposed to under *in situ* conditions. The degree of such effects on the rock's transport properties depends on the local stress field to which the rock sample was exposed under *in situ* conditions (and thus the depth of the sample) and the rock type (e.g. isotropic vs. anisotropic texture). Similarly, the drilling process might disrupt the original rock texture and create additional pore space in the outermost zone of a drillcore. Both these processes result in an increase of the original porosity and permeability that are present under *in situ* conditions. During core drilling such induced perturbations of the rock texture might potentially favour a penetration of drilling fluid during the drilling process and thus a contamination of the originally present porewater.

Effects of stress release are often used to explain differences in experimentally derived porosity and diffusion coefficients of crystalline rocks. Laboratory through-diffusion experiments to derive diffusion coefficients of crystalline rocks have tended to focus on thin (a few cm) rock slices to reduce experimental time (e.g. /Skagius and Neretnieks 1986, Johansson et al. 1997, Vilks et al. 2003/. However, when using drillcore material, it became obvious that there was a large spread of diffusivity values measured in samples taken close together from the same drillcore specimen and also when using samples of different thicknesses (cf. e.g. /Ohlsson and Neretnieks 1995, Liu et al. 2006, Selnert et al. 2008/). Such discrepancies have often been attributed to stress release effects incurred when removing the drillcore from depth resulting in an enhanced porosity via an increase in open-pore connections (e.g. /Schild et al. 2001, Ota et al. 2003, Tullborg and Larson 2006/). Therefore, small and thin laboratory samples might be expected to result in higher diffusivities than large and thick samples.

Such observations appear to be in contrast to petrophysical modelling approaches. For example, in the Kola superdeep borehole stress release effects calculated on the basis of the elastic moduli of the rock forming minerals in biotite gneisses appear to be negligible down to a depth of 800–1,000 m depth in this area /Gorbatsevich 2003/.

Nevertheless, the accuracy and strength of porewater investigations might be affected by such perturbing effects and their influence on the performed porewater extraction experiments needs to be understood and quantified. This was accomplished by performing two drilling campaigns using drilling fluid traced with different combinations of iodide, bromide and uranine. Information about possible penetration of drilling fluid into the drillcore – and thus a perturbation of the *in situ* porewater – was then obtained by analysing the out-diffusion experimental solutions for the tracer concentration and applying transport model calculations.

The first such experiments were conducted at the Äspö HRL at the 420 m level by drilling a new borehole horizontally from the tunnel wall into the Äspö diorite rock matrix. This tunnel had been excavated in 1995 and it can be assumed that the rock in the immediate vicinity is stress released and re-equilibrated with respect to porewater. This experiment therefore aimed to investigate the potential influence of drilling fluid during drilling in a rock no longer affected by stress release, but only by the disturbed zone induced by the drilling process itself.

The second experiment was conducted in the Forsmark borehole KFM02B at 560–574 m borehole length (–544 m to –558 m elevation). The core obtained from this depth consists of medium-grained metamorphic granodiorite and was affected by stress release as well as the drilling process.

4.1 Drilling disturbed zone: Borehole KA3386A06, Äspö HRL

Effects of the drilling process and related potential contamination of the drillcore by drilling fluid were investigated in borehole KA3386A06 drilled at the Äspö HRL at the 420 m level in March 2005. This borehole was drilled horizontally from the tunnel wall to a depth of about 5 m into Äspö diorite and with a core diameter of 61.7 mm.

Figure 4-1 shows schematically the location of the porewater samples investigated from this borehole. Drilling was conducted with a drilling fluid traced with iodide, bromide and uranine for the first about 2.5 m where a strongly conducting fracture was encountered. Behind this fracture, drilling continued with uranine as the only tracer. On each side of the water-conducting fracture, two samples were collected for porewater investigations. On-site sample conditioning, storage, transport and laboratory treatment of the samples was exactly the same as applied to the porewater samples collected from the SKB site investigation deep boreholes.

The four samples used for out-diffusion experiments consisted of reddish-coloured, hydrothermally altered Äspö diorite. Thus, these altered samples have water contents and a water-content (connected) porosity (Table 4-1) that is in the upper half of the range of other Äspö diorite samples (cf. /Smellie et al. 2003/).

The concentration of tracers Br^- and I^- used in the drilling fluid is given in Table 4-2. The composition of the fracture groundwater encountered at about 2.5 m in the rock differs from that of the drilling fluid having a much higher Cl^- content and much lower Br^- and I^- contents which resulted in greatly different Br/Cl and I/Cl ratios (Table 4-2). Monitoring of the drilling fluid showed an increase in Cl^- content and dilution of the tracer concentrations during drilling of the A-2 sample behind the

Table 4-1. Average water content by drying at 105°C and water-content porosity of rock samples from borehole KA3386A06, Äspö HRL.

Sample No	Number of samples	Water Content (wt.%)	Error (1 σ) (wt.%)	WC-Porosity (Vol.%)	Error (1 σ) (Vol.%)
A-1	2	0.281	0.060	0.76	0.16
A-2	2	0.287	0.049	0.77	0.13
A-3	2	0.247	0.008	0.66	0.02
A-4	2	0.211	0.013	0.57	0.03

Table 4-2. Anion composition of drilling fluid and fracture groundwater of borehole KA3386A06, Äspö HRL.

Sample	Water Type	Cl^- (mg/L)	Br^- (mg/L)	I^- (mg/L)	Br/Cl (mg/mg)	I/Cl (mg/mg)	Br/I (mg/mg)
SKB006420	Drilling Fluid	78	1,280	832	16.41	10.67	1.54
SKB006423	A-2 Drilling Fluid	1,567	1,070	688	0.68	0.44	1.56
SKB006431	Fracture water	6,609	79	< 1	0.012	< 0.0002	< 0.01

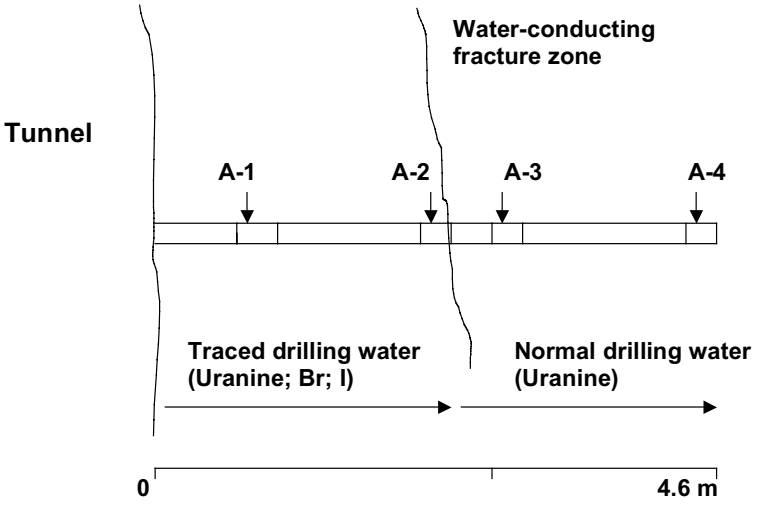

Figure 4-1. *Location of porewater samples and type of drilling fluid used in the borehole at the Äspö HRL.*

water-conducting fracture, indicating that the drilling fluid became increasingly mixed with fracture groundwater. The composition of the returned drilling fluid during drilling is also given in Table 4-2 ("A-2 Drilling Fluid"). It seems plausible that sample A-2 has been mainly exposed to this type of drilling fluid composition. For samples A-3 and A-4 the exact mixing proportions are less well established as they were affected by a largely unknown, but lower, tracer concentration. They are thus less suited for the quantitative investigation of possible drilling-fluid contamination. Nevertheless, they can be used for a qualitative judgment.

Thus, if the drilling process would lead to a contamination, the porewater would have been affected in the first sample, A-1, by drilling fluid alone, by a large proportion of drilling fluid with some fracture water in sample A-2, and by an unknown mixed drilling fluid–fracture groundwater in samples A-3 and A-4. The expected effects in the experimentally derived porewater composition would then be a dilution of Cl^- and enrichment in Br^- and I^- in the first two samples and an enrichment of all three compounds, though less pronounced for Br^- and I^-, in the last two samples because of the high Cl^-, but low Br^- and I^- fracture groundwater relative to the drilling fluid. As can be seen from Table 4-3, no such behaviour is observed in the four samples. In the contrary, the first sample (A-1) has the overall highest Cl^-, Br^- and I^- concentrations in the porewater, while the other samples have similar porewater anion concentrations. It should further be noted that the concentrations of Br^- and I^- are very low in the experiment solutions with the I^- concentrations being hardly above the detection limit of the applied ion-chromatographic method (Table 4-3). This induces an additional uncertainty on the calculated porewater concentrations without changing the fact that these concentrations are low.

Although the dilution of the possibly contaminated porewater in the experiment was rather high with a test water to porewater ratio between 23 and 33 in the out-diffusion experiments, these very low concentrations (considering the high tracer concentrations) already indicate that contamination with drilling fluid is only minor if at all resolvable by the applied techniques. The fact that sample A-1 collected close to the tunnel wall has significantly higher concentrations of the conservative anions appears to be due to an enrichment of these compounds due to the evaporation induced in the excavation disturbed zone (EDZ) at the tunnel surface.

Table 4-3. Anion concentrations in out-diffusion experiment solutions and calculated porewater concentrations of the drillcore samples from borehole KA3386A06, Äspö HRL.

Porewater Rock Type	Units	A-1 Äspö diorite	A-2 Äspö diorite	A-3 Äspö diorite	A-4 Äspö diorite
Depth below surface	m	420	420	420	420
Mass Rock	g	1,468.600	1,472.100	1,448.200	1,439.400
Vol. Porewater	cm^3	4.13	4.23	3.58	3.03
Vol. Experiment Water	cm^3	100.60	99.90	102.47	102.47
Anions in Out-Diffusion Experiment Solution					
Chloride (Cl^-)	mg/L	165.6	120.4	102.7	94.6
Bromide (Br^-)	mg/L	2.1	1.3	0.9	0.5
Iodide (I^-)	mg/L	0.7	0.2	0.4	< 0.2
Anions Calculated to Porewater Concentrations					
Chloride (Cl^-)	mg/kg $_{H2O}$	4,199	2,966	3,033	3,291
– error	mg/kg $_{H2O}$	705	412	91	187
+ error	mg/kg$_{H2O}$	1,085	579	97	212
Bromide (Br^-)	mg/kg $_{H2O}$	54.3	31.3	27.7	18.2
– error	mg/kg $_{H2O}$	9.1	4.3	0.9	1.0
+ error	mg/kg $_{H2O}$	14.0	6.1	1.0	1.2
Iodide (I^-)	mg/kg $_{H2O}$	17.3	4.4	12.8	< 3.5
– error	mg/kg $_{H2O}$	2.9	0.6	0.4	
+ error	mg/kg $_{H2O}$	4.4	0.9	0.4	
Ion-Ion Ratios					
Br/Cl	mg/mg	0.0129	0.0105	0.0091	0.0055
I/Cl	mg/mg	0.0041	0.0015	0.0042	–
Br/I	mg/mg	3.1	7.1	2.2	–

The ion-ion ratios of Br/Cl and I/Cl also serve as indicators of the presence or absence of contamination of the porewater by drilling fluid. In the traced drilling fluid, these ratios are very high (16.41 and 10.67, respectively; cf. Table 4-2). In the porewater, however, these ratios are 3-4 orders of magnitude lower (Table 4-3) and well comparable with fracture groundwater of the Äspö HRL. Based on simple mixing calculations, it can be shown that contamination by drilling fluid of 1% would yield Br/Cl, I/Cl and Br/Cl ratios in the experiment solutions that are much higher than those observed. For example, in the experiment solution of sample A-2, contamination of 1% by the "A-2 drilling fluid" (notably already modified by fracture water) would result in a Br/Cl ratio of 0.0141, a I/Cl ratio of 0.0038 and a Br/Cl ratio of 3.7 compared to the observed ratios of 0.0105, 0.0015, and 7.1, respectively.

Further support for low or negligible contamination comes from the evolution of the ion-ion ratios in the out-diffusion experiment solutions as a function of time. Contamination of the porewater with drilling fluid would be most pronounced in the outermost pore space of the core rim and decrease towards the centre of the core. In the out-diffusion experiment solution, this would result in Br/Cl and I/Cl ratios similar to that of the drilling fluid in the very first hours. They might then be expected to decrease and become more similar to the actual porewater in the following days and towards the end of the experiment, assuming equal transport velocities for the three anions. As shown in Figure 4-2, the measured ion-ion ratios in the experiment solutions are, however, constant over the entire out-diffusion time with only small variations barely exceeding the analytical uncertainty occurring in the first 4-6 days of the experiments. Together with the above mass balance arguments and the 3-4 orders of magnitude lower ratios in the experiment solution (or porewater, respectively) compared to those in the drilling fluid, this indicates that the drilling fluid contamination of porewater induced by the drilling disturbed zone is low, probably below 1%.

The evolution of the anion concentrations during potential contamination by the drilling process and the following out-diffusion experiment in the laboratory have been investigated for sample A-2 using FLOTRAN /Lichtner 2007/, a reactive transport model code capable of simulating 2-D radial diffusion with heterogeneous transport domains. The evolution with time of the measured anion concentrations in the out-diffusion experiment solution of sample A-2 is shown in Figure 4-3. These solutes present in the external solution originate from the porewater in the undisturbed rock, as well as from the contamination by drilling fluid, if present. For the added tracers Br and I, the latter contribution would be positive (i.e. addition to the porewater) while for Cl this could be expected to be negative (i.e. dilution of the porewater) because of the low Cl concentration in the drilling fluid (Table 4-2).

The concept behind the model exercises is also shown in Figure 4-3. In a first step it was evaluated whether the measured data can be adequately described using homogenous transport parameters over the entire drillcore. Although barely exceeding the analytical uncertainty, the slight change in slope of the concentration increase and the small variations of the ion-ion ratios in the first 3-6 days (cf. Figures 4-2 and 4-3) might indeed suggest different transport properties in a thin rim compared to the bulk of the core. The simulations showed, however, that the evolution of the concentrations for all anions can be adequately approximated using a homogeneous pore diffusion coefficient, D_p, of 1×10^{-10} m^2/s at the experiment temperature of 45°C and neglecting any contamination (not shown). Such a value of D_p is similar to the D_p values obtained for Ävrö granite (average of $1.18\times10^{-10} \pm 5.40\times10^{-11}$ m^2/s at 45°C) and quartz monzodiorite (average of $1.68\times10^{-10} \pm 5.40\times10^{-10}$ m^2/s at 45°C) from the deep boreholes of the Laxemar subarea /Waber et al. 2009/.

In the second step, the effect of contamination by drilling fluid was evaluated. Sample A-2 had been in contact with the traced drilling fluid for about 2 hours. The left-side panels in Figure 4-4 show profiles of the progressive change of the anion concentrations during the diffusive exchange with the drilling fluid in the borehole and the following out-diffusion into the de-ionised test water during the laboratory experiment as a function of time. In these simulations the initial porewater concentrations of Cl^-, Br^-, and I^- were calculated according to (Equation 3) and assuming that the possible contamination is neither large enough to significantly modify the initial concentration in the centre of the core nor the final concentrations of out-diffused anions (i.e. the concentrations in the final experiment solution). Both of these assumptions are justified considering the transport properties of the rock relative to the contact time with drilling fluid and the expected differences in mass and anion concentrations between the porewater and the possible contamination by drilling fluid in the

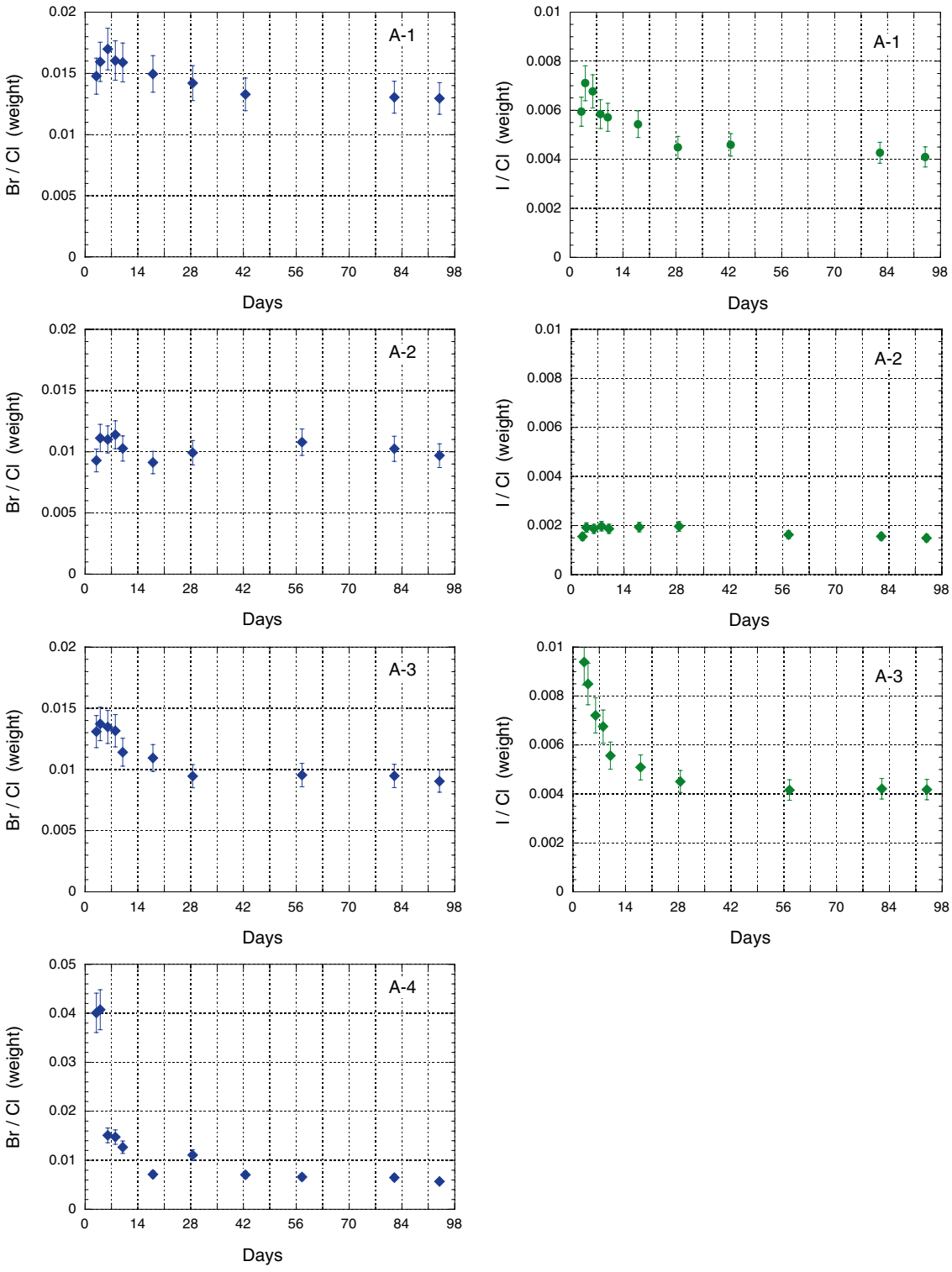

Figure 4-2. *Evolution of the Br/Cl and I/Cl ratios in out-diffusion experiment solutions (sampled in the time-series samples) and as a function of time. The drilling fluid used to drill samples A-1 and A-2 had a Br/Cl ratio of 16.41 and an I/Cl ratio of 10.67. The fracture groundwater that mixed at unknown proportions with the drilling fluid during drilling of samples A-3 and A-4 had ratios of 0.012 and < 0.0002, respectively. Note that dilution with the de-ionised experiment water does not alter the ion-ion ratios and the observed ratios are thus mainly those of the porewater.*

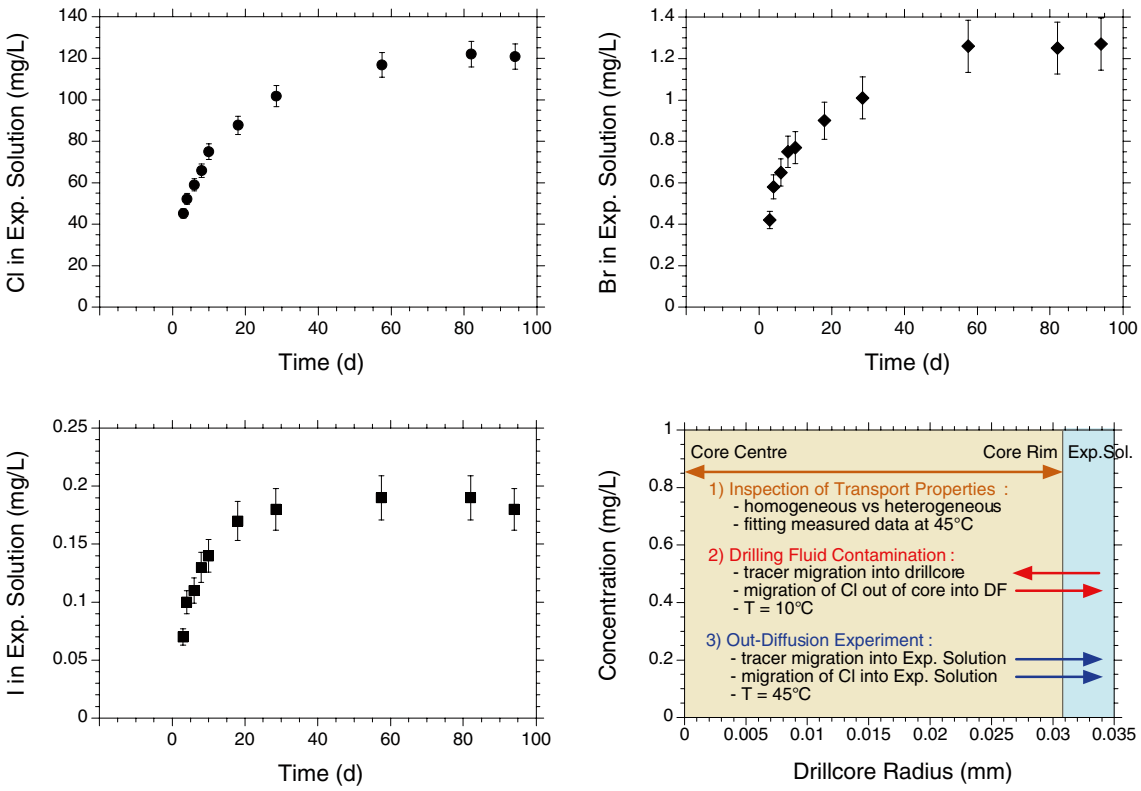

Figure 4-3. *Anion concentrations measured in the out-diffusion experiment as a function of time in small scale time-series samples. The concentrations are corrected according to (Equation 3-3) for the mass and volume removed by these samples from the initial solution. The analytical error is ± 5% for Cl^- and ± 10% for Br^- and I^-. The lower right panel shows the conceptual model used for modelling the observed time-series data (see text).*

newly created pore space. Over a contact time of two hours between the drillcore and drilling fluid, steep concentration gradients would theoretically develop in a contaminated zone of about 2.7 mm in thickness at the outermost rim of the core with a total radius of 30.85 mm (Figure 4-4, left). For Cl^-, contamination would result in a dilution to about half of the initial concentration close to the external side due to the low Cl^- content in the drilling fluid (Table 4-2). In contrast, the concentrations of Br^- and I^- would be increased many times over the initial concentration in the same zone. The extent of this theoretical chemically disturbed zone depends, of course, on the estimated contact time between drilling fluid and porewater (i.e. in this case 2 hours) and the estimated D_p.

Assuming this theoretical chemically disturbed zone also corresponds to reality, the calculated subsequent out-diffusion of the anions should adequately describe the data measured in the out-diffusion experiments. This was evaluated in step 3 of the modelling exercise. The left-side panels of Figure 4-4 also show the evolution of the simulated anion concentration profiles during out-diffusion for various times, whereas the right-hand panels show the behaviour of measured and simulated anion concentrations in the experiment solution during the out-diffusion experiments. It can be seen that the scenario of a 2 hours contact time between drilling fluid and porewater can adequately describe the Cl^- data because of the minor influence of the low Cl drilling fluid on the high Cl porewater. The actual concentration of the tracers Br^- and I^- are, however, grossly overestimated by the calculations. This indicates that either the thickness of the chemically contaminated zone is overestimated due to a too high D_p used in the calculations, or the contact time between the drilling fluid and the core is overestimated. The latter information can be easily obtained and thus seems to be better supported. In general, the overestimation of the I^- and Br^- concentrations just show that the contamination must have been much less than assumed in this scenario.

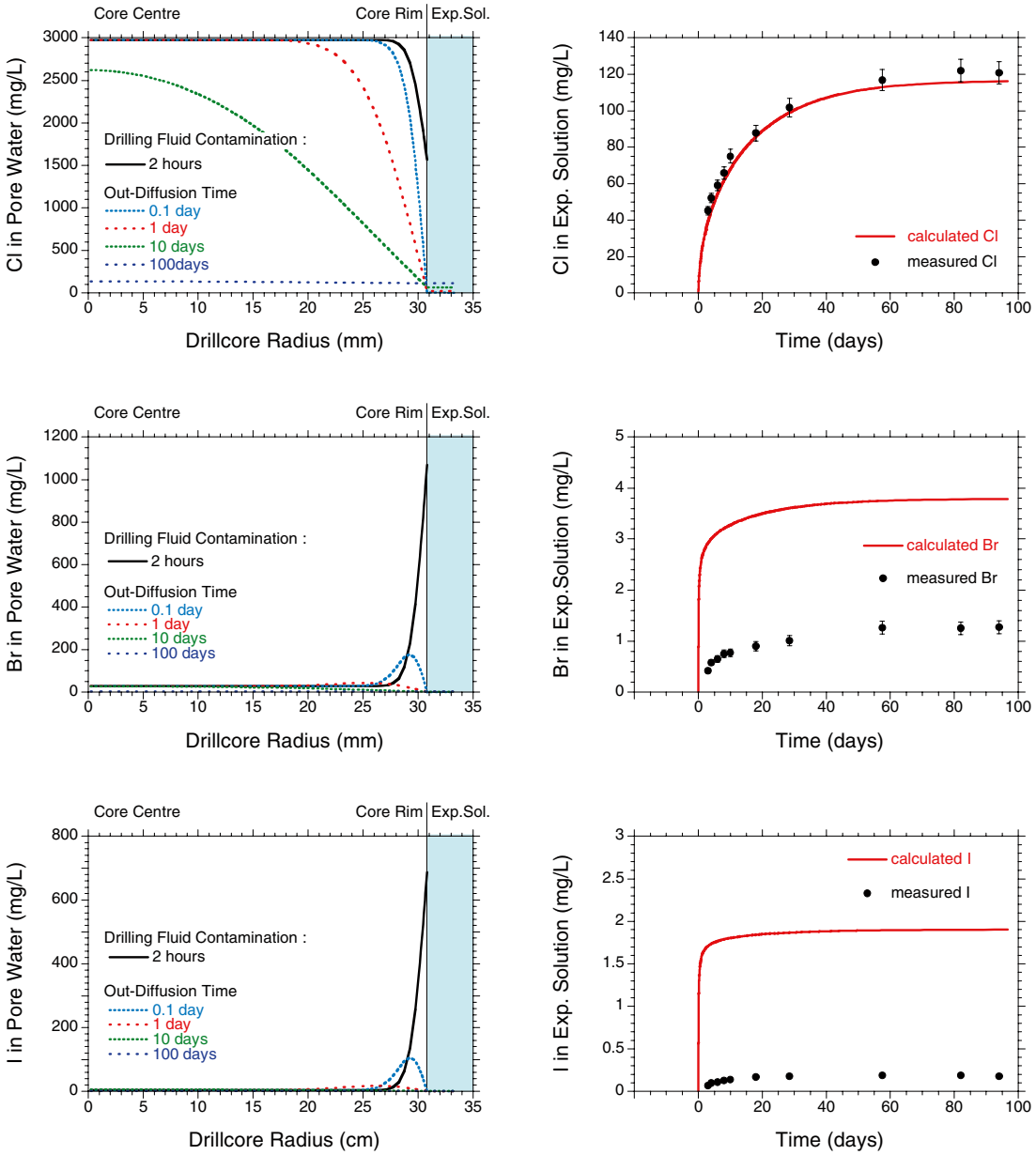

Figure 4-4. *Effect of a 2 hour drilling fluid contamination on porewater anion concentration in the drillcore (left-side panels, black solid lines) and the progressive anion concentrations as a function of time in the following out-diffusion experiment (left-sided panels, dotted coloured lines). For the equilibrium state between porewater and test water after 100 days of out-diffusion time the calculated concentrations of Br^- and I^- grossly overestimate the concentrations measured in the out-diffusion experiment solutions (right-side panels).*

In the next simulation, the data were further evaluated by varying the solute mass originating from the contamination (by varying the contamination time or contamination distance) and the initial anion concentrations in the porewater (Figure 4-5). For the Cl^- concentrations, the initial concentration was kept as in the previous simulations (i.e. calculated from measured data according to (Equation 3-3)) based on the experience gained form the previous simulations (very small or no effect by drilling fluid). Shorter contact times with the drilling fluid result in slightly better fits of the measured Cl^- data compared to a 2 hours contamination. The best fit is, however, attained by zero contamination with drilling fluid (Figure 4-5, upper left). Yet, all simulation results lie within the uncertainty band of the Cl^- data and therefore do not allow a definitive final statement.

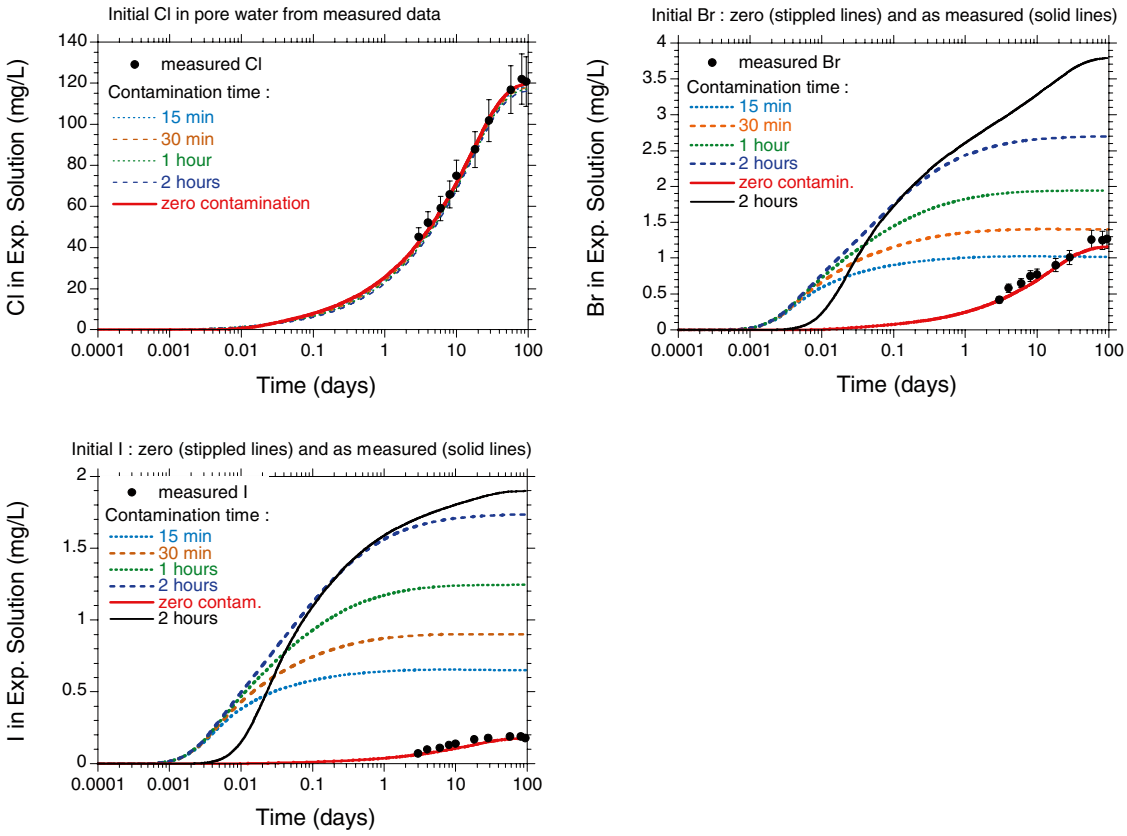

Figure 4-5. *Effect of a drilling-fluid contamination over variable time periods on the anion concentration in the out-diffusion experiment solutions. For the tracers Br^- and I^- the initial concentration before a potential contamination is set to zero (all Br^- and I^- from drilling fluid, dotted lines) and to the porewater concentration as calculated according to (Equation 3-3) (i.e. all Br^- and I^- uniformly distributed in the porewater, solid lines). Note that any contamination by drilling fluid would result in a much earlier breakthrough of Br^- and I^- compared to that measured in the experiment solution and therefore the data can only be fitted with zero contamination.*

Large differences between calculated and measured data are, however, observed for the two tracers Br and I. Thus, the two extreme scenarios were tested which are: a) the calculation of the concentrations assuming that the initial concentration in the porewater is zero, i.e. all Br^- and I^- would stem from the drilling fluid, for different time periods of contamination, and b) for zero contamination, i.e. all Br^- and I^- would stem from the porewater. As shown in Figure 4-5, none of these scenarios can describe the measured data, except for that with zero contamination. Most prominent is the fact that contamination would result in a much earlier breakthrough of Br^- and I^- than observed in the out-diffusion experiments because, in this situation, large amounts of Br^- and I^- would be in the outermost pore space of the drillcore (Figure 4-5).

Based on the above calculations, the drilling fluid contamination has affected the pore volume of a rim sector of the drillcore to a maximum thickness of 0.1 mm. This chemically disturbed zone corresponds to about 0.66% of the total pore volume of the drillcore. Such a low affected pore volume is consistent with the maximum contamination of the porewater by < 1% drilling fluid as calculated from the mass balance of the I^- concentrations. It should be noted, however, that the so derived chemically disturbed zone assumes a homogeneous distribution of the diffusion-accessible pore space. In reality, the mechanically disturbed zone may extend further into the drillcore heterogeneously along grain boundaries and be non-existent where mineral grains form the boundary. The total affected volume will, however, be the same.

The drilling-fluid contamination experiment conducted on a stress-released drillcore from the Äspö HRL thus revealed that:

- Modelling with a homogeneous diffusion coefficient D_p adequately describes the measured data.
- The chemically disturbed zone extends to a maximum of 0.1 mm into the drillcore, corresponding to about 0.66% of the total pore volume; this is consistent with a maximum contamination of < 1% derived from tracer mass-balance considerations.
- The mechanically disturbed zone might be more heterogeneous and extend somewhat further into the drillcore (along grain boundaries), but the total affected pore volume is that derived from the chemically disturbed zone.
- During a contact time of 2 hours the ingress of drilling fluid, i.e. contamination, in the drilling disturbed zone (DDZ) is negligible and does not affect the calculated original porewater composition.

4.2 Stress release effects: Borehole KFM02B, Forsmark

For the first time, the effects of drilling-fluid contamination on the drillcore have been quantitatively investigated in a deep borehole drilled into crystalline rock. This has been performed by adding iodide as an inorganic tracer to the drilling fluid for the drilling of the last 15 metres of borehole KFM02B. This borehole was drilled in the candidate area at Forsmark from the hanging wall bedrock segment into the footwall bedrock segment at greatest depth below deformation zone ZFMF1. Iodide was employed in addition to uranine, routinely used to trace the drilling fluid contamination in fracture groundwater samples. The experiment was designed to give insight into possible drilling fluid contamination induced by immediate stress release of the rock in the borehole during drilling (and thus during contact with the drilling fluid) in addition to the possibility of contamination in the drilling disturbed zone (DDZ). As shown in the previous section, the effects of contamination in the DDZ induced by the drilling process alone (i.e. without stress release) appear to be negligible in the investigated granitic rocks.

The samples used in this experiment from borehole KFM02B are located in the footwall bedrock segment in the deeper part of fracture domain FFM01 that is not visibly affected by the overlying deformation zone ZFMF1. /Martin 2007/ derived for the interval between 400–600 m depth in the target area within the footwall bedrock segment a maximum horizontal stress of 29.5+0.023z, where z is depth. At a depth of 600 m this corresponds to a horizontal stress of σ_H = 43.3 MPa. In spite of this considerable stress the same author states, based on numerous stress measurements on drillcores and in boreholes from the Forsmark area: "There was no evidence from the stress-strain behaviour of laboratory samples to depths of 700 m that the *in situ* stress magnitudes were sufficient to create significant stress-induced micro-cracking". Although large effects of drilling fluid contamination in the out-diffusion experiments might not be expected based on stress measurements, the effect, if present at all, needs to be quantified in order to narrow the uncertainty band related to the calculated elemental concentrations in the porewater.

Borehole KFM02B was drilled at an inclination of 80° down to 573.87 m borehole length (–557.89 m of elevation). The five drillcore samples collected from the interval drilled using traced drilling fluid at the end of the borehole were conditioned and prepared for porewater investigations in the same way as all other porewater samples. The samples used for out-diffusion experiments all consist of medium-grained, slightly foliated, metamorphic granodiorite. The water content and water-content (connected) porosity of the samples (Table 4-4) falls within the range given by the 34 other kilogramme size samples from the same borehole (0.143–0.342 wt.% and 0.38–0.90 Vol.%). Over the entire borehole length there is no correlation established between the water content and the depth of the samples. The water content of the kilogramme size samples used in the out-diffusion experiments agrees within the uncertainty band with that determined by drying small-sized samples and by the largely independent isotope diffusive-exchange technique, except for sample KFM02B-42 where pronounced textural differences are observed among the various subsamples (cf. Chapter 5).

The composition of the iodide traced drilling fluid is given in Table 4-5. For comparison some typical (fracture) groundwater compositions that could be expected to occur in the fractures of borehole KFM02B and mix with the drilling fluid are also given. From samples of shallower depth in borehole KFM02B it is known that the porewater in these rocks is of a dilute Na-HCO_3 type with Cl^- contents typically around 1,000 mg/kg_{H2O} (cf. Chapter 7). Based on the drilling-fluid composition given in Table 4-5, it can be seen that a possible contamination induced by immediate stress release would not only result in an increased I^- concentration, but also increased concentrations of Cl^- and Br^- due to the higher mineralised drilling fluid compared to the expected porewater.

The concentrations of the out-diffusion experiment solutions and the calculated porewater concentrations (assuming no contamination) for samples KFM02B-39 to-43 are given in Table 4-6. As indicated from the shallower samples, the porewater Cl^- concentration varies around 1,000 mg/kg_{H2O}. Groundwater with such Cl^- contents commonly has a Br^- concentration of a few mg/L at the most and I^- concentrations in the low µg/L range. For samples KFM02B-39 to -43, the calculated concentrations of I^- and, to some degree, of Br^- in the porewater are, however, somewhat higher and intermediate between the drilling fluid and the known groundwater (Table 4-5). The ion-ion ratio of I/Cl in the porewater varies between 5.9×10^{-3} and 3.3×10^{-2}, while this ratio is at least two orders of magnitude lower in known fracture groundwater compositions. This suggests that some contamination of the drillcore material has occurred by drilling fluid during drilling.

The slightly differing slopes described by the Cl^- and I^- concentrations in the out-diffusion experiment solutions in the transient phase during the first days of out-diffusion (Figure 4-6) and the decreasing I/Cl ratio with time (Figure 4-7) yield further indications for some contamination. Without contamination by drilling fluid, the I/Cl ratio would be constant with time (both for homogeneous and heterogeneous diffusion coefficients D_p within the core, see below).

The maximum contamination is given by assuming that the porewater contained initially no iodide (0 mg/kg_{H2O}) and thus 100% of the I^- found at equilibrium in the out-diffusion experiment stems from drilling fluid. Such an assumption is in agreement with the suggested low Cl^- concentration in the porewater. For sample KFM02B-41, for example, the volume of the contaminating drilling fluid would be 0.054 mL based on such iodide mass balance calculation. This small volume of drilling fluid, which represents 2.4% of the porewater (total porewater volume = 2.33 mL), would contribute 8.4% (gross, i.e., considering the total Cl^- mass in the 0.054 mL drilling fluid) or 6.1% (net, i.e. when accounting only for the excess Cl^- mass compared to the initial porewater content) of the mass of Cl^- found in the out-diffusion experiment. For this maximum contamination by drilling fluid, the calculated initial porewater concentration is 915 mg/kg_{H2O} as compared to 974 mg/kg_{H2O} without any contamination, which is a difference equal to the percentage of the net Cl^- contamination (i.e. about 6.1%). As can be seen from Table 4-6, such a difference is well within the error range given for the porewater Cl^- concentration and based on the uncertainty band attached to the determination of the water content.

Contamination of the core samples by drilling fluid can only occur as long as the core is in contact with the drilling fluid, i.e. in the time interval in which the core is drilled until its arrival at the surface. The duration of this time interval depends on the time used to drill the core (i.e. the core length) and the depth at which the core is drilled (i.e. the time required to bring the core to the surface). In the boreholes drilled at Forsmark, this time interval varied between about 1 to 4 hours. It should be noted that the contact between drilling fluid and drillcore occurs under pressurised conditions for the drilling fluid. On the other hand, the drillcore is within the drill stem until its arrival at the surface, and therefore the volume of drilling fluid around the core is limited. Furthermore, the constriction of the drillcore by the drill stem will inhibit significant stress release and resulting increase in the core volume, for example, due to formation of micro-cracks. As mentioned above, the *in situ* stress field at Forsmark is given by a strong horizontal to sub-horizontal stress, whereas the vertical stress $\sigma1$ is subordinate /Martin 2007/. The strongest stress release effects would therefore be expected along the horizontal axis of the core where the core is constricted by the drill stem (note that the borehole inclination was only 80°). Thus, the majority of stress release might indeed occur only at the time the core is removed from the drill stem, i.e. at a time the core is no longer in contact with drilling fluid. Obviously, these occurrences would limit the possibility of a contamination of the drillcore by drilling fluid.

Table 4-4. Average water content by drying at 105°C and water-content porosity of rock samples from borehole KFM02B, Forsmark.

SKB Sample No	UniBern Lab-Sample	Rock Mass (wet, g)	Bulk Density (g/cm³) [1]	Water Content (wt.%) [2]	WC-Porosity (Vol.%) [2]
SKB012601	2B-39	615.578	2.63	0.235	0.62
SKB012603	2B-40	981.065	2.64	0.239	0.63
SKB012604	2B-41	977.289	2.63	0.238	0.62
SKB012605	2B-42	976.949	2.61	0.329	0.85
SKB012607	2B-43	985.522	2.65	0.208	0.55

[1] Relative to dry weight.
[2] Relative to wet weight.

Table 4-5. Anion composition of drilling fluid of borehole KFM02B and typical groundwater compositions from Forsmark.

Borehole/Sample	Water Type	Cl (mg/L)	Br (mg/L)	I (mg/L)	Br/ Cl (mg/mg)	I / Cl (mg/mg)	Br/I (mg/mg)
KFM02B	Drilling Fluid	3,400	14.2	899	4.18E–3	2.64E–1	0.016
SICADA	Av. Baltic	2,817	9.5	0.015	3.39E–3	2.8E–6	650.5
KFM03A-270	Saline	10,500	94.4	0.630	8.99E–3	6.0E–5	149.8
KFM01D-202	Brackish	5,960	46.4	0.321	7.79E–3	5.4E–5	144.5
	Av. Sea water [1]	19,350	67.3	0.062	3.48E–3	3.2E–6	1,085.5

[1] From /Nordstrom et al. 1979/.

Table 4-6. Anion concentrations in out-diffusion experiment solutions and calculated porewater concentrations of the drillcore samples from borehole KFM02B, Forsmark.

KFM02B Rock Type	Units	2B-39	2B-40	2B-41	2B-42	2B-43
		Meta-granodiorite				
Elevation	m	–544.09	–546.69	–549.46	–553.45	–557.67
Mass Rock	g	615.578	981.065	977.289	976.949	987.576
Vol. Porewater	cm^3	1.45	2.35	2.33	3.21	2.06
Vol. Exp. Water	cm^3	72.44	113.44	109.45	109.13	111.04
Anions in Out-Diffusion Experiment Solution						
Chloride (Cl^-)	mg/L	20.0	20.7	20.4	22.4	17.0
Bromide (Br^-)	mg/L	< 0.2	0.26	0.20	< 0.2	0.21
Iodide (I^-)	mg/L	0.12	0.24	0.45	0.74	0.21
Anions Calculated to Porewater Concentrations						
Chloride (Cl^-)	mg/kg $_{H2O}$	1,014	1,018	974	781	926
– error	mg/kg $_{H2O}$	90	91	87	69	83
+ error	mg/kg $_{H2O}$	111	111	106	84	101
Bromide (Br^-)	mg/kg $_{H2O}$	–	12.2	9.0	–	11
– error	mg/kg $_{H2O}$		1.1	0.8		1.0
+ error	mg/kg $_{H2O}$		1.3	1.0		1.2
Iodide (I^-)	mg/kg $_{H2O}$	6.0	11.8	21.6	25.9	9.0
– error	mg/kg $_{H2O}$	0.5	1.0	1.9	2.3	0.8
+ error	mg/kg $_{H2O}$	0.7	1.3	2.3	2.8	1.0
Ion–Ion Ratios						
Br/Cl	mg/mg	–	1.19E–2	9.19E–3	–	1.17E–2
I/Cl	mg/mg	5.89E–3	1.16E–2	2.22E–2	3.32E–2	1.25E–2
Br/I	mg/mg	–	1.0	0.4	–	0.9

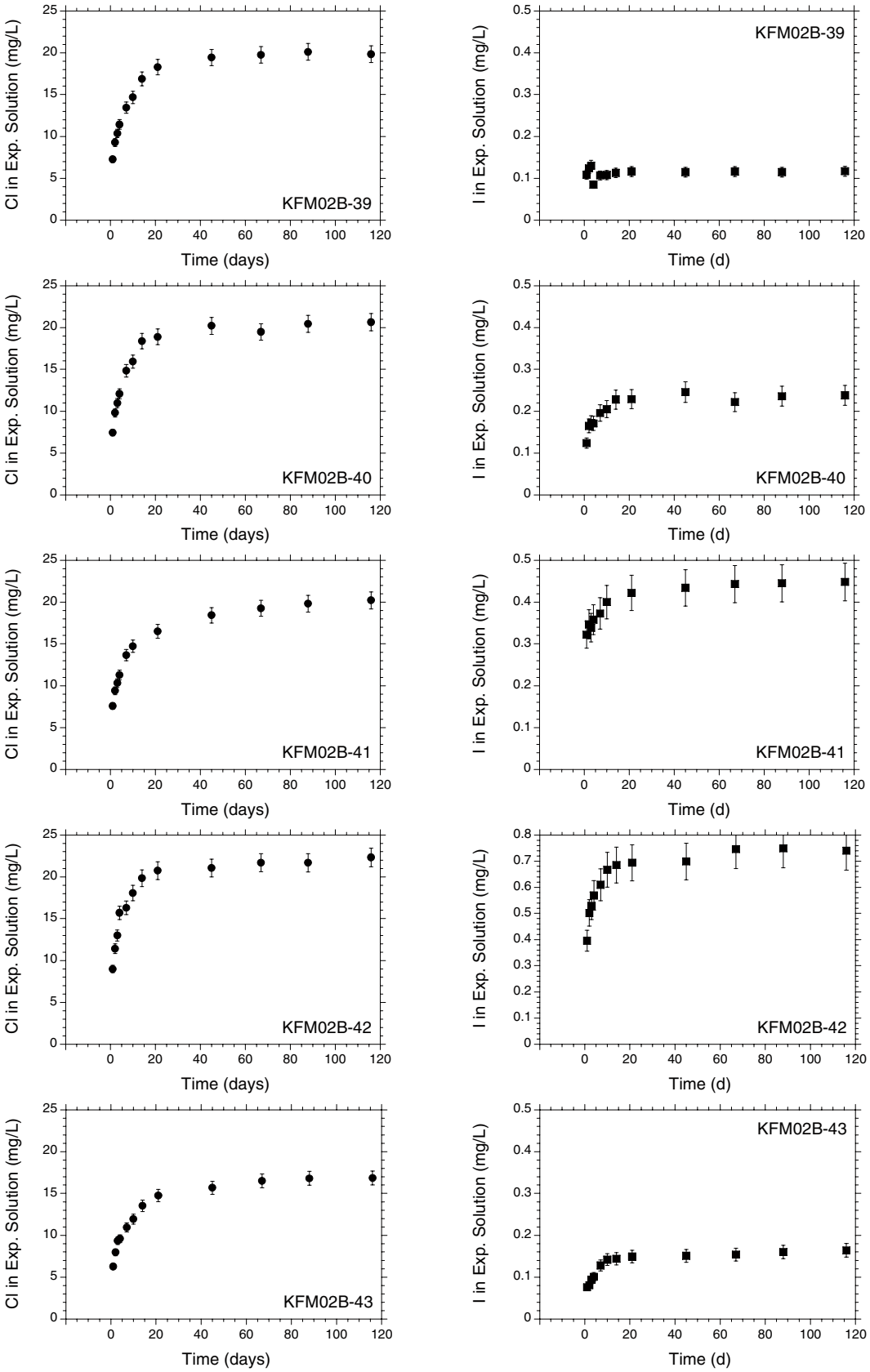

Figure 4-6. *Time series of Cl^- and I^- concentrations during out-diffusion at 45°C of the drillcore samples KFM02B-39 to -43 drilled with traced drilling fluid.*

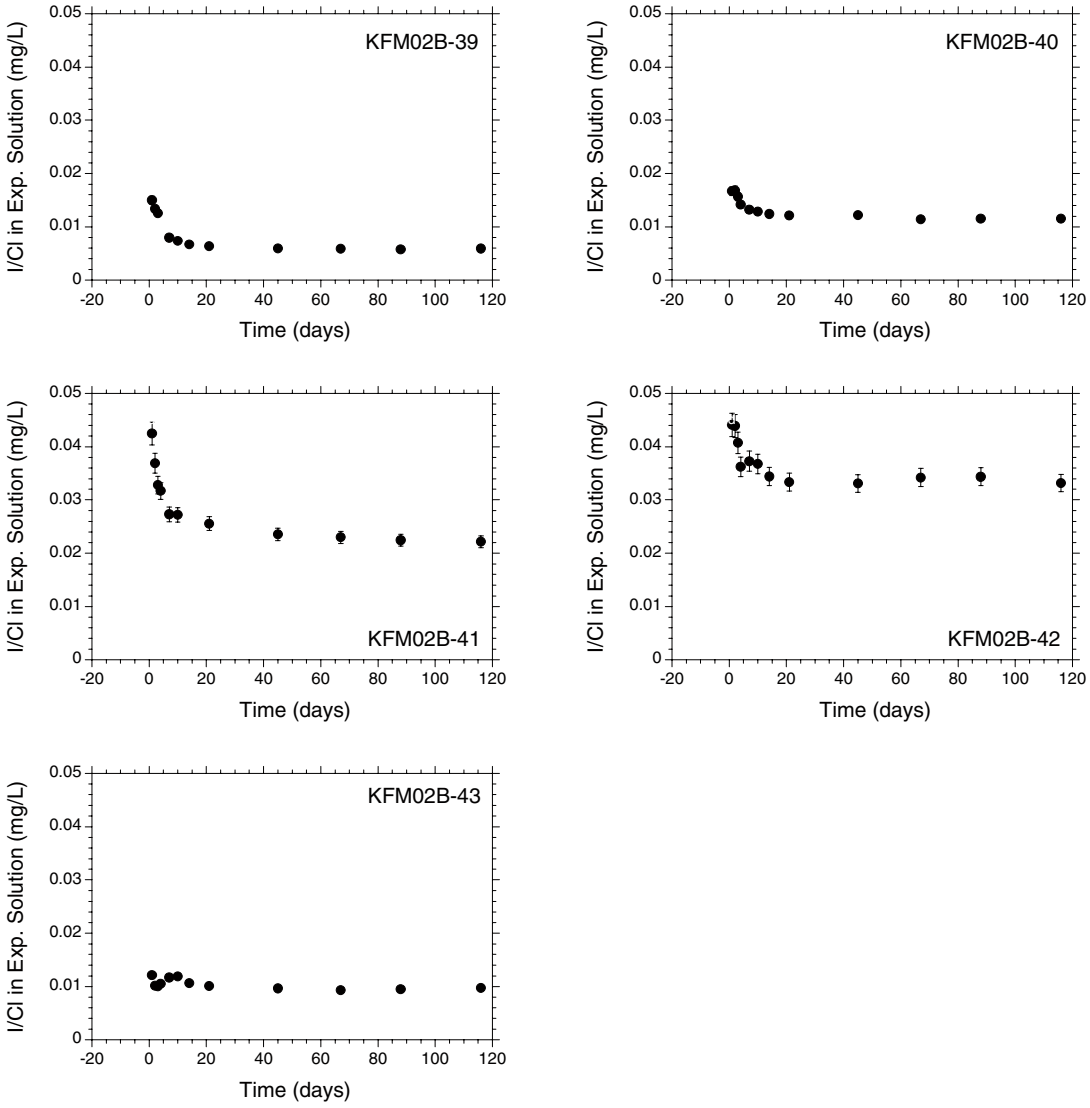

Figure 4-7. *Progressive Cl/I ratios during out-diffusion at 45°C of the drillcore samples KFM02B-39 to -43 drilled with traced drilling fluid.*

The evolution of the anion concentrations during the out-diffusion experiments was quantitatively evaluated for sample KFM02B-41 for possible perturbations by drilling fluid contamination. The cylindrical drillcore sample KFM02B has a diameter of 50 mm, a length of 190 mm and a total wet mass of 977.289 g. The modelling concept and tools used are those described above in Section 4.1. In contrast to the stress-released core form the Äspö HRL, however, the more heterogeneous behaviour of the anion concentrations during out-diffusion in the transient state of all samples (Figure 4-6) suggests that heterogeneous transport properties across the core must also to be considered. Thus, calculations were also performed with heterogeneous diffusion properties in the core centre and up to two sectors at the core rim.

Figure 4-8 shows the modelled results for the Cl^- and I^- concentrations and the I/Cl ratio assuming no contamination, homogeneous diffusion properties across the entire core and using variable diffusion coefficients, D_p. As can be seen, the relatively fast initial increase of the measured Cl^- and especially of the I^- concentrations and the slower later increase (leading to a relatively flat slope in the log-log plot) cannot be satisfactorily modelled with these assumptions. The measured concentrations are underestimated in the initial transient phase as best observed in the log-log plot with all different D_p values used.

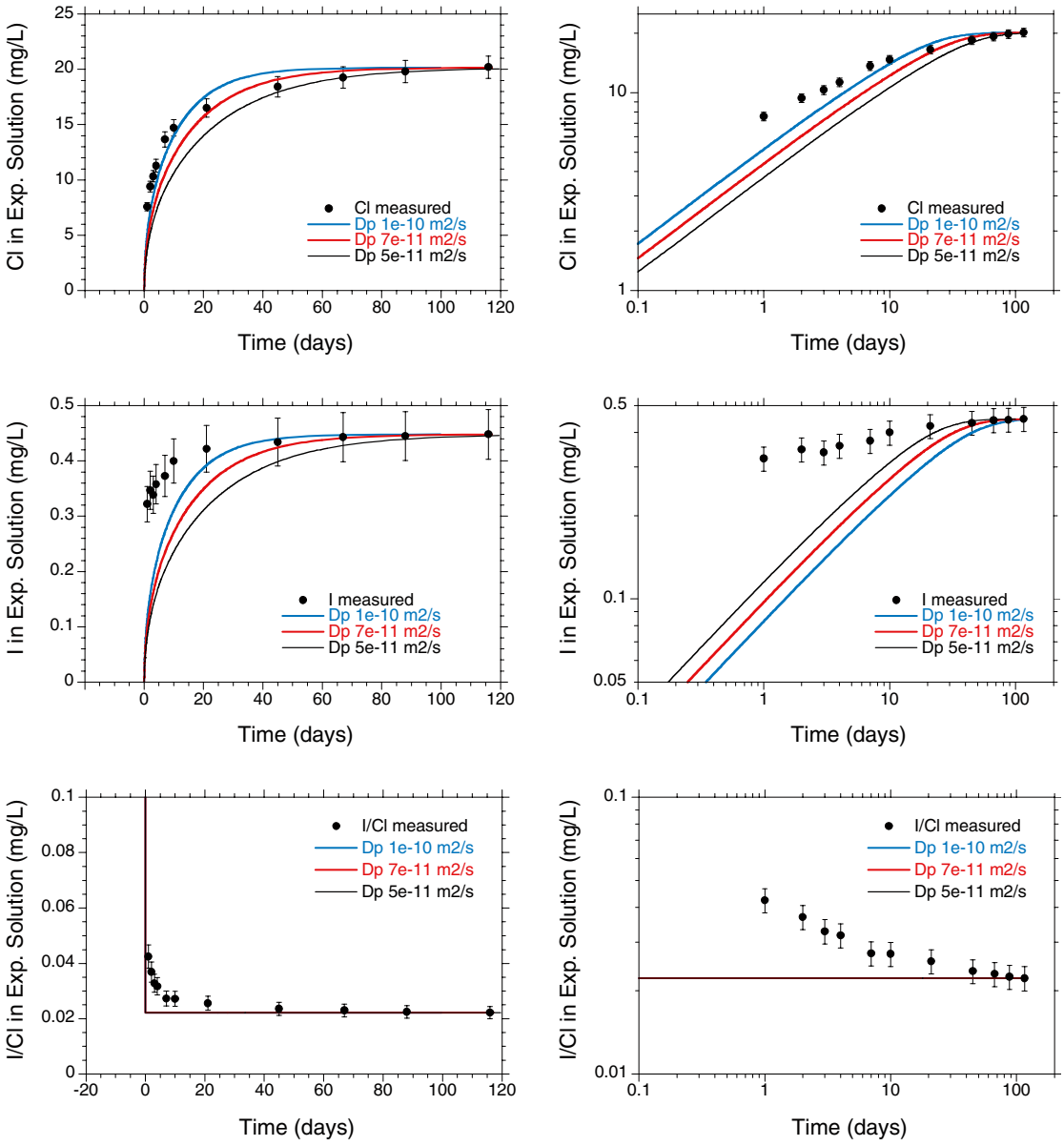

Figure 4-8. *Calculated concentrations of Cl^- and I^- and the Cl/I ratio (solid lines) during out-diffusion at 45°C of the drillcore samples KFM02B-41 compared to the measured values assuming no contamination or the maximum contamination of 0.3 mm external rim, homogeneous diffusion properties and a D_p of 1×10^{-10} m^2/s. Left: linear scale, right: log-log scale to highlight the discrepancy in the early phase of the transient state.*

A better fit of the measured Cl^- data is obtained when using heterogeneous diffusion properties across the core, but still assuming zero contamination. Figure 4-9 shows the results of such simulations with the core being subdivided into three segments of radius of 0–19 mm, 19–22 mm, and 22–25 mm with corresponding D_p values of 5×10^{-11} m^2/s, 1×10^{-10} m^2/s, and 2×10^{-10} m^2/s, respectively. A flatter slope of the concentration *versus* time in the log-log plot can be obtained by assuming heterogeneous diffusion coefficients, with larger values in the outer part of the core (Figure 4-9). However, no simultaneous fit for the Cl^-, I^-, and I/Cl data can be obtained. Also, assuming zero contamination, the simulated I/Cl ratio is flat for homogeneous (Figure 4-8) as well as heterogeneous diffusion properties (Figure 4-9), in contrast to the measured data. From all these observations, it is concluded that a certain degree of contamination with drilling fluid must have occurred and that heterogeneous diffusion properties prevail in the drillcore.

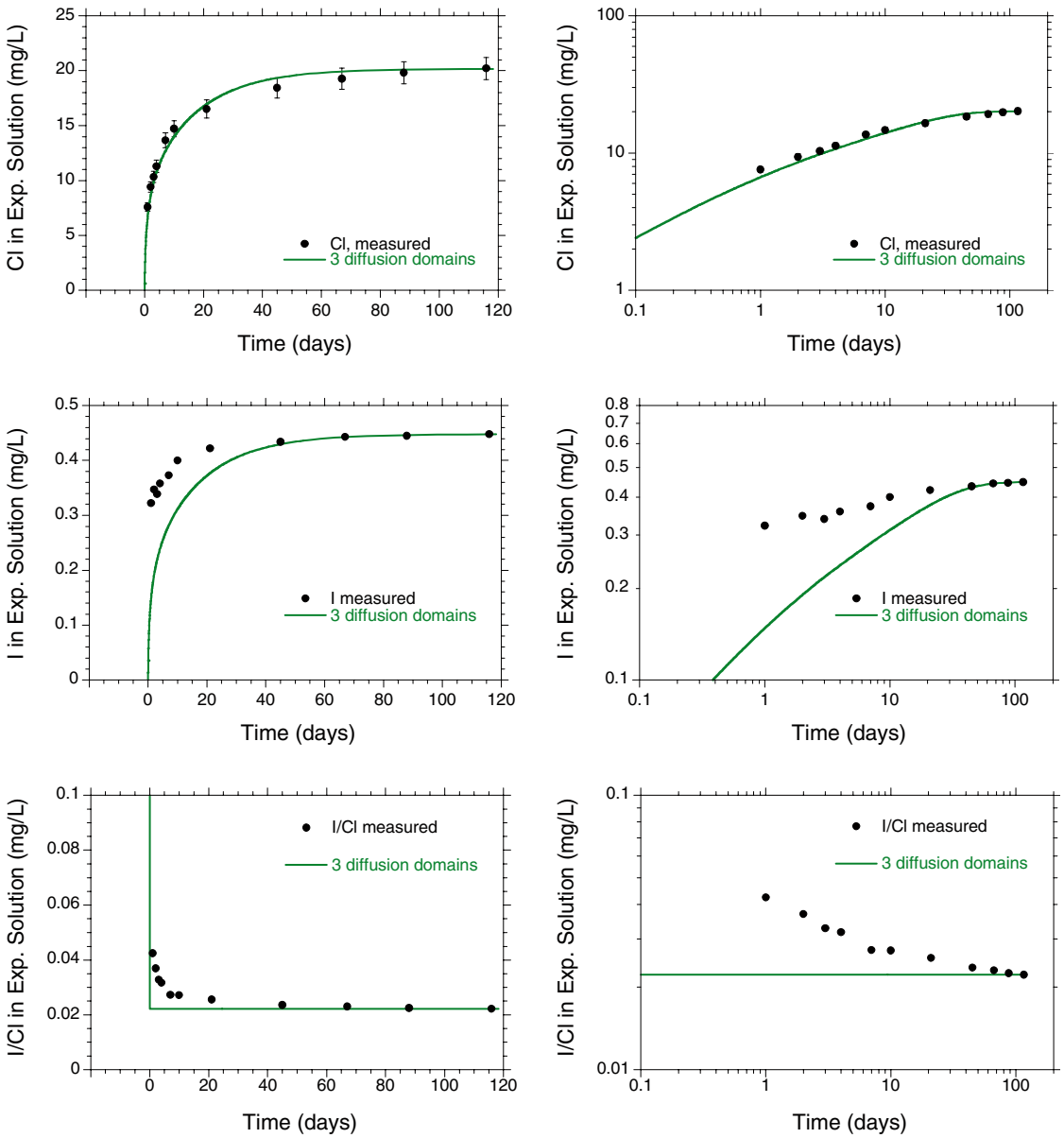

Figure 4-9. *Calculated out-diffusion results for Cl^- and I^- and the Cl/I ratio (solid lines) during out-diffusion at 45°C of the drillcore samples KFM02B-41 assuming no contamination, but heterogeneous diffusion properties from 0–19 mm, 19–22 mm, and 22–25 mm radial distance and with D_p values of 5×10^{-11} m²/s, 1×10^{-10} m²/s, and 2×10^{-10} m²/s, respectively. Left: linear scale, right: log-log scale.*

In the next step, the effect of the maximum contamination was examined, first assuming homogeneous diffusion properties across the entire core. The maximum contamination is derived from mass balance considerations of the I^- concentrations under the assumption that the *in situ* porewater has (within uncertainty) no measurable I^-. As mentioned above, this is a plausible assumption considering the low Cl^- concentration in the porewater of these samples of only about 1,000 mg/L. Assuming that all I^- in the out-diffusion experiment originated from contamination, then the extent of the zone where the porewater was completely flushed out by drilling fluid is at most 0.306 mm (corresponding to 2.4% of the porewater volume, see above). Considering a larger extent completely flushed with drilling fluid, the total mass of I^- within the sample would be considerably larger than what was obtained in the out-diffusion experiment. Thus, in the simulations shown in Figure 4-10, a maximum chemically contaminated zone of 0.3 mm was considered and is shown in comparison to the zero contamination scenario. As can be seen from this figure, a slightly better fit compared to assuming zero contamination is obtained for the measured chloride time-series (top panels), but the calculated out-diffusion of I^- is much too fast (middle panels), resulting also in an overestimation of the I/Cl

ratio (bottom panels) in the initial transient phase. The same picture arises when using a lower diffusion coefficient of 5×10^{-11} m²/s. An even lower diffusion coefficient seems unlikely, because the simulated out-diffusion of Cl^- is already too slow for a coefficient of 5×10^{-11} m²/s.

It has been shown, therefore, that only poor fits of the measured iodide time-series can be achieved when it is assumed that all I^- originates from contamination of the outermost rim alone. This result is derived from the transient phase of the out-diffusion experiment, which shows that the I^- and Cl^- from the contamination would diffuse out of the core within a relatively short time (10 minutes to about 2 hour, depending on the assumed D_p). According to the simulations for maximum contamination, at the time of the first measurement (1 day) all I^- has already disappeared from the core. In contrast, the I^- out-diffusion data show a significant increase from 1 day until about 40 days, similar to that of the Cl^- data. This suggests that a significant fraction of the I^- comes from central parts of the core, and not from the rim. Therefore, assuming a fully contaminated zone of 0.3 mm (maximum), the simulated I^- concentrations after 1 day are always overestimated and the Cl^- concentrations underestimated in comparison with the measurements, leading to initially too high I/Cl ratios.

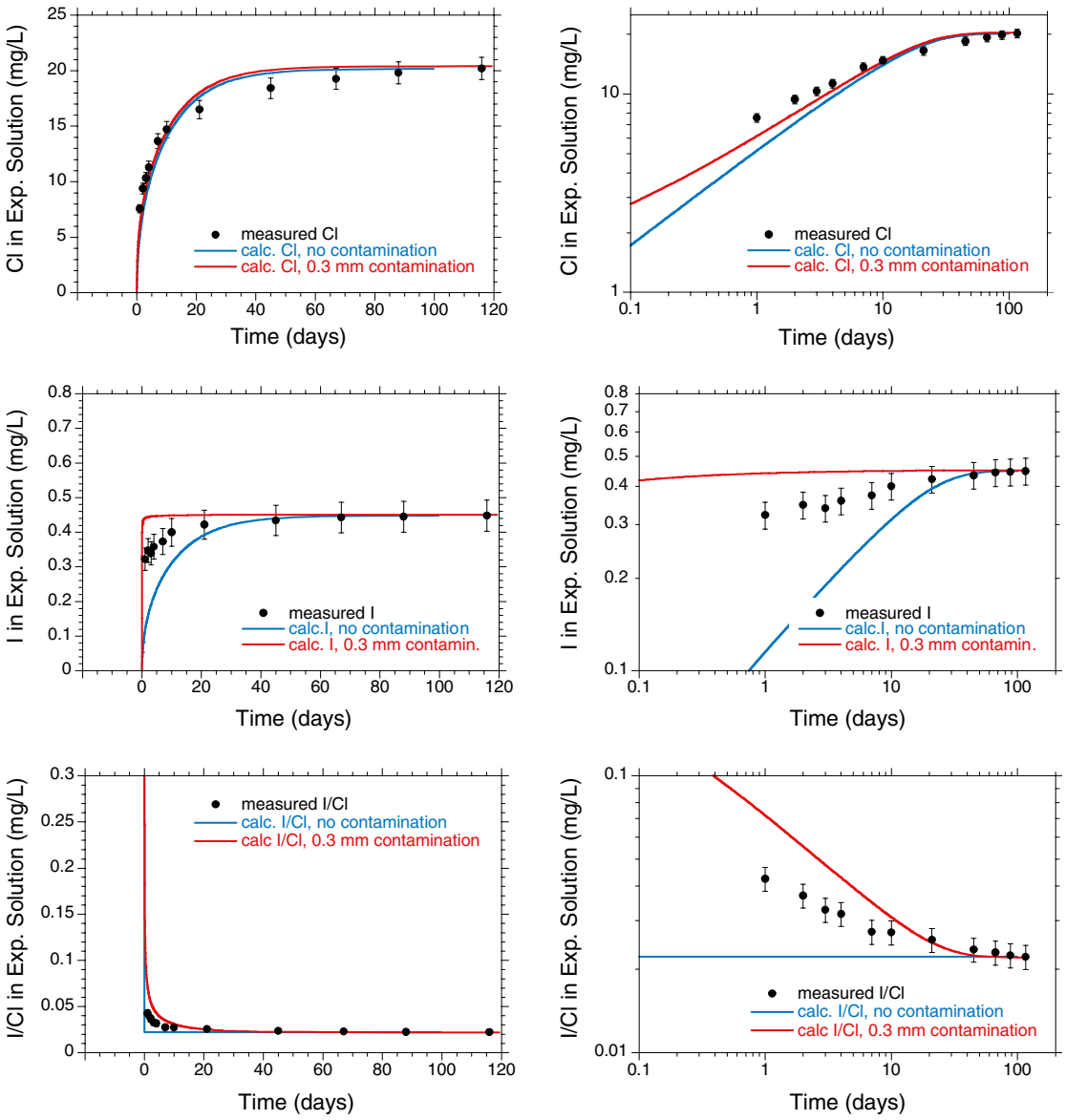

Figure 4-10. *Calculated concentrations of Cl^- and I^- and the Cl/I ratio (solid lines) during out-diffusion at 45°C of the drillcore samples KFM02B-41 compared to the measured values assuming no contamination or the maximum contamination of 0.3 mm external rim and homogeneous diffusion properties and a D_p of 1×10^{-10} m²/s. Left: linear scale, right: log-log scale to highlight the discrepancy in the early phase of the transient state.*

Acceptable matches between simulations and data at earlier times can be obtained for a contaminated zone of 0.2 mm or 0.15 mm (Figure 4-11). In the first case, about 5% or 4% of the Cl^- mass (gross or net contamination, respectively) would originate from contamination, and in the second case about 4% or 3%, respectively. Therefore, the initial porewater concentrations calculated for a contaminated zone of 0.2 mm would become: $I^- = 7.7$ mg/kg$_{H2O}$ and $Cl^- = 954$ mg/kg$_{H2O}$, and for a contaminated zone of 0.15 mm: $I^- = 11.3$ mg/kg$_{H2O}$ and $Cl^- = 963$ mg/kg$_{H2O}$, respectively. While these Cl^- concentrations are within the uncertainty of the porewater Cl^- concentration for sample KFM02B-41, the I^- concentrations seem high and the I/Cl ratios of 8.1×10^{-3} and 1.2×10^{-2} are 2-3 orders of magnitude higher than any known groundwater from the Forsmark area (cf. Table 4-5). The reason for this behaviour is as yet unknown. Possibilities include strong sorption of I^- on the large surface of the core or analytical problems related to the very low concentrations of I in the experimental solution.

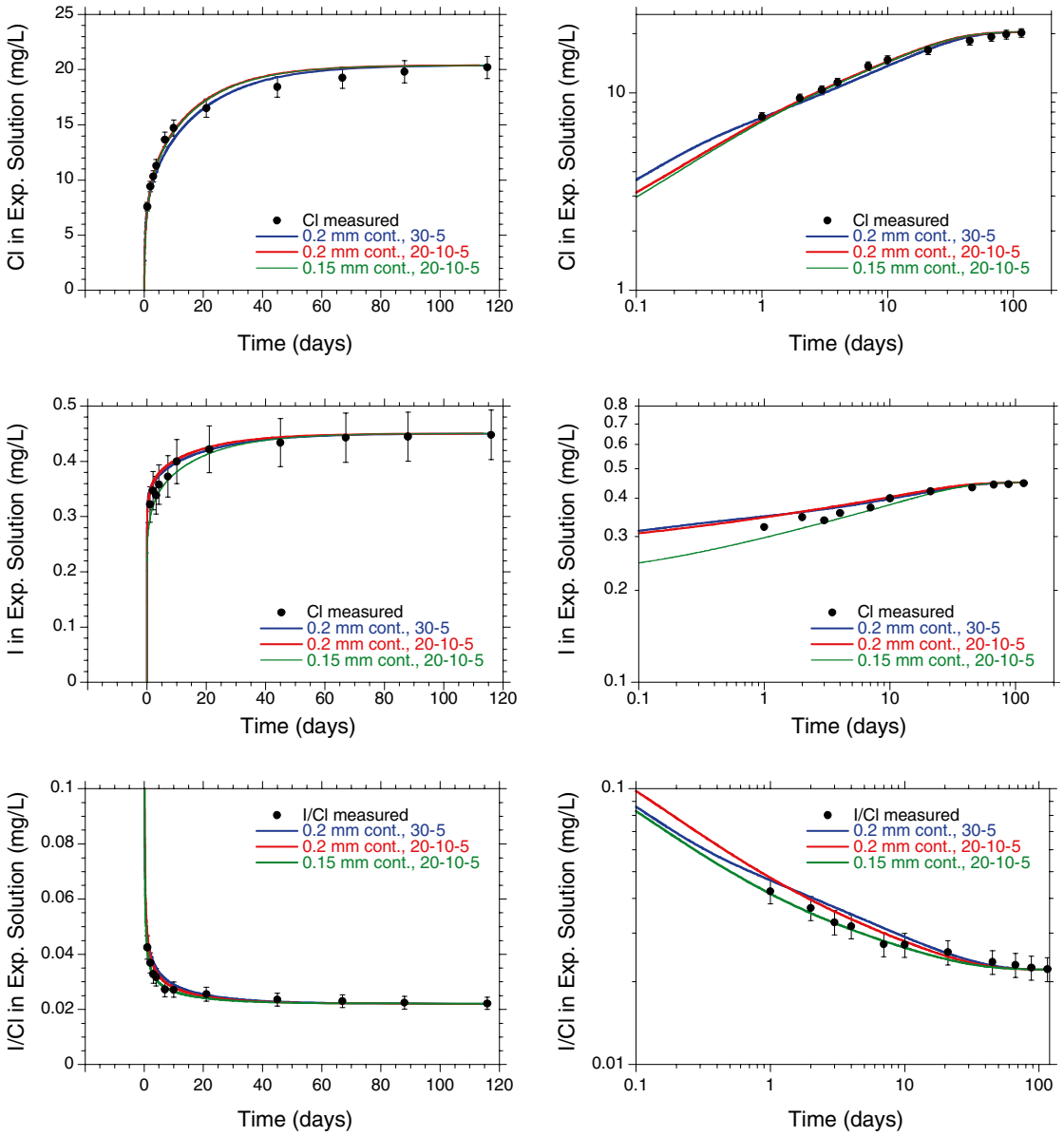

Figure 4-11. *Calculated out-diffusion results for Cl^- and I^- and the Cl/I ratio (solid lines) during out-diffusion at 45°C of the drillcore samples KFM02B-41 assuming a contamination of the external 0.2 or 0.15 mm of the core and heterogeneous diffusion coefficients (case 30-5: 5×10^{-11} m²/s from 0–22 mm and 3×10^{-10} m²/s from 22–25 mm radial distance; case 20-10-5: 5×10^{-11} m²/s from 0–19 mm, 1×10^{-10} m²/s from 19–22 mm, and 2×10^{-10} m²/s from 22–25 mm radial distance).*

Summary

The drilling-fluid contamination experiment conducted on drillcore from about 550 m depth in borehole KFM02B at Forsmark has revealed that:

- Modelling with a homogeneous diffusion coefficient, D_p, cannot adequately describe the measured data.
- The extent of the mechanically disturbed zone, i.e. heterogeneous diffusion properties, may cover about the outermost 6 mm of the drillcore
- The chemically disturbed zone extends to a maximum 0.3 mm into the drillcore based on mass balance considerations of the tracer concentration and 0.15 mm to 0.2 mm into the drillcore based on fitting the observed artificial (I^-) and natural (Cl^-) tracer data. This corresponds to a maximum of 2.4% of the total pore volume being affected by the drilling-fluid contamination.
- The maximum contamination of the porewater Cl^- concentration is about 8%.
- Being less than 10%, the Cl^- contamination by drilling fluid of the drillcores from the boreholes of the Forsmark area is therefore within the uncertainty band of the porewater determinations, which is given essentially by the measurement of the water content and connected porosity, respectively.

4.3 Data uncertainty

From (Equation 3-3) it can be seen that the calculated concentration of Cl^- (or any other chemically conservative element) in the porewater from out-diffusion concentrations is inversely proportional to water content. The uncertainty of the indirectly derived porewater concentrations thus strongly depends on the accuracy of the water-content determination and the degree to which the measured values represent *in situ* conditions. This becomes especially important in rocks with low water content such as the crystalline rocks of Forsmark.

Effects that could deviate the measured water-content from *in situ* conditions are related to desaturation, stress release and the drilling disturbed zone. By applying adequate handling techniques (e.g. immediate vapour-tight packing on-site after recovery of the core), desaturation can be minimised if not excluded. By applying the same handling methods, the effects of stress release are limited to the time the core is in contact with the drilling fluid. As shown in the previous sections, the effect of drilling fluid contamination induced by stress release could be quantified as being less than 10% and the effect of the drilling disturbed zone on the porewater content and composition is less than 1%. It can thus be concluded that the combined perturbation effects of the measurement of the *in situ* water content and the measurement of conservative porewater compounds can be minimised to less than 10% by adequate sample handling and conditioning in these low permeability and porosity rock types.

The uncertainty of porewater concentrations for conservative compounds is thus mainly related to textural heterogeneity of the rock and how well the sample mass used for the water-content determination takes account of such heterogeneity. This is because effects of textural heterogeneity (and possible influences by stress release) will result in a deviation of the measured water content that is inversely proportional to the mass of sample aliquots used. This results in a larger standard deviation for groups of samples with lower masses. The uncertainty band of a porewater concentration of a chemically conservative compound such as Cl^- or Br^- is thus best described by the standard deviation of water contents derived from multiple samples and/or to the analytical error of the water content determination in the case of a large kilogramme size sample as used in the present out-diffusion experiments.

The uncertainty of the porewater isotope composition using the isotope diffusive-exchange technique is appropriately described by the error propagated according to Gauss. As shown by /Waber and Smellie 2008/ in the case of Forsmark, contamination by drilling fluid would affect the calculated isotope composition only in the case where such contamination would exceed about 10%. Based on the above investigations, such a high contamination can be excluded here.

For the Forsmark area, it can thus be concluded that the water contents and water-content porosity, the chemical and isotopic composition of porewater, and the pore diffusion coefficients derived by the applied indirect methods, appear indeed to represent *in situ* conditions within the given analytical uncertainties.

5 Water content and water-loss porosity

Water content, bulk density, and water-loss porosity were determined on originally saturated drillcore material on 48 samples from the footwall bedrock s.l. and 46 samples from the hanging wall bedrock s.l. of the Forsmark candidate area. The samples collected for porewater investigations were not aimed to be representative for the occurrence of different lithologies in the Forsmark model area. Thus, the petrophysical and transport properties determined on these samples might serve as a complement (but not replacement) to the laboratory measurements for the transport properties performed on a much more representative sample selection with respect to the various lithologies /Selnert et al. 2008/.

Porewater investigations were almost exclusively performed on fracture-free rock samples with little or no alteration. By far the majority of porewater samples consist of metagranite to granodiorite (footwall s.l.: 33, hanging wall s.l.: 44), followed by aplitic granite (footwall: 8, hanging wall: 0), fine-grained granite (footwall s.l.: 3, hanging wall s.l.: 2), granite to tonalite (footwall s.l.: 4, hanging wall s.l.: 0) and two highly altered episyenite samples in the footwall s.l.. Because of the strong bias towards samples of granite to metagranite composition there is only a weak dependence between the rock lithology and the petrophysical parameters water content and water-loss porosity is observed in the present data set. The only exceptions are two highly altered metagranites (episyenite) collected from the footwall bedrock s.l. (boreholes KFM08C and KFM09B). In contrast, differences in petrophysical parameters are observed between the rocks of the footwall bedrock s.l. and those of the hanging wall bedrock s.l. even when taking into account the bias towards a greater amount of samples from greater depth in the footwall bedrock s.l.. Therefore, the discussion of the petrophysical parameters will mainly distinguish between rocks from the footwall bedrock s.l. and rocks from the hanging wall bedrock s.l., but not between different lithologies, except for the above mentioned two episyenite samples.

5.1 Water content

5.1.1 Water content by gravimetry

The water content, determined gravimetrically by drying the samples at 105°C to stable weight conditions, is below 0.3 wt.% for most samples of the Forsmark model area (Table A-1). Such small water contents are sensitive to even small influences of contamination by drilling fluid and/or evaporation during sample handling. As shown in the previous chapter, chemical effects on the porewater composition by drilling fluid contamination are less than 10% based on *in situ* experiments performed with traced drilling fluid. This maximum chemical contamination corresponds to about 2.4% of the total pore volume of the rock samples. Even in the most conservative consideration, assuming that the entire 2.4% of the total pore space would have been newly created by effects of stress release and drilling process, such perturbation does not alter the water content measured on originally saturated rock samples outside the analytical error. Therefore, the *in situ* water content of the rocks has not been altered to a measurable degree during the drilling process.

Evaporation of original porewater from the surfaces of the rocks sampled and during sample preparation is the next possible process that may lead to a deviation of the measured water content from that existing under *in situ* conditions. The effect of possible evaporation can be evaluated by comparing the water contents obtained by two largely independent methods, i.e. determination of the water content by gravimetry, WC_{Drying}, and by the diffusive isotope exchange technique, $WC_{IsoExch}$ (cf. /Waber and Smellie 2008/ for discussion). As can be seen from Figure 5-1, the water contents derived by these two methods agree well for most samples although a somewhat larger spread is observed for the rocks of the hanging wall. Larger deviations in water contents obtained by the two methods are only observed for a few samples located in the near vicinity of water-conducting fractures, i.e. in tectonically altered zones, and/or for samples with closed fractures with abundant clay minerals. The latter might indeed influence the water content determined by the diffusive isotope exchange technique due to the large amounts of bound water on their surfaces (cf. /Pearson et al. 2003/ for discussion). Evaporation of porewater during sampling and sample preparation seems therefore either negligible or at the maximum of the analytical uncertainty. It can be concluded that the majority of the water contents obtained from originally saturated samples represent the water content present in the rock under *in situ* conditions within the analytical uncertainty and larger deviations are due to textural heterogeneity of the subsamples used for different measurement and methods.

The majority of rock samples from the footwall bedrock s.l. (boreholes KFM01D, lower part of KFM06A, KFM08C and KFM09B, cf. Figure 2-3) have very similar water contents that fall within a narrow range (Table A-1). For the small sample aliquots with total weights between about 100 g and 400 g, the gravimetric water content ranges from 0.07–0.23 wt.% with an average of 0.11 ± 0.03 wt.% (n = 46). The large size samples used for out-diffusion experiments with total weights between about 650 g and 1,000 g have almost identical water contents (Figure 5-2) ranging from 0.09–0.20 wt.% with an average of 0.12± 0.02 wt.% (n = 34). The small difference is attributed to the higher susceptibility of small samples to effects by sample preparation (e.g. sawing), evaporation and textural heterogeneity. The difference is, however, well within the analytical uncertainty given by the standard deviation of multiple samples and the ±5% relative analytical error associated to the large size samples (Figure 5-2). The only exceptions to this general pattern are two episyenite samples with gravimetric water contents of 3.08 wt.% (sample KFM08C-4) and 0.61 wt.% (sample KFM09B-1, Table A-1).

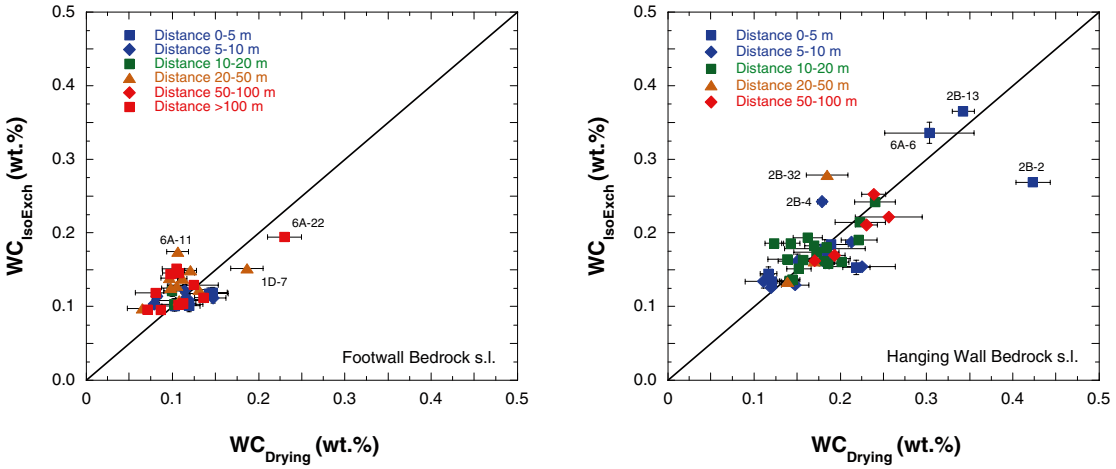

Figure 5-1. Comparison of the gravimetric water content derived by drying to stable weight conditions and the water content derived by the diffusive isotope exchange techniques as a function of the distance between the porewater sample and the next water-conducting fracture. Left: rocks from the footwall bedrock s.l., right: rocks from the hanging wall bedrock s.l. Note that not all samples have been subjected to the isotope diffusive exchange technique.

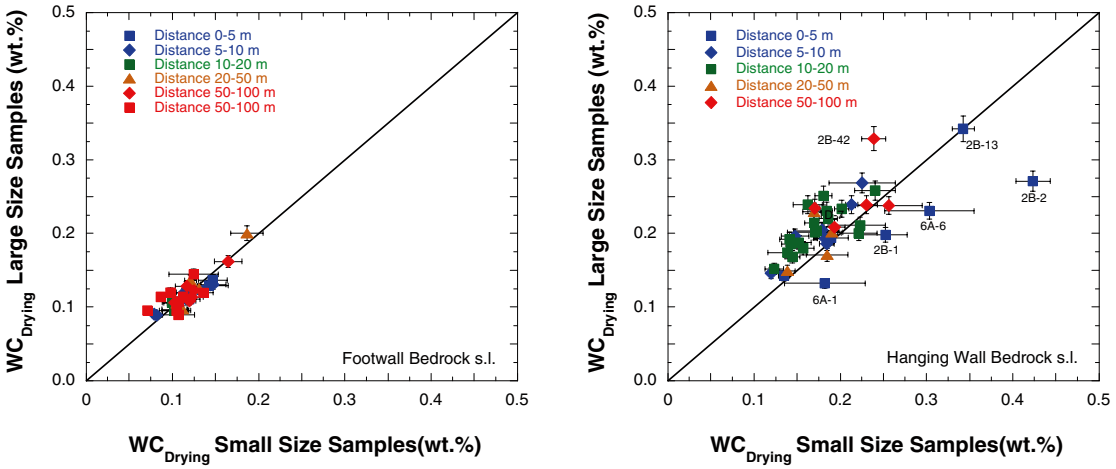

Figure 5-2. Comparison of the gravimetric water content of small size subsamples and the large size samples used for out-diffusion experiments as a function of the distance between the porewater sample and the nearest water-conducting fracture. Left: rocks from the footwall bedrock s.l., right: rocks from the hanging wall bedrock s.l. Note that water contents have not been determined on all large size samples (cf. Tables A-1 and A-2).

Generally higher water contents and a larger spread are observed for samples from the hydraulically higher transmissive hanging wall bedrock s.l. represented by borehole KFM02B and the upper part of borehole KFM06A (cf. Figure 2-3). Because most of these samples are also of granite to metagranite composition, the higher water contents seem to be related more to the shallow to intermediate depths sampled (above about 500 m) and therefore mostly collected within the zones with a high fracture frequency closer to water-conducting fractures (Figure 5-1). For the small sample aliquots with total weights between about 100 g and 250 g, the gravimetric water content ranges from 0.11–0.42 wt.% with an average of 0.19± 0.06 wt.% (n = 46). In comparison to fracture domain FFM01 in the footwall bedrock, a much larger spread is observed between water contents of the small size samples and the large size sample used for out-diffusion experiments (Figure 5-2). These latter samples with total weights between about 650 g and 1,000 g have generally higher water contents (Figure 5-2) ranging from 0.13–0.34 wt.% with an average of 0.21± 0.04 wt.% (n = 41). Because measurable contamination induced by stress release and the drilling process can be excluded, the slightly higher

water contents measured in the large size samples seem mainly due to the higher susceptibility to evaporation effects of the low amounts of rock material available for the small size samples (average of about 200 g). For a few samples collected close to water-conducting fractures and at shallow depth, the large size samples show lower water contents compared to the small size aliquots. Most of these samples also show larger deviations between the gravimetric water content and that obtained by isotope diffusive exchange suggesting that these few samples may have experienced some perturbation(s) no longer resolvable (note that such data are not available for all samples, cf. Table A-1).

5.1.2 Water content by the diffusive isotope exchange technique

For the rocks from the footwall bedrock s.l. the water content derived via isotope exchange between porewater and test water using the gas phase as a diaphragm is similar or identical to the gravimetric water content (Figure 5-1, Table A-1) for most samples. It ranges from 0.09–0.19 wt.% and averages at 0.12 ± 0.02 wt.%.

As for the gravimetric water contents, slightly higher values and a larger spread is observed for the water content by isotope exchange of the rocks from the hanging wall bedrock s.l. For these samples, the water content by isotope exchange ranges from 0.13–0.37 wt.% and averages at 0.19 ± 0.05 wt.%.

In both the sampled localities larger deviations between water contents determined by the different methods are associated with shallow samples collected close to water-conducting zones and/or samples that have visible closed fissures with clay infills. In spite of these few exceptions, the water contents derived by the diffusive isotope exchange technique and those derived by gravimetric methods generally agree well providing confidence that the measured values represent the water content as present under *in situ* conditions for most samples.

5.2 Bulk density

Bulk density measurements were derived from the wet mass and volume of the large size drillcore samples used in the out-diffusion experiments (Table A-2). For all rocks, the measured density values are consistent with the mineralogical composition and highlight the rather monotonous mineralogy of the rocks.

For the granitic rocks of the footwall bedrock s.l. the bulk wet density ranges from 2.59–2.68 g/cm^3 with an average of (2.64 ± 0.02 g/cm^3, n = 46). Average values of the different lithologies show only small differences (Table 5-1) and the rather large range is more related to local differences in the contents of the mafic minerals. Significantly lower bulk wet density values are recorded for the episyenite sample with values of 2.45 g/cm^3 (sample KFM08C-4) and 2.56 g/cm^3 (sample KFM09B-1) in agreement with the intense alteration of these samples.

For the rocks of the hanging wall bedrock s.l. mainly comprising granite to metagranite, the bulk wet density shows less variation and ranges from 2.62–2.67 g/cm^3 with an average of (2.64 ± 0.01 g/cm^3, n = 46).

5.3 Water-loss porosity

The water-loss or connected porosity determined on originally saturated rock material differs for rocks from the footwall and hanging wall bedrocks. In the footwall bedrock (fracture domain FFM01) the water-loss porosity of the various granitic rocks varies for the large size samples used in the out-diffusion experiments from 0.23–0.42 Vol.% for most samples from boreholes KFM01D, the lower part of KFM06A, KFM08C and KFM09B. Exceptions include one altered sample at about 365 m depth in borehole KFM01D (KFM01D-7) with 0.52 Vol.% and the episyenite samples with 1.55 Vol.% (KFM09B-1) and 8.86 Vol.% (KFM0C-4, Tables A-1 and A-2). The average water-loss porosity shows little or no variation among the different rock types and between the large size samples used for out-diffusion experiments and the small size subsamples specifically used for gravimetric water content measurements without ever having been immersed in the test water (Table 5-1). Thus, the rocks from the footwall (fracture domain FFM01) do not seem to be affected by stress release that takes place at the surface resulting in potential new pore space that would become saturated during the out-diffusion experiments. Further support in this direction comes from the absence of any variation of the water-loss porosity with depth (Figure 5-3). Such variation might be expected because of the increasing *in situ* stress on the rock with increasing depth.

In the hanging wall bedrock s.l. (i.e. fracture domain FFM03 including the upper part of borehole KFM06A representing fracture domain FFM02 and the upper part of fracture domain FFM01), the water-loss porosity of the granitic rocks is higher compared to the rocks of the footwall bedrock s.l. (i.e. fracture domain FFM01 and including the lower part of borehole KFM06A representing also fracture domain FFM06) and a larger variation is established.

For the large size samples used in the out-diffusion experiments the water-loss porosity in the hanging wall bedrock s.l. varies between 0.35–0.90 Vol.%. In contrast to the rocks from the footwall bedrock, the large size samples of the hanging wall bedrock s.l. tend to have on average a slightly higher water-loss porosity compared to the small size samples (Table 5-1). As in the footwall bedrock s.l., the water-loss porosity varies, however, not with depth, but is related to the distance of the collected porewater samples to the various deformation zones encountered in borehole KFM02B (i.e.ZFM866, ZFMA3, ZFMA2, ZFMF1) and in the upper part of borehole KFM06A (i.e. ENE0060B and ENE0060A, cf. Figure 2-3). Thus, samples in borehole KFM02B collected from within the two gently dipping brittle deformation zones, ZFMA2 and ZFMF1 between about 410 m and 520 m depth have water-loss porosity values that differ by almost a factor of 3 within only a few metres of depth (Figure 5-3). Currently, it is not well understood if the difference in water-loss porosity between the small size and the large size samples is due to stress release that took place at the surface and resulted in new pore space that became saturated during the out-diffusion experiments. Stress release effects do not seem, however, to be a plausible explanation based on the *in situ* stress field, which seems lower in the hangning wall bedrock segement compared to the footwall bedrock segment /Martin 2007/.

Table 5-1. Average bulk density and water-loss porosity of the different rock types used for porewater investigations in comparison with water-loss porosity values generated by resaturation.

Rock Type	Bulk Density	WL-Porosity	WL-Porosity	WL-Porosity
	(wet)	Large size samples	Small size samples	/Selnert et al. 2008/
State of rock sample		originally saturated	originally saturated	resaturated
Sample weight		650–1,000 g	100–400 g	mainly < 100 g
	g/cm^3	Vol.%	Vol.%	Vol.%
Footwall bedrock s.l. (fracture domains FFM01 and FFM06, excluding the upper part of borehole KFM06A to 340 m depth)				
Metagranite to granodiorite	2.64 ± 0.02 (n=24)	0.31 ± 0.06 (n=24)	0.30 ± 0.07 (n=31)	0.25 ± 0.15 (n=96)
Granodiorite to tonalite	2.65 ± 0.03 (n=4)	0.31 (n=1)	0.38 ± 0.15 (n=4)	0.23 ± 0.14 (n=11)
Fine-grained granite	2.64 ± 0.02 (n=3)	0.28 ± 0.05 (n=3)	0.30 ± 0.04 (n=3)	0.36 (n=1)
Aplitic granite	2.62 ± 0.01 (n=8)	0.31 ± 0.04 (n=5)	0.27 ± 0.04 (n=8)	0.22 ± 0.06 (n=2)
Hanging wall bedrock s.l. (fracture domain FFM03 including FFM01 in borehole KFM02B and FFM02 and FFM01 in the upper 340 m of borehole KFM06A)				
Metagranite to granodiorite	2.64 ± 0.01 (n=44)	0.56 ± 0.12 (n=39)	0.50 ± 0.16 (n=44)	0.26 ± 0.17 (n=39)
Fine-grained granite	2.64 ± 0.02 (n=2)	0.50 ± 0.18 (n=2)	0.45 ± 0.14 (n=2)	0.28 (n=1)

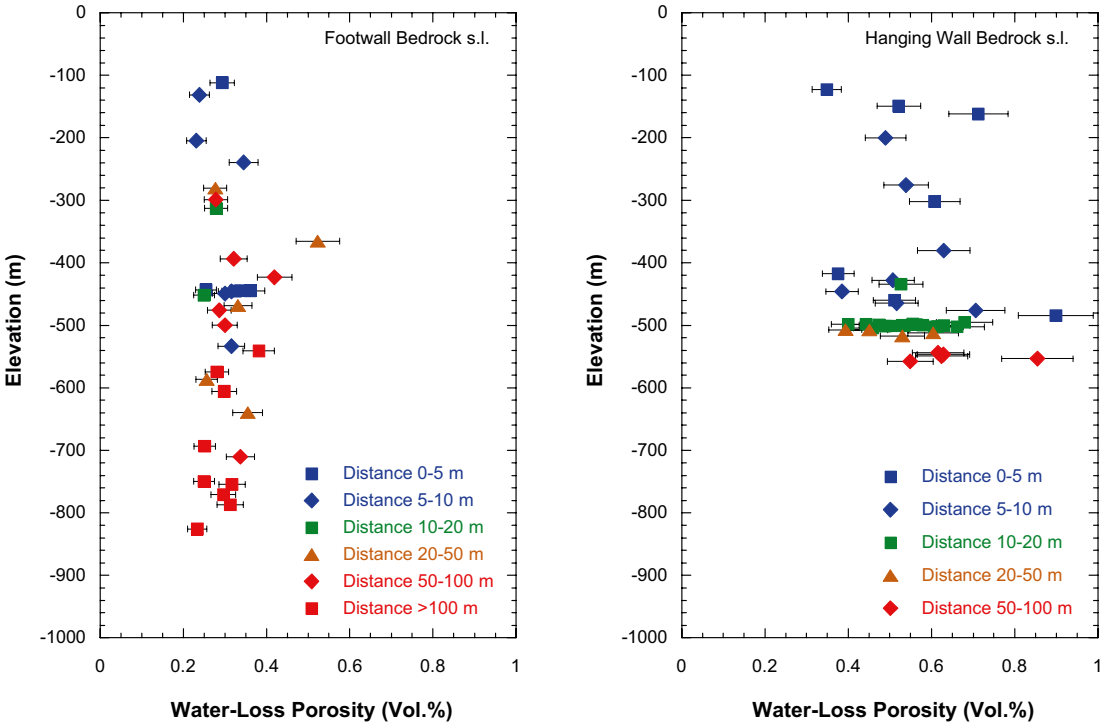

Figure 5-3. *Water-loss (connected) porosity as a function of distance of the porewater sample to the next water-conducting fracture versus elevation (m a.s.l.) for rock samples from the footwall bedrock s.l. (left) and the hanging wall bedrock s.l. (right). See Figure 2-3 for allocation of footwall bedrock s.l and hanging wall bedrock s.l.*

In Table 5-1 the water-loss porosity obtained from originally saturated samples used for porewater characterisation are compared to values obtained by the resaturation technique. These samples consisted of drillcore section of 0.5 to 5 cm in length with a mass of mainly less than 100 g /Selnert et al. 2008/. The samples were first dried at 70°C to constant weight, then resaturated with water under vacuum for 4 days and again dried to constant weight. The water-loss porosity obtained by this method results in lower values, which is especially pronounced for rocks from the hanging wall bedrock s.l. (Table 5-1). The water-loss porosity values obtained by resaturation are lower than the capacity factor obtained by through-diffusion experiments performed on the very same samples (cf. Figure 4-18 in /Selnert et al. 2008/). According to theory, however, these two parameters should be identical in the case of the non-sorbing tracer ^{3}H as used in the through-diffusion experiments. /Selnert et al. 2008/ explain the difference by mineral reactions that may affect porosity during the approximately 8 months duration period of the diffusion experiments. In comparison with the water-loss porosity data obtained from originally saturated samples, it seems, however, more likely that the duration of resaturation (4 days) was not long enough to completely resaturate the samples. In addition, it might be difficult to effectively resaturate all the pores and replace the air present in the pores with water. In this context it is further interesting to note that drying to constant weight of the porewater samples lasted several weeks for the small size samples and up to 8 months for the large size samples (cf. /Waber and Smellie 2005, 2007, 2009/) suggesting that 4 days might indeed be insufficient for complete resaturation even when applying vacuum pressure. To finally resolve this issue it would be interesting to monitor the resaturation with and without vacuum pressure as a function of time.

6 Transport properties of rock matrix

In order to interpret the porewater data in a hydrogeological sense, the solute transport properties of the rock matrix need to be known. For the scale of the obtained rock samples, such information has been derived from measurements and modelling of Cl^- concentration time series obtained from the out-diffusion experiments as explained in sections 6.1 and 6.2. In section 6.3, the possible spatio-temporal evolution of porewater is discussed in response to the concentrations in the water-conducting fractures, using the obtained transport properties of the matrix.

6.1 Theoretical background

The out-diffusion experiments were performed on rock cores of about 200 mm in length and 50 mm in diameter, which were emplaced in vapour-tight containers containing water initially devoid of chloride (Section 3.2.2). The cores were completely immersed in this experiment solution such that all surfaces were exposed to the fluid. Note that most of the diffusion parameters have been derived from originally saturated core material with a total mass of about 1 kg (Table A-2), compared to conventional through-diffusion experiments performed on much smaller sized (about 50–100 g) and often re-saturated samples (e.g. /Skagius and Neretnieks 1986, Ohlsson 2000/).

In view of the dimensions of the core with its large cylindrical outer surface compared to the top and bottom surfaces, transport through the latter was neglected for the modelling and diffusion across the mantle surface only was considered. This allowed using a one-dimensional radial transport equation to describe diffusion within the rock:

$$\theta \frac{\partial C}{\partial t} = \frac{1}{r}\frac{\partial}{\partial r}\left(rD_e \frac{\partial C}{\partial r}\right), \quad (0 < r < a) \qquad \text{(Equation 6-1)}$$

where θ : volumetric water content accessible for Cl (equal to the water-loss or connected porosity if no anion exclusion occurs), C : porewater concentration, D_p : pore diffusion coefficient, $D_e = \theta D_p$: effective diffusion coefficient, a : radius of the core, r : space coordinate, and t : time.

The containers were gently rotated throughout the experiment to ensure complete mixing of the experiment solution. Thus, mixing of the fluid surrounding the core is much faster than the (expected) diffusion within the pores of the rock. It is then justified to assume that the solutes diffusing out of the core spread quickly within the surrounding experiment solution such that their concentration is uniform. In this case, the boundary condition at $r = a$ (i.e. at the interface of the core and the experiment solution) becomes:

$$V_w \frac{\partial C_w}{\partial t} = -AD_e \left.\frac{\partial C}{\partial r}\right|_{r=a} \qquad \text{(Equation 6-2)}$$

where V_w : volume of the experiment solution surrounding the core, $C_w = C(r = a,t)$: concentration in the experimental solution, $A = 2\pi aL$: cylindrical outer surface of the core, and L : length of the core. At $r = 0$, a zero gradient boundary condition applies. Initially, the concentration in the surrounding experiment solution is zero, whereas for the porewater a homogeneous value is assumed of $C(r < a, t = 0) = C_i$. This last assumption is reasonable considering the generally good match between data and the simulation results of the out-diffusion experiments.

An analytical solution for the above equations describing diffusion out of a cylinder into a well-mixed reservoir is /Crank 1975/:

$$C(r,t) = C_{eq} - (C_i - C_{eq}) \sum_{n=1}^{\infty} \frac{4(\alpha+1)\exp\left(-D_p q_n^2 t/a^2\right)}{\left(4 + 4\alpha + \alpha^2 q_n^2\right)} \frac{J_0(q_n r/a)}{J_0(q_n)} \qquad \text{(Equation 6-3)}$$

Here, $\alpha = V_w/(\pi a^2 L\theta)$: ratio of the reservoir volume to the volume of porewater within the cylinder, $C_{eq} = C_i/(\alpha + 1)$: final equilibrium concentration, and the q_ns are the positive, non-zero roots of

$$\alpha q_n J_0(q_n) + 2J_i(q_n) = 0 \qquad \text{(Equation 6-4)}$$

which were obtained for each value of α numerically with a Newton-Raphson algorithm. The $J_0(x)$ and $J_1(x)$ are Bessel functions of the first kind of order zero and one, respectively. In applying the above solution, the small effect of the removal of the 0.5 mL aliquots from the reservoir solution (about 70–80 mL and 100–110 mL for core length of 120 mm and 190 mm, respectively) on the transient phase is neglected. However, this effect was accounted for when calculating the initial concentration C_i from the final equilibrium concentration C_{eq} and the corresponding mass balance.

6.2 Diffusion coefficient of chloride

As discussed in Chapter 4, the effect on the transport properties of the rocks by the drilling process and stress release are minimal. This justifies the assumption that solute transport across the drillcore samples is dominated by diffusion also for the remaining originally saturated porewater samples. Modelling of the time series data for dissolved Cl^- of the investigated porewater samples revealed that the only transport mechanism that can adequately describe equilibration between the porewater and the surrounding experiment solution is diffusion. Equilibrium conditions with respect to Cl^- concentrations in the experiment solution and the remaining porewater were commonly achieved within about 50 to 80 days of the total out-diffusion time of more than 100 days (Figure 6-1). The obtained pore-diffusion coefficients for $Cl^-$are tabulated in Table A-2 and the model fits graphically reproduced in Figures A-1 to A-5.

In the rocks of the footwall bedrock s.l., the pore diffusion coefficients for Cl^- are largely independent of rock type and the sample depth (Figure 6-2). For all rocks they vary within about a factor of 4 between 5.2×10^{-11} m^2/s and 2.3×10^{-10} m^2/s. The average pore diffusion coefficient of Cl^- for the metagranite to granite rocks is 1.2×10^{-10} m^2/s ± 0.40×10^{-10} m^2/s (n = 21), for the granodiorite to tonalite rocks 8.1×10^{-11} m^2/s (n = 1), for

the aplitic granite 9.4×10^{-11} m^2/s ± 4.2×10^{-11} m^2/s (n = 5), and for thefine-grained granite 1.1×10^{-10} m^2/s ± 0.38×10^{-10} m^2/s (n = 3) at a temperature of 25°C. No correlation is established between the chloride pore diffusion coefficient and the sample depth and the same range of diffusion coefficients is common at all depth intervals (Figure 6-2). Because the water-loss porosity of the modelled samples shows no correlation with depth, but is rather homogenously distributed between about 0.23 and 0.53 wt.% (Figure 6-2), there is also no trend between the effective diffusion coefficient for Cl^-, $D_e = \theta D_p$, and the sample depth. For the rocks in the footwall bedrock s.l. the effective diffusion coefficient values for Cl^- at 25°C vary between 1.6×10^{-13} and 9.0×10^{-13} m^2/s for all samples (Table A-1).

The lack of any depth dependence of these parameters in the rocks of the footwall bedrock s.l. is additional supporting evidence that the samples did not suffer from significant perturbations induced by stress release because a positive correlation with depth would be expected in such a case.

From the hanging wall bedrock s.l. pore diffusion coefficients for Cl^- are only available for meta-granite to granodiorite rock samples. Pore diffusion coefficient for Cl^- of these samples display a similar variation compared to the equivalent rock type from the footwall bedrock s.l. and range between 4.6×10^{-11} m^2/s and 1.7×10^{-10} m^2/s and average at a slightly lower value of 9.0×10^{-11} m^2/s ± 0.33×10^{-11} m^2/s (n = 19). The greatest variation in the pore diffusion coefficient occurs in samples collected next to each other, or within a few metres as observed in the depth interval covering the deformation zone ZFMF1 between about 447–497 m depth (Figure 6-2). A similar distribution with depth is also obtained for the water-loss porosity of the modelled samples (Figure 6-2). Consequently, the effective diffusion coefficient for Cl^-, $D_e = \theta D_p$, shows the greatest variation in the rocks collected from the deformation zone ZFMF1 in the hanging wall bedrock s.l. (Table A-1).

Figure 6-3 shows the relationship between the effective diffusion coefficient $D_e = \theta D_p$ of Cl^- at 25°C and the water-loss porosity of the corresponding rock samples. In the rocks from the footwall bed-rock s.l., no trend is established between these two parameters for any of the rock types (Figure 6-3, top-left). In contrast, a tendency is observable towards higher diffusion coefficients with increasing proximity of the sample to a water-conducting fracture in the borehole (Figure 6-3, bottom-left). No such trend seems developed in the rocks of the hanging wall s.l. (Figure 6-3, right) where most of the samples come from deformation zones. In this case, the limitation of borehole investigations to the 3-dimensional distribution of structural features has to be accounted for.

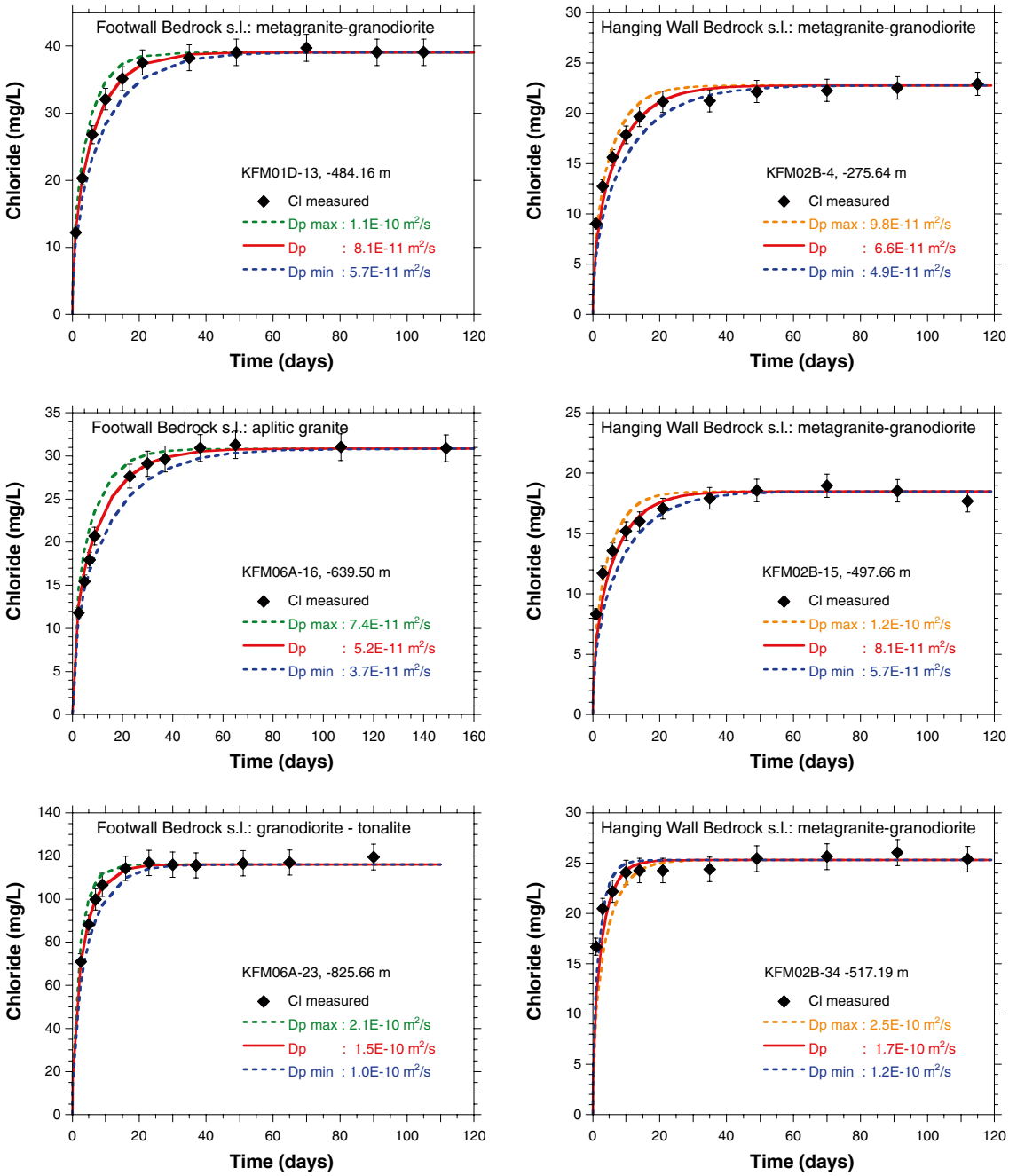

Figure 6-1. *Model fits to the measured chloride time-series data of the out-diffusion experiments. The examples show the best-fit curves (red) delivering the pore diffusion coefficient, D_p, for chloride at 25°C. On the left D_{p-Cl} is shown for different rock types in the footwall bedrock s.l. and on the right of samples from outside (KFM02B-4) and within (KFM02B-15, KFM02B-34) the deformation zones ZFMA2 and ZFMF1 in the hanging wall bedrock s.l. The uncertainty range (D_p min and D_p max) is given by a factor of 2 around the best-fit value.*

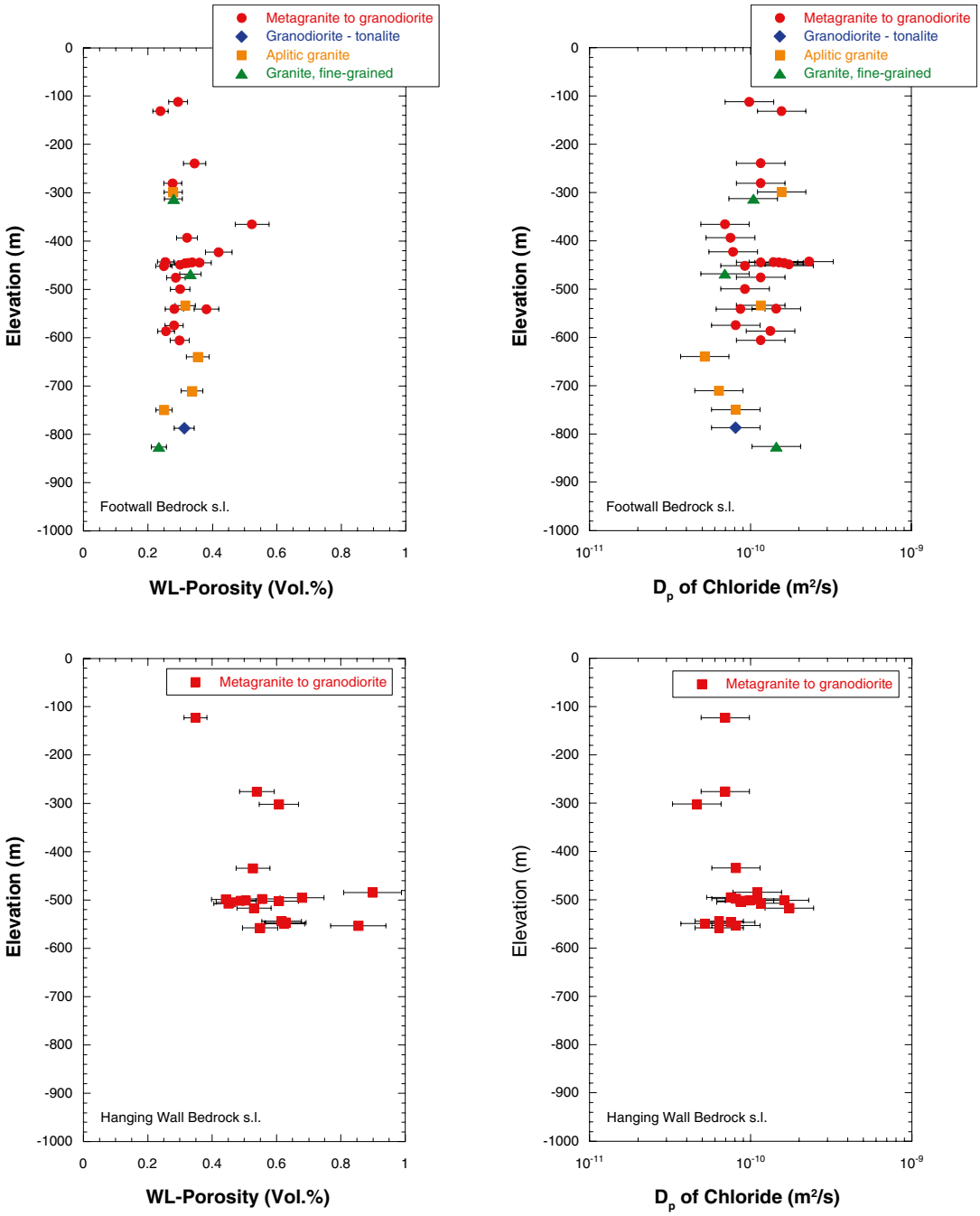

Figure 6-2. *Pore diffusion coefficients of chloride at 25°C (right) and water-loss porosity of corresponding samples (left) as a function of rock type and elevation of porewater samples for the rocks from the footwall bedrock (top) and the hanging wall bedrock s.l. (bottom). Error bars indicate ±10% for the water-loss porosity of the large size core samples and the uncertainty range for the pore-diffusion coefficients given by a factor of 2 around the modelled best fit to the measured data (see text). See Figure 2-3 for allocation of footwall bedrock s.l and hanging wall bedrock s.l.*

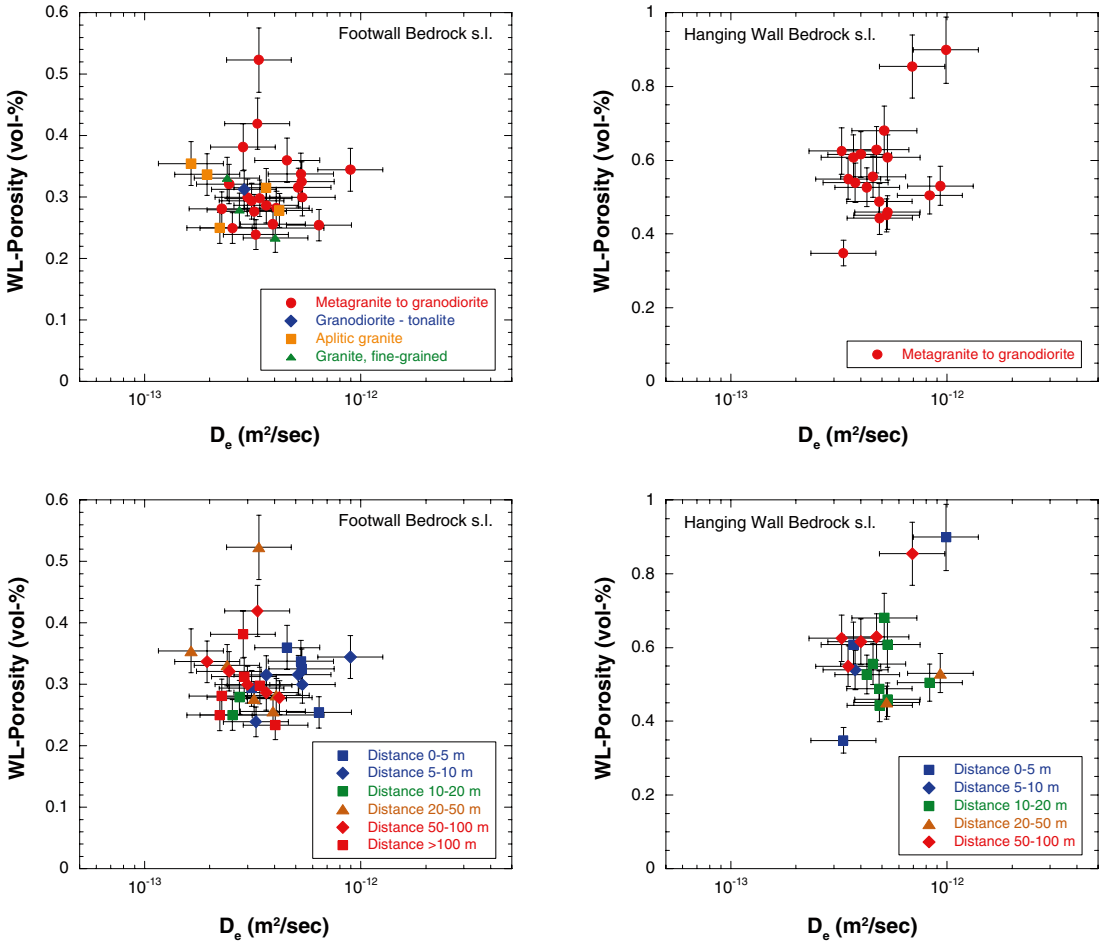

Figure 6-3. *Effective diffusion coefficient of chloride at 25°C versus the water-loss porosity of corresponding large size core samples as a function of rock type (top) and distance of the porewater sample to the next water-conducting fracture (bottom) for the rock samples from the footwall bedrock s.l. (left) and from the hanging wall bedrock s.l. (left). Error bars indicate the uncertainty range of D_e given by the difference of a factor of 2 around the best fit for D_e (see text) and ±10% for the water-loss porosity of the large size core samples. See Figure 2-3 for allocation of footwall bedrock s.l and hanging wall bedrock s.l.*

Figure 6-4 shows a comparison of effective diffusion coefficients derived from the present Cl out-diffusion experiments and effective diffusion coefficients from /Selnert et al. 2008/ determined by through-diffusion experiments using ^{3}H (HTO) as tracer. For the data derived from modelling HTO break-through curves of the through-diffusion experiments /Selnert et al. 2008/ used core sections of mainly 3 cm lengths and estimated an uncertainty of ±25% for the individual D_e values. As can be seen from Figure 6-4 (left) there is good agreement within the uncertainty band for most samples of the footwall bedrock s.l. independent of rock type and depth. A somewhat different picture arises for the hanging wall bedrock s.l.. For samples at around 275 m depth, the effective diffusion coefficient from HTO through-diffusion experiments is almost two orders of magnitude higher than those determined by Cl^- out-diffusion. On the other hand, a few HTO through-diffusion samples between about 200–500 m depth yield significantly lower effective diffusion coefficients compared to the Cl^- out-diffusion. Whereas the

low values seem to be related to a highly tectonised zone that was not sampled for porewater investigations, the lower diffusion coefficients compared to the Cl^- out-diffusion values are not well understood. There is no doubt, however, that the more heterogeneous pattern obtained for rock transport properties in the hanging wall bedrock s.l. reflects the higher degree of deformation in this area.

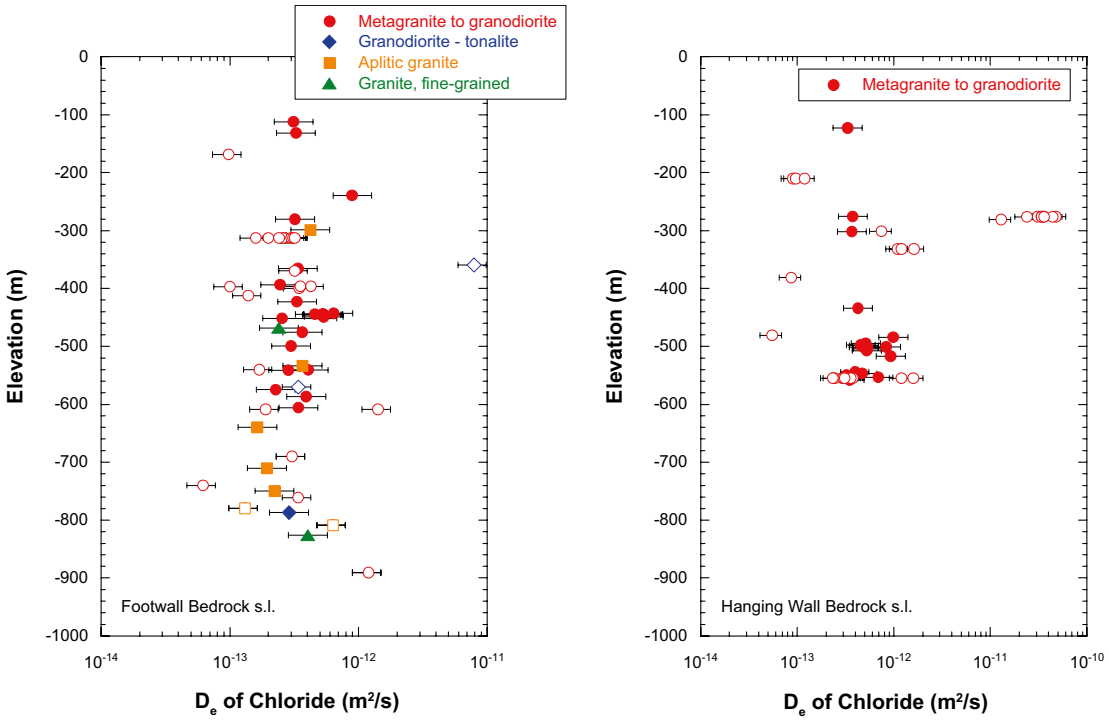

Figure 6-4. *Effective diffusion coefficients of the rocks from the footwall bedrock s.l. (right) and the hanging wall bedrock s.l. versus elevation and derived by Cl-out-diffusion (closed symbols, this study) and HTO through-diffusion (open symbols, /Selnert et al. 2008/). Error bars indicate the uncertainty range for the Cl^- diffusion coefficients given by a factor of 2 around the modelled best fit to the measured data and ± 25% for the HTO diffusion coefficients. See Figure 2-3 for allocation of footwall bedrock s.l and hanging wall bedrock s.l.*

The general agreement between independently derived diffusion coefficients supports the derivation of the porewater composition and their interpretation in a palaeohydrogeological context because this is based on an accurate derivation of the rock transport properties. Furthermore, the agreement in effective diffusion coefficients derived by HTO through-diffusion and Cl^- out-diffusion for samples from borehole KFM02B from a depth around 550 m (Figure 6-4, right) also supports the conclusion made from the drilling fluid contamination study described in Chapter 4.

6.3 Scenarios of diffusive exchange

With diffusion being identified as the dominant solute transport process in the rock matrix, the chemical and isotopic concentration of the porewater sample can be brought into an evolutionary context as a function of time (or space) using the fracture groundwaters as boundary conditions for the diffusion domain. Figure 6-5 illustrates schematically the concentration change induced in a pore-water sample as a function of distance to the nearest water-conducting fracture and for time periods of 2,000, 6,000, 12,000 and 30,000 years. In such a hypothetical system this could, for example, approximately correspond to the time span covered by present day type Baltic Sea water conditions (2,000 years), the time of ingress of Littorina Sea water (6,000 years), and time periods of glacial water infiltration during the last glaciation (12,000 and 30,000 years), respectively. A pore-diffusion coefficient for chloride, D_{pCl}, at 25°C of 1.29×10^{-10} m²/s was used for the calculations, corresponding about to the average of the measured values for the metagranite to granodiorite rocks comprising the footwall bedrock. Note that at present day *in situ* temperatures of 10°C the D_{pCl} would be reduced by about a factor of 1.5 and the distances shown in Figure 6-5 and given below would be reduced by about a factor of 1.2 ($\sqrt{1.5}$).

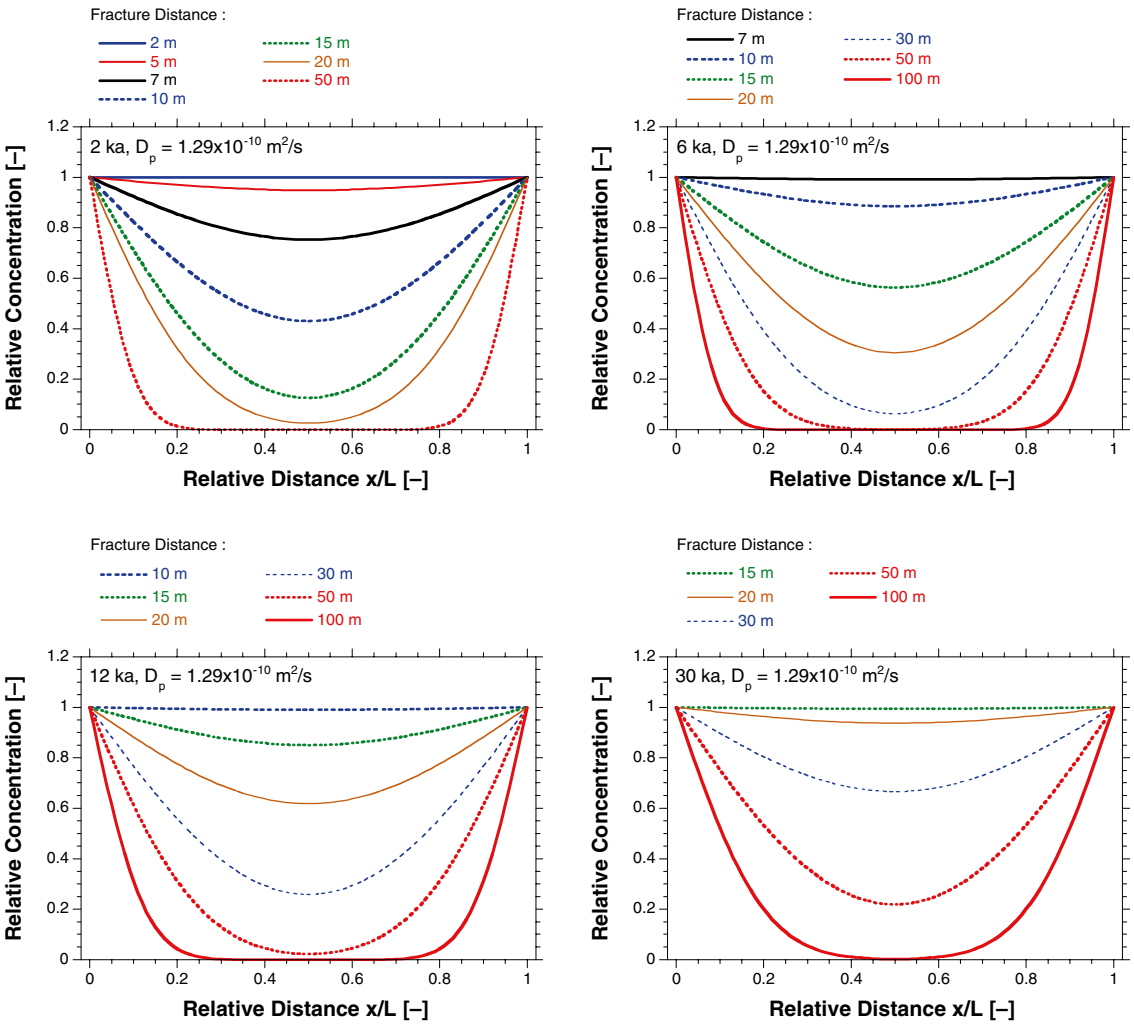

Figure 6-5. *Relative concentration changes induced on the porewater composition of a sample located at different distances between two water-conducting fractures for a time period of 2,200, 6,000, 12,000 and 30,000 years. A pore-diffusion coefficients for chloride of $D_{pCl,} = 1.29 \times 10^{-10}$ m²/s was used in the calculations, corresponding to about the average of the measured values for the metagranite to granodiorite rocks comprising the footwall bedrock.*

From Figure 6-5 it can be seen, for example, that any signature present some 2,000 years ago in a porewater sample located 1 metre or less from a fracture above and below (i.e. distance between fractures = 2 m or less) would be completely exchanged by the signature prevailing in the fractures since this time (Figure 6-4, top-left) given that the fracture groundwater composition remained constant over this time period. A signature of a once established chloride content of Littorina water (e.g. 6,500 mg/L) would be completely diluted in a porewater sample located 3.5 metres or less from a fracture above and below (i.e. distance between fractures = 7 m or less) or reduced by about 90% (i.e. to about 650 mg/L) in a porewater sample located 5 metres from a fracture above and below, if fresh water would have circulated in both these fractures over the last 6,000 years (Figure 6-5, top-right).

Similarly, a once established glacial isotope signature in a porewater sample (e.g. glacial meltwater with a $\delta^{18}O$ of –21‰ VSMOW) would be completely erased over a distance of 5 metres or less from a fracture, changed to about 40% of the fracture-groundwater value (e.g. to about –16.6‰ VSMOW with a fracture groundwater of –10‰ VSMOW) over a distance of 10 metres, and only be preserved at a distance of more than about 25 metres between the two fractures, assuming constant isotope composition in the fracture groundwater over 12,000 years of interaction (Figure 6-5, bottom-left). Under the conditions used in these scoping calculations, signatures that were developed more than 30,000 years ago would be preserved only in a porewater sample located at least 50 m away from the nearest water-conducting fracture.

All further interpretations of porewater data and their comparison with present day and past fracture groundwater should be consistent with such basic type scenarios. However, it has to be borne in mind: 1) the possible limitations of a one dimensional interpretation of the borehole data, and 2) that in the scoping calculations constant fracture groundwater composition and a constant removal of the solute entering the fracture groundwater from the porewater are assumed. Both these simplifications might not apply to the natural occurrences at the Forsmark investigation site. This is because steeply dipping fractures close to a collected porewater sample might not be detected by the borehole, but could still affect the porewater sample data.

7 Porewater composition

Concentrations of chemically conservative elements dissolved in the matrix porewater were derived by non-destructive out-diffusion experiments and mass balance calculations using water-content data of the investigated rock samples (cf. Section 3.2.2). For chemically reactive elements, additional geochemical modelling is required to account for mineral reactions during the experiment.

Non-destructive experiments are a prerequisite for matrix porewater charactersiation because of the different fluid reservoirs that exist in crystalline rocks. Besides the porewater in the connected pore space of the rock matrix, the fluid trapped in mineral fluid inclusions is of importance in this context because of its often very high salinity. During destructive extraction techniques, the salts of such inclusions will be released and inhibit the derivation of the matrix porewater concentrations even for conservative elements. The out-diffusion experiments used here to derive the porewater concentrations were carefully tested for such possible perturbations and found to be free of any measurable influence by fluid inclusion leakage (cf. /Waber and Smellie 2006/).

For the Forsmark investigations site, a total of 48 samples from boreholes KFM01D, KFM06A (lower part; fracture domains FFM01 and FFM06), KFM08C and KFM09B from the footwall bedrock s.l. were subjected to out-diffusion experiments and for 45 the final experiment solution was analysed for its chemical and isotopic composition. Of these drillcore samples 31 consist of metagranite to granodiorite, 3 of granodiorite to tonalite, 6 of aplitic granite and 3 of fine-grained granite. From borehole KFM02B in the hanging wall bedrock s.l. (fracture domains FFM03 and FFM01, deformation zones ZFMA3, ZFMA2 and ZFMF1) and including the upper part of KFM06A (comprising fracture domain FFM02 and the upper part of fracture domain FFM01), 46 samples were subjected also to the experiments and all of them were analysed. Except for 2 fine-grained granite samples, all samples from the hanging wall bedrock s.l. consist of metagranite to granodiorite. The complete datasets of the out-diffusion experiments can be found in /Waber and Smellie 2005, 2007, 2009/.

7.1 Chloride in matrix porewater

Chloride concentrations in matrix porewater of the rocks at the Forsmark investigation site cover a large range of about 600 mg/kg_{H2O} to more than 14,600 mg/kg_{H2O} (Table A-3). They show a distinction between the footwall bedrock s.l. and the hanging wall bedrock s.l. (cf. Figure 2-3 for allocation of footwall bedrock s.l. and hanging wall bedrock s.l.). The footwall bedrock s.l. is characterised by low transmissivity and low frequency of water conducting fractures, whereas the hanging wall bedrock s.l. are characterised by high transmissivity and a high frequency of water conducting fractures.

In spite of differences related to the occurrence of the five sampled boreholes with respect to the major deformation zones, there are also some general similarities between the porewater compositions in the rock matrix and their spatial distribution and relation to structural features in these boreholes:

- In all boreholes, porewater Cl^- concentrations generally increase towards greater depth, but the concentrations differ greatly between porewater in the footwall bedrock and the hanging wall bedrock and domain FFM02.
- In all boreholes, changes in the porewater Cl^- concentrations are related to the frequency and transmissivity of water-conducting fractures as observed by differential flow logging (PFL) and injection tests (PSS) as seen from Figures 7-1 to 7-3.
- In all boreholes the first increase in the porewater Cl^- concentration to values higher than 4,000 mg/kg_{H2O} is associated with a distinct change in the chemical type of the porewater (cf. Section 6.2.1).
- In all boreholes localised zones of higher transmissivity and frequency of water-conducting fractures might lead to a deviation from the general patterns given by the porewater compositions.

The relation between porewater Cl^- concentrations, or other natural tracers such as the porewater oxygen and hydrogen isotope composition (Section 7.3) and the frequency and transmissivity of water-conducting fractures, is not a simple one and cannot be described by a simple correlation. This is because the exchange between porewater and fracture groundwater occurs by diffusion. Unlike mixing, where the different concentrations of two (or more) fracture groundwaters are immediately equilibrated, the slow exchange by diffusion between porewater and fracture groundwater might not have attained equilibrium at the time of sample collection and a transient state is still prevailing. The relation between porewater Cl^- concentrations and frequency and transmissivity of water-conducting fractures is thus not a simple correlation between only two independent variables. Much more the relationship depends on a) the initial condition in the matrix, b) the time period of constant boundary conditions (i.e. fracture-groundwater concentration), c) the diffusion properties of the rock matrix, and d) the distance from the porewater sample to a water-conducting fracture. Depending on the length of the time periods with constant fracture-groundwater concentrations, and the distance of the porewater sample to the conducting fracture, the time lag induced by the exchange by diffusion might also result in the superposition of successive different concentrations in the fracture groundwater (e.g. dilute meteoric followed by glacial and brackish-marine water).

A simple correlation between porewater Cl^- concentrations and frequency and transmissivity of water-conducting fractures cannot, therefore, be expected and the data have to be interpreted by taking all the dependences into account. In addition, it has to be kept in mind that the borehole information is limited with respect to the occurrences of water-conducting fractures and their detection because the drillcores only provide a one-dimensional section of a rock volume, i.e. along the borehole length. Nevertheless, the interpretation of porewater data can provide valuable information about the palaeohydrogeological evolution of a site over the last few thousand to hundreds of thousands of years that might not any longer be derived from the dynamic fracture groundwater system.

7.1.1 Spatial distribution of Cl^- concentrations in porewater

In the footwall bedrock s.l., most of the porewater Cl^- concentrations are between 2,000 and 3,500 mg/kg_{H2O} down to about 700 m borehole length (about 540 m depth) in borehole KFM01D (Figure 7-1) and down to about 420 m (350 m depth) in borehole KFM08C (Figure 7-2). Porewater Cl^- concentrations in these shallow to intermediate depth intervals are rather constant and are similar in depth intervals characterised by a high frequency of water-conducting fractures and correspondingly depth intervals with a low frequency of water-conducting fractures as, for example, in borehole KFM01D between 100–200 m and 200–700 m borehole length, respectively (Figure 7-1). Similar observations have been noted in borehole KFM08C at shallow to intermediate depths (Figure 7-2). Towards the end of both these boreholes the Cl^- concentrations increase to about 5,700 mg/kg_{H2O} in borehole KFM01D and to about 10,600 mg/kg_{H2O} in borehole KFM08C. Whereas the increase is smooth in borehole KFM01D, it is more irregular in borehole KFM08C where the highest porewater Cl^- concentration recorded (about 14,600 mg/kg_{H2O}) already occurs at 750 m borehole length (623 m depth).

Porewater Cl^- concentrations between 2,000 and 3,500 mg/kg_{H2O} are also observed in borehole KFM06A in the footwall bedrock s.l. below deformation zone ENE0060A in fracture domain FFM01 (cf. Figure 2-3) between about 400–760 m borehole length (340–640 m depth, Figure 7-3). At these intermediate depths only very few water-conducting fractures were encountered in this borehole as in the other two ones. Towards greater depth, porewater Cl^- concentrations in borehole KFM06A increase irregularly to a maximum of about 11,400 mg/kg_{H2O}.

Porewater investigations in borehole KFM09B focussed on a narrow depth interval below a water-conducting, highly porous episyenite zone at around 570 m borehole length (about 440 m depth). The porewater of the altered and fractured metagranite sample adjacent to the episyenite zone has a Cl^- concentration of about 10,500 mg/kg_{H2O} (Figure 7-2). Within only one metre from the episyenite into the intact metagranite rock matrix, the Cl^- concentration in the porewater dropped to about 4,800 mg/kg_{H2O}, and this concentration is maintained over the next two metres before it increases gradually to about 8,600 mg/kg_{H2O} at a distance of 13 metres from the contact. From the contact to that depth the hydraulic transmissivity derived from single-hole injection tests (PSS, /Gustavsson et al. 2006/) is below the detection limit of this method (Figure 7-2).

In the hanging wall bedrock s.l., porewater Cl^- concentrations are generally lower compared to those in the footwall bedrock s.l. Chloride concentrations are mainly below 1,500 mg/kg_{H2O} down to the bottom of borehole KFM02B at 573 m borehole length (about 578 m depth) and also down to 300 m borehole length (about 250 m depth) in the upper part of borehole KFM06A (Figure 7-3). These depth intervals are characterised by a high frequency of highly transmissive fractures in fracture domains FFM03 and FFM01, in particular associated with the two major gently dipping deformation zones ZFMA2 and ZFMF1 (borehole KFM02B), and equally transmissive parts in the upper part of borehole KFM06A, mostly in fracture domains FFM02 and FFM01 associated with the steeply dipping deformation zones ENE0060B and ENE0060A. In borehole KFM02B this pattern is interrupted with increased contents up to 3,000 mg/kg_{H2O} between about 430–460 m borehole length (about 417–445 m depth), which coincide with an increased accumulation of water-conducting fractures and the intersection of deformation zones ZFMA2 and ZFMF1 (Figure 7-3). In borehole KFM06A a similar irregular behaviour of chloride occurs between 250–400 m borehole length (245–340 m depth), the interval with a high frequency of water-conducting fractures mainly related to the steeply dipping deformation zones ENE0060B and ENE0060A (Figure 7-3).

7.1.2 Relation between porewater and structural features

As mentioned above the composition of rock matrix porewater depends on the time of interaction with a specific fracture groundwater composition and the distance of the porewater sample to the nearest water-conducting fracture. In order to allow a comparison of porewater compositions and structural features among different boreholes from the footwall bedrock and the hanging wall bedrock, the porewater Cl-concentrations are plotted in Figure 7-4 as a function of elevation (i.e. metres above sea level).

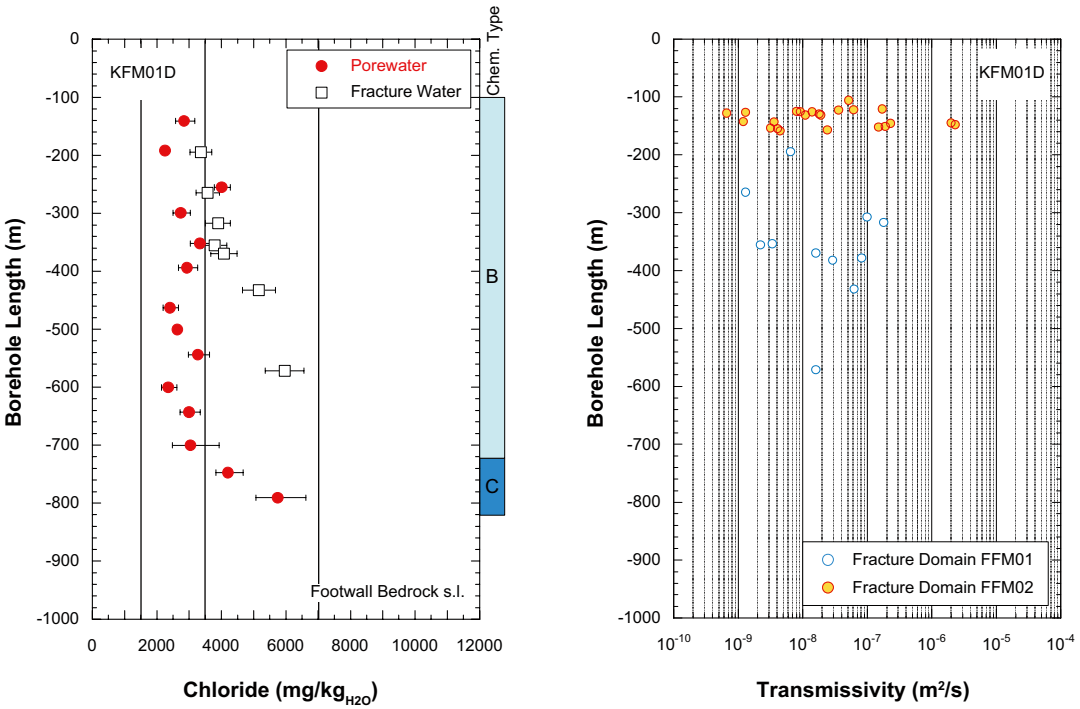

Figure 7-1 Borehole KFM01D, footwall bedrock s.l. *Left: chloride concentration in porewater (closed symbols) and fracture groundwater (open symbols) as a function of sampling depth. Right: measured hydraulic transmissivity of water-conducting fractures (PFL data from /Väisävaara et al. 2006a/) in relation to fracture domains and deformation zones (data from /Olofsson et al. 2007/). General chemical types of porewater are: B = dilute Na-Ca-HCO_3 type, C = brackish Na-Ca-Cl-(HCO_3) type; vertical lines indicate concentration ranges used in the site visualisation model /Smellie et al. 2008/.*

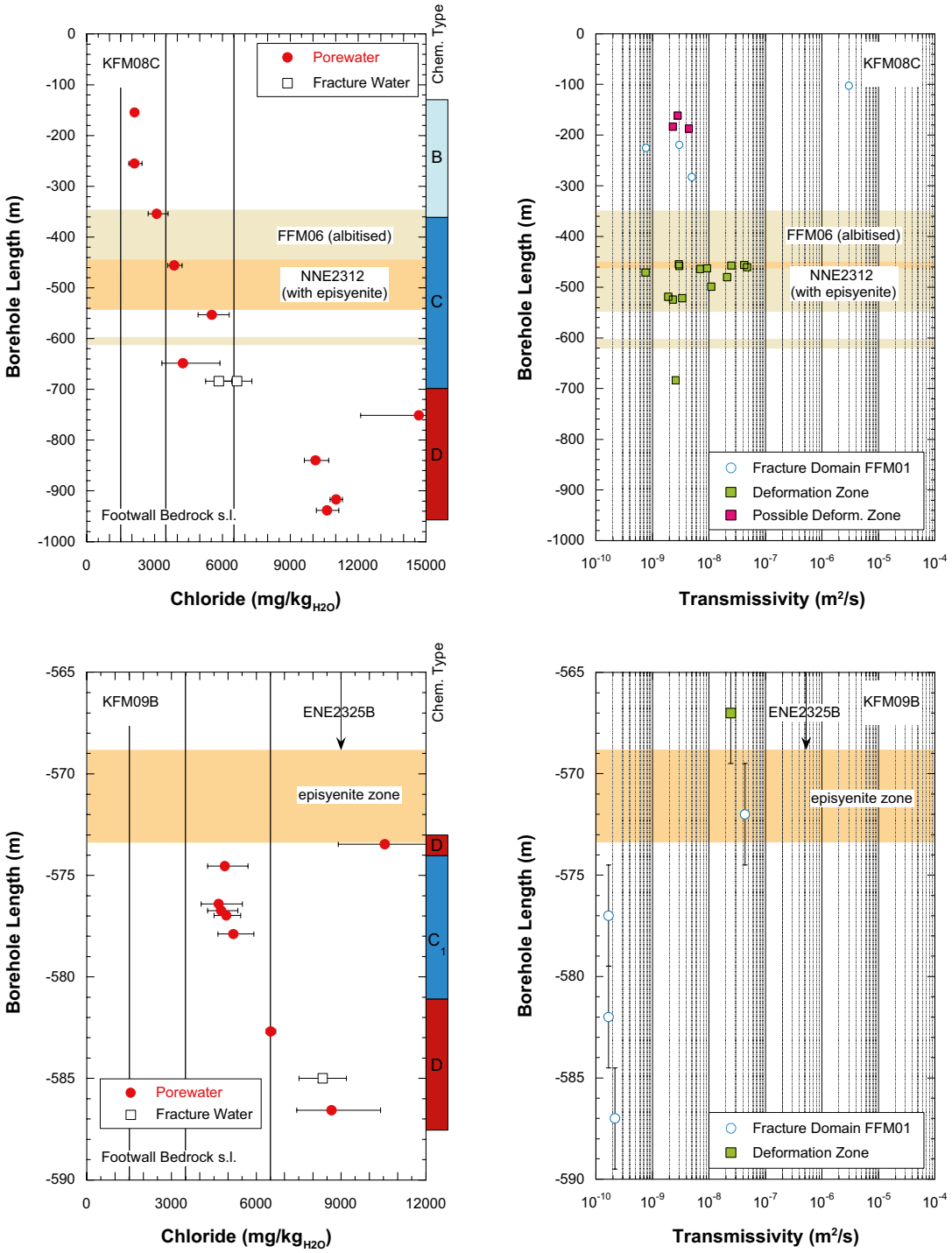

Figure 7-2. *Boreholes KFM08C (top) and KFM09B (bottom), footwall bedrock s.l.: Chloride concentration in porewater (closed symbols) and fracture groundwater (open symbols) as a function of sampling depth (left) and compared to the measured hydraulic transmissivity of water-conducting fractures (right, PFL data for KFM08C from /Väisävaara et al. 2006b/, PSS data for KFM09B from /Gustavsson et al. 2006/) in relation to fracture domains and deformation zones (data from /Olofsson et al. 2007/). General chemical types as in Figure 7-1; vertical lines indicate concentration ranges used in the site visualisation model /Smellie et al. 2008/.*

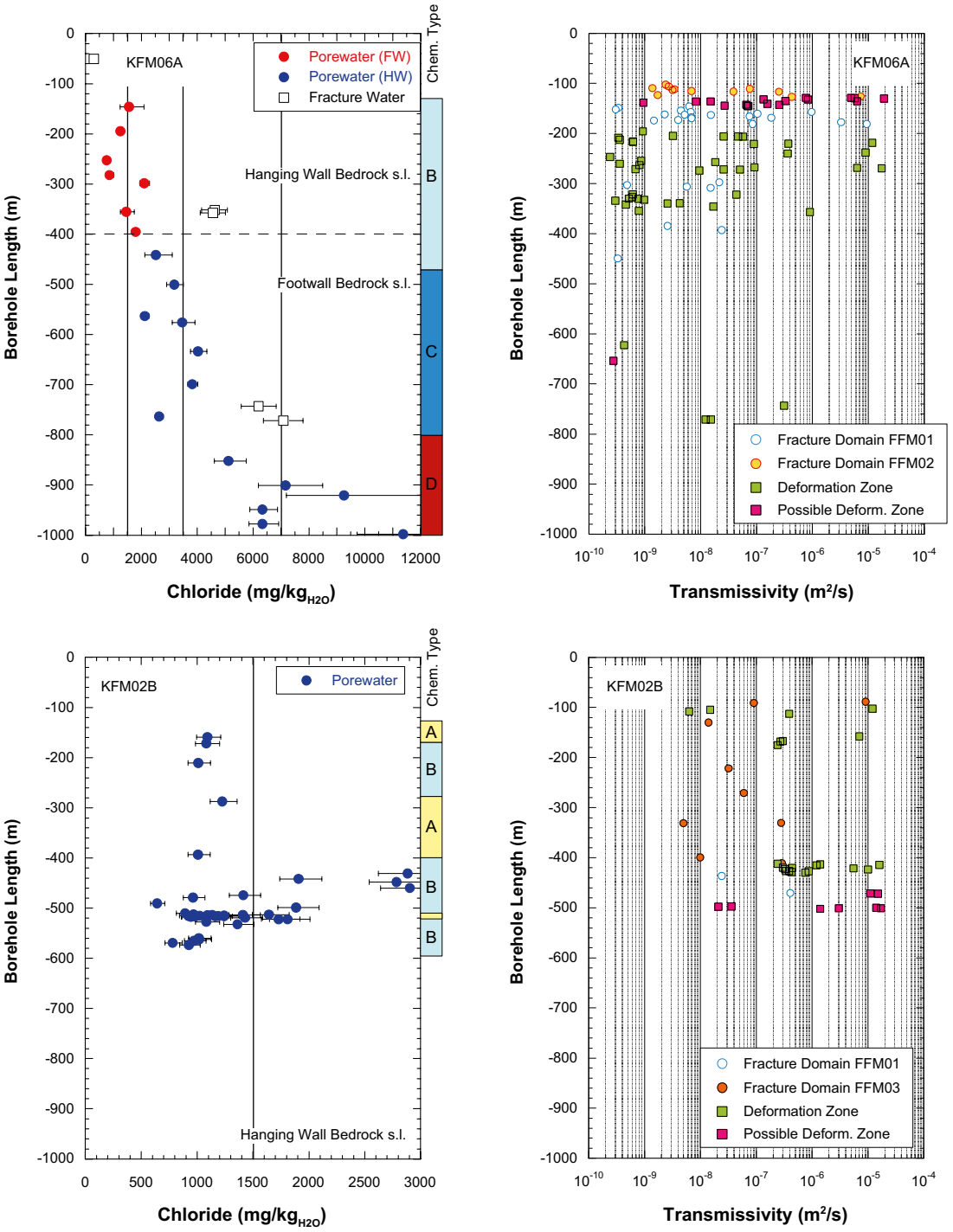

Figure 7-3. *Borehole KFM06A (top) and and KFM02B (bottom), hanging wall bedrock s.l. and footwall bedrock s.l., respectively: Chloride concentration in porewater (closed symbols) and fracture groundwater (open symbols) as a function of sampling depth (left) and compared to the measured hydraulic transmissivity of water-conducting fractures (right, PFL data from /Rouhiainen and Sokolnicki 2005, Väisäsvaara and Pöllänen 2007/) in relation to fracture domains and deformation zones (data from /Olofsson et al. 2007, Stephens et al. 2008a/). General chemical types of porewater as in Figure 7-1. See Figure 2-3 for allocation of footwall bedrock s.l and hanging wall bedrock s.l.*

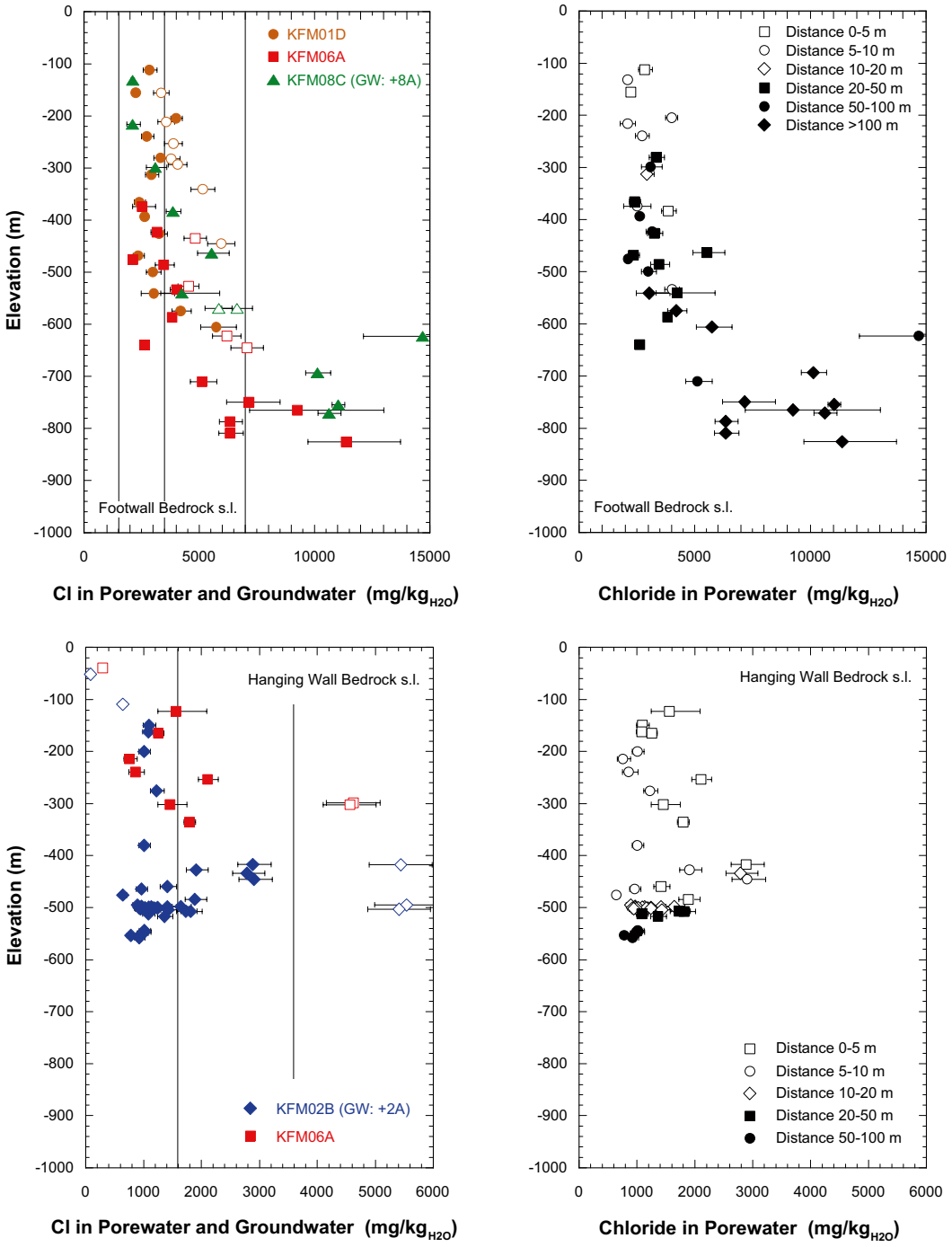

Figure 7-4. *Chloride concentration in porewater (closed symbols) as a function of the borehole from which the core sample was collected (left) and the distance between the porewater sample and the nearest water-conducting facture (right) versus elevation (m a.s.l.) for the footwall bedrock s.l. (top) and the hanging wall bedrock s.l. (bottom). Chloride concentrations of fracture groundwaters (open symbols in right panels) collected from the same boreholes are given for comparison (cf. Sicada dataset, data freeze Forsmark 2.3). See Figure 2-3 for allocation of footwall bedrock s.l and hanging wall bedrock s.l.*

In the porewater of the footwall bedrock s.l., Cl^- concentrations between 2,000 and 3,500 mg/kg_{H2O} down to about 540 m depth in borehole KFM01D and down to about 350 m depth in borehole KFM08C are largely independent of the distance between the porewater sample and the nearest water-conducting fractures as identified in the differential flow log (PFL). Similar porewater Cl^- concentrations occur in samples collected within 5 metres of the nearest water-conducting fracture as well as in samples collected more than 50 metres away from such a fracture in the borehole (Figure 7-4 top). Similar relationships occur for samples between about 340–600 m depth in borehole KFM06A.

On first sight, it seems reasonable to relate the Cl^- concentrations of porewater samples located within a few metres from the nearest water-conducting fracture to fracture groundwater influenced by Littorina and Baltic Sea waters, respectively. Indications of porewater influenced by Littornia Sea water indeed exist in samples located less than 5–10 metres from the nearest water-conducting fractures in borehole KFM01D at shallow depths down to about 200 m depth (i.e. fracture domain FFM02), and in borehole KFM06A for a sample at an intermediate depth of –373.70 m elevation in fracture domain FFM01 (Figure 7-4 top). All these samples have elevated Mg^{2+} concentrations measured in the out-diffusion experiment solution, whereas Mg^{2+} is below detection in the other experiment solutions (cf. Section 7.2.2). As pointed out by /Smellie et al. 2008/ elevated Mg^{2+} concentrations in fracture groundwater are usually indicative of a marine component (e.g. Baltic and/or Littorina Sea). However, the fact that porewater samples over much greater distances also have very similar Cl^- concentrations between 2,000 and 3,500 mg/kg_{H2O} cannot be explained in this way because a much longer time of exchange between, for example Littorina-type fracture groundwater and porewater, would be required to impose a likewise signature on the porewater. Furthermore, based on the discrete fracture network model /Fox et al. 2007/ there is also no necessity to suppose that at intermediate to greater depths the large distances observed in the boreholes between certain porewater samples and water-conducting fractures would be greatly reduced by different fracture orientations not encountered by the borehole. Therefore, the porewater data, transport properties of the rock, discrete fracture network model and Holocene palaeo-hydrology consistently indicate that the Cl^- concentrations in samples at greater distances from the nearest water-conducting fractures have evolved from old brackish fracture groundwater that circulated in the fractures long before the two presently known salinity sources, i.e. Littorina and Baltic Sea water.

From about 550–850 m depth porewater Cl^- concentrations increase to their highest values in all three boreholes in a more or less regular way. All these porewater samples come from distances of more than 20 m and most from more than 50 m from the nearest water-conducting fracture (Figure 7-4, top). This indicates that the brackish to saline signatures preserved in these porewaters have been produced a very long time ago, certainly long before the Weichselian glaciation.

Further support for the circulation of old brackish water in the fractures at shallow and intermediate depths comes from the Cl^- concentration distribution in porewaters adjacent to the porous and conductive episyenite zone in Borehole KFM09B. The strong decline of the porewater Cl^- concentrations to less than half of that of the porewater sample adjacent to the episyenite within a distance of only one metre indicates that the system is in a transient state on the decametre scale (Figure 7-2). It further shows that the circulation of saline water in the episyenite, which created the Cl^- signature in the porewater sample adjacent to the episyenite, did not occur over a very long time period, otherwise it would have to extended a greater distance into the rock matrix. Fracture groundwater sampled from the episyenite zone in the neighbouring borehole KFM09A has a Cl^- concentration of 14,800 mg/kg_{H2O} (cf. Sicada dataset, data freeze Forsmark 2.3). This is about 30% higher than the Cl^- concentration in the porewater adjacent to the episyenite (10,500 mg/kg_{H2O}) and about three times the concentration of the porewater samples following at greater depths below (about 4,800 mg/kg_{H2O}). The porewater data along this profile thus clearly indicate that prior to this still present saline water a dilute to brackish water must have circulated in this fracture. Based on the distances to the water-conducting zone and the fact that the out-diffusion experiment solutions of these samples are free of Mg^{2+}, this brackish fracture groundwater cannot have been of Littorina-type origin, but must have been considerably older. Furthermore, the circulation of the old brackish fracture groundwater must have lasted for a considerable time period as indicated by the decrease in Cl^- concentration in the porewater from the deepest sample some 13 metres from the contact to the episyenite (about 8,600 mg/kg_{H2O}) to those some 3–4 metres from the contact (about 4,800 mg/kg_{H2O}). The presence of a much older brackish non-marine fracture groundwater is in accordance with the conceptual model presented in /Smellie et al. 2008/.

A different picture arises for the porewater samples in the hanging wall bedrock s.l., here represented by porewater samples from borehole KFM02B and the upper part of KFM06A (cf. Figure 2-3 for allocation of footwall bedrock s.l. and hanging wall bedrock s.l.). As a consequence of the high frequency of water-conducting fractures the porewater samples down to 520 m depth in borehole KFM02B and down to 340 m depth in borehole KFM06A come from a distance of less than 10 m from the nearest water-conducting fracture (Figure 7-4, bottom). Only the deepest samples in borehole KFM02B belonging to fracture domain FFM01, i.e. outside the influence of deformation zones, appear to be further distant from the nearest water-conducting fracture. However, this might not reflect the real situation because no differential flow logging could be performed along the final 10 m of this borehole due to instrumental limitations /Väisäsvaara and Pöllänen 2007/.

Porewater samples with highest Cl^- concentrations up to 3,000 mg/kg_{H2O} between about 417–445 m depth adjacent to deformation zone ZFMA2 in borehole KFM02B are also located very close to the nearest water-conducting fracture. In addition, these samples have the overall highest Mg^{2+} concentrations measured in the out-diffusion experiment solutions (cf. Section 7.2.2) suggesting a considerable influence of Littorina-type fracture groundwater. Magnesium concentrations in the experiment solutions above the detection limit are also present in most other samples. Combined with the proximity of the samples to the nearest water-conducting fracture this suggests that a Littorina-type component is present in most of these porewaters.

Based on the Cl^- concentrations alone it cannot be decided if the observed porewater Cl^- concentrations of mainly less than 1,500 mg/kg_{H2O} are a remnant of a porewater that was once in equilibrium with Littorina Sea water of the maximum salinity stage (Cl^- of about 6,500 mg/L) and which has been continuously diluted since then, or if there is still a dilute pre-Littorina signature present that has not been completely overprinted by the Littorina Sea water. This is complicated by the fact that the porewater Cl^- concentrations reached during the Littorina Sea stage are not known. Based on the calculations shown in Section 6.3 an equilibriation of the porewater with the fracture groundwater of the maximum salinity stage of the Littorina Sea seems not plausible for most samples. This is because for a sample at a distance of 2.5 metres from a water-conducting fracture (i.e. fracture distance of 5 m) such interaction would have required more than 2,000 years for equilibration while the maximum salinity stage of the Littorina Sea lasted only for about 500 years /Söderbäck 2008/. As shown in Section 7.3, the oxygen and hydrogen isotope composition of the porewater indicates, however, that a component of meteoric water of pre and post Littorina stage origin is still preserved in these porewaters and as a function of sample depth.

7.1.3 Relation between porewater and fracture groundwater

In the footwall bedrock s.l. the Cl^- concentrations in porewater and nearest fracture groundwater are in a transient state in the shallow and intermediate zone except for two samples from borehole KFM01D at –204.6 m and –280.5 m elevation (Figure 7-4, top left). As shown in section 7.3, these two porewaters differ greatly from the fracture groundwater in their isotope composition suggesting that the total porewater composition is in a transient state with the surrounding fracture groundwaters. Generally, the fracture groundwaters down to about 500 m depth have higher Cl^- concentrations compared to the porewater and contain a large component of Littorina-type water /Smellie et al. 2008/. Between 500–650 m the Cl^- concentrations in porewater and fracture groundwater become more similar due to the general concentration increase in the porewater. Below 650 m depth no more fracture groundwater data are available for comparison due to the scarcity of water-conducting fractures at these levels.

In the hanging wall bedrock s.l. a transient state is established for the Cl^- concentrations between porewater and fracture groundwater (Figure 7-4, bottom left). Fracture groundwater at shallow levels down to 100 m depth (i.e. fracture domain FFM02 in the upper part of borehole KFM06A) has lower Cl^- concentrations compared to the porewaters just a few metres below in the upper part of fracture domain FFM01 in borehole KFM06A and in fracture domain FFM03 in borehole KFM02B. Between 300–500 m depth the fracture groundwaters related to deformation zones ZFMA2 and ZFMF1 in borehole KFM02B and the steeply dipping deformation zone ENE0060A in borehole KFM06A then have two to three times the Cl^- concentrations contained in the porewaters.

7.2 Porewater types

7.2.1 Correction for reactions during the experiment

The general chemical type of a pore (or fracture) water reflects to some extent the geochemical evolution of the water including possibly involved reactions such as mineral dissolution and bacterially mediated redox reactions as well as possible mixing of different water types. For the porewater, the chemical type also carries information about the palaeohydrochemical evolution of the site.

The concentrations of chemically reactive elements in the experiment solution analysed at the conclusion of an out-diffusion experiment are the sum of the concentration of a specific element in the porewater and the contribution to this element by mineral dissolution reactions during the experiment. Estimates of the reactive element inventories from dissolution reactions were obtained by modelling these geochemical processes during the experiment as a weathering process of a granitic rock with a modal composition and mineral chemistry similar to that of the metagranite-granodiorite rocks of the Forsmark candidate area. These calculations are of special interest with respect to the Mg^{2+} concentrations released by weathering reactions during the experiment and to the potential use of the Mg^{2+} concentrations of the *in situ* porewater as an indicator for any influence by Littorina and/or Baltic Sea water on the porewater to the same degree of success accomplished for the fracture groundwaters /Smellie et al. 2008/. Microprobe analyses of metagranite-granodiorite and tonalite-granodiorite samples from borehole KFM06A (samples KFM06A-7, -12 and 15) showed that biotite is the main magnesium bearing mineral phase in these rocks with magnesium contents of about 7-9 wt.%. In contrast, chlorite and epidote, which also occur in the rock matrix, are essentially free of magnesium. For the modelling a biotite composition corresponding to the measured average composition of metagranite-granodiorite and tonalite-granodiorite rocks was used.

The calculations were performed using the geochmical code PHREEQC (v. 2–13, 2006, /Parkhurst and Appelo 1999/) and the kinetic rate laws given in the database of this code. Biotite was considered as the only magnesium bearing mineral phase in the rock. Figure 7-5 shows the evolution of the cation concentration during this type of simulation as a function of time. The concentrations released by mineral dissolution after 100 days of experimental time are in the order of about 3.3×10^{-6} to 2.3×10^{-5} mol/L for all major cations. These concentrations are less than 1% of the concentrations measured in the experiment solutions and are thus within the analytical uncertainty. The Mg^{2+} concentration released from biotite by weathering the rock over 100 days at 45°C in out-diffusion experiment is calculated to be about 7.9×10^{-6} mol/L or 0.19 mg/L. The detection limit for Mg^{2+} of the ion-chromatographic technique applied to analyse the final experiment solutions was at 0.5 mg/L, except for the samples from borehole KFM02B where it has been reduced to 0.3 mg/L. This means that those measured Mg^{2+} concentrations higher than the detection limit by more than 0.2 mg/L are mainly derived from the *in situ* porewater and therefore, in a semi-quantitative way, the measured Mg^{2+} concentrations can be used to estimate the potential influence of Littorina and/or Baltic Sea water in the porewater.

In the scoping calculations, the highest concentrations are calculated for Si and Al. No secondary minerals were allowed to precipitate in the simulation and the calculated concentrations of Si and Al appear be overestimated. This is indicated by the calculated oversaturation with respect to kaolinite from 100 days onwards of experimental time. Measured concentrations of Si and Al in the final experiment solutions after 90–110 days average 10.4±2.6 mg/L (n = 79; 3.73×10^{-4} mol/L, log mol = –3.4) and 0.083±0.035 mg/L (n = 72; 3.1×10^{-6} mol/L, log mol = –5.5), respectively. The measured Si concentrations correspond to about quartz saturation and compare well with the concentrations calculated by the artificial weathering of granite (Figure 7-5). In contrast, the calculated Al concentration is more than one order of magnitude higher than that measured. This is because no secondary minerals such as gibbsite and kaolinite were allowed to precipitate during the simulation, but which are known to occur in nature and influence the experiment. In the simulated solution both these phases are oversaturated. Because Al and Si are derived from alumino-silicate and quartz dissolution, the comparison of Al and Si concentrations in the experiment solution with those calculated supports the calculated low cation concentrations. Thus, the simulations show consistently that the contribution of major cations from mineral dissolution during the experiment seem negligible.

In conclusion, the model calculations show that the input of element concentrations by mineral dissolution reactions induced in the experiment seem negligible for the major cations and also very minor for Mg^{2+}. Thus, most concentrations in the experiment solution measured after equilibration with respect to Cl^- can be used together with those of the anions to derive the general chemical

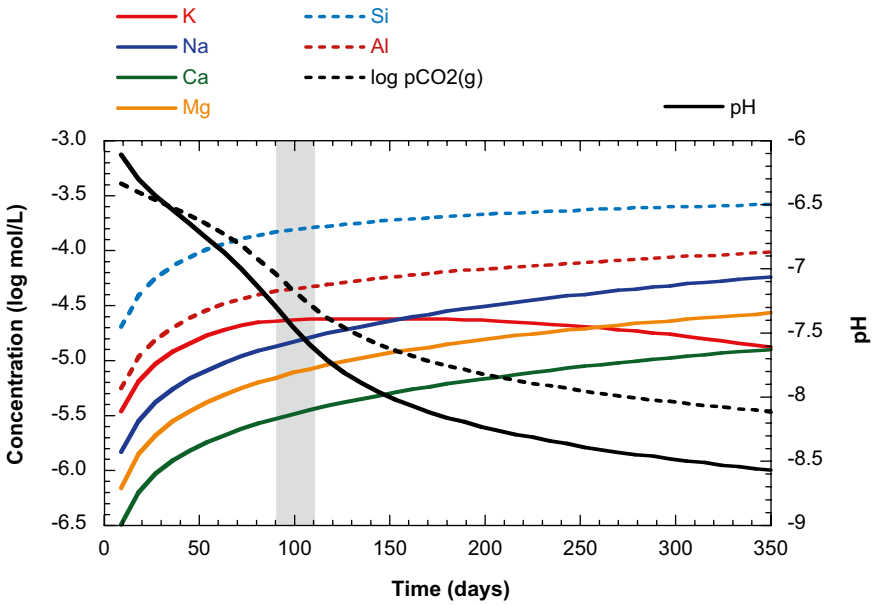

Figure 7-5. *Calculated cation concentrations, $pCO_{2(g)}$, and pH during kinetic weathering of a metagranite at 45°C. The shaded area gives the experiment time of the out-diffusion experiment conducted with the drill core material from boreholes used for porewater investigations from the Forsmark area. Note that suppression of cation concentrations by secondary minerals was not allowed in this scoping simulation.*

type of the *in situ* porewater. The experiments were, however, not designed to deliver data about pH and the carbonate system of the porewater. Therefore, there are too few equations to solve for all unknowns and no unique *in situ* porewater composition can be modelled with the present data. However, based on experience of natural crystalline groundwater systems and the simulations above, it can be estimated that the concentrations of dissolved CO_2 and bicarbonate (HCO_3) will decrease with increasing salinity and become minor anions in the saline porewaters /Nordstrom et al. 1989, Michard et al. 1996/.

7.2.2 General chemical type

The out-diffusion experiment solution of porewater samples from the Forsmark area are of four major types. As outlined above, to a large extent these chemical types also represent the chemical type of the *in situ* porewater and extrapolation yields a dilute Ca-Na-HCO_3 type (type A), a dilute Na-Ca-HCO_3 type (type B), a brackish Na-Ca-Cl-(HCO_3) type (type C, with subtype C_1 = Ca-Na-Cl-(HCO_3) type) and a saline Ca-Na-Cl type (type D).

In the footwall bedrock s.l. chemical type A porewater is absent. Porewater chemical type B occurs at shallow to greater depths in borehole KFM01D and at shallow to intermediate depths in boreholes KFM08C and KFM09B (Figure 7-1 and Figure 7-2). Chemical type C (including C_1) occurs at greatest depth in borehole KFM01D and at intermediate depth in boreholes KFM08C and KFM06A. Saline type D is only present in boreholes KFM08C, KFM06A and KFM09B at greatest depth. With one exception in borehole KFM09B (cf. Figure 7-2), the chemical types of porewater in the footwall are correlated with depth although the distribution varies in absolute terms.

In the hanging wall bedrock s.l., only the dilute chemical types A and B occur (Figure 7-3). Whereas porewater in the upper part of borehole KFM06A is mainly of the chemical Type B, these two types in borehole KFM02B alternate with depth and are related to the various deformation zones with high frequencies of water-conducting fractures.

7.2.3 Chemical indicators of porewater origin

In the fracture groundwaters the concentrations of Mg^{2+} have been used successfully to trace post-glacial melt water, brackish-marine (e.g. Littorina/Baltic Sea) and recent meteoric end member types in the bedrock groundwater system. In Section 7.2.1 it was outlined that elevated Mg^{2+} concentrations in the out-diffusion experiment solution might well represent porewater concentrations to a large degree because of the minimal contribution of Mg^{2+} from mineral reactions during the experiment.

Concentrations of Mg^{2+} in the experiment solutions above detection limit are present in 4 experiment solutions of samples from the footwall bedrock s.l. and in 34 experiment solutions of samples from the hanging wall bedrock s.l.. Extrapolating these concentrations to approximate porewater concentrations using (Equation 3-4) the Mg^{2+} concentration in these porewaters would vary between about 10–200 mg/L This range covers that in the experiment solutions from values at the detection limit of 0.3–0.5 mg/L to the highest value of 3.1 mg/L.

Figure 7-6 shows the extrapolated Mg^{2+} concentration in porewater versus the elevation of the porewater samples. These concentrations should not be mistaken for the real *in situ* porewater concentrations. Nevertheless, and in combination with the Cl^- concentrations, such Mg^{2+} values above 200 mg/kg_{H2O} are indicative of the presence of a Littorina Sea component, whereas values between about 20–100 mg/kg_{H2O} might be more indicative for a Littorina and/or Baltic Sea water component. It appears that such influence is almost absent in the porewater samples from the footwall bedrock, except for the shallowest three samples in borehole KFM01D, the sample at –373.7 m elevation near-by a water-conducting fracture in fracture domain FFM01 in borehole KFM06A, and the two samples collected adjacent to conductive episyenite zones in boreholes KFM08C and KFM09B (Figure 7-6, left). The three shallow samples in borehole KFM01D show similar relationships with respect to Cl^- and Mg^{2+} concentrations to the fracture groundwaters sampled from these zones with the sample at 200 m depth being at steady state with the present day fracture groundwater (cf. Figure 7-2 and Figure 7-6). The latter has been interpreted to have a significant Littorina Sea water component (p. 166 in /Smellie et al. 2008/). Also, the Cl^- concentration of the episyenite sample from borehole KFM08C would allow a component of Littornia water to be present; however its Mg/Cl ratio is too low for such a component. In contrast, the Cl^- concentration of the episyenite sample from borehole KFM09B of about 10,500 mg/kg_{H2O} is too high and, in combination with the Cl^- concentration profile away from the episyenite zone, no such component can be present in this porewater.

In contrast to porewater in the footwall bedrock s.l., almost all samples in the hanging wall s.l. bedrock have elevated Mg^{2+} concentrations (Figure 7-6, right). In porewaters from borehole KFM02B and KFM06A down to about 400 m depth equal Mg^{2+} concentrations occur that correspond to the Mg^{2+} concentrations in the fracture groundwater of this depth interval. Conspicuously elevated Mg^{2+} concentrations are observed in the highly transmissive interval at the bottom of deformation zone ZFMA2 at around 420 m depth. These high concentrations also correspond to those observed in fracture groundwater from this depth. Further down in deformation zone ZFMF1 at around 500 m depth, the porewater has still elevated Mg^{+2} concentrations, but now significantly lower than the corresponding fracture groundwater.

In all porewater samples with measurable Mg^{2+} concentrations in the out-diffusion experiment solutions positive trends are established between the apparent Mg^{2+} concentrations and the Cl^- concentrations in the porewater (Figure 7-7). The only exceptions include the two samples from the episyenite zones in boreholes KFM08C and KFM09B for reasons mentioned above and these samples are, therefore, not included in Figure 7-7. For all other samples two different trends between the apparent Mg^{2+} concentrations and the Cl^- concentrations are observed: In samples from the bottom of deformation zone ZFMA2 at around 420 m depth in borehole KFM02B and the shallowest samples from fracture domain FFM02 and deformation zones ENE0060B and ENE0060A (KFM06A) and borehole KFM01D in the footwall bedrock, a trend with a steep slope and an average Mg/Cl mass ratio of 0.051 is established, whereas the samples from below deformation zone ZFMF1 at around 512 m depth in borehole KFM02B, the sample from –373.7 m elevation borehole KFM06A (fracture domain FFM01), and the sample at –204.6 m elevation in borehole KFM01D (fracture domain FFM01), describe a less steep slope with an average Mg/Cl mass ratio of about 0.024 (Figure 7-7). The fracture groundwaters from about the same depth in KFM01D also plot along the less steep slope whereas none of the fracture groundwaters from the hanging wall s.l. plot along either of the trend lines described by the porewaters.

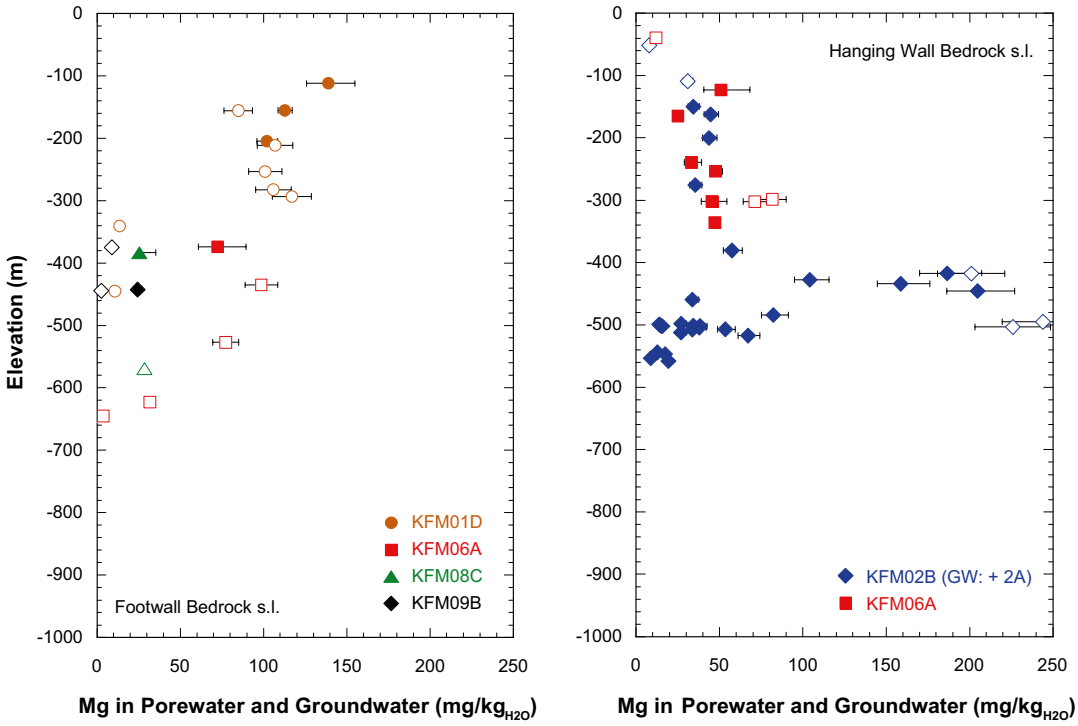

Figure 7-6. *Apparent concentrations of Mg^{2+} in porewater from the footwall bedrock s.l. (left) and the hanging wall bedrock s.l. (right). The samples from boreholes KFM08C and KFM09B in the footwall come from adjacent locations to the conducting episyenite zones. Note that Mg^{2+} does not behave conservatively during the out-diffusion experiments (see text). See Figure 2-3 for allocation of footwall bedrock s.l and hanging wall bedrock s.l.*

The elevated Mg^{2+} concentrations in these porewaters suggest the presence of a Littorina and/or Baltic Sea water component because such high Mg^{2+} concentrations cannot be generated by water-rock interactions (cf. Section 7.2.1). The fracture groundwaters from the same depth intervals as the porewater samples are interpreted to contain a large component of Littorina Sea water based on chemical composition and average residence time /Smellie et al. 2008/. Consequently, the source of Mg in the porewater must also be Littornia Sea water (Mg^{+2} = 244 mg/L, Cl^{-} =5,540 mg/L, cf. /Smellie et al. 2008/) and not the younger Baltic Sea water. Thus, two possible mechanisms could produce the different slopes observed for the Mg/Cl ratio in the porewater (Figure 7-7): Firstly, Mg^{2+} and Cl^{-} might undergo fractionation during the exchange by diffusion between porewater and fracture groundwater due to retardation of Mg^{2+} (e.g. by sorption). Secondly, the interaction with Littorina Sea water occurred with a different porewater composition having been present in the two groups of samples. In the first case, a relation between different Mg/Cl ratios and the distance between porewater sample and the nearest water-conducting fracture would be expected. As shown in Figure 7-7 (bottom) no such relation seems to be developed. In the second case, the porewater that became later modified by exchange with fracture groundwater of Littorina type Sea water must have had already low Cl^{-} concentrations in the samples now displaying a high Mg/Cl ratio along the trend line with the steep slope. In contrast, the samples now displaying a lower Mg/Cl ratio along the trend line with the less steep slope must have had moderately high, brackish Cl^{-} concentrations with associated low Mg^{2+} concentrations before the exchange with Littorina type Sea water. This implies that porewater in samples from the bottom of deformation zone ZFMA2 at around 420 m depth in borehole KFM02B and the shallow samples from borehole KFM06A down to the end of deformation zone ENE0060A (358 m depth), and from borehole KFM01D in fracture domain FFM02, were strongly influenced by meteoric water prior to the interaction with Littorina type sea water. In turn, such influence is less pronounced in the deeper sample at –373.7 m elelvation from borehole KFM06A in fracture domain FFM01 below deformation zone ENE0060A and mainly absent in the shallow sample at –204.6 m elevation in borehole KFM01D in fracture domain FFM01. As shown in Section 7.3, this complex scenario is further supported by the porewater isotope data.

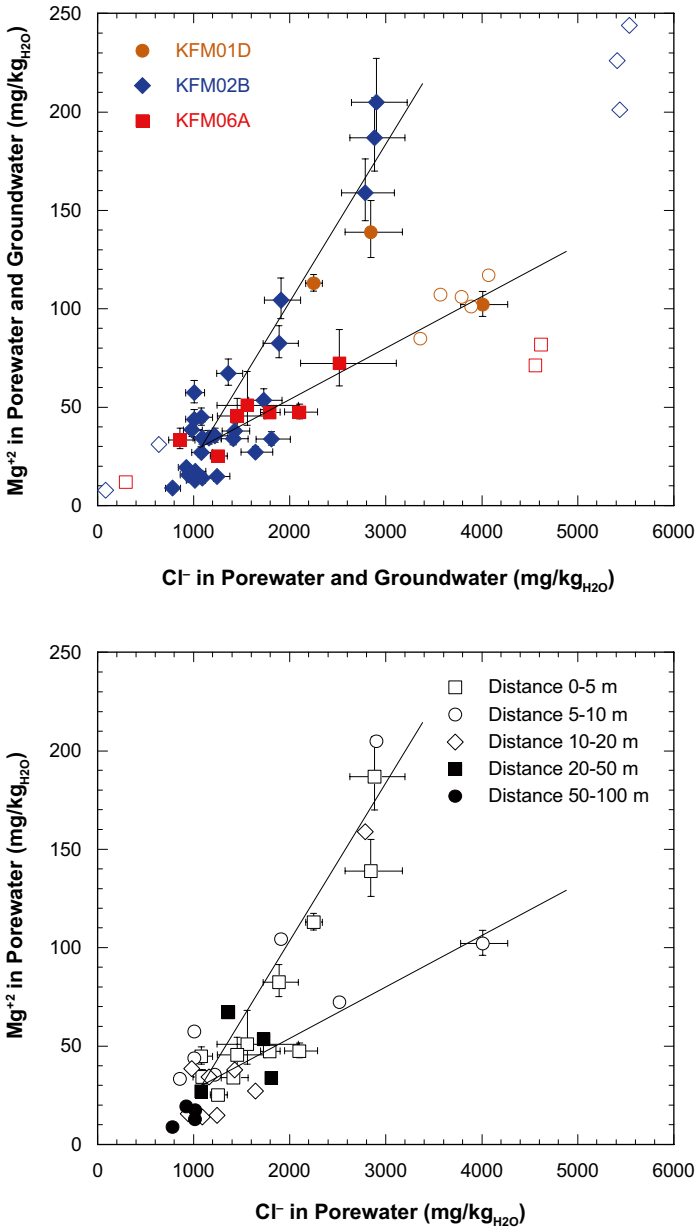

Figure 7-7. *Upper graph: Apparent concentrations of Mg^{2+} versus Cl^- concentrations in porewater (closed symbols) from the hanging wall bedrock s.l. and the footwall bedrock s.l. Two different trends are established in the porewater indicating different amounts of Littorina and/or Baltic Sea water components in the porewater. Fracture groundwater compositions (open symbols) from corresponding depth intervals in the same boreholes are given for comparison. Lower graph: The same concentration plot with the samples now distinguished according to the distance to the nearest water-conducting fracture. Note that Mg^{2+} does not behave conservatively during the out-diffusion experiments (see text).*

7.2.4 Cl-isotope composition

The ratio of the stable isotopes of dissolved chloride ^{35}Cl and ^{37}Cl, expressed as $\delta^{37}Cl$, might serve as a useful tracer to track porewater–fracture groundwater interaction because unlike the total Cl^- concentrations, the isotope ratio is independent of porosity. In turn, however, fractionation of the chlorine isotopes occurs during diffusive transport of chloride /Desaulniers et al. 1986, Eggenkamp et al. 1994/. In contrast to other isotope pairs, this fractionation is measurable mainly due to the large difference in the natural abundance of the two stable isotopes ^{35}Cl and ^{37}Cl. Generic diffusion calculations using isotope-specific diffusion coefficients show that the $\delta^{37}Cl$ values of two reservoirs will become equal after steady state conditions with respect the Cl^- concentration is attained between the two reservoirs /Gimmi and Waber 2004/. In the out-diffusion experiments performed on drillcore material from the Forsmark investigation site, steady state conditions were attained as shown in Chapters 4 and 5. Therefore, the $\delta^{37}Cl$ value measured in the out-diffusion solution is representative for that of the *in situ* porewater. For the porewater–fracture groundwater system, the evaluation of steady state versus transient state between porewater and fracture groundwater with respect to the chlorine isotopes also has to be made in combination with the total Cl^- concentrations and steady state conditions are only attained if both, the isotope ratio and the total concentration, are in equilibrium.

Within the Forsmark site investigation programme, chlorine isotope ratios were only determined on samples from borehole KFM06A. The $\delta^{37}Cl$ values of porewater fall in the range of 0.1–1.9‰ SMOC, except for one sample (KFM06A-15) with an exceptionally high value of 3.3‰ SMOC (Table A-4). The reason for this very high $\delta^{37}Cl$ value is yet unknown. However, because the chemical and other isotope compositions of this sample compare well with the surrounding samples an analytical artefact seems most likely. The chlorine isotope ratios show no systematic trend with the porewater Cl^- concentrations, except for a tendency towards a larger variation related to the lower porewater Cl^- concentrations of samples from the hanging wall bedrock s.l. (Figure 7-8). This becomes even more obvious in the distribution of the $\delta^{37}Cl$ values with sample depth (Figure 7-9). In the upper part of borehole KFM06A down to about 400 m borehole length (340 m depth; fracture domain FFM02, upper part of fracture domain FFM01, deformation zones ENE0060B, ENE0060A) and characterised by a high frequency of water-conducting fractures, the $\delta^{37}Cl$ values in porewater are generally higher than those from the footwall bedrock s.l. below. The least variation is observed at greatest depth in the porewater of the saline Ca-Na-Cl type porewaters.

Compared to the fracture groundwater, the $\delta^{37}Cl$ values of the porewater are generally more positive although at some locations (e.g. around 360 m and 760 m borehole length) similar chlorine isotope compositions are observed in porewater and fracture groundwater (Figure 7-9). However, the total

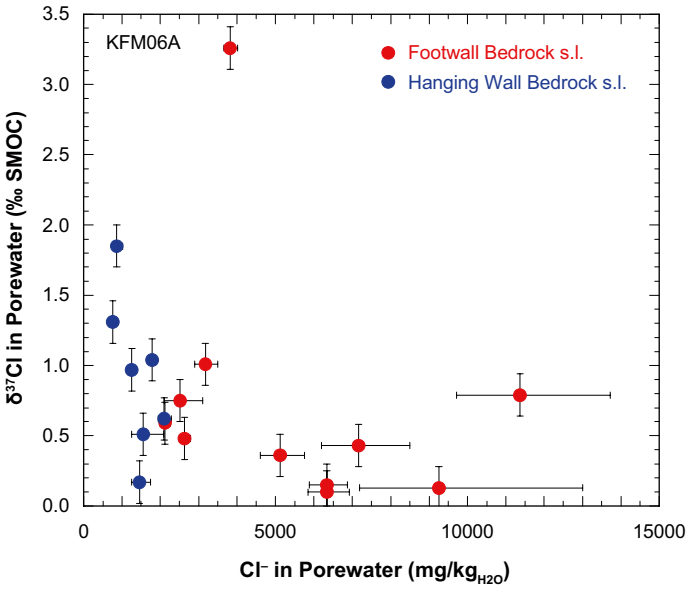

Figure 7-8. *Chlorine isotope composition, $\delta^{37}Cl$, versus Cl^- concentrations in porewater from borehole KFM06A. Error bars are the propagated error for Cl^- concentrations and the analytical error of 0.15‰ for $\delta^{37}Cl$. See Figure 2-3 for allocation of footwall bedrock s.l and hanging wall bedrock s.l.*

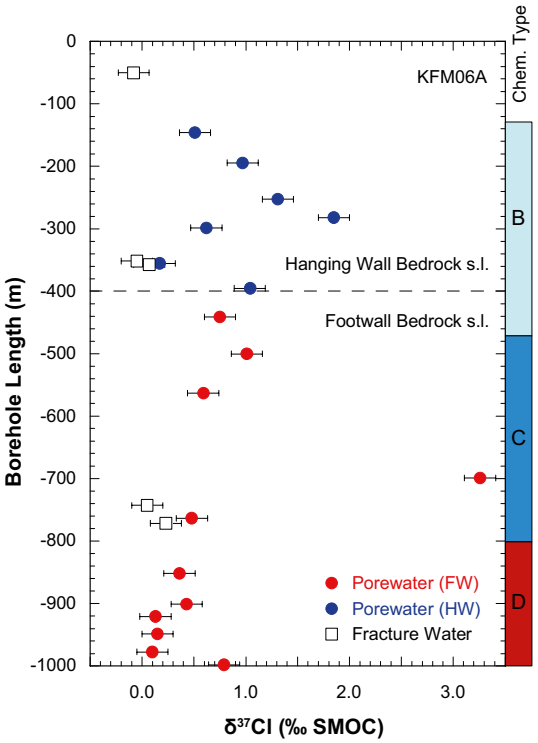

Figure 7-9. *Chlorine isotope composition of porewater (closed symbols) and fracture groundwater (open symbols) from borehole KFM06A. Error bars are the analytical error of 0.15‰ for $\delta^{37}Cl$; porewater chemical types as in Figure 7-3. See Figure 2-3 for allocation of footwall bedrock s.l and hanging wall bedrock s.l.*

Cl^- concentrations of porewater and fracture groundwater differ greatly at these locations indicating transient conditions (cf. Figure 7-3). This is further support of the complex evolution of the porewater–fracture groundwater system with superimposed chemical and isotopic signatures from subsequent events (i.e. changes in fracture groundwater composition).

7.2.5 Sr-isotope composition

Strontium is chemically reactive and is involved in mineral dissolution reactions during the out-diffusion experiments. The concentration measured in the out-diffusion experiment solutions can, therefore, not be directly extrapolated to a porewater concentration as for chloride. Nevertheless, some insight about the porewater composition and about mineral dissolution reactions during the out-diffusion experiment can be gained from the total Sr concentration and the Sr-isotope ratio, $^{87}Sr/^{86}Sr$.

Depending on the total mineralisation of the *in situ* porewater, the effect of mineral dissolution reactions on the total Sr^{2+} concentration, Sr_{tot}, in the experiment solution will be minimal. This is due to the occurrence of Sr (generally less than 1%) as a trace element in the rock-forming minerals. As shown in section 7.2.1, the contribution of major elements from mineral dissolution during the out-diffusion experiment is in the order of 10^{-5} to 10^{-6} mol/L and consequently the contribution of Sr^{2+} can be expected to be even smaller by at least one order of magnitude. Nevertheless, the Sr^{2+} concentrations have to be evaluated for such a contribution because they were analysed with high precision and low detection limit by mass spectrometry.

In contrast to the Sr^{2+} concentration, the effect on the Sr-isotope ratio, $^{87}Sr/^{86}Sr$, in the experiment solution is expected to be bigger. This is because radiogenic ^{87}Sr, which is continuously produced by the natural decay of ^{87}Rb, is retained in the minerals unless it becomes released by recrystallisation and/or dissolution processes. During the induced mineral dissolution (e.g. feldspars, biotite) in the out-diffusion experiment, the small amounts of Sr^{2+} released from such minerals will thus be highly radiogenic, i.e. have a high $^{87}Sr/^{86}Sr$ ratio. In addition, the $^{87}Sr/^{86}Sr$ ratio obtained for the experiment solutions might also depend on the rock type in spite for their similar mineralogy. This is indicated by the large variation in $^{87}Sr/^{86}Sr$ ratios of rocks ranging from 0.7116 in the granodiorite to tonalite to 0.8059 in the metagranite to granodiorite /Sandström et al. 2008/.

The information obtained from the comparison of Sr_{tot} and the Sr-isotope ratio in the experiment solution with those in the fracture groundwater thus depends on the total Sr^{2+} concentration. At low Sr^{2+} concentrations in the experiment solution and fracture groundwater, equal Sr-isotope ratios would indicate that the isotope ratio in the fracture groundwater is attained rather quickly being derived from the same mineral dissolution reactions that occur during the out-diffusion experiment in the laboratory. In this situation no independent information can be gained for the porewater because the porewater signature is masked by the experiment. However, at total Sr^{2+} concentrations significantly higher than that contributed by mineral dissolution during the out-diffusion experiment, the $^{87}Sr/^{86}Sr$ ratio of the experiment solution will be more similar to that of the *in situ* porewater. In this situation, information about chemical and isotopic relationships of strontium between porewater and fracture groundwater can be obtained.

Concentrations of Sr_{tot} measured in the experiment solutions by mass spectrometry are generally higher for rocks from the footwall bedrock s.l. (0.071–0.587 ppm, episyenite samples excluded) compared to rocks in the hanging wall bedrock s.l. (0.068–0.259 ppm, Table A-4). In the footwall bedrock s.l., total Sr_{tot} correlates with the Cl^- concentrations in the experiment solutions independent of rock type whereas no such correlation is established in the experiment solutions of rocks from the hanging wall bedrock (Figure 7-10). This suggests that a large portion of the Sr^{2+} in experiment solutions from footwall bedrock s.l. samples comes from the porewater where the Sr^{2+} concentrations increase with increasing rock-water interaction as indicated by the increasing Cl^- concentrations. In contrast, in the rocks from the hanging wall bedrock s.l. the lack of a correlation between Sr^{2+} and Cl^- inhibits the identification of such a porewater component.

In the experiment solutions of rocks from the footwall bedrock s.l. the $^{87}Sr/^{86}Sr$ ratio depends on the rock type. It is highest for experiment solutions of metagranite to granodiorite rocks with $^{87}Sr/^{86}Sr$ between 0.7210–0.7433, similar for the granodiorite to tonalite rocks and the fine-grained granite with $^{87}Sr/^{86}Sr$ between 0.7193–0.7259, and lowest for solutions of aplitic granite rock samples with $^{87}Sr/^{86}Sr$ between 0.7153–0.7210 (Figure 7-11, Table A-4). A weak trend towards higher $^{87}Sr/^{86}Sr$ ratios with increasing Cl^- concentrations is present in the metagranite to granodiorite, but absent in experiment solutions of the other rock types. Compared to whole rock $^{87}Sr/^{86}Sr$ ratios, the ratios in the out-diffusion experiment solutions of metagranite to granodiorite rock samples are still lower (whole rock $^{87}Sr/^{86}Sr$ = 0.7525–0.8059, /Sandström et al. 2008/), but similar in the solutions of granodiorite to tonalite rock samples (whole rock $^{87}Sr/^{86}Sr$ = 0.7116, /Sandström et al. 2008/). As a function of sample depth, a large scatter in the $^{87}Sr/^{86}Sr$ ratio of the experiment solutions is observed for shallow and intermediate samples. At greater depth the isotope signatures remain rather constant around the value of the whole rock in the granodiorite to tonalite and aplitic granite, but still increases with increasing depth in the metagranite to granodiorite (Figure 7-12).

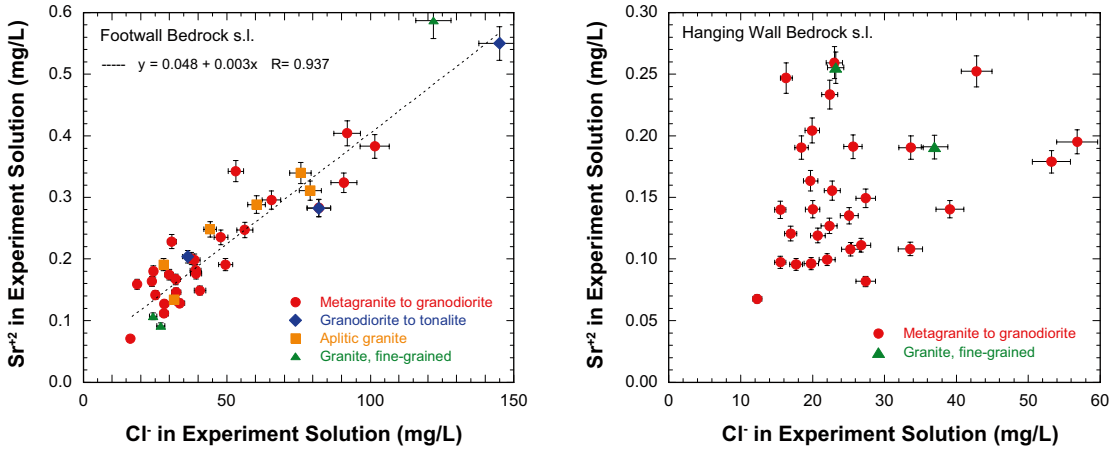

Figure 7-10. *Strontium versus chloride concentrations in out-diffusion experiment solutions as a function of rock type in the footwall bedrock s.l. (left) and the hanging wall bedrock s.l. (right). Error bars indicate the relative analytical error of ±5%. See Figure 2-3 for allocation of footwall bedrock s.l and hanging wall bedrock s.l.*

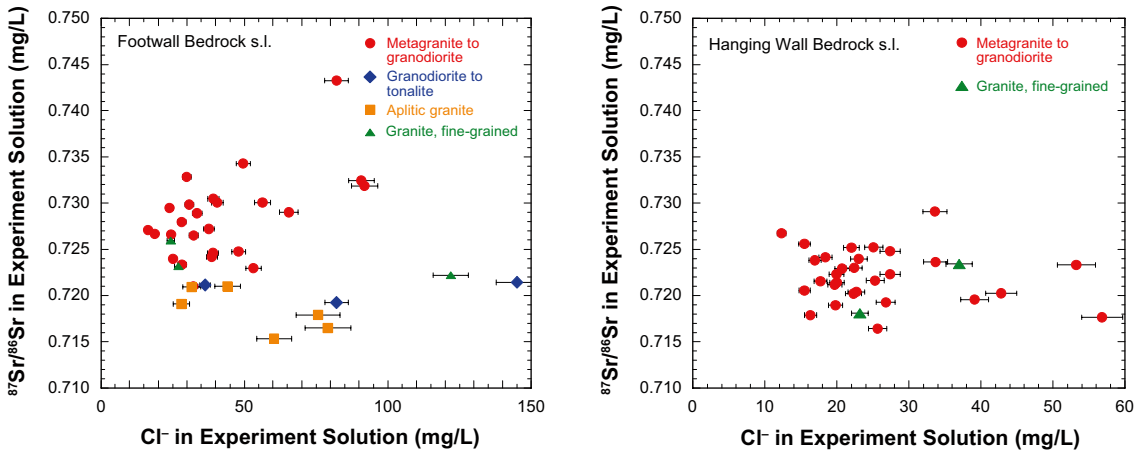

Figure 7-11. *Strontium isotope ratio, $^{87}Sr/^{86}Sr$ chloride concentrations in out-diffusion experiment solutions as a function of rock type in the footwall bedrock s.l. (left) and the hanging wall bedrock s.l. (right). Error bars indicate the relative analytical error of ±5% for Cl^- and 2σ absolute for the $^{87}Sr/^{86}Sr$ ratio (smaller than the size of the symbols in the plots). See Figure 2-3 for allocation of footwall bedrock s.l and hanging wall bedrock s.l.*

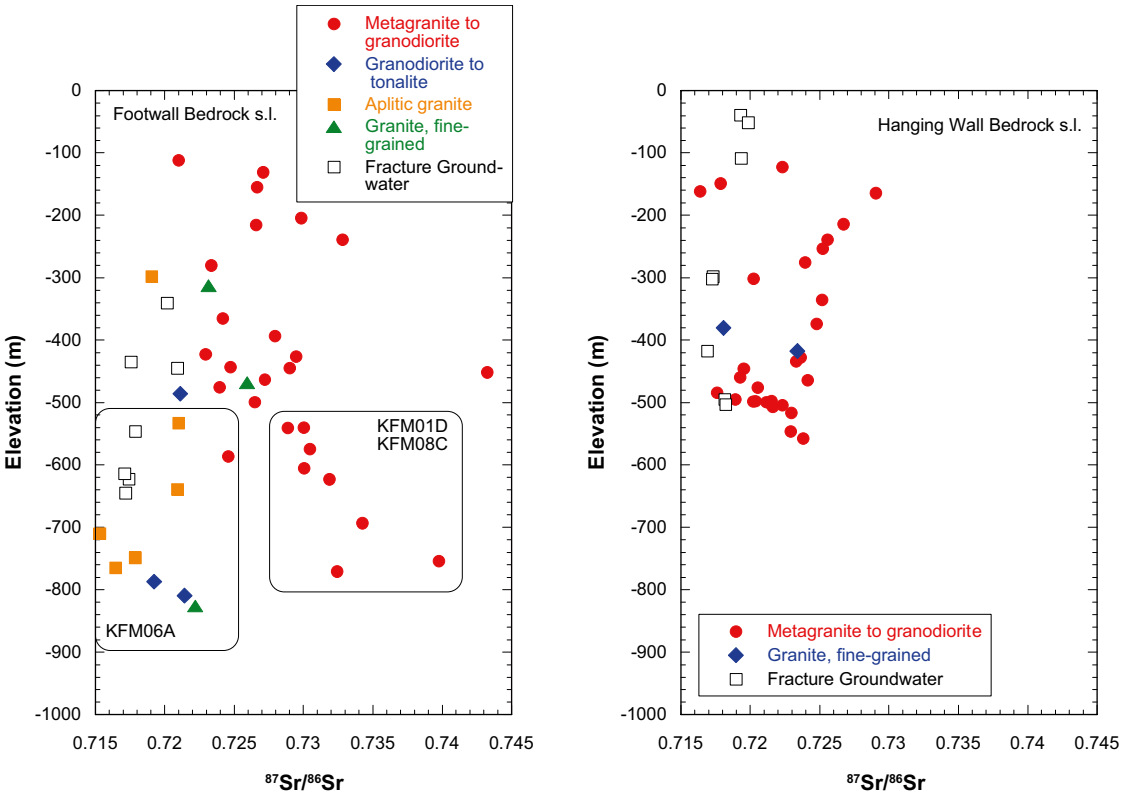

Figure 7-12. *Strontium isotope ratio, $^{87}Sr/^{86}Sr$ in out-diffusion experiment solutions (closed symbols) versus sample elevation and as a function of rock type in the footwall bedrock s.l. (left) and the hanging wall bedrock s.l. (right). The $^{87}Sr/^{86}Sr$ ratios of fracture groundwater (open symbols) are given for comparison. Error bars indicate 2σ absolute for the $^{87}Sr/^{86}Sr$ ratio (smaller than the size of the symbols in the plots). See Figure 2-3 for allocation of footwall bedrock s.l and hanging wall bedrock s.l.*

In the experiment solutions of rocks from the hanging wall bedrock s.l. no trend among different rock types or with the Cl^- concentrations is established with the $^{87}Sr/^{86}Sr$ ratio of the experiment solution, which are all much lower than the $^{87}Sr/^{86}Sr$ ratios of the corresponding whole rock (Figure 7-11). In these rock samples there is also no trend established between sample depth and $^{87}Sr/^{86}Sr$ ratio of the experiment solution (Figure 7-12).

All this information combined suggests that in the footwall bedrock s.l. in the more fine-grained granodiorite to tonalite and aplitic rocks with larger reactive surface areas, the contact time between porewater and rock was long enough to approach equilibrium with respect to the Sr-isotopes. In the medium-grained granodiorite this is not yet the case and the increasing $^{87}Sr/^{86}Sr$ ratios of the experiment solution towards the whole rock Sr-isotope composition with increasing sample depth and Cl-concentration suggests that this process is still ongoing. Converted to signatures in the porewater, it appears that the Sr^{2+} concentration and the $^{87}Sr/^{86}Sr$ ratio of porewater from the intermediate to greater depths in the footwall bedrock is mainly rock dominated.

In contrast, the Sr^{2+} concentration and the $^{87}Sr/^{86}Sr$ ratio of porewater in the hanging wall s.l. seems to be more determined by the fracture groundwater than by extensive rock-water interaction. This is supported by the greater similarity in the $^{87}Sr/^{86}Sr$ ratio between fracture groundwater in the hanging wall bedrock s.l. and the experiment solution compared to the footwall bedrock s.l. (Figure 7-11). The Sr^{2+} concentrations and the $^{87}Sr/^{86}Sr$ ratios of the experiment solutions (and indirectly for the porewater) therefore indicate generally longer residence times for the porewater in the footwall bedrock s.l. compared to the hanging wall bedrock s.l. This is consistent with the other chemical and isotopic indicators of the porewaters from these two areas.

7.3 $\delta^{18}O$ and $\delta^{2}H$ of porewater

The water isotope composition of the porewater, expressed as $\delta^{18}O$ and $\delta^{2}H$, has been determined by the diffusive-exchange technique. During the course of the Forsmark site investigation programme, the propagated error of the isotope diffusive-exchange technique was significantly reduced from the first samples collected from borehole KFM06A to the last ones collected from borehole KFM02B (cf. Section 3.2.3). Yet, the overall uncertainty attached to these data is still at the upper end of that attached to the chloride content, certainly for deuterium.

The ratio of the stable isotopes of infiltrating water is, among others, dependent on the temperature and moisture source. This makes the stable isotopes valuable indicators of possible different origins of waters that have similar Cl^- concentrations such as glacial water and present day infiltration. In contrast to the chloride isotopes, no fractionation is yet known for the oxygen and hydrogen isotopes during diffusion of water through the matrix of a crystalline rock. From the chemical point of view, the interaction between porewater and fracture groundwater can thus be treated for the stable isotopes of water in the same way as for the conservative solute Cl^-. From the physical point of view, however, the water isotopes appear to diffuse faster than dissolved Cl^- in low-permeability rock environments up to a factor of about 2 due to the different accessible porosity for the two components /Gimmi and Waber 2004, Mazurek et al. 2009/. During the interpretation of water isotope and chloride porewater data, it has to be kept in mind that changes in the fracture groundwater composition might strongly affect the porewater $\delta^{18}O$ and $\delta^{2}H$ values, but not the chloride in the porewater (e.g. glacial versus meteoric) and *vice-versa* (e.g. Littorina versus Baltic Sea water, brine versus warm-climate meteoric).

Repeating climatic cycles with similar or identical isotope composition in the fracture groundwater will also leave their traces in the porewater and superimpose on each other. Porewater isotope signatures obtained from individual samples collected at greater intervals (about 50 m in all boreholes except for boreholes KFM09B and KFM02B) might therefore not resolve a single event during the palaeohydrogeologcal evolution of the system. Exceptions are locations where extreme signatures that can be related to a unique source (e.g. glacial melt water) would have been preserved under certain circumstances. In contrast, a higher resolution and more information about the palaeohydrogeological evolution can be gained from porewater samples collected along a continuous profile as collected in borehole KFM02B.

The water-isotope composition of matrix porewater in rocks of the Forsmark candidate area covers a large range of $\delta^{18}O$ values between –14.9‰ and –2.1‰ VSMOW and $\delta^{2}H$-values between about –120‰ and –14‰ VSMOW (Table A-3). The oxygen and hydrogen isotope compositions of porewater in rocks from the footwall bedrock s.l. (fracture domains FFM01 and FFM06 in boreholes KFM01D, KFM08C, KFM09B and the lower part of KFM06A, cf. Figure 2-3), differ clearly from that of porewater sampled in rocks from the hanging wall bedrock s.l. (fracture domains FFM03 and FFM01 in borehole KFM02B and fracture domains FFM02 and FFM01 in the upper part of borehole KFM06A, cf. Figure 2-3) as best shown in the conventional $\delta^{18}O$–$\delta^{2}H$ diagram (Figure 7-13). Porewater in the footwall bedrock s.l. is generally more enriched in the heavy isotopes compared to

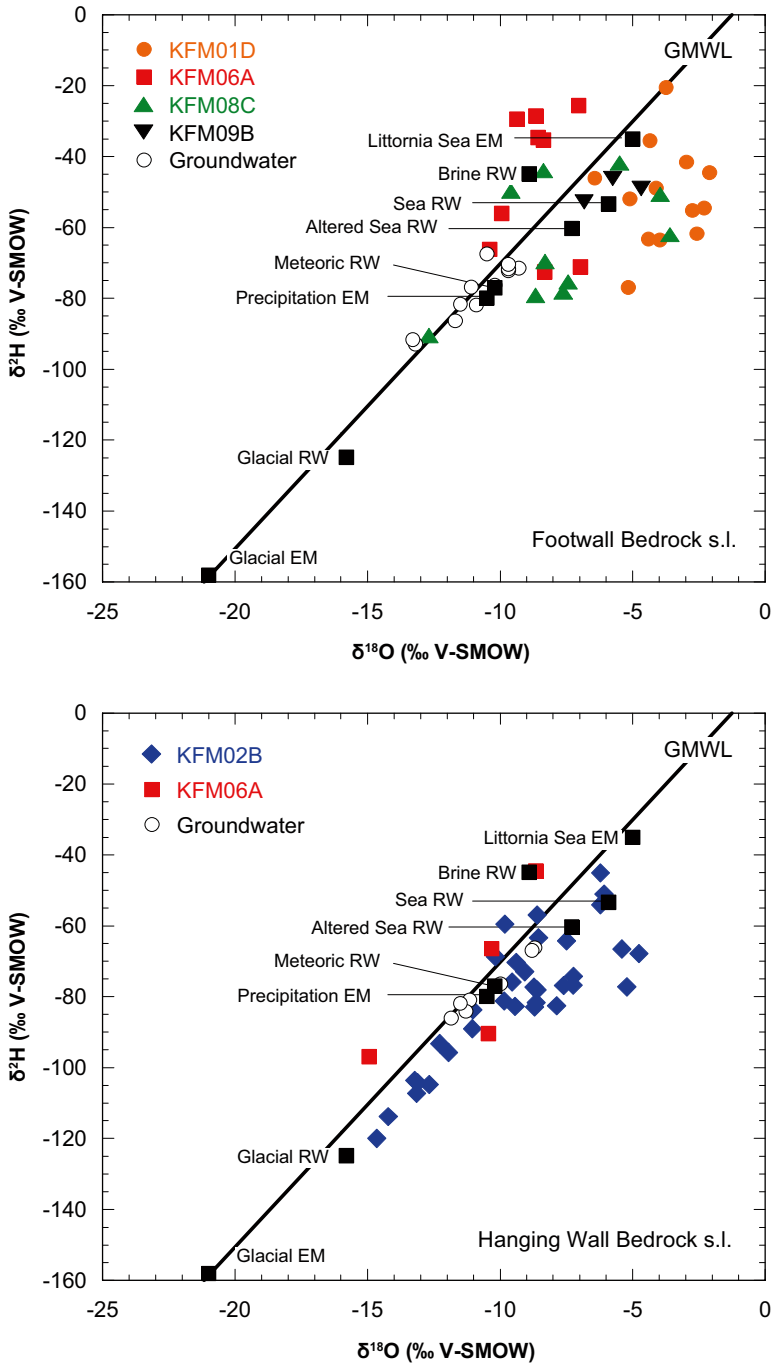

Figure 7-13. *$\delta^{18}O$–$\delta^{2}H$ diagram of porewater as a function of the footwall bedrock s.l. (top) and hanging wall bedrock s.l. (bottom). The isotope composition of end member and reference fracture groundwaters is given for comparison (data from /Laaksoharju et al. 2008/. GMWL: Global Meteoric Water Line; error bars are omitted in this figure for better legibility). See Figure 2-3 for allocation of footwall bedrock s.l and hanging wall bedrock s.l.*

porewater of the hanging wall bedrock s.l. and also compared to the fracture groundwater sampled from this area. Furthermore, porewater from boreholes KFM01D and KFM08C in the footwall bedrock s.l. with low to moderate chloride contents plot further to the right of the Global Meteoric Water Line (GMWL) than sea water, suggesting the presence of a warm climate component. In turn, some of the most saline porewaters from greater depth below 600 m in boreholes KFM06A and KFM08C within the footwall bedrock s.l. plot to the left of the GMWL near-by the Brine end member suggesting extended water-rock interactions for these deep-seated porewater samples at great distances from water-conducting fractures (Figure 7-13, top). In contrast, porewater from the hanging wall s.l. bedrock plots over a large range of isotope compositions parallel to the GMWL, with the bulk of samples being located between the end-member compositions of sea water and present day infiltration (Figure 7-13, bottom). Here, the porewater seems isotopically more similar to the fracture groundwaters sampled from this area. As shown below, and based on the oxygen isotope composition, these differences result also in different distribution patterns with depth.

Considering the relationships of $\delta^{18}O$ and $\delta^{2}H$ in porewater, their absolute values, the distance between porewater samples and nearest water-conducting fracture, and the Cl^- concentration and chemical type of the porewater, four different groups of porewater can be distinguished. These are from young to old: 1) porewater with a present day type meteoric water and Littorina Sea (and possibly Baltic Sea) water influence, 2) porewater with a cold climate to glacial water and Littorina Sea (and possibly Baltic Sea) water influence, 3) porewater with an origin from warm climate brackish non-marine fracture groundwater of old origin (certainly pre-Weichselian stage), and 4) porewater with a strong saline component of very old origin.

Because most of the water isotope compositions of porewater appear to plot along lines which run parallel to the GMWL, the trends for $\delta^{18}O$ and $\delta^{2}H$ with depth will be similar and so only the $\delta^{18}O$ values will be plotted against depth (Figures 7-14 to 7-16) and discussed in detail. All $\delta^{18}O$ and $\delta^{2}H$ data are given relative to VSMOW.

7.3.1 Spatial distribution and relationship to structural features

In the footwall bedrock s.l., porewater with isotope compositions most enriched in ^{18}O and $\delta^{18}O$ values between –2‰ and –6‰ VSMOW occur along the entire length of borehole KFM01D (Figure 7-14) largely independent of Cl^- concentration. The least depleted isotope signatures with $\delta^{18}O$ values between –5‰ and –6‰ VSMOW occur down to about 300 m borehole length (250 m depth) at distances of less than 10 m to the nearest water-conducting fracture (Figure 7-17). These samples show measurable Mg^{2+} concentrations in the out-diffusion experiment solutions and are influenced by Littorina-type fracture groundwater consistent with their short distance to the nearest fracture. As shown in Section 7.2.3, the sample at –204.6 m elevation in borehole KFM01D must have contained a brackish type porewater before the interaction with Littorina Sea water. This brackish type porewater, still not affected by Littorina Sea water, is present in the deeper-seated samples down to about 700 m borehole length (about 540 m depth) in borehole KFM01D as indicated by the moderate Cl^- concentrations (2,000 and 3,500 mg/kg_{H2O}), the large distances between porewater sample and water-conducting fractures, and the absence of measurable Mg^{2+}. The isotope signature of these samples indicates an origin from meteoric fracture groundwater that infiltrated during a significantly warmer climate compared to today. Although the exact origin can no longer be identified based on the available data, these porewater chemical and isotope signatures are best explained by a long-lasting, very old (most probably pre-Pleistocene) interaction with warm climate meteoric to brackish water including extended water-rock interaction.

Somewhat less depleted isotope signatures with $\delta^{18}O$ values between –6‰ and –8‰ VSMOW are recorded for the porewaters of similar Cl^- concentrations (2,000 and 3,500 mg/kg_{H2O}) in boreholes KFM08C and the lower part of KFM06A within those depth intervals with a low frequency of water-conducting fractures down to 420 m borehole length (about 350 m depth, Figure 7-15) and between 500–760 m borehole length (about 420–640 m depth, Figure 7-16), respectively. These porewater samples have otherwise similar characteristics to the old porewaters in borehole KFM01D, i.e. no measurable Mg^{2+} concentrations in the out-diffusion experiment solutions and large distances to the nearest water-conducting fracture. Thus, they might also represent remnants of such a very old interaction, and the less enriched isotope values can be explained by a somewhat increased interaction with later fracture groundwater as also suggested by the higher Cl^- concentrations compared to the KFM01D porewaters (cf. Section 7.1).

In borehole KFM08C at greatest depth, the most saline porewaters of the general Ca-Na-Cl type have $\delta^{18}O$ values of around –4‰ VSMOW (Figure 7-15). Porewater of the same general chemical type, but with slightly lower Cl^- concentrations also occur just below the porous and conductive episyenite zone in borehole KFM09B (cf. Figure 7-2). The isotope composition of these porewaters varies between about –5‰ and –7‰ VSMOW (Figure 7-15). This seems to corroborate the above hypothesis that in the course of the hydrogeological evolution the interaction of very old meteoric to brackish porewater with more saline fracture groundwater can result in less enriched isotope signatures, but also elevated Cl^- concentrations as suggested for porewater in borehole KFM08C. Further support in this direction comes from the fracture groundwater sampled from the episyenite zone in the neighbouring borehole KFM09A, which has a Cl^- concentration of 14,800 mg/kg_{H2O} (cf. Section 7.1.2) and a $\delta^{18}O$ value of –13.3‰ VSMOW (cf. Sicada dataset, Data freeze Forsmark 2.3). The isotope signature of this saline fracture groundwater clearly suggests the presence of a glacial type component /Smellie et al. 2008/. Interaction of very old meteoric to brackish porewater with such type of fracture groundwater will result in some increase of the Cl^- concentration in the porewater and a pronounced depletion of ^{18}O and ^{2}H.

The $\delta^{18}O$ and $\delta^{2}H$ isotope signatures of porewater from the hanging wall bedrock s.l. differ greatly from those in the footwall bedrock s.l.; they plot along the GMWL and are generally depleted in the heavy isotopes compared to the porewaters in the footwall bedrock s.l.. Porewaters down to about 400 m depth in borehole KFM02B (fracture domain FFM03) and in the upper part of borehole KFM06A (fracture domain FFM02 and the upper part of fracture domain FFM01) have very similar isotope signatures corroborating the hydrogeological similarity of the fractured domains in these two boreholes, which are otherwise associated with different geologically-defined bedrock segments.

In boreholes KFM02B and KFM06A the most depleted porewater $\delta^{18}O$ values of –14.7‰ and –14.9‰ VSMOW occur at borehole lengths of about 171 m and 194 m, respectively (Figure 7-16), which correspond to approximately the same depth below the surface. These samples are located close to water-conducting fractures (Figure 7-17) and the isotope signatures thus indicate the presence of a cold climate and/or glacial component of the last glaciation present in these porewaters.

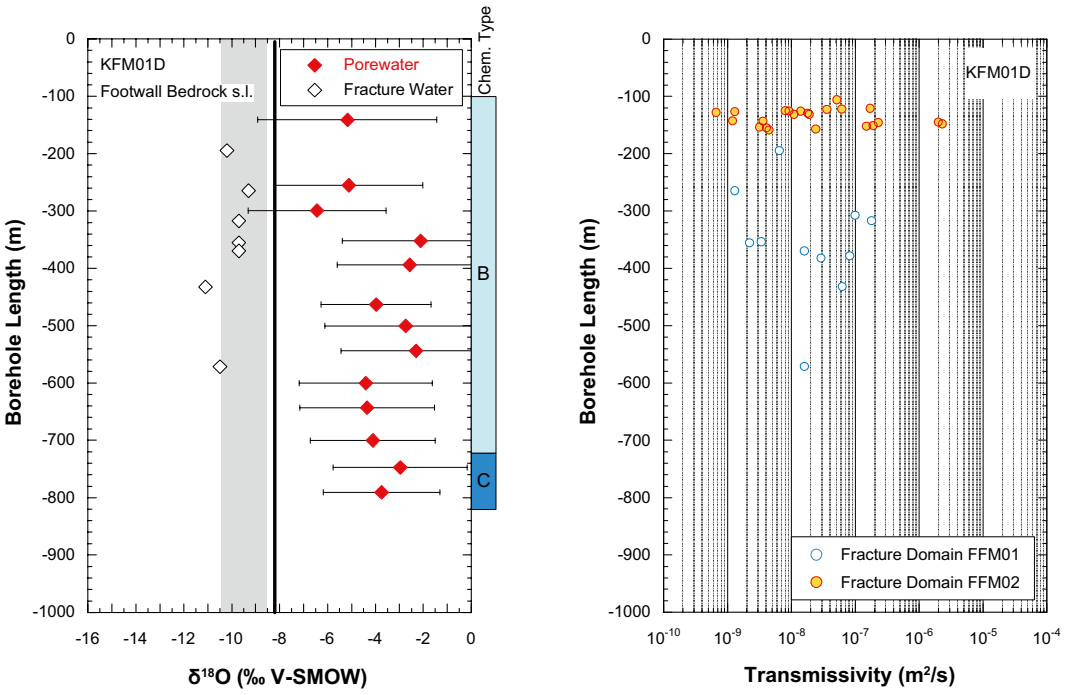

Figure 7-14. *Borehole KFM01D, footwall bedrock s.l.: $\delta^{18}O$ of porewater (closed symbols) and fracture groundwater (open symbos) as a function of sampling depth (left) compared to the measured hydraulic transmissivity of water-conducting fractures (right, PFL data from /Väisävaara et al. 2006a/) in relation to fracture domains and deformation zones (data from /Olofsson et al. 2007/). Error bars give propagated error calculated according to Gauss; grey-shaded area indicates brackish marine Littorina-type signature, black line indicates present Baltic Sea signature; general chemical types of porewater (B and C) as in Figure 7-1. See Figure 2-3 for allocation of footwall bedrock s.l and hanging wall bedrock s.l.*

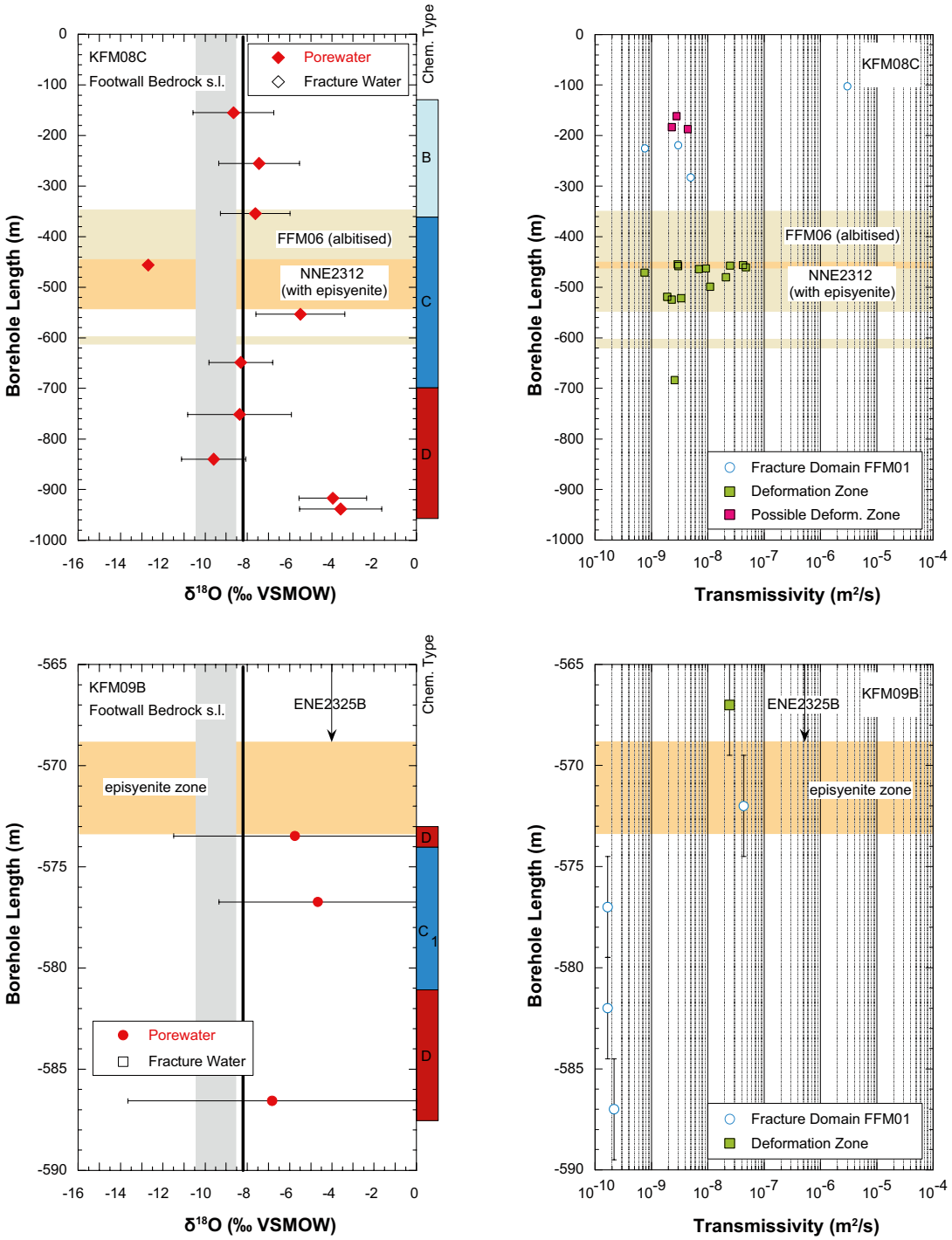

Figure 7-15. *Boreholes KFM08C (top) and KFM09B (bottom), footwall bedrock: $\delta^{18}O$ of porewater and groundwater as a function of sampling depth (left) compared to the measured hydraulic transmissivity of water-conducting fractures (right, PFL data for KFM08C from /Väisävaara et al. 2006b/, PSS data for KFM09B from /Gustavsson et al. 2006/) in relation to fracture domains and deformation zones (data from /Olofsson et al. 2007/). Error bars give propagated error calculated according to Gauss; grey shaded area as in Figure 7-14; general chemical types of porewater (B, C and D) as in Figure 7-2. See Figure 2-3 for allocation of footwall bedrock s.l and hanging wall bedrock s.l.*

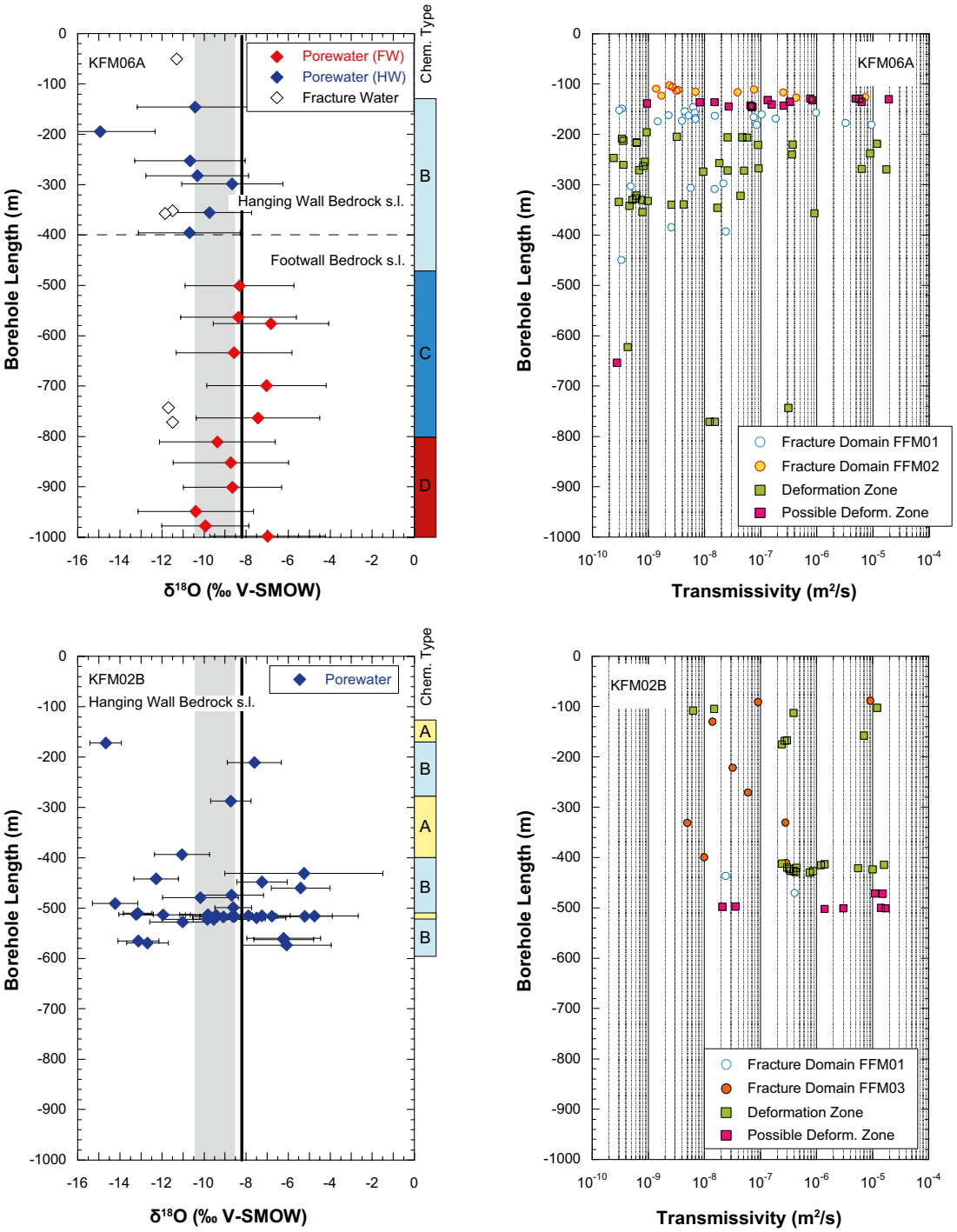

Figure 7-16. *Boreholes KFM06A (top) and KFM02B (bottom), footwall and hanging wall bedrock, respectively: $\delta^{18}O$ of porewater and groundwater as a function of sampling depth (left) compared to the measured hydraulic transmissivity of water-conducting fractures (right, PFL data from /Rouhiainen and Sokolnicki 2005, Väisäsvaara and Pöllänen 2007/) in relation to fracture domains and deformation zones (data from /Olofsson et al. 2007, Stephens et al. 2008a/). Error bars give propagated error calculated according to Gauss; grey shaded area as in Figure 7-14, and general chemical types of porewater (A-D) as in Figure 7-3. See Figure 2-3 for allocation of footwall bedrock s.l and hanging wall bedrock s.l.*

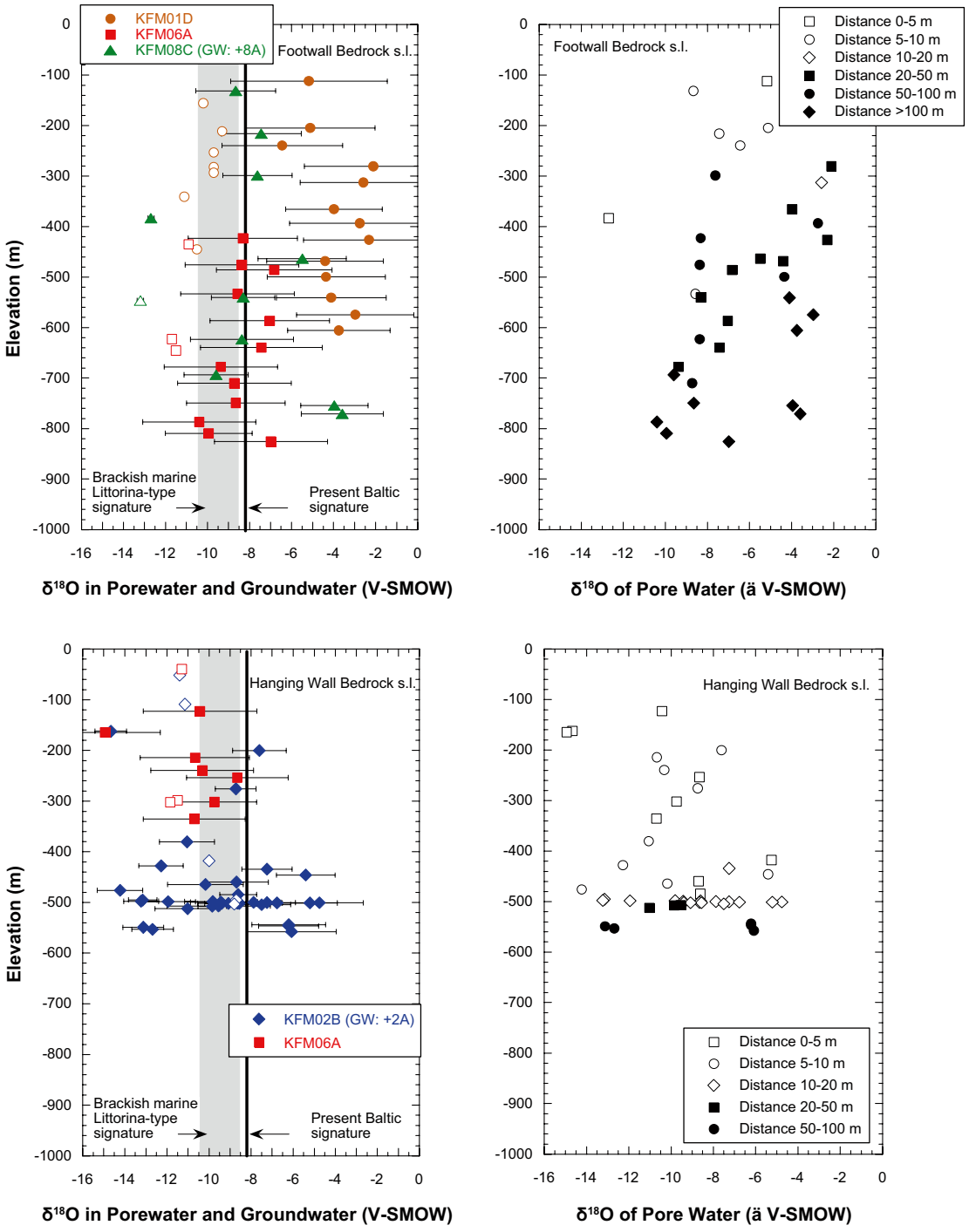

Figure 7-17. *$\delta^{18}O$ of porewater (closed symbols) as a function of the borehole from which the core sample was collected (left) and the distance between the porewater sample and the nearest water-conducting facture (right) versus elevation (m a.s.l.) for the footwall bedrock s.l. (top) and the hanging wall bedrock s.l. (bottom). $\delta^{18}O$ values of fracture groundwaters (open symbols in right panels) collected from the same boreholes are given for comparison (cf. Sicada dataset, Data freeze Forsmark 2.3). See Figure 2-3 for allocation of footwall bedrock s.l and hanging wall bedrock s.l.*

Between about 200–350 m depth the isotope signatures become enriched in ^{18}O with $\delta^{18}O$ values between those of Baltic Sea water and brackish marine Littorina-type signature, or present day meteoric water, respectively. In borehole KFM02B, the water isotope signatures become again increasingly depleted in ^{18}O and ^{2}H towards cold climate type signatures down to about 440 m borehole length (Figure 7-16). In one dimension, all these samples are between 5–10 m away from the nearest water-conducting fracture (Figure 7-17) with a transmissivity of about 10^{-8} m^2/s. Between 410–450 m borehole length at the intersection of borehole KFM02B with deformation zone ZFMA2, and where an increased frequency of highly transmissive fractures occur with the highest recorded Cl^- and apparent Mg^{2+} concentrations in the porewater (cf. Sections 7.1 and 7.2), the isotope composition of the porewater becomes again enriched in ^{18}O and ^{2}H. Although the variation is large, at least two samples show isotope compositions similar to that of brackish marine water (Littorina and/or Baltic Sea water).

Large variations in the porewater isotope composition are also observed at the intersection of borehole KFM02B with deformation zone ZFMF1 and their associated high frequency of highly conducting fractures starting from about 490 m borehole length (Figure 7-16). Within short distances cold temperature to glacial isotope signatures with $\delta^{18}O$ and $\delta^{2}H$ values between about –13‰ to –14.5‰ VSMOW and –105‰ to –114‰ VSMOW, respectively, alternate with brackish marine-type signatures similar to those of Littorina and Baltic Sea water. Close examination of the data reveals that such variations are repeated three times where the distance along the borehole to the next water-conducting fracture is within a few metres only (Figure 7-17). The most negative isotope compositions occur at borehole lengths of 490 m, 509–512 m and 565–569 m and coincide with the lowest Cl^- concentrations and the lowest or non-detectable apparent Mg^{2+} contents. At each of these locations, the gradients described by the porewater isotope compositions are steep and the transition from cold temperature glacial-type to brackish marine-type isotope signatures occurs within some decimetres to a few metres. Considering the transport properties of the rock (cf. Chapter 5), these steep gradients over short distances between different porewater samples clearly indicate that these isotope (and chemical) signatures were developed in the most recent past during Holocene times. This is consistent with the observations made above based on the porewater Mg^{2+} concentrations that porewater in samples from the bottom of deformation zone ZFMA2 and at around 420 m depth in borehole KFM02B, and the samples down to deformation zone ENE0060A from the upper part of borehole KFM06A, were strongly influenced by meteoric water prior to the interaction with Littorina Sea water (cf. Section 7.2.4).

7.3.2 Relation between porewater and fracture groundwater

In the footwall bedrock s.l. the porewater isotope composition is generally enriched compared to that of the fracture groundwater along the sampled profile to maximum depth (Figure 7-17). Therefore, a transient state is established almost throughout the footwall bedrock s.l. between porewater and fracture groundwater with respect to the oxygen and hydrogen isotope compositions. Interestingly, such a transient state is also still established in the shallowest zone, although less pronounced, where the distance between porewater samples and water-conducting fractures is rather short (Figure 7-17). This indicates that the circulation of fracture groundwater, which nowadays has a strong brackish marine Littorina type signature (cf. /Smellie et al. 2008/), is limited. In fact, as already suggested from the Cl^- and Mg^{2+} concentrations (cf. Sections 7.1 and 7.2), the still strongly ^{18}O enriched isotope signature of the porewaters also indicates that the circulation of cold temperature and/or glacial type water in the footwall bedrock s.l. did, if at all, only occur in discrete zones because otherwise the isotope signature of the porewaters would have been changed rather quickly in the shallow zone.

The only exception to the general pattern given by the isotope composition of porewaters in the footwall bedrock s.l. is the sample at 380 m depth in borehole KFM08C that shows a depleted $\delta^{18}O$ value of –12.7‰ VSMOW (Figure 7-17). This sample was collected from within 5 m of a water-conducting episyenite zone in fracture domain FFM06. The depleted isotope signature of this porewater suggests the presence of a cold climate or possible glacial component in the still brackish Na-Ca-Cl-(HCO_3) type porewater. In fact, fracture groundwater with a similarly depleted isotope signature could be sampled from the neighbouring borehole KFM08A at some 100 m greater depth (Figure 7-17).

In the hanging wall bedrock s.l., porewater and groundwater show steady state at shallow depths down to about 150 m depth where the groundwater is dominated by present day type infiltration (cf. /Smellie et al. 2008/). There is also an indication at greater depth towards the end of borehole KFM02B that a

situation equal to or close to steady state is established between porewater and fracture groundwater in spite of the large variations in the isotopic compositions (Figure 7-17). This is consistent with the generally short distances between porewater sample and water-conducting fractures and the high frequency of such fractures in this bedrock segment. The obvious cold climate to glacial type isotope signatures present in the porewater of rocks from the hanging wall bedrock s.l. (including the upper part of borehole KFM06A) indicate that this bedrock underwent interaction with dilute meteoric water prior to the interaction with Littorina Sea water what is consistent with the Cl^- and Mg^{2+} concentrations of these porewaters (cf. Sections 7.1 and 7.2). This demonstrates that in the hanging wall bedrock s.l. the hydraulic system has been and still is more active compared to the footwall bedrock s.l.

8 Palaeohydrogeochemical implications

Solute transport in the intact rock matrix of the rocks from the Forsmark investigation site has been identified to occur predominantly by diffusion. This puts a time constraint on the interaction between matrix porewater and fracture groundwater circulating in more transmissive zones. In the absence of absolute time measurements, the knowledge of the pore diffusion coefficient for solutes allows estimates of the interaction time based on the distance between the porewater in a specific rock matrix sample and the groundwater in the nearest water-conducting fracture. Therefore, the compositional differences in the porewater as a function of depth and distance to the nearest water-conducting fracture allow, in combination with the fracture groundwater data, a (partial) reconstruction of the palaeohydrogeological evolution of the site. In addition, hydrogeological events that occurred during Holocene, Pleistocene and possibly even further back in time and that are no longer resolvable in the fracture groundwater, can still be identified in the porewater.

The chemical and isotopic compositions of porewater are distinct for the rock matrix of the footwall bedrock segment (including the lower part of borehole KFM06A) and the hanging wall bedrock segment (including the upper part of borehole KFM06A). The differences indicate that they cover largely different time periods of the hydrogeological evolution of site being mainly pre-Weichselian glaciation in the footwall bedrock s.l. and post-Weichselian glaciation in the hanging wall bedrock. Exceptions include the shallowest zone down to about 150 m depth and, at deeper levels, a few specific more conductive zones (e.g. episyenite zones) in the footwall bedrock s.l. where porewater also records Holocene influences.

In the footwall bedrock s.l., the rather continuous zonation of porewater chemical types as a function of depth from dilute Na-Ca-HCO_3 type to brackish Na-Ca-Cl-(HCO_3) type and saline Ca-Na-Cl type suggests a porewater evolution under limited hydraulic activity in the fracture network, although local differences are present and the changes in chemical type occur at different depths in the different boreholes. The chemical composition of the dilute Na-Ca-HCO_3 type and brackish Na-Ca-Cl-(HCO_3) porewater types (i.e. moderate Cl^- concentration, absence of Mg^{2+}, rock-water interaction controlled Sr^{2+}) indicates that influences of the most recent hydrologic events such as Littorina and/or Baltic Sea water and present day meteoric water are absent in these porewaters. Furthermore, the Sr-isotopes seem to have evolved mainly from rock-water interaction compared to exchange with different types of fracture groundwaters. Similarly, the absence of a distinct cold climate type $\delta^{18}O$ and $\delta^{2}H$ signature indicates that the porewaters were not subjected to an interaction with cold climate type water, certainly not with glacial water from the last glaciation cycle. On the other hand, the isotope signature indicates that these porewaters have originated from interaction with fracture groundwater of meteoric origin. Based on enriched $\delta^{18}O$ and $\delta^{2}H$ values this meteoric water infiltrated under warmer climatic conditions than today and during Pleistocene times, i.e. the water probably infiltrated during Tertiary times.

The preservation of such very old signatures implies either large distances between porewater and the nearest fracture groundwaters and/or strongly reduced hydraulic activity in the fracture network. Both these criteria seem to apply for most of the footwall bedrock s.l., certainly at intermediate to great depths. Below 200 m depth the distance between porewater and the nearest water-conducting fractures is mainly between 5–10 m and below about 300 m depth already more than 20 m for most samples due to the rapid decrease in fracture frequency with increasing depth. However, even at shallow depth, where there is still a considerable frequency of water-conducting fractures, porewater and fracture groundwater are at a transient state with respect to chemical and isotopic composition. Groundwater at these depths has a considerable component of Littorina type sea water, which imposed its traces on the more dilute porewater down to about 200 m depth in borehole KFM01D, but not in borehole KFM08C. In addition, a steady state situation is not established in borehole KFM01D. The impact of this Holocene fracture groundwater event on the porewater is thus very limited even at these depths. Furthermore, at intermediate to great depth a transient state between porewater and fracture groundwater prevails down to at least about 640 m depth with the fracture groundwater being distinctly more mineralised and less enriched in ^{18}O and ^{2}H than the porewater. Based on ^{36}Cl and ^{4}He the average residence time in the underground of some fracture groundwaters collected from these depths can be estimated to be more than at least 1 Ma /Smellie et al. 2008/.

The prevailing transient state between porewater and fracture groundwater, in combination with the large distances between porewater and fracture groundwater at these depths, indicates that the origin of the porewater dates back to even older times. This is also supported by the presence of the saline Ca-Na-Cl type porewater preserved at greatest depths in boreholes KFM01D, KFM08C and KFM06A characterised by the lowest fracture frequency. These porewaters show the greatest chemical and isotopic affinity to the different rock types and their compositions seem to be largely controlled by rock-water interactions. Although there are no data available on fracture groundwaters at these depths for comparison, similar groundwater chemical types are to be expected based on the Forsmark area as a whole.

The porewaters in the footwall bedrock s.l. thus indicate that before the beginning of the Pleistocene the entire rock volume was saturated with dilute meteoric water of warm climate origin, possibly as far back as Tertiary times, down to at least about 640 m depth. Changes induced by fracture groundwater from Pleistocene times either did not occur or were so minimal that they cannot be resolved. Similarly, changes induced by the intrusion of the last deglaciation meltwater and post-glacial brackish marine water types in the fracture network resulted only in discrete traces in the porewater associated with the shallowest zone of the footwall bedrock s.l. (fracture domain FFM02).

In the steeply dipping defomation zones, the porewater appears to record rather recent imprints of higher saline groundwater in the first few metres from a water-conducting zone, for example, as evidenced by the samples taken adjacent to vuggy episyenite in borehole KFM09B. This suggests that the saline groundwater similar to the present one was circulating in the fractures to depths of at least 440 m in the last few thousands of years. This might suggest that the present day level of groundwater of similar high salinity, and believed to have originated by upconing from depths greater than 1,000 m in boreholes KFM07A and KFM09C, may at one time have existed at much shallower levels in the bedrock. The timing and exact processes of such ‘upconing’ of deeper, more saline and evolved groundwaters cannot be further defined based on the present data. However, based on the time required to produce these singatures it seems highly unlikely that they are the result of anthropogenic ‘upconing’ if compared to present groundwater data /Smellie et al. 2008/.

A completely different picture arises for the hanging wall bedrock s.l. (including the upper part of borehole KFM06A). Here, the porewater is generally more dilute and the porewater chemical types of dilute Ca-Na-HCO_3 type and Na-Ca-HCO_3 type alternate irregularly with depth, but are more correlated to major deformation zones. Down to the maximum depths sampled (about 560 m depth), the porewaters display greatly variable chemical and isotopic compositions as a function of depth. Compositional changes to the porewater produced by the superimposition of distinct fracture groundwater signatures are mainly related to the short distances to nearby water-conducting fractures within rather restricted time periods of a few thousands of years. The large compositional variability preserved in porewater samples located at similar distances from different water-conducting fractures indicates that the porewater composition is fracture groundwater dominated and the hydraulic system is more active in the hanging wall bedrock compared to the footwall bedrock.

Porewater in the hanging wall bedrock s.l. is the result of interaction with fracture groundwater of meteoric origin ranging from cold to present day climatic conditions according to their oxygen and hydrogen isotope composition with all the $\delta^{18}O$ and $\delta^{2}H$ values plotting parallel to the Global Meteoric Water Line. The majority of the porewaters from this area have conspicuously elevated Mg^{2+} concentrations and reflect an interaction with brackish marine water of either Littornia and/or Baltic Sea water type. The shallowest porewater samples down to about 150 m depth at similar distances to water-conducting fractures have higher Cl^- concentrations, but similar isotopic compositions as fracture groundwaters further up indicating a transient state in the chemical composition between porewaters and fracture groundwaters, while a situation closer to steady state is suggested for the isotope composition. Whereas the fracture groundwater at these levels is dominated by present day meteoric infiltration with low Cl^- concentrations, the porewaters still retain a previous interaction with brackish marine water based on Cl^- and Mg^{2+}. The situation closer to steady state suggested by the isotope composition is inconclusive because the isotope signature of so-called brackish marine Littorina type sea water and present day infiltration are almost indistinguishable /Smellie et al. 2008/. Only at a distance of a few metres into the intact rock matrix does porewater display characteristic, but altered, cold climate isotope signatures with Cl^- and Mg^{2+} concentrations clearly above that of glacial meltwater. This is also observed at greater depth close to the abundant fractures related to deformation zones ZFMF1 and ZFMA2.

Along the entire depth down to about 560 m in the hanging wall bedrock s.l. a transient state between porewater and fracture groundwater is established with respect to Cl^- concentrations, with the concentrations being higher in the fracture groundwater. In contrast, the isotope composition might reflect a situation close to steady state at certain locations. This highlights the above discussion of limitation in resolving the stable isotopes with fracture groundwater of different origin having equal or similar isotope compositions. In combination with other conservative tracers and also non-conservative parameters such as Mg^{2+} and Sr^{2+}, a transient state is well established. As mentioned above, the elevated Mg^{2+} concentrations reflect an interaction with brackish marine water of either Littorina and/or Baltic Sea water type. The high Mg/Cl ratios developed in the porewater indicate that the interaction of such marine water must have occurred with a dilute porewater that was previously present in the rock matrix. This dilute porewater was of cold climate (glacial) origin as indicated by the depleted $\delta^{18}O$ values of less than –13‰ VSMOW further away from the water-conducting fracture. The distance between porewater samples and the nearest water-conducting fractures of generally less than 10 m further constrains this cold climate signature to the last glaciation (Weichselian) and such cold climate glacial water was circulating for a considerable time period in the fractures at these depths. Since the last deglaciation, this cold climate porewater signature has become overprinted with a brackish marine-type signature as indicated by Cl^-, Mg^{2+} and $\delta^{18}O$ in porewaters sampled closer to the water-conducting fracture. In the shallow zone, this brackish marine signature is now becoming overprinted by the circulation of present-day meteoric groundwaters.

9 Conclusions

The chemical and isotopic composition of porewater in the matrix of the rocks from the Forsmark investigation site acts as an archive for the exchange between different types of fracture groundwater circulating in the connected fracture network and the porewater in connected porosity of the rock matrix of the crystalline rock. The variable but long-lasting exchange processes between fracture groundwater and porewater have been identified to occur mainly by diffusion and extend far into the intact rock matrix. Diffusive processes are much slower than the mixing processes in the dominant fracture-groundwater system characterised by advection so that the records preserved in the porewater composition may be used to reconstruct parts of the palaeohydrogeological evolution that can no longer be deduced from fracture groundwater data alone.

The quantitative interpretation of the porewater-fracture groundwater interaction as a function of time is complex and depends on many factors such as the transport properties in the rock matrix, the distance to the nearest water-conducting fracture, and the time period of fracture groundwater circulation with constant chemical and isotopic conditions, etc. Most demanding in such an interpretation is the case if a transient state (i.e. a difference in the chemical and isotopic composition between porewater and fracture groundwater) is established because of the unknown conditions at the start of the interaction (initial conditions). In the situation of a steady state, on the other hand, at least a minimum and maximum time of interaction can be deduced more easily. In both cases, however, changes in the boundary conditions (i.e. the fracture groundwater composition) may become masked and superimposed in the course of the interaction. Furthermore, changes in the boundary conditions might not be equally present for all components. For example, the Cl^- concentration in fracture groundwater might grossly change with time while the water isotope composition remains similar as, for example, in the case of Littorina and Baltic Sea water, or the Cl^- concentration might remain similar whereas the water isotope composition changes dramatically as, for example, in the case of present day infiltration and glacial meltwater. For the quantitative interpretation of the porewater-fracture groundwater interactions, observations from several independent natural tracers (such as Cl^-, ^{18}O, ^{2}H, noble gases etc) are required. Depending on the specific geologic and (palaeo) hydrogeological situation non-conservative element concentrations and isotope compositions might be of additional support. In the data interpretation, however, the limitations of borehole observations with respect to the 3-dimensional distribution of water-conducting fractures and rock matrix transport properties have to be respected.

Based on the conducted characterisation of the porewater chemical and isotopic composition, geochemical modelling and the quantitative description of natural tracer profiles in porewater from rocks of the Forsmark site, the following conclusions emerge:

- Porewater acts as an archive of the past hydrogeological history at the Forsmark investigation site and its composition puts strong constraints on the interpretation of the palaeohydrogeological evolution of the site.
- Solute transport in the intact rock matrix appears to be dominated by diffusion, and matrix diffusion was identified to occur at least over several decametres into the rock matrix. Experimentally derived average pore diffusion coefficients for Cl^- are: metagranite to granodiorite = 1.2×10^{-10} $m^2/s \pm 0.40\times10^{-10}$ m^2/s (n = 21), granodiorite to tonalite = 8.1×10^{-11} m^2/s (n = 1), aplitic granite = 9.4×10^{-11} $m^2/s \pm 4.2\times10^{-12}$ m^2/s and fine-grained granite = 1.1×10^{-10} $m^2/s \pm 0.38\times10^{-10}$ m^2/s (n = 3) at a temperature of 25°C.
- The composition of porewaters are distinct in the rocks from the footwall bedrock s.l. (i.e. target volume; fracture domains FFM01 and FFM06 and in this study including the lower part of fracture domain FFM01 in borehole KFM06A) to the north-west, and the hanging wall bedrock s.l. (i.e. fracture domain FFM03 and in this study including the upper part of borehole KFM06A comprising fracture domain FFM02 and the upper part of fracture domain FFM01) to the south-east, and clearly discern between two different hydraulic regimes with a different palaeohydrogeological evolution.

- Depending on the distance to the nearest water-conducting fracture and the depth of the rock sample, the porewater preserves signatures of exchange with fracture groundwaters during Holocene, Pleistocene and pre-Pleistocene times.
- In the footwall bedrock s.l. porewater, only locally in the shallowest levels down to about 200 m depth, a weak influence of Holocene time fracture groundwater is developed that can be associated to the exchange with brackish marine Littorina type fracture groundwater.
- In the footwall bedrock s.l. below 200 m depth, porewater is dilute to moderately brackish in composition with isotope signatures depleted in the heavy isotopes down to about 640 m depth. A transient state with respect to higher mineralised fracture groundwater is established. These porewaters have evolved from pre-Pleistocene meteoric to brackish fracture groundwater of warm climate origin and support the very long average residence time derived for some groundwaters from this area.
- In the footwall bedrock s.l. at the greatest depths sampled, the origin of the saline Ca-Na-Cl type porewater cannot be related to any fracture groundwater because of the absence of such data. Their origin is, however, even older than that of the brackish type porewaters at intermediate depths.
- In general, the porewater composition of the footwall bedrock s.l. suggests an evolution with a well-developed component of rock-water interaction in a weakly active hydraulic system (mainly limited to the shallow zone) at least during Holocene and Pleistocene times.
- In the hanging wall bedrock s.l., porewater is generally dilute and has characteristic signatures of interaction with glacial and brackish marine type fracture groundwaters. Compositional changes are related to the fracture frequency (mainly deformation zones ZFMF1 and ZFMA2) and do not show a regular distribution with depth.
- In the hanging wall bedrock s.l., the porewater composition indicates that the system became essentially saturated with dilute glacial type water after the last glaciation (Weichselian) and such cold climate glacial water was circulating for a considerable time period in the fractures down to more than 500 m depth. Since the last deglaciation, this cold climate porewater signature has become overprinted with a brackish marine Littorina type signature as indicated by Cl^{-}, Mg^{2+} and $\delta^{18}O$ in porewaters sampled closer to the conducting fracture.
- In the shallow zone of the hanging wall bedrock, the brackish marine Littorina and/or Baltic Sea signature is now becoming overprinted by the circulation of present-day meteoric groundwaters.
- In the hanging wall bedrock s.l., the porewater is dominated by rapid exchange with fracture groundwater within a few thousands of years in a hydraulically very active system.

10 Acknowledgements

Much appreciation is given to Kenneth Åkerström (SKB) for the on-site selection and packaging and rapid dispatching of the drillcore samples to the University of Bern. The support and patience of Anne-Chatrin Nilsson (SKB) throughout the study is much appreciated. We are grateful for the anlytical support from R. Maeder, F. Eichinger, C. Läderach and G. Chevalier (solution chemistry) at the Institute of Geological Sciences, University of Bern. Many thanks are also due to B. Kalinowski (SKB) for the editorial handling of this report.

11 References

Carlsten S, Döse C, Samuelsson E, Gustafsson J, Petersson J, Stephens M, Thunehed H, 2007. Forsmark site investigations. Geological single-hole interpretation of KFM02B. SKB P-07-107, Svensk Kärnbränslehantering AB.

Crank J, 1975. The mathematics of diffusion. 2nd addition. Oxford University Press.

Desaulniers D E, Kaufmann R S, Cherry J A, Bentley H W, 1986. ^{37}Cl-^{35}Cl variations in a diffusion-controlled groundwater system. Geochim. Cosmochim. Acta 50, 1757–1764.

Eggenkamp H G M, Middelbourg J J, Kreulen R, 1994. Preferential diffusion of ^{35}Cl relative to ^{37}Cl in sediments of Kau Bay, Halmahera, Indonesia. Chem. Geol. 116, 317–325.

Follin S, Levén J, Hartley L, Jackson P, Joyce S, Roberts D, Swift B, 2007. Hydrogeological characterisation and modelling of deformation zones and fracture domains, Forsmark modelling stage 2.2. SKB R-07-48 Svensk Kärnbränslehantering AB.

Follin S, 2008. Bedrock hydrogeology Forsmark. Site descriptive modelling, SDM-Site Forsmark. SKB R-08-95, Svensk Kärnbränslehantering AB.

Fox A, La Pointe P, Hermanson J, Öhman J, 2007. Statistical geological discrete fracture network model. Forsmark modelling stage 2.2. SKB R-07-46, Svensk Kärnbränslehantering AB.

Gimmi T, Waber H N, 2004. Modelling of tracer profiles in porewater of argillaceous rocks in the Benken borehole: Stable water isotopes, chloride, and chlorine isotopes. Nagra Technical Report NTB 04-05, Wettingen, Switzerland.

Gorbatsevich F F, 2003. Decompaction mechanism of deep crystalline rocks under stress relief. Tectonophysics, 370, 121–128.

Gustavsson E, Ludvigson J-E, Gokall-Norman K, 2006. Forsmark site investigations. Single-hole injection tests in borehole KFM09B. SKB P-06-122, Svensk Kärnbränslehantering AB.

Johansson H, Byegård J, Skarnemark G, Skålberg M, 1997. Matrix diffusion of some alkali- and alkaline earth metals in granitic rocks. In: W.J. Gray, I.R. Triay (Eds.), Scienific Basis for Nuclear Waste Management XX, Vol. 465.

Laaksoharju M, Smellie J, Tullborg E-L, Gimeno M, Hallbeck L, Molinero J, Waber H N, 2008. Bedrock hydrochemistry Forsmark. Site descriptive modelling, SDM-Site Forsmark. SKB R-08-47, Svensk Kärnbränslehantering AB.

Lichtner P C, 2007. FLOTRAN Users Manual: Two-phase non-isothermal coupled thermal-hydrologic-chemical (THC) reactive flow and transport code, Version 2, Los Alamos National Laboratory, Los Alamos, New Mexico.

Liu J, Löfgren M, Neretnieks I, 2006. SR-Can: Data and uncertainty assessment, Matrix diffusivity and porosity in situ. SKB R-06-111, Svensk Kärnbränslehantering AB.

Martin C D, 2007. Quantifying in situ stress magnitudes and orientations for Forsmark, Design Step D2. SKB R-06-111, Svensk Kärnbränslehantering AB.

Mazurek M, Alt-Epping P, Bath A, Gimmi T, Waber H N, 2009. Natural Tracer Profiles Across Argillaceous Formations: The CLAYTRAC Project. Nuclear Energy Agency – Radioactive Waste Management, NEA No.6253, OECD Paris, France.

Michard G, Pearson F J, Gautschi A, 1996. Chemical evolution of waters during long term interaction with granitic rocks in northern Switzerland. Appl. Geochem. 11, 757–774.

Neretnieks I, 1980. Diffusion in the rock matrix: an important factor for radionuclide retardation? J. Geophys. Res. 85, 4379–4397.

Nordqvist R, Gustafsson E, Andersson P, Thur P, 2008. Groundwater flow and hydraulic gradients in fractures and fracture zones at Forsmark and Oskarshamn. SKB R-08-103, Svensk Kärnbränslehantering AB.

Nordstrom D K, Plummer L N, Wigley T M L, Wolery T J, Ball J W, Jenne E A, Bassett R L, Crerar D A, Florence T M, Fritz B, Hoffman M, Holdren G R Jr, Lafon G M, Mattigod S V, McDuff R E, Morel F, Reddy M M, Sposito G, Thrailkill J, 1979. A comparison of computerized chemical models for equilibrium calculations in aqueous system. In: E.A. Jenne (ed.), Chemical Modeling in aqueous systems, speciation, sorption, solubility, and kinetics, American Chemical Society, Series 93, p. 857–892.

Nordstrom, D K, Ball, J W, Donahoe, R J, Whittemore, D, 1989. Ground water chemistry and water-rock interactions at Stripa. Geochim. Cosmochim. Acta 53, 1727–1740.

Norton D, Knapp R, 1977. The nature of porosity. Am. J. Sci., 277, 913–936.

Ohlsson Y, Neretnieks I, 1995. Literature survey of matrix diffusion theory and of experiments and data including natural analogues. SKB TR 95-12, Svensk Kärnbränslehantering AB.

Ohlsson Y, 2000. Studies of Ionic Diffusion in Chrystalline Rock. PhD thesis, Royal Institute of Technology KTH, Stockholm, Sweden. ISBN 91-7283-025-5.

Olofsson I, Simeonov A, Stigsson M, Stephens M, Follin S, Nilsson A-C, Röshoff K, Lindberg U, Lanaro F, Fredriksson A, Persson L, 2007. Site descriptive modelling Forsmark, stage 2.2. A fracture domain concept as a basis for the statistical modelling of fractures and minor deformation zones, and interdisciplinary coordination. SKB R-07-15, Svensk Kärnbränslehantering AB.

Ota K, Möri A, Alexander W R, Frieg B, Schild M, 2003. Influence of the mode of matrix porosity determination on matrix diffusion calculations. J. Cont. Hydrol., 61, 131–145.

Parkhurst D L, Appelo C A J, 1999. User's Guide to PHREEQC (Version 2) – A Computer Program for Speciation, Batch-Reaction, One-Dimensional Transport, and Inverse Geochemical Calculations: Denver, CO, U. S. Geological Survey, Water-Resources Investigations Report 99-4259; v. W2-13, 2006.

Pearson F J, 1999. What is the porosity of a mudrock? In: A.C. Aplin, A.J. Fleet, J.H.S. Macquaker (Eds.), Muds and Mudstones: Physical and Fluid Flow Properties. London, Geol. Soc. Spec. Publ. 158, 9–21.

Pearson F J, Arcos D, Bath, A, Boisson, J Y, Fernandez, A M, Gaebler, H E, Gaucher E C, Gautschi A, Griffault L, Hernan P, Waber H N, 2003. Mont Terri Project – Geochemistry of Water in the Opalinus Clay Formation at the Mont Terri Rock Laboratory. Reports of the Federal Office of Water and Geology (FOWG), Geology Series No. 5.

Petersson J, Skogsmo G, Berglund J, Stråhle A, 2005. Forsmark site investigation. Boremap mapping of telescopic drilled borehole KFM06A and core drilled borehole KFM06B. SKB P-05-101, Svensk Kärnbränslehantering AB.

Petersson J, Skogsmo G, von Dalwigk I, Wängnerud A, Berglund J, 2006a. Forsmark site investigation. Boremap mapping of telescopic drilled borehole KFM01D. SKB P-06-132, Svensk Kärnbränslehantering AB.

Petersson J, Wängnerud A, von Dalwigk I, Berglund J, Andresson U B, 2006b. Forsmark site investigation. Boremap mapping of telescopic drilled borehole KFM08C. SKB P-06-203, Svensk Kärnbränslehantering AB.

Petersson J, Skogsmo G, von Dalwigk I, Wängnerud A, Berglund J, 2006c. Forsmark site investigation. Boremap mapping of core drilled borehole KFM09B. SKB P-06-131, Svensk Kärnbränslehantering AB.

Rogge T, 1997. Eine molekular-diffusive Methode zur Bestimmung des Porenwassergehaltes und der Zusammensetzung von stabilen Isotopen im Porenwasser von Gestein. Unpubl. Diploma Thesis, Institut für Umweltphysik, University of Heidelberg (in German).

Rouhiainen P, Sokolnicki M, 2005. Forsmark site investigation: Difference flow logging in borehole KFM06A. SKB P-05-15, Svensk Kärnbränslehantering AB.

Rübel A P, 2000. Stofftransport in undurchlässigen Gesteinsschichten – Isotopenuntersuchungen im Grund- und Porenwasser. PhD Thesis, Institut für Umweltphysik, Unversity of Heidelberg, Der Andere Verlag, Osnabrück, Germany (in German).

Samuelsson E, Dahlin P, Lundberg E, 2007. Forsmark site investigation. Boremap mapping of telescopic drilled borehole KFM02B. SKB P-07-102, Svensk Kärnbränslehantering AB.

Sandström B, Tullborg E-L, Smellie J, MacKenzie A B, Suksi J, 2008. Fracture mineralogy of the Forsmark site. SDM-Site Forsmark. SKB R-08-102, Svensk Kärnbränslehantering AB.

Schild M, Siegesmund S, Vollbrecht A, Mazurek M, 2001. Characterisation of granite matrix porosity and pore-space geometry by in situ and laboratory methods. Geophys. J. Int., 146, 111–125.

Selnert E, Byegård J, Widestrand H, 2008. Forsmark site investigation. Laboratory measurements within the site investigaion programme for the transport properties of the rock. Final report. SKB R-07-13, Svensk Kärnbränslehantering AB.

Skagius K, Neretnieks I, 1986. Diffusivity measurements and electrical-resistivity measurements in rock samples under mechanical stress. Water Resour. Res., 22, 570–580.

Smellie J A T, Waber H N, Frape S K (eds.), 2003. Matrix fluid chemistry experiment. Final Report. SKB TR-03-18, Svensk Kärnbränslehantering AB.

Smellie J, Tullborg E-L, Nilsson A-C, Sandström B, Waber H N, Gimeno M, Gascoyne M, 2008. Explorative analysis of major components and isotopes. SDM-site Forsmark. SKB R-08-84, Svensk Kärnbränslehantering AB.

Stephens M B, Simeonov A, Isaksson H, 2008a. Bedrock geology Forsmark, Modelling stage 2.3. Implications for and verification of deterministic geological models based on complementary data. SKB R-08-64, Svensk Kärnbränslehantering AB.

Stephens M B, Bergman T, Isaksson H, Petersson J, 2008b. Bedrock geology Forsmark Modelling stage 2.3. Description of the bedrock geological map at the ground surface. SKB R-08-128, Svensk Kärnbränslehantering AB.

Söderbäck B (ed.), 2008. Geological evolution, palaeoclimate and historical development of the Forsmark and Laxemar-Simpevarp areas. Site descriptive modelling, SDM-Site. SKB R-08-19, Svensk Kärnbränslehantering AB.

Tullborg E-L, Larson, S Å, 2006. Porosity in crystalline rocks – A matter of scale. Eng. Geol., 84, 75–83.

Vilks P, Cramer J J, Jensen M, Miller N H, Miller H G, Stanchell F W, 2003. In situ diffusion experiment in granite: Phase I. J. Contam. Hydrol. 61, 191–202.

Väisäsvaara J, Leppänen H, Pekkanen, J, 2006a. Forsmark site investigations: Difference flow logging in borehole KFM01D. SKB P-06-161, Svensk Kärnbränslehantering AB.

Väisäsvaara J, Leppänen H, Pekkanen J, Pöllänen, J, 2006b. Forsmark site investigations: Difference flow logging in borehole KFM08C. SKB P-06-189, Svensk Kärnbränslehantering AB.

Väisäsvaara J, Pöllänen J, 2007. Forsmark site investigations: Difference flow logging in borehole KFM02B. SKB P-07-83, Svensk Kärnbränslehantering AB.

Waber H N, Smellie J A T, 2005. Forsmark site investigation. Borehole KFM06A: Characterisation of porewater. Part I: Diffusion experiments. SKB P-05-196, Svensk Kärnbränslehantering AB.

Waber H N, Smellie J A T, 2006. Oskarshamn site investigation. Borehole KLX03: Characterisation of porewater. Part 2: Rock properties and diffusion experiments. SKB P-06-77, Svensk Kärnbränslehantering AB.

Waber H N, Smellie J A T, 2007. Forsmark site investigation. Borehole KFM01D, KFM08C, KFM09B: Characterisation of porewater. Part I: Diffusion experiments and porewater data. SKB P-07-119, Svensk Kärnbränslehantering AB.

Waber H N, Smellie J A T, 2008. Characterisation of porewater in crystalline rocks. Appl. Geochem. 23, 1834–1861.

Waber H N, Smellie J A T, 2009. Forsmark site investigation. Borehole KFM02B: Characterisation of porewater. Part I: Diffusion experiments and porewater data. SKB P-09-14, Svensk Kärnbränslehantering AB.

Waber H N, Gimmi T, Smellie J A T, deHaller A, 2009. Porewater in the rock matrix. Site descriptive modelling, SDM-Site Laxemar. SKB R-08-112, Svensk Kärnbränslehantering AB.

Appendix A

Data Tables

Table A-1. Geological information and water content of rock samples used for porewater investigations from boreholes KFM01D, KFM02B, KFM06A, KFM08C and KFM09B (shaded: hanging wall bedrock s.l., cf. Figure 2-3).

SKB Sample No	UniBern Sample No	Average borehole length	Average Elevation [1]	Lithology	Fracture Domain/ Deform. Zone	Rock Unit	Fracture intensity [2]	Distance to conducting fracture [3]	No of samples	Water content by drying at 105°C (average) [4]		Water content by diffusive isotope exchange [5]	
		(m)	(m)					(m)		(wt.%)	(stdev)	(wt.%)	(stdev)
SKB12108	KFM01D-1	140.69	–112.13	granite – granodiorite	FFM02	RU1	high	2.2	5	0.119	0.012	0.101	0.008
SKB12109	KFM01D-2	191.73	–155.30	granite – granodiorite	FFM02	RU2	high	2.7	3	0.087	0.003		
SKB12110	KFM01D-3	255.13	–204.57	granite – granodiorite	FFM01	RU2	low	9.2	4	0.082	0.005	0.114	0.007
SKB12111	KFM01D-4	299.09	–239.33	granite – granodiorite	FFM01	RU2	low	8.4	1	0.147	0.015	0.112	0.007
SKB12112	KFM01D-5	352.07	–280.50	granite – granodiorite	FFM01	RU2	moderate	35.2	1	0.105	0.010	0.128	0.008
SKB12113	KFM01D-6	393.69	–312.47	granite – granodiorite	FFM01	RU2	moderate	11.7	1	0.100	0.010	0.121	0.007
SKB12114	KFM01D-7	462.79	–365.42	granite – granodiorite	FFM01	RU3	low	31.3	1	0.186	0.019	0.152	0.007
SKB12115	KFM01D-8	500.05	–393.49	granite – granodiorite	FFM01	RU4	low	68.6	2	0.125	0.003	0.133	0.009
SKB12116	KFM01D-9	544.23	–426.54	granite – granodiorite	FFM01	RU4	low	27.0	1	0.097	0.010	0.139	0.008
SKB12117	KFM01D-10	600.25	–468.02	granite, fine–grained	FFM01	RU4	low	29.0	1	0.131	0.013	0.123	0.007
SKB12118	KFM01D-11	643.12	–499.49	granite – granodiorite	FFM01	RU4	low	71.9	2	0.123	0.013	0.122	0.007
SKB12121	KFM01D-12	700.25	–541.00	granite – granodiorite	ENE0061	RU4	moderate	129.1	2	0.125	0.028	0.129	0.007
SKB12122	KFM01D-13	747.29	–574.82	granite – granodiorite	FFM01	RU4	low	176.1	2	0.107	0.001	0.102	0.006
SKB12124	KFM01D-14	790.56	–605.62	granite – granodiorite	FFM01	RU4	low	219.4	4	0.112	0.015	0.104	0.005
SKB12400	KFM02B-1	158.91	–149.20	metagranite – granodiorite	ZFMA3	RU1a	high	0.4	1	0.252	0.025	–	
SKB12401	KFM02B-2	171.83	–161.94	metagranite – granodiorite	ZFMA3	RU1a	high	2.4	3	0.423	0.020	0.269	0.002
SKB12402	KFM02B-3	210.64	–200.21	metagranite – granodiorite	FFM03	RU1a	high	8.7	3	0.184	0.008	0.172	0.002
SKB12403	KFM02B-4	287.16	–275.64	metagranite – granodiorite	FFM03	RU1a	high	7.8	3	0.179	0.005	0.243	0.002
SKB12404	KFM02B-5	393.29	–380.24	granite, fine-grained	FFM03	RU2	high	6.1	3	0.213	0.007	0.188	0.002
SKB12405	KFM02B-6	430.74	–417.14	granite, fine-grained	ZFMA2	RU2	high	1.2	3	0.135	0.007	–	
SKB12406	KFM02B-7	441.45	–427.68	metagranite – granodiorite	FFM01	RU1b	high	7.0	3	0.182	0.009	0.160	0.002
SKB12407	KFM02B-8	448.06	–434.19	metagranite – granodiorite	FFM01	RU1b	high	13.6	3	0.222	0.021	0.190	0.002
SKB12408	KFM02B-9	459.84	–445.79	metagranite – granodiorite	FFM01	RU1b	high	9.7	3	0.120	0.002	0.126	0.002
SKB12409	KFM02B-10	474.07	–459.79	metagranite – granodiorite	ZFMF1	RU1b	high	4.6	3	0.189	0.020	0.184	0.003
SKB12410	KFM02B-11	478.89	–464.54	metagranite – granodiorite	ZFMF1	RU1b	high	9.4	3	0.147	0.016	0.129	0.002
SKB12411	KFM02B-12	490.46	–475.92	metagranite – granodiorite	ZFMF1	RU1b	high	9.0	3	0.225	0.039	0.154	0.002
SKB12412	KFM02B-13	498.84	–484.16	metagranite – granodiorite	ZFMF1	RU1b	high	0.8	3	0.343	0.013	0.365	0.003
SKB12413	KFM02B-14	509.81	–494.95	metagranite – granodiorite	ZFMF1	RU1b	high	10.2	3	0.241	0.024	0.242	0.002
SKB12414	KFM02B-15	512.57	–497.66	metagranite – granodiorite	ZFMF1	RU1b	high	13.0	3	0.223	0.029	0.214	0.002
SKB12415	KFM02B-16	512.96	–498.04	metagranite – granodiorite	ZFMF1	RU1b	high	13.4	3	0.123	0.011	0.186	0.003
SKB12416	KFM02B-17	513.34	–498.41	metagranite – granodiorite	FFM01	RU1b	high	13.7	3	0.144	0.009	0.137	0.002

SKB Sample No	UniBern Sample No	Average borehole length (m)	Average Elevation [1] (m)	Lithology	Fracture Domain/ Deform. Zone	Rock Unit	Fracture intensity [2]	Distance to conducting fracture [3] (m)	No of samples	Water content by drying at 105°C (average) [4] (wt.%)	(stdev)	Water content by diffusive isotope exchange [5] (wt.%)	(stdev)
SKB12417	KFM02B-18	513.68	–498.75	metagranite – granodiorite	FFM01	RU1b	high	14.1	3	0.170	0.011	0.183	0.002
SKB12418	KFM02B-19	514.04	–499.11	metagranite – granodiorite	FFM01	RU1b	high	14.9	3	0.157	0.013	0.163	0.002
SKB12419	KFM02B-20	514.47	–499.50	metagranite – granodiorite	FFM01	RU1b	high	14.9	3	0.171	0.032	–	
SKB12420	KFM02B-21	514.84	–499.89	metagranite – granodiorite	FFM01	RU1b	high	15.2	3	0.186	0.011	0.158	0.002
SKB12421	KFM02B-22	515.19	–500.23	metagranite – granodiorite	FFM01	RU1b	high	15.6	3	0.162	0.017	0.193	0.002
SKB12422	KFM02B-23	515.54	–500.58	metagranite – granodiorite	FFM01	RU1b	high	15.9	3	0.172	0.026	0.174	0.003
SKB12423	KFM02B-24	515.85	–500.89	metagranite – granodiorite	FFM01	RU1b	high	16.3	3	0.141	0.011	0.135	0.003
SKB12424	KFM02B-25	516.12	–501.15	metagranite – granodiorite	FFM01	RU1b	high	16.5	3	0.152	0.014	0.151	0.002
SKB12425	KFM02B-26	516.42	–501.44	metagranite – granodiorite	FFM01	RU1b	high	16.8	3	0.142	0.010	0.186	0.002
SKB12426	KFM02B-27	516.72	–501.74	metagranite – granodiorite	FFM01	RU1b	high	17.1	3	0.201	0.008	0.160	0.002
SKB12427	KFM02B-28	517.03	–502.04	metagranite – granodiorite	FFM01	RU1b	high	17.4	3	0.184	0.006	0.180	0.002
SKB12428	KFM02B-29	517.34	–502.34	metagranite – granodiorite	FFM01	RU1b	high	17.7	3	0.180	0.010	0.162	0.002
SKB12435	KFM02B-30	519.54	–504.51	metagranite – granodiorite	FFM01	RU1b	high	19.9	3	0.139	0.023	0.164	0.002
SKB12443	KFM02B-31	522.11	–507.04	metagranite – granodiorite	FFM01	RU1b	high	22.5	3	0.139	0.009	0.134	0.003
SKB12444	KFM02B-32	522.39	–507.31	metagranite – granodiorite	FFM01	RU1b	high	22.8	3	0.185	0.024	0.279	0.002
SKB12458	KFM02B-33	527.55	–512.38	metagranite – granodiorite	FFM01	RU1b	high	27.9	3	0.169	0.013	0.162	0.002
SKB12471	KFM02B-34	532.44	–517.19	metagranite – granodiorite	FFM01	RU1b	high	32.8	3	0.190	0.007	–	
SKB12601	KFM02B-39	559.83	–544.09	metagranite – granodiorite	FFM01	RU1b	high	60.2	3	0.170	0.006	0.163	0.003
SKB12603	KFM02B-40	562.47	–546.69	metagranite – granodiorite	FFM01	RU1b	high	62.9	3	0.231	0.013	0.211	0.003
SKB12604	KFM02B-41	565.29	–549.46	metagranite – granodiorite	FFM01	RU1b	high	65.7	3	0.256	0.039	0.222	0.002
SKB12605	KFM02B-42	569.35	–553.45	metagranite – granodiorite	FFM01	RU1b	high	69.8	3	0.239	0.014	0.253	0.003
SKB12607	KFM02B-43	573.65	–557.67	metagranite – granodiorite	FFM01	RU1b	high	74.1	3	0.193	0.012	0.170	0.003
SKB08550	KFM06A-1	146.08	–122.69	metagranite – granodiorite	FFM01	RU1a	high	3.0	3	0.182	0.047	0.179	0.012
SKB08551	KFM06A-2	194.69	–164.70	metagranite – granodiorite	ENE0060B	RU1a	high	3.4	3	0.219	0.016	0.153	0.010
SKB08552	KFM06A-3	252.41	–214.22	metagranite – granodiorite	ENE0060B	RU1a	high	5.8	3	0.150	0.022	0.162	0.010
SKB08553	KFM06A-4	281.82	–239.33	metagranite – granodiorite	FFM01	RU1a	high	8.6	3	0.183	0.028	0.165	0.010
SKB08554	KFM06A-5	298.49	–253.54	metagranite – granodiorite	FFM01	RU1a	high	0.3	3	0.117	0.010	0.145	0.009
SKB08555	KFM06A-6	355.29	–301.74	metagranite – granodiorite	ENE0060A	RU1a	high	2.0	3	0.303	0.052	0.336	0.015
SKB08556	KFM06A-7	395.40	–335.50	metagranite – granodiorite	FFM01	RU1a	high	2.0	3	0.121	0.007	0.134	0.009
SKB08557	KFM06A-8	440.98	–373.70	metagranite – granodiorite	FFM01	RU1a	high	7.5	3	0.111	0.021	0.134	0.009
SKB08558	KFM06A-9	500.02	–422.92	pegmatitic granite	FFM01	RU1a	low	51.8	3	0.165	0.016	0.166	0.010
SKB08559	KFM06A-10	563.38	–475.44	metagranite – granodiorite	FFM01	RU1a	low	60.3	3	0.120	0.008	0.132	0.009
SKB08560	KFM06A-11	575.94	–485.84	metagranite – granodiorite	FFM01	RU2	low	47.8	3	0.106	0.012	0.174	0.009
SKB08561	KFM06A-12	594.62	–501.28	granodiorite – tonalite	FFM01	RU2	low	29.1	3	0.110	0.012	–	

SKB Sample No	UniBern Sample No	Average borehole length (m)	Average Elevation [1] (m)	Lithology	Fracture Domain/ Deform. Zone	Rock Unit	Fracture intensity [2]	Distance to conducting fracture [3] (m)	No of samples	Water content by drying at 105°C (average) [4] (wt.%)	(stdev)	Water content by diffusive isotope exchange [5] (wt.%)	(stdev)
SKB08562	KFM06A-13	633.56	–533.40	metagranite, aplitic	FFM01	RU3	moderate	9.9	3	0.113	0.008	0.109	0.008
SKB08563	KFM06A-14	660.89	–555.84	metagranite, aplitic	FFM01	RU3		7.2	3	0.078	0.007	–	
SKB08564	KFM06A-15	698.81	–586.41	metagranite – granodiorite	FFM01	RU1b	low	44.6	3	0.112	0.005	0.138	0.010
SKB08565	KFM06A-16	763.59	–639.50	aplitic granite	ENE0725	RU4	moderate	19.8	3	0.121	0.007	0.149	0.009
SKB08566	KFM06A-17	810.84	–677.59	aplitic granite	FFM06	RU4	low	41.9	3	0.098	0.011	0.125	0.009
SKB08567	KFM06A-18	851.71	–710.24	aplitic granite	FFM06	RU4	low	82.8	3	0.117	0.013	0.131	0.010
SKB08568	KFM06A-19	900.97	–749.37	aplitic granite	FFM06	RU4	low	132.1	3	0.105	0.017	0.151	0.010
SKB08569	KFM06A-20	920.69	–764.95	aplitic granite	FFM06	RU4	low	151.8	3	0.081	0.023	0.119	0.009
SKB08570	KFM06A-21	948.77	–786.98	granodiorite – tonalite	FFM06	RU5	low	179.9	3	0.136	0.011	0.112	0.009
SKB08571	KFM06A-22	977.36	–809.33	granodiorite – tonalite	NNE2280	RU5	low	208.5	3	0.230	0.020	0.194	0.010
SKB08572	KFM06A-23	998.32	–825.66	granodiorite – tonalite	FFM06	RU5	low	229.4	3	0.107	0.018	0.146	0.009
SKB12119	KFM08C-1	154.69	–131.16	metagranite – granodiorite	FFM01	RU1a	moderate	6.6	3	0.079	0.003	0.103	0.006
SKB12120	KFM08C-2	254.92	–215.87	metagranite – granodiorite	FFM01	RU1a	high	27.9	3	0.119	0.016	0.103	0.006
SKB12123	KFM08C-3	353.92	–298.58	aplitic granite	FFM06	RU2a	low	71.1	3	0.103	0.015	0.091	0.003
SKB12125	KFM08C-4	455.72	–383.03	aplitic granite (episyenite)	NNE2312	RU2a	moderate	0.2	4	3.083	0.970	2.731	0.028
SKB12126	KFM08C-5	553.20	–463.19	metagranite – granodiorite	FFM01	RU1b	low	28.6	3	0.065	0.017	0.097	0.004
SKB12127	KFM08C-6	648.58	–540.69	metagranite – granodiorite	FFM01	RU1c	low	34.4	3	0.108	0.030	0.108	0.004
SKB12128	KFM08C-7	751.45	–623.27	metagranite – granodiorite	FFM01	RU1c	low	67.9	3	0.069	0.015	0.097	0.005
SKB12129	KFM08C-8	839.74	–693.38	metagranite – granodiorite	FFM01	RU1d	low	156.1	3	0.071	0.004	0.096	0.004
SKB12130	KFM08C-9	917.21	–754.37	metagranite – granodiorite	FFM01	RU1d	low	233.6	3	0.098	0.002	0.144	0.005
SKB12131	KFM08C-10	938.30	–770.85	metagranite – granodiorite	FFM01	RU1d	low	254.7	3	0.087	0.004	0.095	0.004
SKB12100	KFM09B-1	573.47	–442.43	metagranite – granodiorite	FFM01	RU4b	moderate	1.0	3	0.612	0.120	0.525	0.010
SKB12101	KFM09B-2	574.55	–443.17	metagranite – granodiorite	FFM01	RU4b	low	2.5	3	0.103	0.015	–	
SKB12102	KFM09B-3	576.41	–444.47	metagranite – granodiorite	FFM01	RU4b	low	4.5	3	0.142	0.022	–	
SKB12103	KFM09B-4	576.73	–444.70	metagranite – granodiorite	FFM01	RU4b	low	4.8	3	0.147	0.017	0.119	0.007
SKB12104	KFM09B-5	576.98	–444.87	metagranite – granodiorite	FFM01	RU4b	low	5.0	1	0.134			
SKB12105	KFM09B-6	577.89	–445.50	metagranite – granodiorite	FFM01	RU4b	low	5.8	3	0.118	0.014	–	
SKB12106	KFM09B-7	582.69	–448.84	metagranite – granodiorite	FFM01	RU4b	low	10.6	3	0.114	0.003	–	
SKB12107	KFM09B-8	586.57	–451.52	metagranite – granodiorite	FFM01	RU4b	low	14.5	3	0.102	0.017	0.105	0.008

[1] Reference elevation relative to sea level and corrected for altitude.
[2] Fracture intensity above and below sample (see text for references).
[3] Approximate distance from the pore water sample to next water-conducting fracture in the borehole according to the borehole difference flow login (see text for references).
[4] Error is standard deviation of multiple samples and assumed to be 10% in case of a single sample.
[5] Error calculated using Gauss' error propagation (see text).

Table A-2. Water-loss porosity and pore diffusion coefficients for chloride of rock samples used for porewater investigations from boreholes KFM01D, KFM02B, KFM06A, KFM08C and KFM09B (shaded: hanging wall bedrock s.l., cf. Figure 2-3).

UniBern Sample No	Average borehole length	Average Elevation	Lithology	Distance to nearest water-cond. fracture [1]	Mass of Core in Out-Diff. Exp.	Bulk density (wet) [2]	WL-P of Core in Out–Diff. Exp	Number of samples	Water-loss porosity WL-P (average) [3]		D_p chloride (25°C)	D_p uncertainty range [4]	
	(m)	(m)			(g)	(g/cm^3)	(vol.%)		(vol.%)	(stdev)		(+ error)	(– error)
KFM01D-1	140.69	–112.13	granite – granodiorite	2.2	999.542	2.66	0.30	5	0.32	0.03	9.8E–11	4.1E–11	2.9E–11
KFM01D-2	191.73	–155.30	granite – granodiorite	2.7	984.537	2.64		3	0.23	0.01	–		
KFM01D-3	255.13	–204.57	granite – granodiorite	9.2	963.832	2.62	0.23	4	0.21	0.01	–		
KFM01D-4	299.09	–239.33	granite – granodiorite	8.4	611.572	2.64	0.35	1	0.39	0.04	1.2E–10	4.8E–11	3.4E–11
KFM01D-5	352.07	–280.50	granite – granodiorite	35.2	621.679	2.65	0.28	1	0.28	0.03	1.2E–10	4.8E–11	3.4E–11
KFM01D-6	393.69	–312.47	granite – granodiorite	11.7	981.430	2.65	0.28	1	0.26	0.03	1.0E–10	4.3E–11	3.1E–11
KFM01D-7	462.79	–365.42	granite – granodiorite	31.3	989.546	2.62	0.52	1	0.49	0.05	6.9E–11	2.9E–11	2.0E–11
KFM01D-8	500.05	–393.49	granite – granodiorite	68.6	968.530	2.62	0.32	2	0.33	0.01	7.5E–11	3.1E–11	2.2E–11
KFM01D-9	544.23	–426.54	granite – granodiorite	27.0	615.900	2.65		1	0.26	0.03	–		
KFM01D-10	600.25	–468.02	granite	29.0	619.648	2.65	0.33	1	0.35	0.03	6.9E–11	2.9E–11	2.0E–11
KFM01D-11	643.12	–499.49	granite – granodiorite	71.9	975.538	2.65	0.30	2	0.32	0.03	9.3E–11	3.8E–11	2.7E–11
KFM01D-12	700.25	–541.00	granite – granodiorite	129.1	978.290	2.62	0.38	2	0.33	0.07	8.7E–11	3.6E–11	2.5E–11
KFM01D-13	747.29	–574.82	granite – granodiorite	176.1	980.784	2.63	0.28	2	0.28	0.00	8.1E–11	3.4E–11	2.4E–11
KFM01D-14	790.56	–605.62	granite – granodiorite	219.4	988.322	2.63	0.30	4	0.29	0.04	1.2E–10	4.8E–11	3.4E–11
KFM02B -1	158.91	–149.20	metagranite – granodiorite	0.4	579.935	2.66	0.52	1	0.67	0.03	–		
KFM02B -2	171.83	–161.94	metagranite – granodiorite	2.4	979.235	2.64	0.71	3	1.11	0.05	–		
KFM02B -3	210.64	–200.21	metagranite – granodiorite	8.7	992.617	2.65	0.49	3	0.49	0.02	–		
KFM02B-4	287.16	–275.64	metagranite – granodiorite	7.8	988.984	2.64	0.54	3	0.47	0.01	6.9E–11	2.9E–11	2.0E–11
KFM02B-5	393.29	–380.24	granite, fine-grained	6.1	612.652	2.62	0.63	3	0.56	0.02	–		
KFM02B-6	430.74	–417.14	granite, fine-grained	1.2	615.826	2.65	0.38	3	0.36	0.02	–		
KFM02B-7	441.45	–427.68	metagranite – granodiorite	7.0	629.623	2.65	0.51	3	0.48	0.02	–		
KFM02B-8	448.06	–434.19	metagranite – granodiorite	13.6	1,000.288	2.64	0.53	3	0.58	0.06	8.1E–11	3.4E–11	2.4E–11
KFM02B-9	459.84	–445.79	metagranite – granodiorite	9.7	988.312	2.65	0.39	3	0.32	0.01	–		
KFM02B-10	474.07	–459.79	metagranite – granodiorite	4.6	618.420	2.65	0.51	3	0.50	0.05	–		
KFM02B-11	478.89	–464.54	metagranite – granodiorite	9.4	998.407	2.64	0.52	3	0.39	0.04	–		
KFM02B-12	490.46	–475.92	metagranite – granodiorite	9.0	621.058	2.67	0.71	3	0.60	0.10	–		
KFM02B-13	498.84	–484.16	metagranite – granodiorite	0.8	619.712	2.63	0.90	3	0.90	0.03	1.1E–10	4.6E–11	3.2E–11
KFM02B-14	509.81	–494.95	metagranite – granodiorite	10.2	618.585	2.64	0.68	3	0.63	0.06	7.5E–11	3.1E–11	2.2E–11
KFM02B-15	512.57	–497.66	metagranite – granodiorite	13.0	626.453	2.65	0.56	3	0.59	0.08	8.1E–11	3.4E–11	2.4E–11
KFM02B-16	512.96	–498.04	metagranite – granodiorite	13.4	610.801	2.63	0.40	3	0.32	0.03			
KFM02B-17	513.34	–498.41	metagranite – granodiorite	13.7	982.236	2.64	0.44	3	0.38	0.02	1.1E–10	4.6E–11	3.2E–11

UniBern Sample No	Average borehole length	Average Elevation	Lithology	Distance to nearest water-cond. fracture [1]	Mass of Core in Out-Diff. Exp.	Bulk density (wet) [2]	WL-P of Core in Out–Diff. Exp	Number of samples	Water-loss porosity WL-P (average) [3]		D_p chloride (25°C)	D_p uncertainty range [4]	
	(m)	(m)			(g)	(g/cm³)	(vol.%)		(vol.%)	(stdev)		(+ error)	(– error)
KFM02B-18	513.68	–498.75	metagranite – granodiorite	14.1	624.518	2.62	0.56	3	0.44	0.03			
KFM02B-19	514.04	–499.11	metagranite – granodiorite	14.9	602.977	2.64	0.47	3	0.41	0.03	–		
KFM02B-20	514.47	–499.50	metagranite – granodiorite	14.9	597.663	2.64	0.53	3	0.45	0.08	–		
KFM02B-21	514.84	–499.89	metagranite – granodiorite	15.2	978.324	2.64	0.58	3	0.49	0.03	–		
KFM02B-22	515.19	–500.23	metagranite – granodiorite	15.6	598.639	2.64	0.63	3	0.43	0.04	–		
KFM02B-23	515.54	–500.58	metagranite – granodiorite	15.9	608.625	2.64	0.53	3	0.45	0.07	–		
KFM02B-24	515.85	–500.89	metagranite – granodiorite	16.3	620.086	2.65	0.50	3	0.37	0.03	1.6E–10	6.7E–11	4.7E–11
KFM02B-25	516.12	–501.15	metagranite – granodiorite	16.5	619.087	2.63	0.49	3	0.40	0.04	–		
KFM02B-26	516.42	–501.44	metagranite – granodiorite	16.8	614.313	2.65	0.49	3	0.38	0.03	9.8E–11	4.1E–11	2.9E–11
KFM02B-27	516.72	–501.74	metagranite – granodiorite	17.1	612.645	2.65	0.61	3	0.53	0.02	–		
KFM02B-28	517.03	–502.04	metagranite – granodiorite	17.4	628.536	2.64	0.61	3	0.48	0.02	8.7E–11	3.6E–11	2.5E–11
KFM02B-29	517.34	–502.34	metagranite – granodiorite	17.7	623.052	2.64	0.66	3	0.47	0.03	–		
KFM02B-30	519.54	–504.51	metagranite – granodiorite	19.9	601.863	2.64	0.46	3	0.37	0.06	8.7E–11	3.6E–11	2.5E–11
KFM02B-31	522.11	–507.04	metagranite – granodiorite	22.5	612.115	2.65	0.39	3	0.37	0.02	–		
KFM02B-32	522.39	–507.31	metagranite – granodiorite	22.8	610.514	2.64	0.45	3	0.49	0.06	1.2E–10	4.8E–11	3.4E–11
KFM02B-33	527.55	–512.38	metagranite – granodiorite	27.9	603.422	2.64	0.60	3	0.45	0.03	–		
KFM02B-34	532.44	–517.19	metagranite – granodiorite	32.8	617.691	2.64	0.53	3	0.50	0.02	1.7E–10	7.2E–11	5.1E–11
KFM02B-39	559.83	–544.09	metagranite – granodiorite	60.2	615.578	2.63	0.62	3	0.45	0.02	6.4E–11	2.6E–11	1.9E–11
KFM02B-40	562.47	–546.69	metagranite – granodiorite	62.9	981.065	2.64	0.63	3	0.61	0.03	7.5E–11	3.1E–11	2.2E–11
KFM02B-41	565.29	–549.46	metagranite – granodiorite	65.7	977.289	2.63	0.62	3	0.67	0.10	5.2E–11	2.2E–11	1.5E–11
KFM02B-42	569.35	–553.45	metagranite – granodiorite	69.8	976.949	2.61	0.85	3	0.62	0.04	8.1E–11	3.4E–11	2.4E–11
KFM02B-43	573.65	–557.67	metagranite – granodiorite	74.1	987.576	2.65	0.55	3	0.51	0.03	6.4E–11	2.6E–11	1.9E–11
KFM06A-1	146.08	–122.69	metagranite – granodiorite	3.0	1,010.670	2.64	0.35	3	0.48	0.12	6.9E–11	2.9E–11	2.0E–11
KFM06A-2	194.69	–164.70	metagranite – granodiorite	3.4	1,005.660	2.64	–	3	0.58	0.04			
KFM06A-3	252.41	–214.22	metagranite – granodiorite	5.8	1,030.280	2.65	–	3	0.40	0.06			
KFM06A-4	281.82	–239.33	metagranite – granodiorite	8.6	1,002.990	2.65	–	3	0.48	0.07			
KFM06A-5	298.49	–253.54	metagranite – granodiorite	0.3	1,011.980	2.64	–	3	0.31	0.03			
KFM06A-6	355.29	–301.74	metagranite – granodiorite	2.0	992.700	2.64	0.61	3	0.80	0.14	4.6E–11	1.9E–11	1.4E–11
KFM06A-7	395.40	–335.50	metagranite – granodiorite	2.0	1,014.740	2.64	–	3	0.32	0.02			
KFM06A-8	440.98	–373.70	metagranite – granodiorite	7.5	1,010.420	2.64	–	3	0.29	0.06			
KFM06A-9	500.02	–422.92	metagranite – granodiorite	51.8	993.992	2.59	0.42	3	0.43	0.04	7.8E–11	3.2E–11	2.3E–11
KFM06A-10	563.38	–475.44	metagranite – granodiorite	60.3	1,011.830	2.65	0.29	3	0.32	0.02	1.2E–10	4.8E–11	3.4E–11
KFM06A-11	575.94	–485.84	granodiorite – tonalite	47.8	1,017.305	2.65	–	3	0.28	0.03	–		
KFM06A-12	594.62	–501.28	granodiorite – tonalite	29.1	1,036.810	2.68	–	3	0.29	0.03	–		

UniBern Sample No	Average borehole length	Average Elevation	Lithology	Distance to nearest water-cond. fracture [1]	Mass of Core in Out-Diff. Exp.	Bulk density (wet) [2]	WL-P of Core in Out–Diff. Exp	Number of samples	Water-loss porosity WL-P (average) [3]		D_p chloride (25°C)	D_p uncertainty range [4]	
	(m)	(m)			(g)	(g/cm^3)	(vol.%)		(vol.%)	(stdev)		(+ error)	(– error)
KFM06A-13	633.56	–533.40	metagranite, aplitic	9.9	1,009.386	2.64	0.32	3	0.30	0.02	1.2E–10	4.8E–11	3.4E–11
KFM06A-14	660.89	–555.84	metagranite, aplitic	7.2	1,031.290	2.63	–	3	0.20	0.02	–		
KFM06A-15	698.81	–586.41	metagranite – granodiorite	44.6	1,008.946	2.65	0.26	3	0.30	0.01	1.3E–10	5.5E–11	3.9E–11
KFM06A-16	763.59	–639.50	aplitic granite	19.8	987.028	2.60	0.35	3	0.31	0.02	5.2E–11	2.2E–11	1.5E–11
KFM06A-17	810.84	–677.59	aplitic granite	41.9	1,004.066	2.61	–	3	0.26	0.03	–		
KFM06A-18	851.71	–710.24	aplitic granite	82.8	999.525	2.63	0.34	3	0.31	0.03	6.4E–11	2.6E–11	1.9E–11
KFM06A-19	900.97	–749.37	aplitic granite	132.1	1,004.835	2.63	0.25	3	0.27	0.04	8.1E–11	3.4E–11	2.4E–11
KFM06A-20	920.69	–764.95	aplitic granite	151.8	1,002.250	2.62	–	3	0.21	0.06	–		
KFM06A-21	948.77	–786.98	granodiorite – tonalite	179.9	997.045	2.62	0.31	3	0.36	0.03	8.1E–11	3.4E–11	2.4E–11
KFM06A-22	977.36	–809.33	granodiorite – tonalite	208.5	995.352	2.63	–	3	0.60	0.05	–		
KFM06A-23	998.32	–825.66	granodiorite – tonalite	229.4	999.720	2.62	0.23	3	0.28	0.05	1.4E–10	6.0E–11	4.2E–11
KFM08C-1	154.69	–131.16	metagranite – granodiorite	6.6	640.032	2.65	0.24	3	0.21	0.01	1.6E–10	6.5E–11	4.6E–11
KFM08C-2	254.92	–215.87	metagranite – granodiorite	27.9	1,014.480	2.66	–	3	0.32	0.04	–		
KFM08C-3	353.92	–298.58	aplitic granite	71.1	1,005.285	2.63	0.28	3	0.27	0.04	1.6E–10	6.5E–11	4.6E–11
KFM08C-4	455.72	–383.03	aplitic granite (epi–syen.)	0.2	863.165	2.45	8.55	4	7.29	2.25	–		
KFM08C-5	553.20	–463.19	metagranite – granodiorite	28.6	1,011.509	2.63	–	3	0.17	0.05	–		
KFM08C-6	648.58	–540.69	metagranite – granodiorite	34.4	638.864	2.62	–	3	0.28	0.08	1.4E–10	6.0E–11	4.2E–11
KFM08C-7	751.45	–623.27	metagranite – granodiorite	67.9	641.815	2.65	–	3	0.18	0.04	–		
KFM08C-8	839.74	–693.38	metagranite – granodiorite	156.1	643.845	2.65	0.25	3	0.19	0.01	–		
KFM08C-9	917.21	–754.37	metagranite – granodiorite	233.6	998.070	2.64	0.32	3	0.26	0.01	–		
KFM08C-10	938.30	–770.85	metagranite – granodiorite	254.7	1,001.340	2.61	0.30	3	0.23	0.01	–		
KFM09B-1	573.47	–442.43	metagranite – granodiorite	1.0	646.710	2.56	–	3	1.55	0.30	–		
KFM09B-2	574.55	–443.17	metagranite – granodiorite	2.5	1,012.181	2.65	0.25	3	0.27	0.04	2.3E–10	9.6E–11	6.8E–11
KFM09B-3	576.41	–444.47	metagranite – granodiorite	4.5	1,011.005	2.63	0.34	3	0.37	0.06	1.4E–10	5.8E–11	4.1E–11
KFM09B-4	576.73	–444.70	metagranite – granodiorite	4.8	1,016.001	2.64	0.36	3	0.39	0.04	1.2E–10	4.8E–11	3.4E–11
KFM09B-5	576.98	–444.87	metagranite – granodiorite	5.0	648.114	2.65	0.33	1	0.36		1.5E–10	6.2E–11	4.4E–11
KFM09B-6	577.89	–445.50	metagranite – granodiorite	5.8	909.178	2.63	0.32	3	0.31	0.04	1.6E–10	6.7E–11	4.7E–11
KFM09B-7	582.69	–448.84	metagranite – granodiorite	10.6	1,016.390	2.63	0.30	3	0.30	0.01	1.7E–10	7.2E–11	5.1E–11
KFM09B-8	586.57	–451.52	metagranite – granodiorite	14.5	1,004.191	2.63	0.25	3	0.27	0.04	9.3E–11	1.5E–10	2.7E–11

[1] Approximate distance from the pore water sample to next water-conducting fracture in the borehole according to the borehole difference flow login (see text for references).
[2] Determined from mass and volume of originally saturated (wet) drillcore sample used for out-diffusion experiment (Out-Diff. Exp).
[3] Determined on small-sized aliquots (ca 100–350 g); if only one sample, then error assumed ± 10%.
[4] Uncertainty range for the pore diffusion coefficient is $D_p \cdot \sqrt{2} - D_p$ (+ error) and $D_p - D_p/\sqrt{2}$ (– error) corresponding to a factor of 2 in the diffusion time from the best-fit D_p.

Table A-3. Chloride concentration and $\delta^{18}O$ and $\delta^{2}H$ in porewater of rock samples from boreholes KFM01D, KFM02B, KFM06A, KFM08C and KFM09B (shaded: hanging wall bedrock s.l., cf. Figure 2-3).

UniBern Sample No	Average g borehole length (m)	Average Elevation (m)	Lithology	Distance to nearest water-conducting fracture [1]	Experiment Solution Chemical type [2]	Chloride in Pore Water (mg/kg_{H2O})	+ error [3]	– error [3]	$\delta^{18}O$ [4] (‰ VSMOW)	error [4]	$\delta^{2}H$ [4] (‰ VSMOW)	error [4]
KFM01D-1	140.69	–112.13	granite – granodiorite	2.2	Na-Ca-HCO_3-Cl	2,846	266	328	–5.18	±3.7	–77.0	±37.0
KFM01D-2	191.73	–155.30	granite – granodiorite	2.7	Na-Ca-HCO_3-Cl	2,251	82	89	–		–	
KFM01D-3	255.13	–204.57	granite – granodiorite	9.2	Na-Ca-Cl-HCO_3	4,008	230	260	–5.11	±3.1	–51.9	±26.6
KFM01D-4	299.09	–239.33	granite – granodiorite	8.4	Ca-Na-HCO_3-Cl	2,736	246	301	–6.44	±2.9	–46.1	±25.2
KFM01D-5	352.07	–280.50	granite – granodiorite	35.2	Na-Ca-HCO_3-Cl	3,334	301	367	–2.11	±3.3	–44.5	±23.5
KFM01D-6	393.69	–312.47	granite – granodiorite	11.7	Na-Ca-HCO_3-Cl	2,933	264	323	–2.58	±3.0	–61.8	±24.5
KFM01D-7	462.79	–365.42	granite – granodiorite	31.3	Na-Ca-HCO_3-Cl	2,406	215	263	–3.98	±2.3	–63.6	±17.7
KFM01D-8	500.05	–393.49	granite – granodiorite	68.6	Na-Ca-HCO_3-Cl	2,634	62	65	–2.75	±3.4	–55.2	±29.1
KFM01D-9	544.23	–426.54	granite – granodiorite	27.0	Na-Ca-HCO_3-Cl	3,267	295	360	–2.31	±3.1	–54.5	±24.6
KFM01D-10	600.25	–468.02	granite	29.0	Na-Ca-HCO_3-Cl	2,356	212	259	–4.40	±2.8	–63.3	±23.5
KFM01D-11	643.12	–499.49	granite – granodiorite	71.9	Na-Ca-HCO_3-Cl	2,997	282	349	–4.35	±2.8	–35.5	±21.6
KFM01D-12	700.25	–541.00	granite – granodiorite	129.1	Na-Ca-HCO_3-Cl	3,038	558	887	–4.11	±2.6	–48.9	±21.8
KFM01D-13	747.29	–574.82	granite – granodiorite	176.1	Na-Ca-HCO_3-Cl	4,204	379	463	–2.97	±2.8	–41.5	±22.4
KFM01D-14	790.56	–605.62	granite – granodiorite	219.4	Na-Ca-Cl-HCO_3	5,743	669	875	–3.75	±2.4	–20.6	±18.0
KFM02B -1	158.91	–149.20	metagranite – granodiorite	0.4	Ca-Na-HCO_3	1,092	98	120				
KFM02B -2	171.83	–161.94	metagranite – granodiorite	2.4	Na-Ca-HCO_3-Cl	1,082	96	117	–14.67	±0.7	–119.9	±7.6
KFM02B -3	210.64	–200.21	metagranite – granodiorite	8.7	Na-Ca-HCO_3	1,009	90	110	–7.61	±1.3	–76.9	±9.6
KFM02B-4	287.16	–275.64	metagranite – granodiorite	7.8	Ca-Na-HCO_3-Cl	1,226	109	134	–8.73	±1.0	–77.4	±8.4
KFM02B-5	393.29	–380.24	granite, fine-grained	6.1	Ca-Na-HCO_3-Cl	1,008	90	110	–11.05	±1.3	–89.0	±11.5
KFM02B-6	430.74	–417.14	granite, fine-grained	1.2	Na-Ca-HCO_3-Cl	2,884	259	316	–	–	–	
KFM02B-7	441.45	–427.68	metagranite – granodiorite	7.0	Na-Ca-HCO_3-Cl	1,910	171	208	–12.28	±1.1	–93.2	±10.4
KFM02B-8	448.06	–434.19	metagranite – granodiorite	13.6	Na-Ca-HCO_3-Cl	2,787	249	304	–7.25	±1.2	–74.2	±9.7
KFM02B-9	459.84	–445.79	metagranite – granodiorite	9.7	Na-Ca-HCO_3-Cl	2,904	260	318	–5.40	±1.4	–66.6	±13.4
KFM02B-10	474.07	–459.79	metagranite – granodiorite	4.6	Na-Ca-HCO_3-Cl	1,415	126	154	–8.69	±1.5	–82.9	±12.6
KFM02B-11	478.89	–464.54	metagranite – granodiorite	9.4	Na-Ca-HCO_3	963	86	105	–10.18	±1.8	–68.7	±14.4
KFM02B-12	490.46	–475.92	metagranite – granodiorite	9.0	Na-Ca-HCO_3	642	57	70	–14.23	±1.1	–113.8	±12.4
KFM02B-13	498.84	–484.16	metagranite – granodiorite	0.8	Na-Ca-HCO_3-Cl	1,888	166	203	–8.61	±0.9	–56.9	±7.1
KFM02B-14	509.81	–494.95	metagranite – granodiorite	10.2	Na-Ca-HCO_3-Cl	893	79	97	–13.15	±0.7	–107.2	±7.8
KFM02B-15	512.57	–497.66	metagranite – granodiorite	13.0	Na-Ca-HCO_3-Cl	968	86	106	–13.23	±0.8	–103.6	±10.4
KFM02B-16	512.96	–498.04	metagranite – granodiorite	13.4	Na-Ca-HCO_3-Cl	1,644	148	180	–9.81	±1.3	–59.6	±17.3
KFM02B-17	513.34	–498.41	metagranite – granodiorite	13.7	Na-Ca-HCO_3-Cl	1,411	126	154	–11.95	±1.3	–95.7	±11.8
KFM02B-18	513.68	–498.75	metagranite – granodiorite	14.1	Na-Ca-HCO_3-Cl	1,135	101	124	–8.61	±0.9	–78.0	±9.8

UniBern Sample No	Average g borehole length (m)	Average Elevation (m)	Lithology	Distance to nearest water-conducting fracture [1]	Experiment Solution Chemical type [2]	Chloride in Pore Water (mg/kg_{H2O})	+ error [3]	– error [3]	$\delta^{18}O$ [4] (‰ VSMOW)	error [4]	$\delta^{2}H$ [4] (‰ VSMOW)	error [4]
KFM02B-19	514.04	–499.11	metagranite – granodiorite	14.9	Na-Ca-HCO_3-Cl	1,092	98	120	–9.43	±1.5	–82.7	±14.0
KFM02B-20	514.47	–499.50	metagranite – granodiorite	14.9	Na-Ca-HCO_3-Cl	1,241	111	136	–		–	
KFM02B-21	514.84	–499.89	metagranite – granodiorite	15.2	Na-Ca-HCO_3-Cl	972	87	106	–7.88	±1.3	–82.5	±10.7
KFM02B-22	515.19	–500.23	metagranite – granodiorite	15.6	Na-Ca-HCO_3-Cl	1,024	91	111	–7.25	±1.3	–76.8	±13.1
KFM02B-23	515.54	–500.58	metagranite – granodiorite	15.9	Na-Ca-HCO_3	924	83	101	–4.76	±2.1	–67.8	±18.1
KFM02B-24	515.85	–500.89	metagranite – granodiorite	16.3	Na-Ca-HCO_3-Cl	1,188	106	130	–6.77	±2.1	–	–
KFM02B-25	516.12	–501.15	metagranite – granodiorite	16.5	Na-Ca-HCO_3-Cl	1,162	104	127	–5.21	±1.3	–77.3	±10.5
KFM02B-26	516.42	–501.44	metagranite – granodiorite	16.8	Ca-Na-HCO_3	1,243	111	136	–8.65	±1.0	–81.7	±9.2
KFM02B-27	516.72	–501.74	metagranite – granodiorite	17.1	Ca-Na-HCO_3-Cl	985	88	107	–9.40	±1.1	–70.4	±10.0
KFM02B-28	517.03	–502.04	metagranite – granodiorite	17.4	Ca-Na-HCO_3	947	84	103	–8.56	±0.8	–63.4	±8.3
KFM02B-29	517.34	–502.34	metagranite – granodiorite	17.7	Na-Ca-HCO_3-Cl	945	84	103	–9.08	±1.1	–72.9	±9.6
KFM02B-30	519.54	–504.51	metagranite – granodiorite	19.9	Ca-Na-HCO_3	1,429	128	157	–7.50	±1.4	–64.3	±16.0
KFM02B-31	522.11	–507.04	metagranite – granodiorite	22.5	Na-Ca-HCO_3-Cl	1,731	155	190	–9.55	±2.5	–75.8	±26.5
KFM02B-32	522.39	–507.31	metagranite – granodiorite	22.8	Na-Ca-HCO_3-Cl	1,811	162	198	–9.85	±0.7	–81.3	±6.4
KFM02B-33	527.55	–512.38	metagranite – granodiorite	27.9	Na-Ca-HCO_3	1,082	96	118	–11.03	±1.5	–83.7	±16.0
KFM02B-34	532.44	–517.19	metagranite – granodiorite	32.8	Ca-Na-HCO_3	1,362	122	149	–		–	
KFM02B-39	559.83	–544.09	metagranite – granodiorite	60.2	Na-Ca-HCO_3-Cl	1,014	90	110	–6.21	±1.8	–45.1	±16.4
KFM02B-40	562.47	–546.69	metagranite – granodiorite	62.9	Na-Ca-HCO_3-Cl	1,018	91	111	–6.21	±1.4	–54.1	±12.3
KFM02B-41	565.29	–549.46	metagranite – granodiorite	65.7	Na-Ca-HCO_3	974	87	106	–13.12	±1.0	–104.2	±11.8
KFM02B-42	569.35	–553.45	metagranite – granodiorite	69.8	Na-Ca-HCO_3-Cl	781	69	84	–12.69	±1.0	–104.7	±17.1
KFM02B-43	573.65	–557.67	metagranite – granodiorite	74.1	Na-Ca-HCO_3	926	83	101	–6.08	±2.1	–51.0	±18.4
KFM06A-1	146.08	–122.69	metagranite – granodiorite	3.0	Na-Ca-HCO_3-Cl	1,560	314	531	–10.43	±2.7	–90.4	±27.6
KFM06A-2	194.69	–164.70	metagranite – granodiorite	3.4	Na-Ca-HCO_3-Cl	1,256	83	96	–14.94	±2.6	–96.9	±29.1
KFM06A-3	252.41	–214.22	metagranite – granodiorite	5.8	Na-Ca-HCO_3-(Cl)	759	97	130	–10.67	±2.6	–	
KFM06A-4	281.82	–239.33	metagranite – granodiorite	8.6	Na-Ca-HCO_3-Cl	860	114	155	–10.32	±2.4	–66.5	±23.6
KFM06A-5	298.49	–253.54	metagranite – granodiorite	0.3	Na-Ca-HCO_3-Cl	2,104	157	185	–8.65	±2.4	–44.5	±25.5
KFM06A-6	355.29	–301.74	metagranite – granodiorite	2.0	Na-Ca-HCO_3-Cl	1,455	206	291	–9.74	±2.0	–	
KFM06A-7	395.40	–335.50	metagranite – granodiorite	2.0	Na-Ca-HCO_3-Cl	1,794	94	105	–10.70	±2.4	–	
KFM06A-8	440.98	–373.70	metagranite – granodiorite	7.5	Na-Ca-HCO_3-Cl	2,518	401	592	–		–	
KFM06A-9	500.02	–422.92	metagranite – granodiorite	51.8	Ca-Na-HCO_3-Cl	3,175	271	328	–8.32	±2.6	–72.6	±29.2
KFM06A-10	563.38	–475.44	metagranite – granodiorite	60.3	Na-Ca-HCO_3-Cl	2,127	127	145	–8.36	±2.7	–35.3	±27.9
KFM06A-11	575.94	–485.84	granodiorite – tonalite	47.8	Na-Ca-HCO_3-Cl	3,461	359	454	–6.83	±2.7	–	
KFM06A-12	594.62	–501.28	granodiorite – tonalite	29.1	Na-Ca-HCO_3-Cl	-			–		–	

UniBern Sample No	Average g borehole length (m)	Average Elevation (m)	Lithology	Distance to nearest water-conducting fracture [1]	Experiment Solution Chemical type [2]	Chloride in Pore Water (mg/kg_{H2O})	+ error [3]	– error [3]	$\delta^{18}O$ [4] (‰ VSMOW)	error [4]	$\delta^{2}H$ [4] (‰ VSMOW)	error [4]
KFM06A-13	633.56	–533.40	metagranite, aplitic	9.9	Na-Ca-HCO_3-Cl	4,027	271	313	–8.57	±2.7	–34.6	±29.2
KFM06A-14	660.89	–555.84	metagranite, aplitic	7.2		-			–		–	
KFM06A-15	698.81	–586.41	metagranite – granodiorite	44.6	Na-Ca-HCO_3-Cl	3,824	169	186	–7.04	±2.8	–25.7	±17.0
KFM06A-16	763.59	–639.50	aplitic granite	19.8	Na-Ca-HCO_3-Cl	2,634	137	153	–7.44	±2.9	–	
KFM06A-17	810.84	–677.59	aplitic granite	41.9		-			–9.37	±2.7	–29.5	±29.2
KFM06A-18	851.71	–710.24	aplitic granite	82.8	Ca-Na-Cl-HCO_3	5,123	508	636	–8.73	±2.7	–	
KFM06A-19	900.97	–749.37	aplitic granite	132.1	Na-Ca-Cl-HCO_3	7,165	968	1,332	–8.65	±2.3	–28.5	±31.8
KFM06A-20	920.69	–764.95	aplitic granite	151.8	Ca-Na-Cl-HCO_3	9,255	2,066	3,756	–		–	
KFM06A-21	948.77	–786.98	granodiorite – tonalite	179.9	Ca-Na-Cl-HCO_3	6,339	458	537	–10.39	±2.7	–66.2	±29.2
KFM06A-22	977.36	–809.33	granodiorite – tonalite	208.5	Ca-Na-Cl-HCO_3	6,339	488	580	–9.94	±2.1	–56.0	±20.3
KFM06A-23	998.32	–825.66	granodiorite – tonalite	229.4	Ca-Na-Cl-HCO_3	11,375	1,656	2,347	–6.98	±2.7	–	
KFM08C-1	154.69	–131.16	metagranite – granodiorite	6.6	Na-(Ca)-HCO_3-Cl	2,117	69	74	–8.66	±1.9	–79.2	±16.9
KFM08C-2	254.92	–215.87	metagranite – granodiorite	27.9	Na-Ca-HCO_3-Cl	2,111	248	326	–7.44	±1.9	–75.4	±16.9
KFM08C-3	353.92	–298.58	aplitic granite	71.1	Ca-Na-HCO_3-Cl	3,092	381	507	–7.62	±1.6	–78.2	±15.7
KFM08C-4	455.72	–383.03	aplitic granite (epi–syen.)	0.2	Na-Ca-Cl	3,861	283	346	–12.69	±0.1	–90.4	±1.6
KFM08C-5	553.20	–463.19	metagranite – granodiorite	28.6	Na-Ca-HCO_3-Cl	5,530	605	776	–5.49	±2.1	–41.8	±16.6
KFM08C-6	648.58	–540.69	metagranite – granodiorite	34.4	Na-Ca-HCO_3-Cl	4,249	919	1,633	–8.31	±1.5	–69.7	±13.9
KFM08C-7	751.45	–623.27	metagranite – granodiorite	67.9	Ca-Na-Cl-HCO_3	14,686	2,572	3,971	–8.37	±2.5	–44.0	±23.7
KFM08C-8	839.74	–693.38	metagranite – granodiorite	156.1	Na-Ca-Cl-HCO_3	10,128	515	573	–9.59	±1.5	–49.7	±16.0
KFM08C-9	917.21	–754.37	metagranite – granodiorite	233.6	Ca-Na-Cl-HCO_3	11,032	265	278	–3.96	±1.6	–50.7	±13.9
KFM08C-10	938.30	–770.85	metagranite – granodiorite	254.7	Na-Ca-Cl-HCO_3	10,627	473	519	–3.59	±2.0	–62.0	±16.0
KFM09B-1	573.47	–442.43	metagranite – granodiorite	1.0	Na-Ca-Cl	10,543	1,642	2,446	–5.75	±0.8	–46.2	±6.1
KFM09B-2	574.55	–443.17	metagranite – granodiorite	2.5	Na-Ca-Cl-HCO_3	4,886	615	825	–		–	
KFM09B-3	576.41	–444.47	metagranite – granodiorite	4.5	Ca-Na-HCO_3-Cl	4,666	617	843	–		–	
KFM09B-4	576.73	–444.70	metagranite – granodiorite	4.8	Ca-Na-HCO_3-Cl	4,753	475	595	–4.67	±2.9	–49.0	±26.3
KFM09B-5	576.98	–444.87	metagranite – granodiorite	5.0	Ca-Na-HCO_3-Cl	4,930	430	523	–		–	
KFM09B-6	577.89	–445.50	metagranite – granodiorite	5.8	Na-Ca-HCO_3-Cl	5,199	560	715	–		–	
KFM09B-7	582.69	–448.84	metagranite – granodiorite	10.6	Ca-Na-Cl-HCO_3	6,516	161	170	–		–	
KFM09B-8	586.57	–451.52	metagranite – granodiorite	14.5	Ca-Na-Cl-HCO_3	8,666	1,230	1,723	–6.82	±3.4	–52.8	±32.0

[1] Approximate distance from the pore water sample to next water-conducting fracture in the borehole according to the borehole difference flow login.
[2] Chemical type corresponds to that of pore water except for HCO_3, which might not be a major anion in pore water with $Cl^- > 1{,}500$ mg/kgH_2O (see text).
[3] Uncertainty band calculated form standard deviation of water content measurements.
[4] Error calculated according to Gauss' law of error propagation.

Table A-4. Cl and Sr isotope compositions and Br and Mg concentration of out-diffusion experiment solutions of rock samples from boreholes KFM01D, KFM02B, KFM06A, KFM08C and KFM09B (shaded: hanging wall bedrock s.l., cf. Figure 2-3).

UniBern Sample No	Average borehole length (m)	Average Elevation (m)	Rock Unit	Distance to nearest water-cond. fracture	Experiment Solution Chemical type [1]	Cl^- in Exp. Solution (mg/L)	$\delta^{37}Cl$ in Exp. Solution [2] (‰ SMOC)	Br^- in Exp. Solution [3] (mg/L)	Mg^{+2} in Exp. Solution [3] (mg/L)	Sr^{+2} in Exp. Solution [4] (ppm)	$^{87}Sr/^{86}Sr$	2σ error
KFM01D-1	140.69	–112.13	RU1	2.2	Na-Ca-HCO_3-Cl	32.2	–	< 0.5	1.6	0.167	0.721004	0.000020
KFM01D-2	191.73	–155.30	RU2	2.7	Na-Ca-HCO_3-Cl	18.8	–	< 0.5	1.0	0.159	0.726652	0.000020
KFM01D-3	255.13	–204.57	RU2	9.2	Na-Ca-Cl-HCO_3	30.8	–	< 0.5	0.8	0.228	0.729848	0.000020
KFM01D-4	299.09	–239.33	RU2	8.4	Ca-Na-HCO_3-Cl	29.9	–	< 0.5	< 0.5	0.175	0.732842	0.000024
KFM01D-5	352.07	–280.50	RU2	35.2	Na-Ca-HCO_3-Cl	28.3	–	< 0.5	< 0.5	0.127	0.723355	0.000020
KFM01D-6	393.69	–312.47	RU2	11.7	Na-Ca-HCO_3-Cl	27.0	–	< 0.5	< 0.5	0.092	0.723162	0.000020
KFM01D-7	462.79	–365.42	RU3	31.3	Na-Ca-HCO_3-Cl	38.7	–	< 0.5	< 0.5	0.199	0.724190	0.000020
KFM01D-8	500.05	–393.49	RU4	68.6	Na-Ca-HCO_3-Cl	28.2	–	< 0.5	< 0.5	0.112	0.727976	0.000040
KFM01D-9	544.23	–426.54	RU4	27.0	Na-Ca-HCO_3-Cl	23.9	–	< 0.5	< 0.5	0.164	0.729489	0.000021
KFM01D-10	600.25	–468.02	RU4	29.0	Na-Ca-HCO_3-Cl	24.4	–	< 0.5	< 0.5	0.107	0.725942	0.000024
KFM01D-11	643.12	–499.49	RU4	71.9	Na-Ca-HCO_3-Cl	32.3	–	< 0.5	< 0.5	0.146	0.726497	0.000020
KFM01D-12	700.25	–541.00	RU4	129.1	Na-Ca-HCO_3-Cl	33.6	–	< 0.5	< 0.5	0.128	0.728899	0.000020
KFM01D-13	747.29	–574.82	RU4	176.1	Na-Ca-HCO_3-Cl	39.3	–	< 0.5	< 0.5	0.177	0.730480	0.000020
KFM01D-14	790.56	–605.62	RU4	219.4	Na-Ca-Cl-HCO_3	56.3	–	< 0.5	< 0.5	0.247	0.730069	0.000025
KFM02B -1	158.91	–149.20	RU1a	0.4	Ca-Na-HCO_3	16.3	–	< 0.5	0.5	0.247	0.717882	0.000020
KFM02B -2	171.83	–161.94	RU1a	2.4	Na-Ca-HCO_3-Cl	25.7	–	< 0.5	1.1	0.191	0.716416	0.000020
KFM02B -3	210.64	–200.21	RU1a	8.7	Na-Ca-HCO_3	17.0	–	< 0.5	0.8	–		
KFM02B-4	287.16	–275.64	RU1a	7.8	Ca-Na-HCO_3-Cl	23.0	–	< 0.5	0.7	0.259	0.723976	0.000020
KFM02B-5	393.29	–380.24	RU2	6.1	Ca-Na-HCO_3-Cl	23.2	–	< 0.5	1.3	0.255	0.718090	0.000020
KFM02B-6	430.74	–417.14	RU2	1.2	Na-Ca-HCO_3-Cl	37.0	–	< 0.5	2.4	0.191	0.723406	0.000020
KFM02B-7	441.45	–427.68	RU1b	7.0	Na-Ca-HCO_3-Cl	33.7	–	< 0.5	1.9	0.190	0.723650	0.000029
KFM02B-8	448.06	–434.19	RU1b	13.6	Na-Ca-HCO_3-Cl	53.2	–	< 0.5	3.1	0.179	0.723311	0.000020
KFM02B-9	459.84	–445.79	RU1b	9.7	Na-Ca-HCO_3-Cl	39.1	–	< 0.5	2.8	0.141	0.719554	0.000020
KFM02B-10	474.07	–459.79	RU1b	4.6	Na-Ca-HCO_3-Cl	26.8	–	< 0.5	0.6	0.111	0.719276	0.000020
KFM02B-11	478.89	–464.54	RU1b	9.4	Na-Ca-HCO_3	18.4	–	< 0.5	< 0.3	0.190	0.724150	0.000020
KFM02B-12	490.46	–475.92	RU1b	9.0	Na-Ca-HCO_3	15.5	–	< 0.5	< 0.3	0.140	0.720552	0.000022
KFM02B-13	498.84	–484.16	RU1b	0.8	Na-Ca-HCO_3-Cl	56.8	–	< 0.5	2.5	0.195	0.717642	0.000020
KFM02B-14	509.81	–494.95	RU1b	10.2	Na-Ca-HCO_3-Cl	19.8	–	< 0.5	< 0.3	0.096	0.718947	0.000021
KFM02B-15	512.57	–497.66	RU1b	13.0	Na-Ca-HCO_3-Cl	17.7	–	< 0.5	< 0.3	0.096	0.721540	0.000035
KFM02B-16	512.96	–498.04	RU1b	13.4	Na-Ca-HCO_3-Cl	22.7	–	< 0.5	0.4	0.156	0.720382	0.000024
KFM02B-17	513.34	–498.41	RU1b	13.7	Na-Ca-HCO_3-Cl	22.3	–	< 0.5	< 0.3	0.127	0.720221	0.000024
KFM02B-18	513.68	–498.75	RU1b	14.1	Na-Ca-HCO_3-Cl	23.9	–	< 0.5	< 0.3	–		

UniBern Sample No	Average borehole length (m)	Average Elevation (m)	Rock Unit	Distance to nearest water-cond. fracture	Experiment Solution Chemical type [1]	Cl^- in Exp. Solution (mg/L)	$\delta^{37}Cl$ in Exp. Solution [2] (‰ SMOC)	Br^- in Exp. Solution [3] (mg/L)	Mg^{+2} in Exp. Solution [3] (mg/L)	Sr^{+2} in Exp. Solution [4] (ppm)	$^{87}Sr/^{86}Sr$	2σ error
KFM02B-19	514.04	–499.11	RU1b	14.9	Na-Ca-HCO_3-Cl	17.1	–	< 0.5	0.3	–	–	
KFM02B-20	514.47	–499.50	RU1b	14.9	Na-Ca-HCO_3-Cl	19.7	–	< 0.5	< 0.3	0.164	0.721175	0.000021
KFM02B-21	514.84	–499.89	RU1b	15.2	Na-Ca-HCO_3-Cl	19.7	–	< 0.5	< 0.3	–	–	
KFM02B-22	515.19	–500.23	RU1b	15.6	Na-Ca-HCO_3-Cl	20.5	–	< 0.5	< 0.3	–	–	
KFM02B-23	515.54	–500.58	RU1b	15.9	Na-Ca-HCO_3	16.4	–	< 0.5	< 0.3	–	–	
KFM02B-24	515.85	–500.89	RU1b	16.3	Na-Ca-HCO_3-Cl	20.0	–	< 0.5	< 0.3	0.140	0.721409	0.000023
KFM02B-25	516.12	–501.15	RU1b	16.5	Na-Ca-HCO_3-Cl	19.1	–	< 0.5	0.6	–	–	
KFM02B-26	516.42	–501.44	RU1b	16.8	Ca-Na-HCO_3	18.9	–	< 0.5	0.3	–	–	
KFM02B-27	516.72	–501.74	RU1b	17.1	Ca-Na-HCO_3-Cl	21.2	–	< 0.5	0.8	–	–	
KFM02B-28	517.03	–502.04	RU1b	17.4	Ca-Na-HCO_3	19.7	–	< 0.5	< 0.3	–	–	
KFM02B-29	517.34	–502.34	RU1b	17.7	Na-Ca-HCO_3-Cl	22.5	–	< 0.5	0.4	–	–	
KFM02B-30	519.54	–504.51	RU1b	19.9	Ca-Na-HCO_3	19.9	–	< 0.5	0.6	0.204	0.722313	0.000020
KFM02B-31	522.11	–507.04	RU1b	22.5	Na-Ca-HCO_3-Cl	23.1	–	< 0.5	0.7	–	–	
KFM02B-32	522.39	–507.31	RU1b	22.8	Na-Ca-HCO_3-Cl	25.3	–	< 0.5	0.5	0.108	0.721630	0.000030
KFM02B-33	527.55	–512.38	RU1b	27.9	Na-Ca-HCO_3	22.3	–	< 0.5	0.6	–	–	
KFM02B-34	532.44	–517.19	RU1b	32.8	Ca-Na-HCO_3	22.4	–	< 0.5	1.3	0.234	0.722981	0.000020
KFM02B-39	559.83	–544.09	RU1b	60.2	Na-Ca-HCO_3-Cl	20.0	–	< 0.5	0.3	–	–	
KFM02B-40	562.47	–546.69	RU1b	62.9	Na-Ca-HCO_3-Cl	20.7	–	< 0.5	0.4	0.119	0.722921	0.000020
KFM02B-41	565.29	–549.46	RU1b	65.7	Na-Ca-HCO_3	20.4	–	< 0.5	< 0.3	–	–	
KFM02B-42	569.35	–553.45	RU1b	69.8	Na-Ca-HCO_3-Cl	22.4	–	< 0.5	0.3	–	–	
KFM02B-43	573.65	–557.67	RU1b	74.1	Na-Ca-HCO_3	17.0	–	< 0.5	0.4	0.121	0.723832	0.000025
KFM06A-1	146.08	–122.69	RU1a	3.0	Na-Ca-HCO_3-Cl	27.4	0.51	< 0.5	0.9	0.082	0.722315	0.000042
KFM06A-2	194.69	–164.70	RU1a	3.4	Na-Ca-HCO_3-Cl	33.6	0.97	< 0.5	0.7	0.108	0.729086	0.000022
KFM06A-3	252.41	–214.22	RU1a	5.8	Na-Ca-HCO_3-(Cl)	12.3	1.31	< 0.5	< 0.5	0.068	0.726727	0.000020
KFM06A-4	281.82	–239.33	RU1a	8.6	Na-Ca-HCO_3-Cl	15.5	1.85	< 0.5	0.6	0.097	0.725589	0.000032
KFM06A-5	298.49	–253.54	RU1a	0.3	Na-Ca-HCO_3-Cl	25.1	0.62	< 0.5	0.6	0.135	0.725231	0.000020
KFM06A-6	355.29	–301.74	RU1a	2.0	Na-Ca-HCO_3-Cl	42.8	0.17	< 0.5	1.3	0.252	0.720257	0.000020
KFM06A-7	395.40	–335.50	RU1a	2.0	Na-Ca-HCO_3-Cl	22	1.04	< 0.5	0.6	0.100	0.725174	0.000032
KFM06A-8	440.98	–373.70	RU1a	7.5	Na-Ca-HCO_3-Cl	27.4	0.75	< 0.5	0.8	0.149	0.724792	0.000020
KFM06A-9	500.02	–422.92	RU1a	51.8	Ca-Na-HCO_3-Cl	53.2	1.01	< 0.5	0.5	0.343	0.722954	0.000021
KFM06A-10	563.38	–475.44	RU1a	60.3	Na-Ca-HCO_3-Cl	25.2	0.59	< 0.5	0.5	0.142	0.723958	0.000020
KFM06A-11	575.94	–485.84	RU2	47.8	Na-Ca-HCO_3-Cl	36.4	–	< 0.5	< 0.5	0.204	0.721135	0.000021
KFM06A-12	594.62	–501.28	RU2	29.1	Na-Ca-HCO_3-Cl		–	–	–	–		

UniBern Sample No	Average borehole length (m)	Average Elevation (m)	Rock Unit	Distance to nearest water-cond. fracture	Experiment Solution Chemical type [1]	Cl^- in Exp. Solution (mg/L)	$\delta^{37}Cl$ in Exp. Solution [2] (‰ SMOC)	Br^- in Exp. Solution [3] (mg/L)	Mg^{+2} in Exp. Solution [3] (mg/L)	Sr^{+2} in Exp. Solution [4] (ppm)	$^{87}Sr/^{86}Sr$	2σ error
KFM06A-13	633.56	–533.40	RU3	9.9	Na-Ca-HCO_3-Cl	44.2	–	< 0.5	0.5	0.248	0.721013	0.000020
KFM06A-14	660.89	–555.84	RU3	7.2	-	-	–	–	–	–	–	
KFM06A-15	698.81	–586.41	RU1b	44.6	Na-Ca-HCO_3-Cl	39.1	3.26	< 0.5	< 0.5	0.182	0.724597	0.000020
KFM06A-16	763.59	–639.50	RU4	19.8	Na-Ca-HCO_3-Cl	31.7	0.48	< 0.5	< 0.5	0.134	0.720926	0.000020
KFM06A-17	810.84	–677.59	RU4	41.9	-	-	–	–	–	–	–	
KFM06A-18	851.71	–710.24	RU4	82.8	Ca-Na-Cl-HCO_3	60.4	0.36	< 0.5	0.5	0.289	0.715329	0.000020
KFM06A-19	900.97	–749.37	RU4	132.1	Na-Ca-Cl-HCO_3	75.7	0.43	< 0.5	< 0.5	0.340	0.717890	0.000022
KFM06A-20	920.69	–764.95	RU4	151.8	Ca-Na-Cl-HCO_3	79.1	0.13	< 0.5	0.5	0.311	0.716483	0.000020
KFM06A-21	948.77	–786.98	RU5	179.9	Ca-Na-Cl-HCO_3	82.1	0.15	< 0.5	0.5	0.282	0.719254	0.000020
KFM06A-22	977.36	–809.33	RU5	208.5	Ca-Na-Cl-HCO_3	145.0	0.1	1.0	0.5	0.550	0.721426	0.000020
KFM06A-23	998.32	–825.66	RU5	229.4	Ca-Na-Cl-HCO_3	122.0	0.79	0.6	0.5	0.587	0.722194	0.000020
KFM08C-1	154.69	–131.16	RU1a	6.6	Na-(Ca)-HCO_3-Cl	16.5	–	< 0.5	< 0.5	0.191	0.719081	0.000022
KFM08C-2	254.92	–215.87	RU1a	27.9	Na-Ca-HCO_3-Cl	24.4	–	< 0.5	< 0.5	2.406	0.718564	0.000020
KFM08C-3	353.92	–298.58	RU2a	71.1	Ca-Na-HCO_3-Cl	28.0	–	< 0.5	< 0.5	0.201	0.727218	0.000020
KFM08C-4	455.72	–383.03	RU2a	0.2	Na-Ca-Cl	746.4	–	4.9	4.3	0.149	0.730043	0.000022
KFM08C-5	553.20	–463.19	RU1b	28.6	Na-Ca-HCO_3-Cl	37.7	–	< 0.5	< 0.5	0.404	0.731876	0.000020
KFM08C-6	648.58	–540.69	RU1c	34.4	Na-Ca-HCO_3-Cl	40.6	–	< 0.5	< 0.5	0.191	0.734275	0.000020
KFM08C-7	751.45	–623.27	RU1c	67.9	Ca-Na-Cl-HCO_3	92.0	–	< 0.5	< 0.5	0.383	0.739763	0.000020
KFM08C-8	839.74	–693.38	RU1d	156.1	Na-Ca-Cl-HCO_3	49.6	–	< 0.5	< 0.5	0.324	0.732433	0.000020
KFM08C-9	917.21	–754.37	RU1d	233.6	Ca-Na-Cl-HCO_3	101.5	–	0.8	< 0.5	–	–	
KFM08C-10	938.30	–770.85	RU1d	254.7	Na-Ca-Cl-HCO_3	90.8	–	< 0.5	< 0.5	–	–	
KFM09B-1	573.47	–442.43	RU4b	1.0	Na-Ca-Cl	548.9	–	4.3	1.3	1.631	0.719072	0.000020
KFM09B-2	574.55	–443.17	RU4b	2.5	Na-Ca-Cl-HCO_3	48.0	–	< 0.5	< 0.5	0.235	0.724739	0.000020
KFM09B-3	576.41	–444.47	RU4b	4.5	Ca-Na-HCO_3-Cl	62.9	–	< 0.5	< 0.5	0.296	0.729027	0.000020
KFM09B-4	576.73	–444.70	RU4b	4.8	Ca-Na-HCO_3-Cl	65.6	–	< 0.5	< 0.5	0.283	0.743253	0.000050
KFM09B-5	576.98	–444.87	RU4b	5.0	Ca-Na-HCO_3-Cl	58.8	–	< 0.5	< 0.5	0.071	0.727118	0.000020
KFM09B-6	577.89	–445.50	RU4b	5.8	Na-Ca-HCO_3-Cl	52.7	–	< 0.5	< 0.5	0.180	0.726591	0.000020
KFM09B-7	582.69	–448.84	RU4b	10.6	Ca-Na-Cl-HCO_3	72.0	–	< 0.5	< 0.5	–	–	
KFM09B-8	586.57	–451.52	RU4b	14.5	Ca-Na-Cl-HCO_3	82.1	–	< 0.5	< 0.5	–	–	

[1] Chemical type corresponds to that of porewater except for HCO_3, which might not be a major anion in pore water with Cl^- > 1,500 mg/kgH_2O (see text).
[2] Analytical error ±0.15‰ SMOC (2σ).
[3] Measurements by ion-chromatography, analytical error ±5% (2σ); for Mg more precise measurements with a lower detection limit were performed for samples from borehole KFM02B.
[4] Strontium measurements by MS, analytical error <1% (2σ).

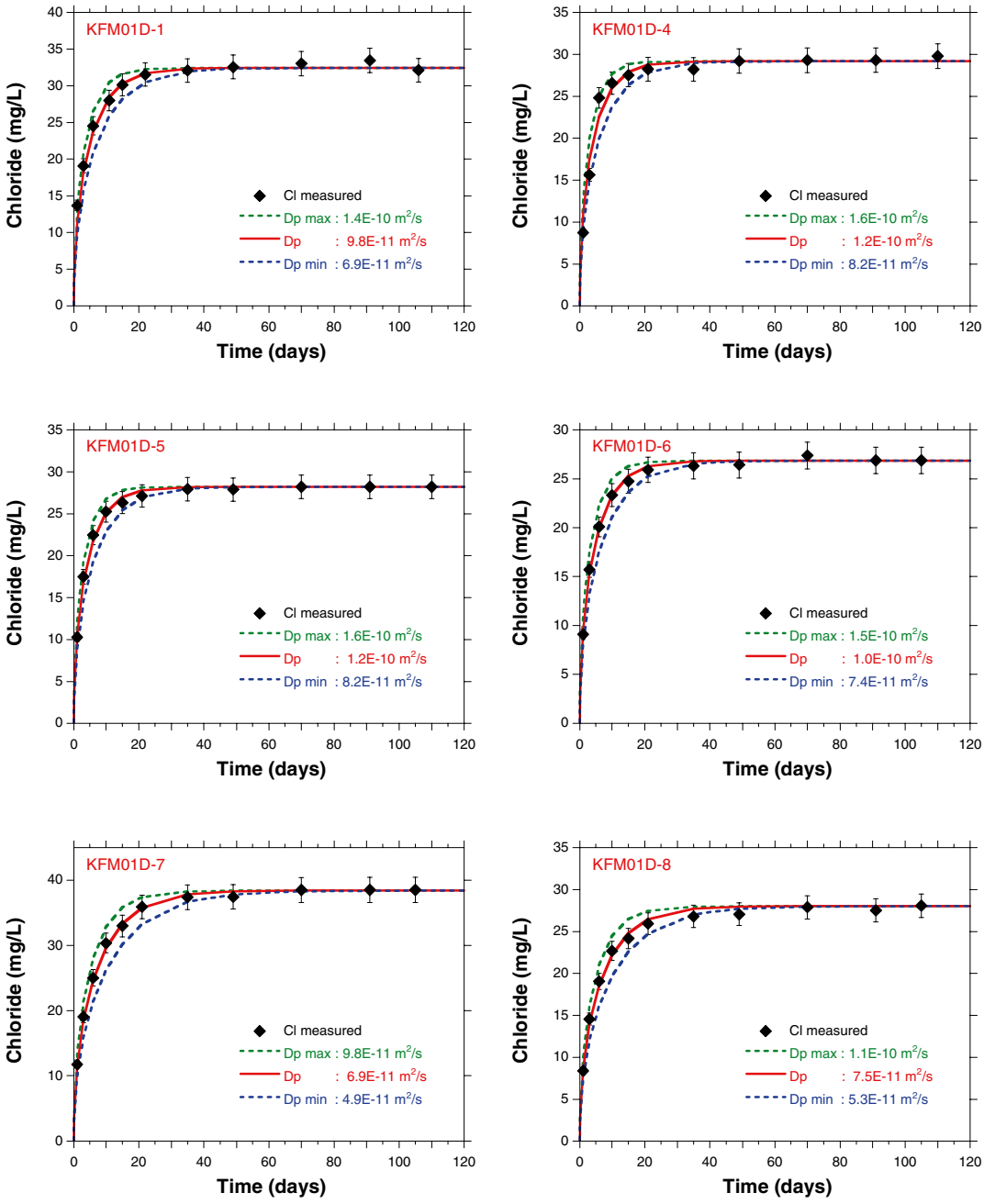

Figure A-1. *Model fits to the measured chloride time-series data of the out-diffusion experiments performed on large size (approx 1 kg) drillcore samples from borehole KFM01D. The best-fit curve delivering the pore diffusion coefficient, D_p, for chloride at 25°C is shown in red. The uncertainty range (D_p min and D_p max) is given by values that are larger/smaller by a factor 1.41 (square root of 2) corresponding to a factor of 2 in the diffusion time (green and blue curves).*

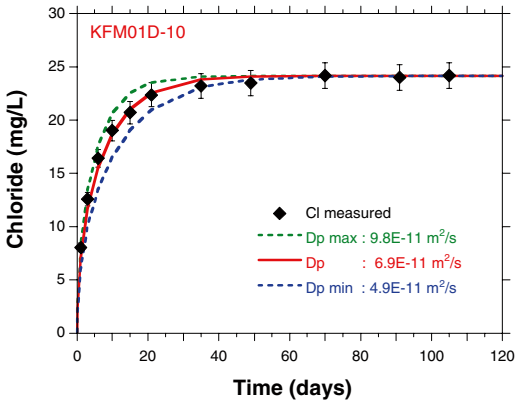

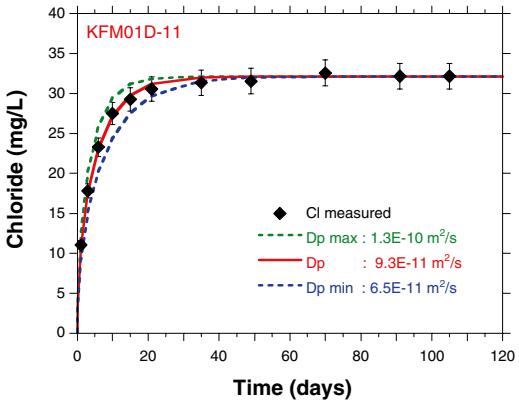

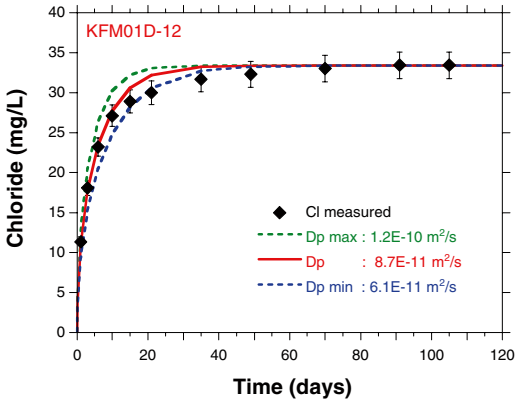

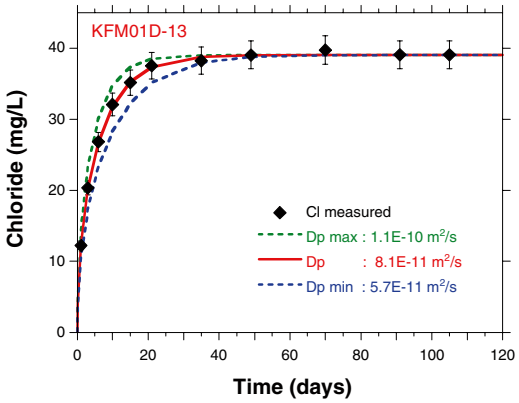

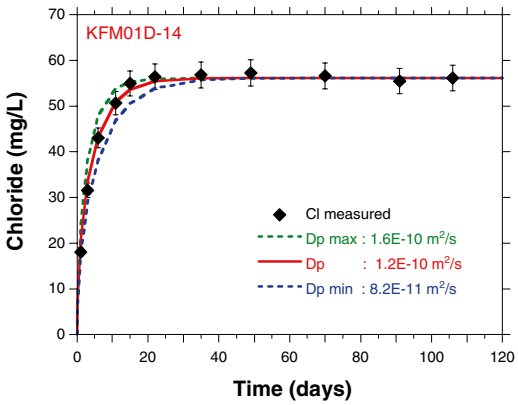

Figure A-1. *Continued.*

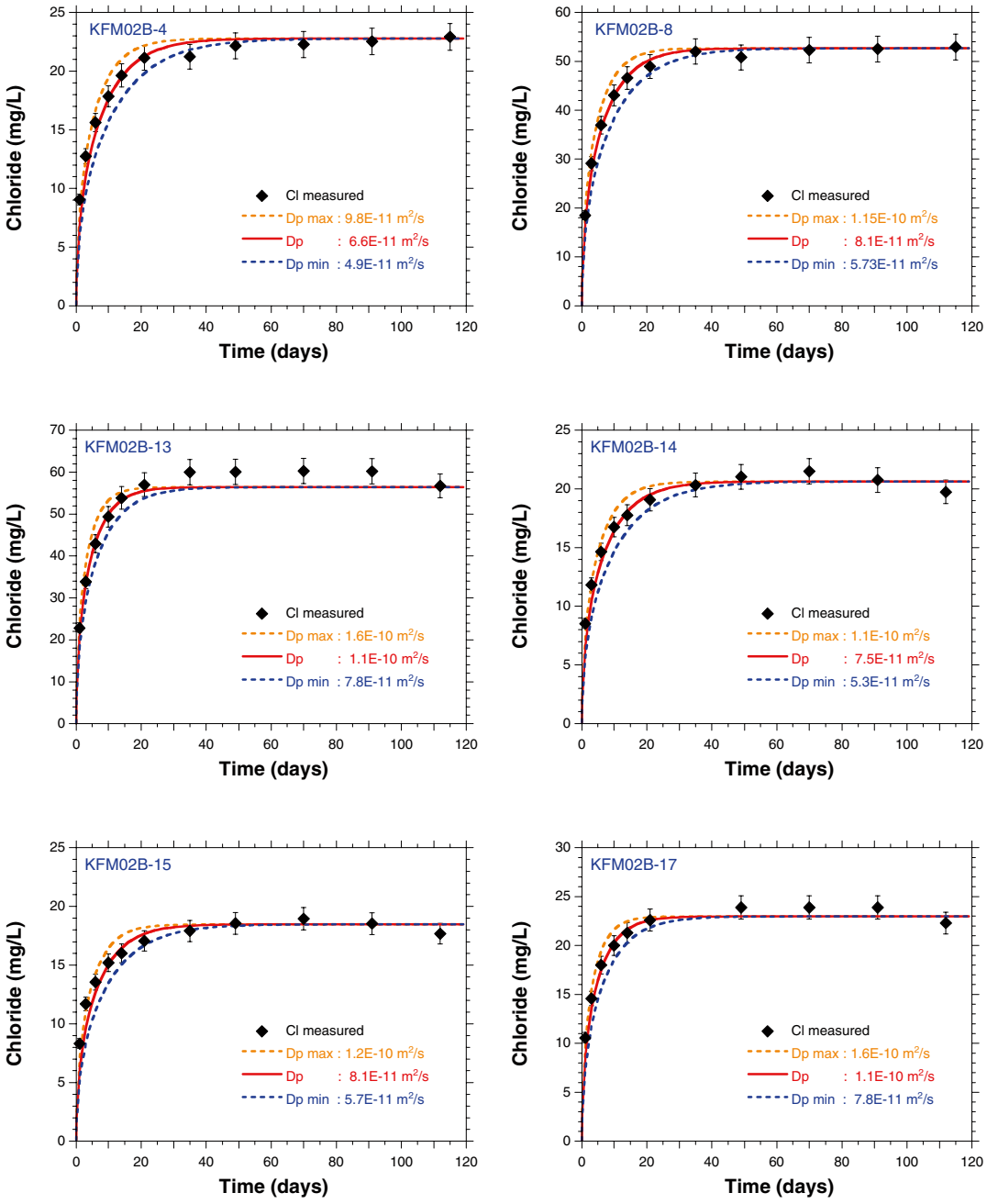

Figure A-2. *Model fits to the measured chloride time-series data of the out-diffusion experiments performed on large size (approx 1 kg) drillcore samples from borehole KFM02B. The best-fit curve delivering the pore diffusion coefficient, D_p, for chloride at 25°C is shown in red. The uncertainty range (D_p min and D_p max) is given by values that are larger/smaller by a factor 1.41 (square root of 2) corresponding to a factor of 2 in the diffusion time (orange and blue curves).*

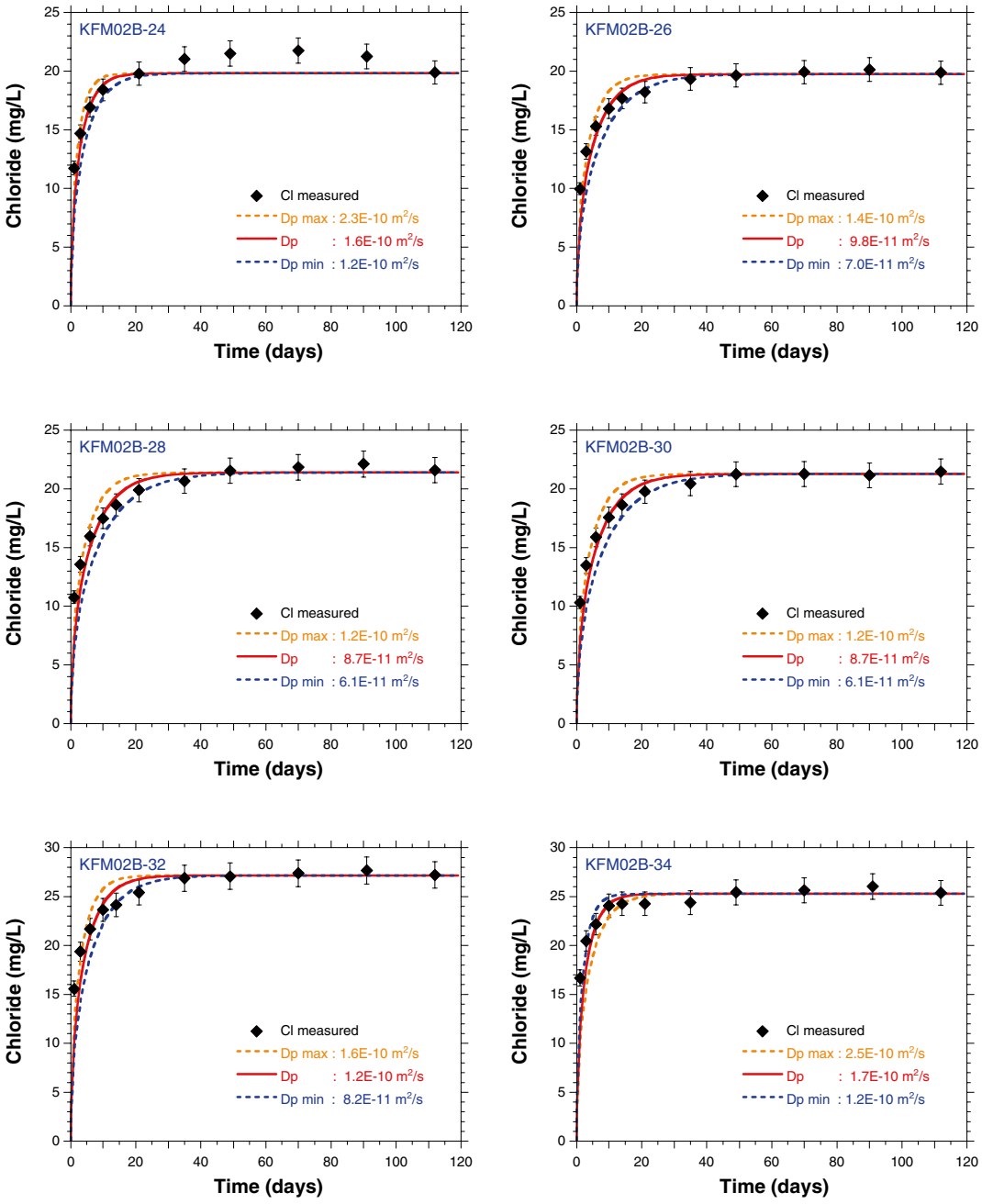

Figure A-2. *Continued.*

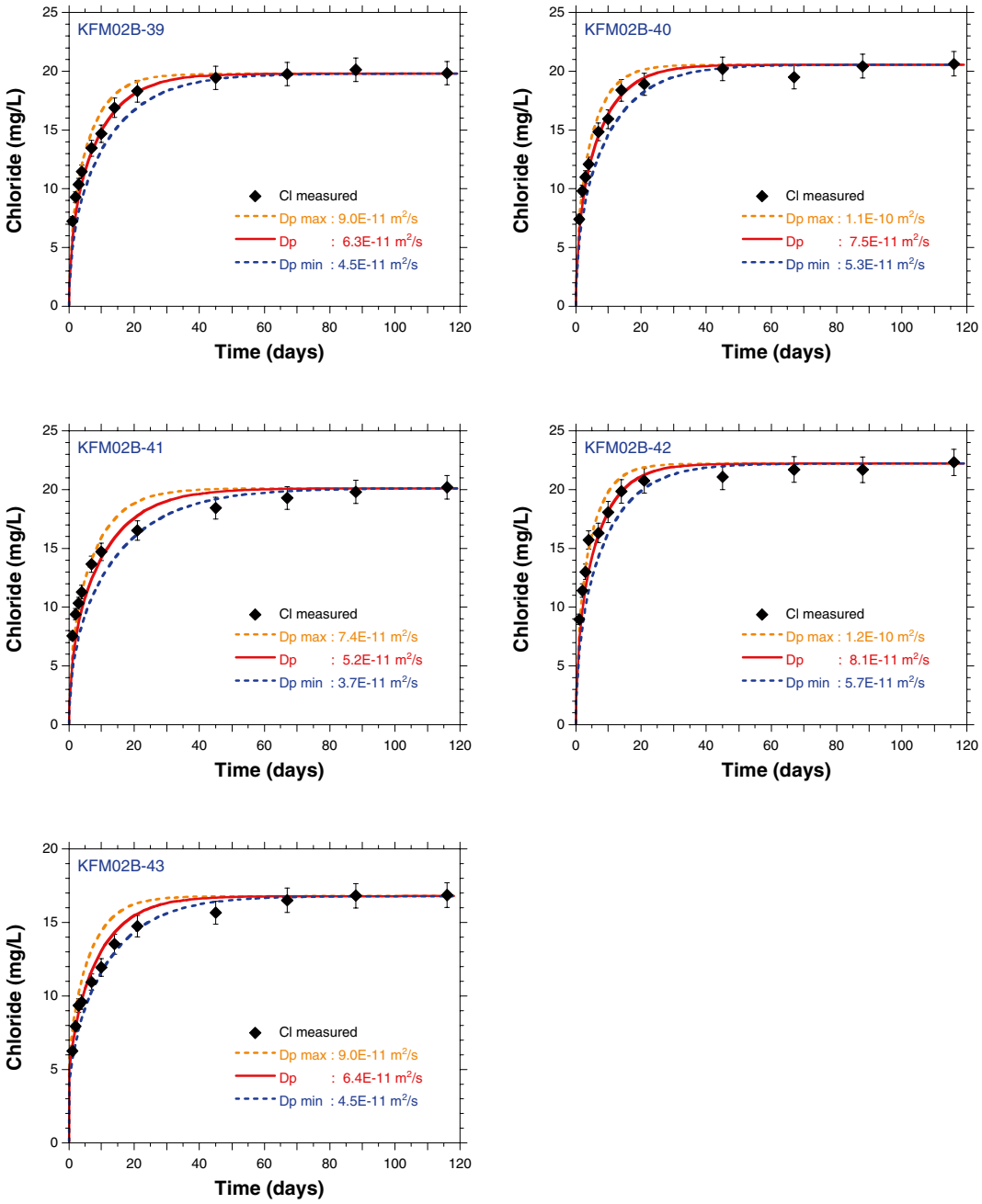

Figure A-2. *Continued.*

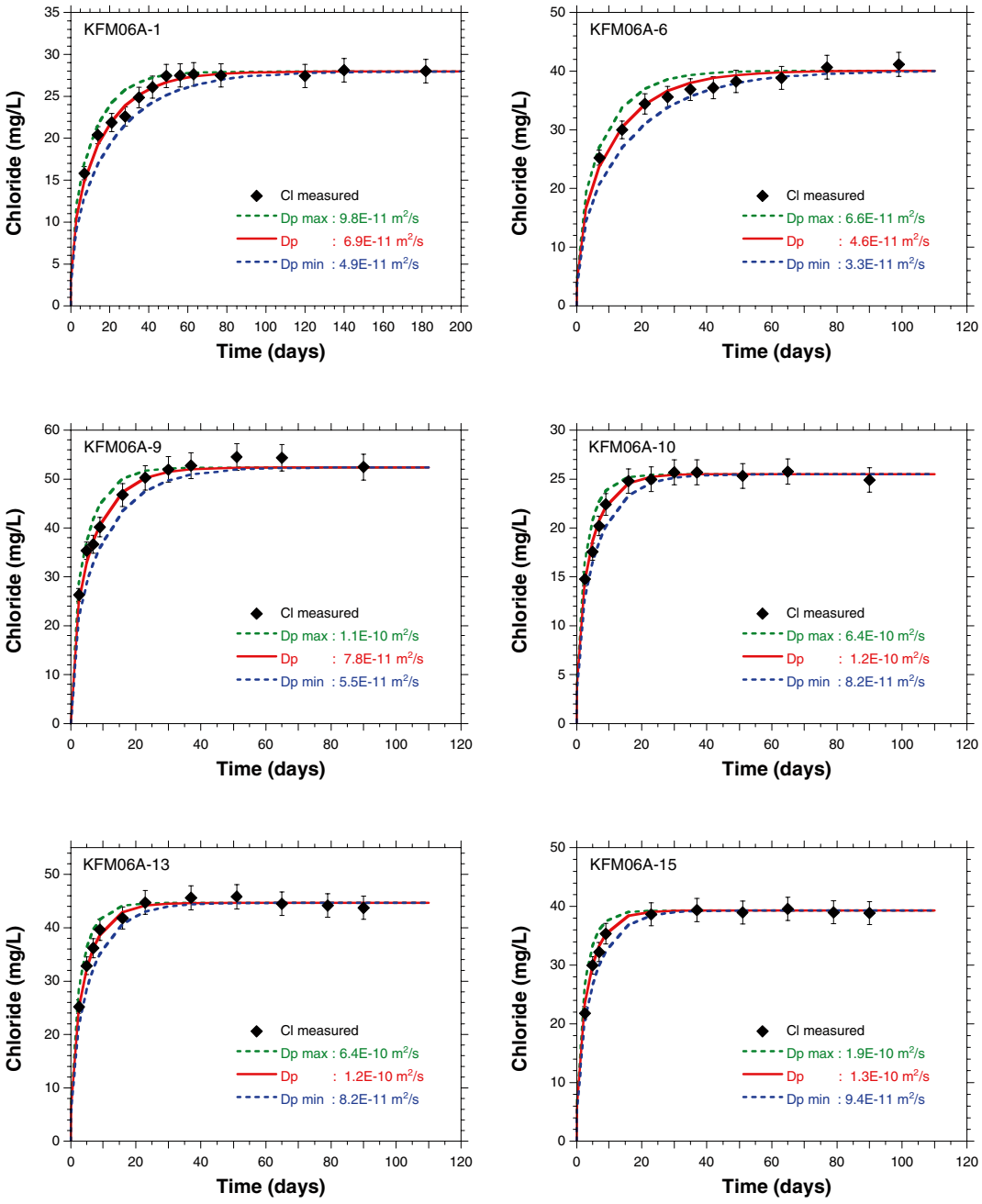

Figure A-3. *Model fits to the measured chloride time-series data of the out-diffusion experiments performed on large size (approx 1 kg) drillcore samples from borehole KFM06A. The best-fit curve delivering the pore diffusion coefficient, D_p, for chloride at 25°C is shown in red. The uncertainty range (D_p min and D_p max) is given by values that are larger/smaller by a factor 1.41 (square root of 2) corresponding to a factor of 2 in the diffusion time (green and blue curves).*

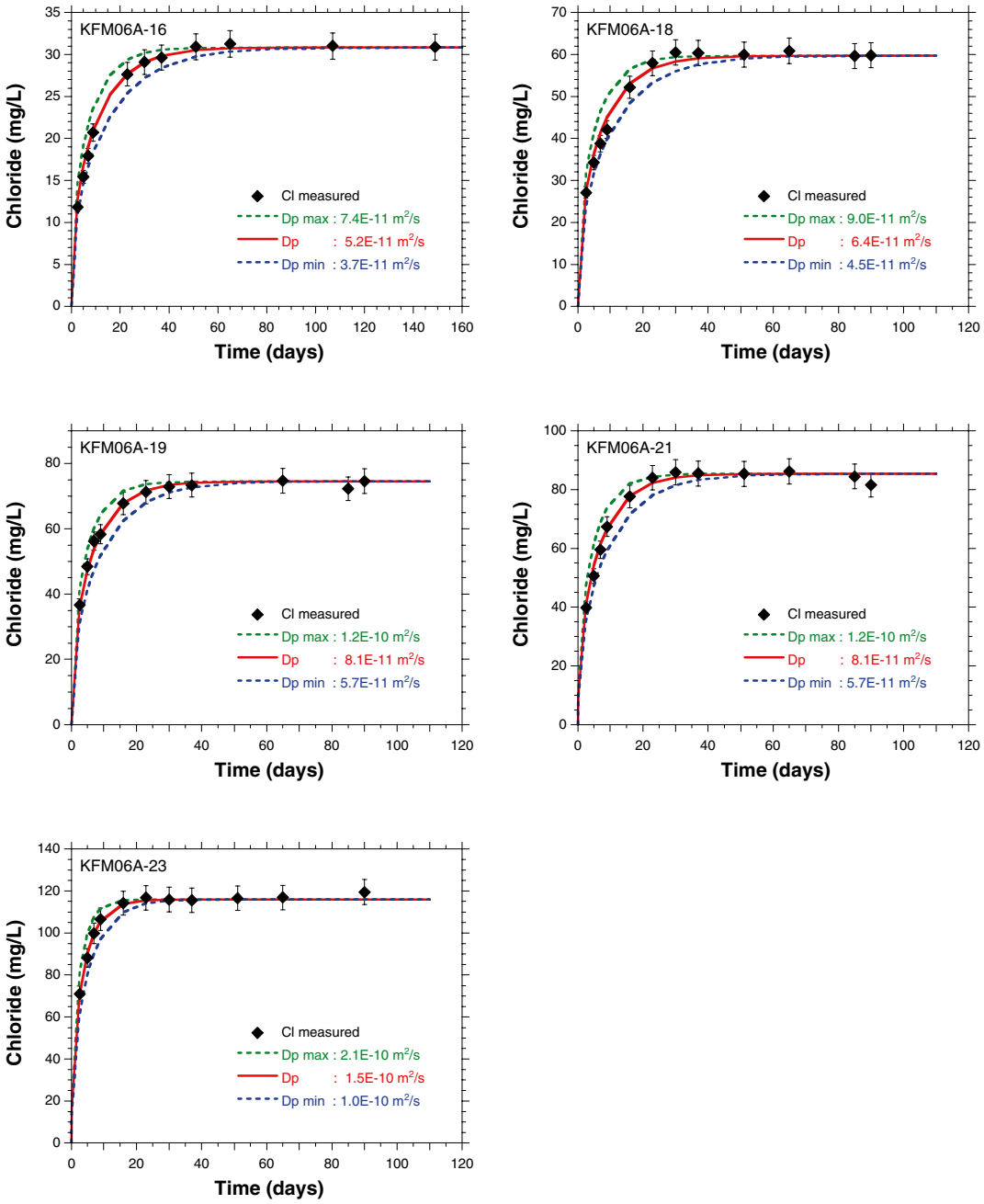

Figure A-3. *Continued.*

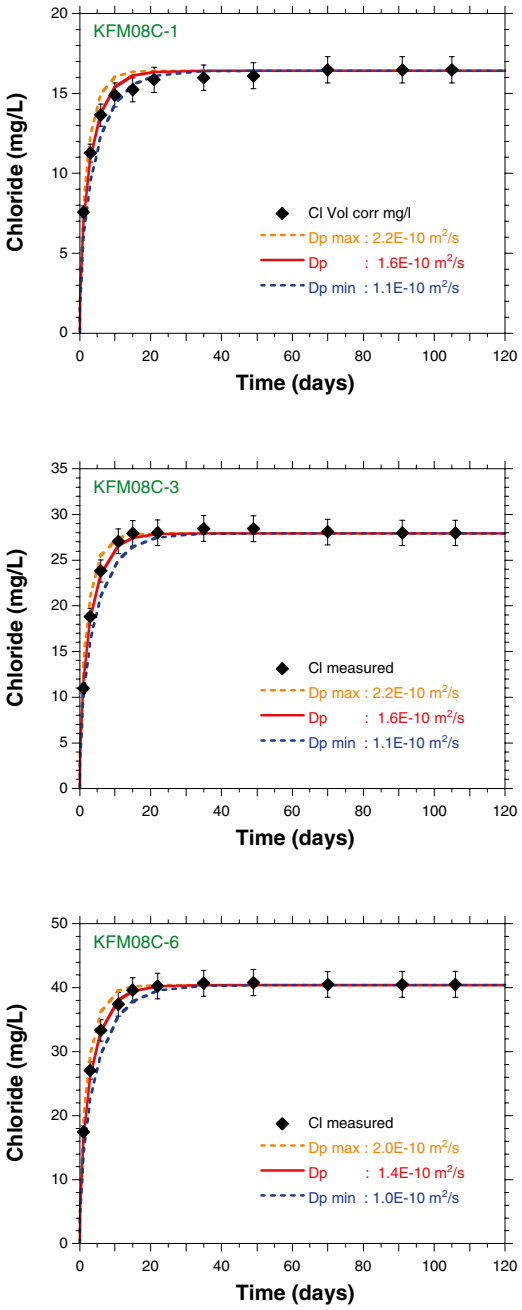

Figure A-4. *Model fits to the measured chloride time-series data of the out-diffusion experiments performed on large size (approx 1 kg) drillcore samples from borehole KFM08C. The best-fit curve delivering the pore diffusion coefficient, D_p, for chloride at 25°C is shown in red. The uncertainty range (D_p min and D_p max) is given by values that are larger/smaller by a factor 1.41 (square root of 2) corresponding to a factor of 2 in the diffusion time (orange and blue curves).*

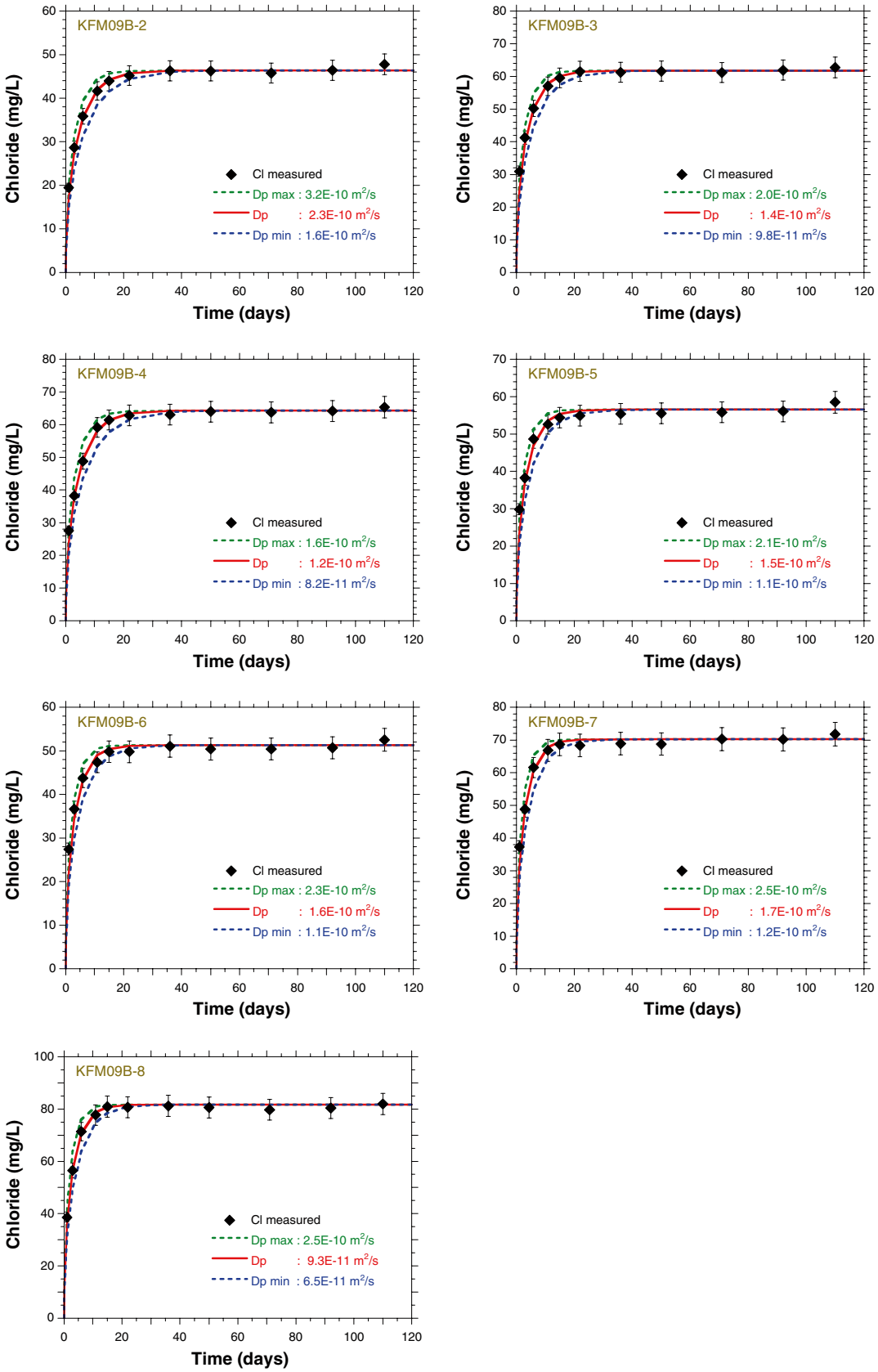

Figure A-5. *Model fits to the measured chloride time-series data of the out-diffusion experiments performed on large size (approx 1 kg) drillcore samples from borehole KFM09B. The best-fit curve delivering the pore diffusion coefficient, D_p, for chloride at 25°C is shown in red. The uncertainty range (D_p min and D_p max) is given by values that are larger/smaller by a factor 1.41 (square root of 2) corresponding to a factor of 2 in the diffusion time (green and blue curves).*